

**THE SYNTHESIS OF NITROGEN DOPED CARBON
SPHERES AS SUPPORTS FOR PALLADIUM
CATALYSTS IN THE HYDROGENATION OF
CINNAMALDEHYDE**

By

Sibongile Mary-Anne Manikai

Student Number: 0702591D

A thesis submitted to the Faculty of Science, University of Witwatersrand,
Johannesburg, in fulfilment of the requirements for the degree of

Doctor of Philosophy in Chemistry

Johannesburg, 2015

DECLARATION

I declare that this Thesis is my own, unaided work. It is being submitted for the Degree of Doctor of Philosophy at the University of the Witwatersrand, Johannesburg. It has not been submitted before for any degree or examination at any other University.



(Sibongile Mary-Anne Manikai)

On this ____ day of _____ 2015

Supervisor:

Professor N. J. Coville

ABSTRACT

The selective hydrogenation of cinnamaldehyde (CALD), an α,β -unsaturated aldehyde, at the carbonyl (C=O) and olefinic (C=C) groups is an important reaction since its products mainly cinnamyl alcohol (CA) and hydrocinnamaldehyde (HCALD) are important intermediates for the production of many chemicals in a wide range of industries (pharmaceuticals, flavouring, agrochemicals, perfume). In this study the synthesis of nitrogen doped carbon spheres (NCSs) as catalyst supports for the hydrogenation of CALD is reported. At the heart of the hydrogenation of CALD is the catalyst, since it provides the surface for the various reactions to take place. In this study, an in-depth study was conducted on the NCSs support, by varying pyrolysis time, pyrolysis temperatures and flow rates of gases to determine the physical and chemical properties. The effects of chemically modifying the surfaces of the NCS supports by functionalization with acid and doping with carbon were also investigated. NCSs which had undergone different pre-treatments procedures were then deposited with Pd nanoparticles using different metal deposition methods and the resultant catalysts tested for the hydrogenation of CALD.

NCSs were successfully synthesized using a non - catalytic chemical vapour deposition (CVD) method using acetonitrile as a N source and acetylene (C_2H_2) as a C source. The influence of synthesis parameters (pyrolysis temperature, time and flow rate of gases) on the product morphology, size, N composition, thermal stability and the degree of crystallinity of the carbon products was studied. The NCSs produced were characterized by TEM, CN elemental analysis, XPS, TGA and Raman spectroscopy. TEM analysis showed that the variation of different CVD parameters produced carbon material that had a spherical morphology that is carbon spheres. The variation of pyrolysis temperature (700, 800, 850, 900, 950 and 1000 °C) had the effect of lowering the N content of the spheres formed. The NCSs produced at 800, 850, 900, 950 and 1000 °C had N concentrations of 4.09, 3.14, 3.30, 2.64 and 2.81

wt.% respectively. This is due to the bond dissociation energies of the C-C bond and the C-N bonds. The thermal stability of the NCSs increased due to the decrease in the number of defects formed in the NCSs at high temperatures. Increasing the pyrolysis time (5, 30, 60, 90, 120, 150, 180 and 240 minutes) had the effect of increasing the average diameters of the NCSs due to the long periods of annealing. The degree of disorder increased due to the N content which increased which meant that there were more defects in the NCSs. Thermal stability decreased because of the defects introduced by the N atoms on the surfaces of the carbon spheres. The variation of flow rate of gases (N_2 and C_2H_2) during the pyrolysis step affected the physical and chemical properties of the resultant NCSs formed. The average diameter and thermal stability of the NCSs decreased upon increasing the C_2H_2 flow rate and eliminating the N_2 introduced during the pyrolysis stage. However the degree of disorder of the NCSs increased due to the increase in the N content. Increasing the C_2H_2 flow rate and decreasing the N_2 flow rate, had the following effect on the NCSs, the average diameter and thermal stability remained nearly constant and the I_D / I_G ratio and N content increased.

NCSs were successfully used as catalyst supports. The Pd nanoparticles that were deposited on the surfaces of NCSs were well dispersed with narrow particle size distribution using the liquid phase reduction method. The Pd particles supported on CSs and NCSs functionalized at different temperatures of 55 % HNO_3 for 24 hours had mean particle sizes ranging between 4.68 and 7.51 nm. The Pd nanoparticles supported on CSs with different N contents had mean particle sizes ranging between 4.15 and 4.82 nm. The amount of oxygen surface groups on the support had an effect on the liquid phase hydrogenation of CALD. Low concentration of oxygen surface groups on catalysts resulted in high catalytic activity (expressed as conversion) of 87 and 91 % for 1 % Pd / fNCSs 40 and 1 % Pd / fNCSs 60 catalysts respectively at reaction time of 3 hours. The conversion of CALD at reaction time 3 hours was 10 % for the 1 % Pd / fNCSs 80 catalyst. The presence of N in the CS supports led to a

significant improvement of catalytic activity compared to N free catalysts. The conversion to CALD of 1 % Pd / fNCSs 40 (3.84 % N), 1 % Pd / fNCSs 40 (2.39 % N), 1 % Pd / fNCSs 40 (0.41 %) and 1 % Pd / fNCSs 40 (0.00 % N) were 59, 91, 54 and 48 % respectively at reaction time of 3 hours. The activity improvement was attributed to the electronic modification of the active phase. The amount of N in the catalysts also affected the activity and selectivity of the catalysts in the hydrogenation of CALD.

The effects of reaction solvents, temperature and flow rates of hydrogen on the hydrogenation of CALD were studied over 1 % Pd / fNCSs 40 catalyst. Optimum conditions were then found to be used in all other hydrogenation reactions to be used in this thesis. The optimum conditions were selected based on high activities and selectivities to HCALD obtained absence of side reactions and catalyst leaching and catalyst stability.

Comparison of the activity of catalysts for the hydrogenation of CALD prepared by two methods of preparation, the incipient wetness impregnation method and liquid phase reduction method were done. The catalyst prepared from the liquid phase reduction method had the best catalytic performance in terms of both CALD conversion and selectivity to HCALD. The conversion to CALD was 100 % at reaction time 4 hours and the selectivity to HCALD was 100 % from reaction time 1 hour to 8 hours for the Polyol 1 % Pd / fNCSs 40 catalyst. However the catalyst activities (expressed in terms of conversion) for the catalysts prepared using the IWI method were 57 % and 42 % for the Impregnation 1% Pd / fNCSs 40 calcined and Impregnation 1 % Pd / fNCSs 40 reduced catalysts respectively. The Impregnation 1 % Pd / fNCSs 40 reduced catalyst was 100 % selective to HCALD throughout the reaction whereas the Impregnation 1% Pd / fNCSs 40 calcined catalysts was selective to both HCALD and 3P1P from reaction time 3 hours.

DEDICATION

This thesis is dedicated to the following people, without whose support, encouragement, love and motivation I would not have been able to complete this endeavour:

- My husband Bothwell Manikai and my kids Ropafadzo and Anesu Manikai
- My parents, Doreen and Russell Dube
- My siblings Masiyiwa, Russell and Sam Dube.

ACKNOWLEDGEMENTS

I would like to express my sincere gratitude to the following people and institutions for their various roles in making this project a success:

- My supervisor, Professor N. J. Coville for his invaluable support, guidance and helpful suggestions and criticisms during this project.
- The staff members of the Microscopy and Microanalysis Unit at the University of the Witwatersrand for assistance with electron microscopy work.
- Dr. R. Erasmus for assistance with Raman spectroscopy analysis.
- Professor H. C. Swart of the University of the Free State for XPS analysis.
- Mr M. F. Philpott from the ARC – Institute for soil, climate and water for CN elemental analysis.
- Many thanks are due to Mr B. Chassoulas for all the technical assistance
- The glassblower, Mr T. Dzara for assistance with the quartz tubes and glassware modifications used for this work.
- My family members for their patience in seeing me through this work.
- All members of the CAT-OM-MAT group of the School of Chemistry at the University of the Witwatersrand for providing a conducive working environment.
- The DST / NRF Nano Flagship Project - PGM beneficiation and the University of the Witwatersrand for financial support.
- Above all to God the almighty for providing strength and protection.

PUBLICATIONS AND PRESENTATIONS

PUBLICATIONS

1. Haifeng Xiong, Mahluli Moyo, Myriam A. M Motchelaho, Zikhona N. Tetana, **Sibongile M. A Dube**, Linda L. Jewell and Neil J Coville, *Fischer-Tropsch synthesis: Iron catalysts supported on N-doped carbon spheres prepared by chemical vapour deposition and hydrothermal approaches*. Journal of Catalysis, 2014. **311**(0): p. 80-87.
2. Thobeka Kente, **Sibongile M. A Dube**, Neil J Coville and Sabelo D. Mhlanga, *Application of Gallium Nitride Nanostructures and Nitrogen Doped Carbon Spheres as Supports for the Hydrogenation of Cinnamaldehyde*. Journal of Nanoscience and Nanotechnology, 2013. **13**(7): p. 4990-4995.
3. W. P. Wright, V. D. Marsicano, J. M. Kearthland, R. M. Erasmus, **S.M. A Dube** and N. J. Coville. *The electrical transport properties of nitrogen doped carbon microspheres*. Materials Chemistry and Physics, 2014. **147**(3): p. 908-914.
4. **Sibongile M. A. Manikai**, Neil J Coville, *The synthesis of nitrogen doped carbon spheres by non - catalytic chemical vapour deposition method*. To be submitted.

PRESENTATIONS

Sibongile, M. A Dube and N. J. Coville, *Nitrogen doped carbon spheres as catalyst supports in the cinnamaldehyde hydrogenation reaction*, (**Oral presentation**), Catalysis Society of South Africa (CATSA) 2012 conference, Langebaan, Capetown, 11 - 14 November 2012.

Sibongile, M. A Dube and N. J. Coville, *Palladium supported nitrogen doped carbon spheres for the hydrogenation of cinnamaldehyde*, (**Oral presentation**), South African Nanotechnology Initiative (SANI), Nanoscience Young Researcher Symposium (NYRS), University of the Witwatersrand, Johannesburg, 7 September 2012.

Sibongile, M. A Dube and N. J. Coville, *Synthesis of nitrogen doped carbon spheres*, (**Oral presentation**), DST / NRF Nano Flagship Project - PGM beneficiation seminar, University of the Western Cape, Capetown, South Africa, 20 September 2010.

TABLE OF CONTENTS

DECLARATION.....	i
ABSTRACT.....	ii
DEDICATION.....	v
ACKNOWLEDGEMENTS.....	vi
PUBLICATIONS AND PRESENTATIONS.....	vii
PUBLICATIONS.....	vii
PRESENTATIONS.....	viii
TABLE OF CONTENTS.....	ix
LIST OF FIGURES.....	xvii
LIST OF TABLES.....	xxiii
LIST OF ABBREVIATIONS.....	xxvi
CHAPTER 1.....	1
INTRODUCTION.....	1
1.1 Background and motivation	1
1.2 Aims and objectives of the study.....	4
1.3 Thesis outline.....	5
1.4 References	6

CHAPTER 2.....	8
LITERATURE REVIEW	8
2.1 Carbon materials as catalyst supports.....	8
2.2 Carbon spheres	8
2.2.1 Modification of carbon nanomaterials	9
2.2.1.1 Functonalization.....	10
2.2.1.2 Doping.....	11
2.2.1.2.1 Nitrogen doping of CSs.....	11
2.3 Synthesis of NCSs	13
2.4 Catalyst preparation methods	23
2.4.1 Impregnation method	23
2.4.1.1 Incipient wetness impregnation method.....	24
2.4.1.2 The liquid phase reduction method / polyol process.....	25
2.5 Carbon spheres used as supports in various catalysis reactions.....	27
2.5.1 Undoped carbon sphere supports	27
2.5.2 Doped carbon sphere supports	30
2.6 Hydrogenation reactions of α,β -unsaturated aldehydes	36
2.6.1 Mechanism of hydrogenation reaction of cinnamaldehyde	36
2.7 Doped and undoped carbon nanomaterials used as supports for the.....	
hydrogenation of CALD	38

2.7.1	Undoped carbon nanomaterials.....	38
2.7.1.1	Pd catalysts supported on undoped carbon nanomaterials for the hydrogenation of CALD	38
2.7.1.2	Other PGM catalysts excluding Pd supported on undoped carbon nanomaterials for the hydrogenation of CALD	39
2.7.2	Nitrogen doped carbon nanomaterials.....	42
2.8	Summary.....	44
2.9	References	45
CHAPTER 3.....		56
The synthesis of nitrogen doped carbon spheres by non - catalytic chemical vapour deposition.*		56
3.1	Introduction	56
3.2	Experimental.....	58
3.2.1	Synthesis of NCSs.....	58
3.2.2	Characterization techniques	60
3.3	Results and Discussion	60
3.3.1	Variation of carbonization temperature.....	61
3.3.2	Variation of carbonization time.....	70
3.3.3	Variation of flow rates of gases.....	80
3.4	Conclusion	89

3.5	References.....	90
CHAPTER 4.....		94
Nitrogen doped carbon spheres as a catalyst support for the hydrogenation of cinnamaldehyde. The effect of support characteristics on the reaction.		94
4.1	Introduction	94
4.2	Experimental.....	99
4.2.1	Synthesis of NCSs.....	99
4.2.1.1	Removal of polycyclic aromatic hydrocarbons (PAHs)	100
4.2.1.2	Functionalization of NCSs	100
4.2.2	Catalyst synthesis	100
4.2.3	Characterization techniques	101
4.2.4	Hydrogenation of cinnamaldehyde (CALD).....	103
4.3	Results and Discussion	104
4.3.1.	Effect of functionalization of undoped and doped carbon supports....	104
4.3.1.1	Support characterization.....	104
4.3.1.2	Characterization of the Pd catalysts.	114
4.3.1.3	Catalytic tests.	123
4.3.2	Effect of N content of the support.....	127
4.3.2.1	Support characterization.....	127
4.3.2.2	Catalyst characterization	131

4.3.2.3	Catalytic test reactions	138
4. 4	Conclusion.....	143
4. 5	References.....	144
CHAPTER 5.....		153
The effect of variation of reaction conditions on the hydrogenation of cinnamaldehyde over palladium supported nitrogen doped catalysts.....		153
5.1	Introduction	153
5.2	Experimental.....	154
5.2.1	Synthesis of NCSs.....	154
5.2.2	Synthesis of catalysts using liquid phase reduction method	155
5.2.3	Characterization	155
5.2.4	Catalyst testing.....	155
5.3	Results and Discussion	157
5.3.1	Support and Catalyst Characterization.....	157
5.3.2	Hydrogenation of CALD.....	159
5.3.2.1	Effect of solvents.....	159
5.3.2.2	Effect of temperature.....	163
5.3.2.3	Effect of hydrogen flowrates.....	165
5.3.2.4	Mass transfer effects.....	168
5.3.2.5	Catalyst leaching and recyclability	169

5.4	Conclusions	171
5.5	References	172
CHAPTER 6.....		174
The effect of different methods of catalyst preparation on the hydrogenation of cinnamaldehyde using nitrogen doped carbon spheres as supports and palladium as metal.....		174
6.1	Introduction	174
6.2	Experimental.....	175
6.2.1	Synthesis of NCSs.....	175
6.2.2	Catalyst preparation.....	175
6.2.2.1	Liquid phase reduction method	176
6.2.2.2	Incipient wetness impregnation method.....	176
6.2.3	Characterization	176
6.2.4	Hydrogenation of CALD.....	177
6.3	Results and Discussion	177
6.3.1	Catalyst characterization results.....	177
6.3.2	Hydrogenation of CALD.....	182
6.4	Conclusion	186
6.5	References.....	186

CHAPTER 7.....	189
Summary and concluding remarks	189
APPENDIX	192
EXPERIMENTAL	192
Materials and chemicals	192
Reagents and Chemicals	192
Gases.....	192
Synthesis of NCSs	193
Functionalization of NCSs.....	194
Catalyst synthesis	194
Liquid phase reduction method.....	194
Incipient wetness impregnation method	195
Characterization techniques.....	196
Transmission Electron Microscopy (TEM)	196
Fourier transform infrared (FTIR) spectroscopy	196
Zeta potential measurements.....	196
Raman spectroscopy	197
Thermogravimetric analysis (TGA).....	197
Nitrogen adsorption / desorption analysis	197

CN elemental analysis	198
X-ray photoelectron spectroscopy (XPS)	198
Powder X-ray diffraction (XRD)	198
Inductively Coupled Plasma - Optical Emission Spectroscopy (ICP - OES)....	199
Temperature programmed reduction (TPR).....	199
Catalytic reaction	200
Data analysis and calculations	202
References.....	203

LIST OF FIGURES

Figure 2.1. The types of nitrogen species that can be incorporated in nitrogen doped carbon nanomaterials: (A) pyridinic N, (B) pyrrolic N, (C) quaternary N and (D) nitrogen oxides [53].	12
Figure 2.2. An example of the schematic illustration of the mechanism of the polyol method [72].	26
Figure 2.3. The various adsorption modes of cinnamaldehyde [90, 91, 93].....	37
Figure 3.1. TEM images and the corresponding size distribution graphs of NCSs synthesized at (a) 800 °C, (b) 850 °C, (c) 900 °C, (d) 950 °C and (e) 1000 °C using C ₂ H ₂ as a carbon source (100 ml / min), CH ₃ CN (80 °C) as a nitrogen source and a carbonization time of 120 minutes.	62
Figure 3.2. TEM images and the corresponding size distribution graphs of NCSs synthesized at (a) 800 °C, (b) 850 °C, (c) 900 °C, (d) 950 °C and (e) 1000 °C.....	63
Figure 3.3. Graph showing average diameter of NCSs as a function of carbonization temperature.....	64
Figure 3.4. N content as a function of carbonization temperature.	64
Figure 3.5. Raman spectra of NCSs synthesized at different carbonization temperature. Carbonization time was kept constant at 120 minutes. C ₂ H ₂ was bubbled through CH ₃ CN at 80 °C.	66
Figure 3.6. (a) TGA and (b) corresponding derivative weight loss graphs of NCSs synthesized at different carbonization temperatures. Carbonization time was kept constant at 120 minutes. C ₂ H ₂ was bubbled through CH ₃ CN at 80 °C.....	67

Figure 3. 7. TEM images of NCSs synthesized at (a) 5 minutes, (c) 30 minutes, (d) 60 minutes, (e) 90 minutes, (f) 120 minutes, (g) 150 minutes, (h) 180 minutes and (i) 240 minutes using C_2H_2 as a carbon source (100 ml / min), CH_3CN (80 °C) as a nitrogen source and carbonization temperature of 950 °C.	71
Figure 3.8. Particle size distribution graphs of (a) NCSs 950 °C / 5 minutes, (b) NCSs 950 °C / 10 minutes, (c) NCSs 950 °C / 30 minutes, (d) NCSs 950 °C / 60 minutes, (e) NCSs 950 °C / 90 minutes and (f) NCSs 950 °C / 120 minutes. C source = C_2H_2 (100 ml / min), N source = CH_3CN (80 °C) and T = 950 °C.	72
Figure 3.9. Particle size distribution graphs of (a) NCSs 950 °C / 150 minutes, (b) NCSs 950 °C / 180 minutes and (c) NCSs 950 °C / 240 minutes. C source = C_2H_2 (100 ml / min), N source = CH_3CN (80 °C) and T = 950 °C.	73
Figure 3.10. Graph showing average diameter of NCSs as a function of carbonization time.	74
Figure 3.11. Graph showing N content as a function of carbonization time.	75
Figure 3.12. Raman graphs of NCSs synthesized at different carbonization times. Carbonization temperature was kept constant at 950 °C. C_2H_2 was bubbled through CH_3CN at 80 °C.	76
Figure 3.13. TGA and corresponding derivative weight loss graphs of NCSs synthesized at different carbonization times. Carbonization temperature was kept constant at 950 °C. C_2H_2 was bubbled through CH_3CN at 80 °C.	78
Figure 3.14. TEM images of NCSs synthesized using different flow rates of acetylene and nitrogen gases during the carbonization step a) NCSs 50 +50, b) NCSs 80 + 20, c) NCSs 100 + 0 and NCSs 200 + 0.	81
Figure 3.15. XPS N1s spectra of NCSs produced using different flow rates of C_2H_2 and N_2 gases during the carbonization step: (a) FR 50 + 50, (b) FR 100 + 0 and (c) FR 200 + 0. C_2H_2 and or N_2 was bubbled through CH_3CN at 80 °C.	82

Figure 3.16. Raman graphs of NCSs synthesized at different flow rates of gases. Carbonization temperature and time were kept constant at 950 °C and 90 minutes respectively. C ₂ H ₂ and or N ₂ were bubbled through CH ₃ CN at 80 °C.....	85
Figure 3.17. TGA and corresponding derivative weight graphs of NCSs synthesized at different flow rates of gases. Carbonization temperature and time were kept constant at 950 °C and 90 minutes respectively. C ₂ H ₂ and or N ₂ were bubbled through CH ₃ CN at 80 °C.....	86
Figure 4.1. Reaction pathway for the selective hydrogenation of cinnamaldehyde. ..	96
Figure 4.2. TEM images of (a) as - synthesized CSs and (b) fCSs 40 supports, (c) as - synthesized NCSs, (d) fNCSs 40, (e) fNCSs 60 and (f) fNCSs 80 supports.	106
Figure 4.3. Zeta potential measurements as a function of pH for as - synthesized and functionalized supports.	108
Figure 4.4. TGA and corresponding derivative weight loss graphs of (a) as - synthesized CSs and (b) fCSs 40 supports, (c) as - synthesized NCSs, (d) fNCSs 40, (e) fNCSs 60 and (f) fNCSs 80 supports.....	111
Figure 4.5. Raman graphs of as - synthesized and functionalized doped and undoped carbon spheres.	112
Figure 4.6. Typical TEM image and palladium particle size histogram of 1 % Pd / fCSs 40 catalyst.....	115
Figure 4.7. Typical TEM image and palladium particle size histogram of 1 % Pd / fNCSs 40 catalyst.....	117
Figure 4.8. Typical TEM image and palladium particle size histogram of 1 % Pd / fNCSs 60 catalyst.....	117

Figure 4.9. Typical TEM image and palladium particle size histogram of 1 % Pd / fNCSs 80 catalyst.....	118
Figure 4.10. EDX spectrum showing the presence of Pd nanoparticles in the 1% Pd / fNCSs 40 catalyst.....	119
Figure 4.11. TGA profiles run in air of (a) fCSs 40 and 1 % Pd / fCSs 40 (b) fNCSs 40 and 1 % Pd / fNCSs 40, (c) fNCSs 60 and 1 % Pd / fNCSs 60 and (d) fNCSs 80 and 1 % Pd / fNCSs 80 catalysts.....	121
Figure 4.12. Powder XRD patterns of 1 wt. % Pd catalysts synthesized using doped and undoped carbon sphere supports functionalized at different temperatures of nitric acid.	123
Figure 4.13. Catalytic activity, expressed in terms of conversion as a function of time for the cinnamaldehyde (CALD) hydrogenation of the different Pd - based CSs and NCSs catalysts.....	125
Figure 4.14. TEM images of (a) 0.00 % N support, (b) 0.41 % N support, (c) 2.39 % N support and (d) 3.84 % N support.	127
Figure 4.15. N1s spectra of a) 0.41 % N, b) 2.39 % N and c) 3.84 % N supports....	129
Figure 4.16. TEM image and corresponding particle size distribution graph of 1 % Pd / fCSs 40 catalyst (0.00 % N).....	132
Figure 4.17. TEM image and corresponding particle size distribution graph of 1 % Pd / fNCSs 40 catalyst (0.41 % N).....	132
Figure 4.18. TEM image and corresponding particle size distribution graph of 1 % Pd / fNCSs 40 catalyst (2.39 % N).....	133
Figure 4.19. TEM image and corresponding particle size distribution graph of 1 % Pd / fNCSs 40 catalyst (3.84 % N).....	133
Figure 4.20. EDX spectrum of 1 % Pd / fNCSs 40 catalyst (3.84 % N).....	134

Figure 4.21. TGA and corresponding derivative weight loss graphs of a) 1 % Pd / fCSs 40 catalyst (0.00 % N), b) 1 % Pd / fNCSs 40 catalyst (0.41 % N), c) 1 % Pd / fNCSs 40 catalyst (2.39 % N) and d) 1 % Pd / fNCSs 40 catalyst (3.84 % N)..... 136

Figure 4.22. Powder XRD patterns of 1 % Pd fNCSs 40 catalysts containing different N contents of support. (X = C)..... 138

Figure 4.23. Catalytic activity, expressed in terms of conversion as a function of time for the CALD hydrogenation of a) 1 % Pd / fCSs 40 catalyst (0.00 % N), b) 1 % Pd / fNCSs 40 catalyst (0.41 % N), c) 1 % Pd / fNCSs 40 catalyst (2.39 % N) and d) 1 % Pd / fNCSs 40 catalyst (3.84 %N).....141

Figure 5.1. Hydrogenation of CALD over 1 % Pd / fNCSs 40 catalyst performed using different solvents. (a) Conversion of CALD as a function of time, (b) HCALD selectivity as a function of time and (c) 3P1P selectivity as a function of time..... 162

Figure 5.2. Hydrogenation of CALD over 1 % Pd / fNCSs 40 catalyst performed at different temperatures. (a) Conversion of CALD as a function of time, (b) HCALD selectivity as a function of time and (c) 3P1P selectivity as a function of time..... 164

Figure 5.3. Hydrogenation results of CALD over 1 % Pd / fNCSs 40 catalyst under different hydrogen flow rates. (a) Conversion of CALD as a function of time, (b) HCALD selectivity as a function of time and (c) 3P1P selectivity as a function of time..... 167

Figure 5.4. CALD conversion as a function of catalyst mass. (Conditions: CALD = 1.26 ml, solvent = hexan-1-ol (100 ml), catalyst weight = 50, 100, 150 and 200 mg, T = 60 °C, reductant = H₂, 50 ml / min). 168

Figure 5.5. Influence of catalyst leaching and stability on the hydrogenation of CALD. (Conditions: CALD = 1.26 ml, solvent = hexan-1-ol (100 ml), catalyst weight = 100 mg, T = 60 °C, reductant = H₂, 50 ml / min).....169

Figure 6.1. TEM images and corresponding particle size distribution graphs of a) Polyol 1 % Pd / fNCSs 40 catalyst, b) Impregnation 1 % Pd / fNCSs 40 calcined catalyst and c) Impregnation 1 % Pd / fNCSs 40 reduced catalyst.....	178
Figure 6.2. EDX spectrum of Impregnation 1 % Pd / fNCSs 40 calcined catalyst...	179
Figure 6.3. TPR profile of Impregnation 1 % Pd / fNCSs 40 reduced catalyst.	181
Figure 6.4. XRD patterns of a) Polyol 1 % Pd / fNCSs 40 catalyst, b) Impregnation 1 % Pd / fNCSs 40 calcined catalyst and c) Impregnation 1 % Pd / fNCSs 40 reduced catalyst.....	182
Figure 6.5. Catalytic activity, expressed in terms of conversion as a function of time for the CALD hydrogenation of the 1 % Pd / fNCSs 40 catalysts prepared by different methods.....	184
Figure A1. The horizontal CVD setup for the synthesis of nitrogen doped carbon spheres.....	193
Figure A2. Experimental setup used for the hydrogenation of cinnamaldehyde.....	200

LIST OF TABLES

Table 2.1. Doping of nitrogen doped carbon spheres (NCSs)	13
Table 2.2. Selected examples of the hydrogenation of cinnamaldehyde using undoped carbon nanostructures.....	40
Table 3.1. CVD experimental conditions ^a	59
Table 3.2. NCSs diameter range, elemental (CN) composition, D, G bands and I _D / I _G ratios and gasification temperature of NCSs synthesized at different temperatures. Carbonization time was kept constant at 120 minutes. C ₂ H ₂ was bubbled through CH ₃ CN at 80 °C.	69
Table 3.3. NCSs diameter range, elemental (CN) composition, D, G bands and I _D / I _G ratios and gasification temperature of NCSs synthesized at different times. Carbonization temperature was kept constant at 950 °C. C ₂ H ₂ was bubbled through CH ₃ CN at 80 °C.	79
Table 3. 4. The nitrogen contents and related detailed breakdown of nitrogen species of NCSs synthesized using different flow rates of acetylene and nitrogen during carbonization step.....	84
Table 3. 5. NCSs diameter range, elemental (CN) composition, XPS analysis results, D, G bands and I _D / I _G ratios and gasification temperatures of NCSs synthesized using different flow rates of C ₂ H ₂ and N ₂ gases during the carbonization step.....	88
Table 4.1. Point of zero charge (PZC) obtained from zeta potential measurements of as - synthesized and functionalized supports.	109

Table 4.2. Decomposition temperatures of as - synthesized and functionalized undoped and doped CSs.	110
Table 4.3. Raman data for as - synthesized and functionalized CSs and NCSs.....	113
Table 4.4. Physical and chemical properties of as - synthesized and functionalized CSs and NCSs supports.....	114
Table 4.5. Physical properties of the catalysts.	120
Table 4.6. TGA data of functionalized carbon supports and the corresponding catalysts.	122
Table 4.7. The effect of support pre - treatment on the hydrogenation of CALD. ...	126
Table 4.8. CN elemental and XPS analysis results.	130
Table 4.9. Physical properties of the catalysts.	135
Table 4.10. Decomposition temperatures of 1 % Pd catalysts containing different N contents of the support.	137
Table 4.11. The effect of different N contents in support on the hydrogenation of CALD.....	142
Table 5.1. Variation of conditions for the hydrogenation of cinnamaldehyde.....	156
Table 5.2. Physical and chemical properties of supports and catalysts.....	158
Table 5.3. CN elemental and XPS analysis results.....	158
Table 5.4. Properties of alcohols used in the study.....	161
Table 5.5. Hydrogenation results of CALD over 1 % Pd / fNCSs 40 catalyst in different solvents.....	161

Table 5.6. Hydrogenation results of CALD over 1 % Pd / fNCSs 40 catalyst under different reaction temperatures of hexan-1-ol.....	165
Table 5.7. Hydrogenation results of CALD over 1 % Pd / fNCSs 40 catalyst under different hydrogen flow rates.....	166
Table 6.1. Physical properties of the catalysts.....	180
Table 6.2. Catalytic activity of 1 % Pd / fNCSs 40 catalysts prepared by different methods for cinnamaldehyde hydrogenation.....	185

LIST OF ABBREVIATIONS

Abbreviation	Description
3P1P	3-phenyl-1-propanol
AC	Activated carbon
AFROX	African Oxygen
BET	Brunauer Emmett and Teller
C ₂ H ₂	Acetylene
CH ₃ CN	Acetonitrile
CA	Cinnamyl alcohol
CALD	Cinnamaldehyde
CCD	Charge couple device
CNFs	Carbon nanofibres
CNTs	Carbon nanotubes
CSs	Carbon spheres
CVD	Chemical vapour deposition
DEG	Di(ethylene glycol)
EDX	Energy dispersive X-ray spectroscopy
EG	Ethylene glycol
FID	Flame ionization detector
FTIR	Fourier transform infrared spectroscopy
fCSs	Functionalized carbon spheres
fNCSs	Functionalized nitrogen doped carbon spheres
GC	Gas chromatography
HCALD	Hydrocinnamaldehyde
HCSs	Hollow carbon spheres
HIV	Human immunodeficiency virus
ICP - OES	Inductively coupled plasma - optical emission spectroscopy
IWI	Incipient wetness impregnation

MCSs	Mesoporous carbon spheres
MCMBs	Mesocarbon microbeads
MF	Melamine - formaldehyde
NCSs	Nitrogen doped carbon spheres
NCS _{hor}	NCSs synthesized on a horizontal CVD
NCS _{hyd}	NCSs synthesized using a hydrothermal method
NCS _{ver}	NCSs synthesized on a vertical CVD
NHCSs	Nitrogen doped hollow carbon spheres
NHGCSs	Nitrogen doped hollow graphitic carbon spheres
NMCNPs	Nitrogen doped magnetic carbon nanoparticles
OPD	<i>o</i> -phenylenediamine
ORR	Oxygen reduction reaction
PEG	Poly(ethylene glycol)
PoPD	poly(<i>o</i> -phenylenediamine)
PPy	Polypyrrole
PZC	Point of zero charge
Si@NCSs	Nitrogen doped carbon spheres containing Si nanoparticles
Si NPs	Silica nanoparticles
SWNTs	Single walled carbon nanotubes
TCD	Thermal conductivity detector
TEM	Transmission electron microscopy
TGA	Thermogravimetric analysis
TPO	Temperature programmed oxidation
XPS	X-ray photoelectron spectroscopy
XRD	X-ray diffraction

CHAPTER 1

INTRODUCTION

1.1 Background and motivation

Catalysis accounts for more than 90 % of the catalytic processes used in the chemical manufacturing industries throughout the world [1]. In many industries, their production processes rely heavily on catalysis e.g. chemical, petroleum, agriculture, pharmaceutical, polymer, and electronics, just to mention a few. The role of the catalyst is to increase the rate and control the selectivity of chemical reactions without the catalyst being used up during the reaction. The catalyst does not change the thermodynamics of the chemical reaction.

The selective hydrogenation of α,β -unsaturated aldehydes is a catalytic reaction that has been the subject of a lot of research interest in the manufacturing industries and scientific fields [2-5]. Cinnamaldehyde (CALD) is a member of the α,β -unsaturated aldehydes. It occurs naturally in the bark of cinnamon trees and other species of the genus *Cinnamomun* like camphor and cassia which are widely used in flavouring food and in some perfumes. Hydrogenation of CALD results in the synthesis of cinnamyl alcohol (CA) and hydrocinnamaldehyde (HCALD) as intermediate products and 3-phenyl-1-propanol (3P1P) as final product. The selective hydrogenation of CALD is a difficult process, the hydrogenation of the C=C group to produce HCALD is thermodynamically more favourable than the C=O group hydrogenation to produce CA. Both HCALD and CA are important products which are used as intermediates in

the production of perfumes, flavouring additives, pharmaceuticals and agrochemicals [6]. Hydrocinnamaldehyde has been found to be an important intermediate in the manufacture of pharmaceutical products used in the treatment of human immunodeficiency virus (HIV) [7]. CA has many applications; it is used in the perfume industry because of its odour characteristics and fixative properties. It is also used as an intermediate for synthesizing pharmaceuticals, such as chloramphenicol which is used as an antibiotic agent in chloromycetin [8]. Lastly it is used as an important building block in organic synthesis.

The major problem in chemoselective hydrogenation is to develop a stable catalyst, which is active and selective, since the activity can increase (or decrease) as the selectivity decreases (or increases). Both the metal and support can have an effect on the activity and selectivity of the final catalyst for supported catalysts. Metals can have different electronic properties, for example due to their different oxidation states, displaying various properties [9]. In addition, a number of metals or metal alloys can be used as active components, and their electronic properties can be altered by the addition of promoters [9-11]. The nature of the support material, like porosity, pore size distribution and reducibility is an important parameter in catalyst preparation. The activity and selectivity of the metal-supported catalysts are also strongly affected by the synthesis variables [12], as the particle size is strongly influenced by the method of preparation and has an important effect on the activity and selectivity of the supported metal catalyst. Lastly the reaction medium can strongly influence the outcome of a catalytic reaction [9].

Carbon materials are now being widely used as supports in heterogeneous catalytic processes because of their ability to be tailored to meet specific needs and to have unique physical and chemical properties [13]. Nitrogen doped carbon materials are attracting a lot of interest in the world of nanoscience and nanotechnology. The most

important use of nitrogen doped carbon nanostructures in catalysis is to anchor metal particles in a stable manner, which promotes high metal dispersion and narrow particle size distributions. The introduction of nitrogen functional groups on carbon nanostructures modifies the electronic and chemical interactions of a metal on the carbon [14]. N atoms on the surface of a carbon material can increase the number of anchorage sites for adsorption of the metal particles. This in turn improves the catalytic activity and selectivity in catalytic reactions as there is better dispersion of metals on the support.

The use of carbon materials as a support in catalysis has another advantage in that precious metals can be easily recovered by combustion of the support in an oxygen atmosphere [1]. This provides a cost effective recovery of precious metals from catalysts. It is very important in the recovery, refining and recycling of precious metals especially if they have a low concentration on a support. This technology also has an added advantage for it does not produce large amounts of solid wastes that need to be land filled.

In this thesis, cinnamaldehyde hydrogenation was used as a showcase to investigate the influence of various parameters on the catalytic action of palladium based catalysts supported on nitrogen doped carbon spheres. Optimization studies on the synthesis of NCSs will be investigated in this thesis.

The materials produced in this study (NCSs) were also used by co-workers and collaborators in other studies. Their results have not been included in this thesis. The electrical properties of NCSs were investigated and depending on the concentration of N in the samples measured by electron paramagnetic resonance spectroscopy (EPR) the samples were found to have either clear semiconducting behavior or a transition

from metallic to semiconducting behavior [15]. In another paper, a comparison study was done by using gallium nitride nanostructures and NCSs as supports in the hydrogenation of CALD [16]. NCSs synthesized using different methods were also used as supports in the Fischer Tropsch synthesis [17].

1.2 Aims and objectives of the study

The aims of this research work are to synthesize nitrogen doped carbon spheres supported Pd catalysts and test their catalytic performance in the hydrogenation of cinnamaldehyde. These aims will be achieved through the following objectives:

- I. To synthesize NCSs from different nitrogen sources using a non - catalytic chemical vapor deposition method (CVD) with acetylene (C_2H_2) as a carbon source, nitrogen (N_2) as a carrier gas and acetonitrile (CH_3CN) as the nitrogen and also a carbon source. The effect of different reaction parameters such as pyrolysis time, pyrolysis temperature and different flow rates of C_2H_2 and N_2 during the pyrolysis step will be investigated.
- II. To functionalize the NCSs using different functionalization conditions.
- III. To characterize the as-synthesized and functionalized NCSs using transmission electron microscopy (TEM), N_2 physisorption, zeta potential measurements, thermogravimetric analysis (TGA), Fourier transform infrared spectroscopy (FTIR), Raman spectroscopy, powder X-ray diffraction (XRD), X-Ray photoelectron spectroscopy (XPS) and CN elemental analysis.
- IV. To load palladium (Pd) on as synthesized and functionalized NCSs using the polyol and incipient wetness impregnation methods.
- V. To characterize the catalysts formed using TEM, TEM coupled with electron dispersive spectroscopy (EDX), N_2 physisorption, TGA, XRD and inductively coupled plasma - optical emission spectrometry (ICP - OES).

- VI. To test the catalytic activity and selectivity of the Pd supported nitrogen doped catalysts.
- VII. To explore issues such as support effects and catalyst preparation methods on the activity and selectivity of the catalysts on the hydrogenation of cinnamaldehyde. The importance lies in the catalyst hydrogenating either the C=C or C=O bond to produce the desired product selectivity. NCSs are going to be used as a novel material in this thesis.

1.3 Thesis outline

Chapter 1 presents the background, motivation as well as the aims and objectives of the research work. Chapter 2 gives a detailed literature review on nitrogen doped carbon spheres. Chapter 3 reports on the “The synthesis of nitrogen doped carbon spheres by non-catalytic chemical vapour deposition”. Chapter 4 reports on the effects of support characteristics in the hydrogenation of cinnamaldehyde. Chapter 5 reports on the activity and selectivity results of the hydrogenation of cinnamaldehyde obtained by variation of different catalytic reaction conditions. Chapter 6 reports on the effect of using different catalyst preparation methods on the hydrogenation of cinnamaldehyde. In Chapter 7 a summary of all results described in preceding chapters is given, together with concluding remarks and suggestions for future work. The appendix section gives a detailed description of experimental procedures used for the synthesis of the carbon supports and Pd catalysts. The experimental setup for the CVD and the catalysis reaction are also illustrated in this section. Calculations for the catalysis reaction are also shown.

1.4 References

1. Roessler, F., *Catalysis in the Industrial Production of Pharmaceuticals and Fine Chemicals*. CHIMIA International Journal for Chemistry, 1996. **50**(3): p. 106-109.
2. Nhut, J.M., R. Vieira, L. Pesant, J. P. Tessonnier, N. Keller, G. Ehret, C. Pham-Huu, and M. J. Ledoux, *Synthesis and catalytic uses of carbon and silicon carbide nanostructures*. Catalysis Today, 2002. **76**(1): p. 11-32.
3. Pham-Huu, C., N. Keller, G. Ehret, L.J. Charbonniere, R. Ziessel, and M.J. Ledoux, *Carbon nanofiber supported palladium catalyst for liquid-phase reactions: An active and selective catalyst for hydrogenation of cinnamaldehyde into hydrocinnamaldehyde*. Journal of Molecular Catalysis A: Chemical, 2001. **170**(1-2): p. 155-163.
4. Koo-amornpattana, W., and J. M. Winterbottom, *Pt and Pt-alloy catalysts and their properties for the liquid-phase hydrogenation of cinnamaldehyde*. Catalysis Today, 2001. **66**(2-4): p. 277-287.
5. Bachiller-Baeza, B., I. Rodríguez-Ramos, and A. Guerrero-Ruiz, *Influence of Mg and Ce addition to ruthenium based catalysts used in the selective hydrogenation of α,β -unsaturated aldehydes*. Applied Catalysis A: General, 2001. **205**(1-2): p. 227-237.
6. Mills, P.L. and R.V. Chaudhari, *Multiphase catalytic reactor engineering and design for pharmaceuticals and fine chemicals*. Catalysis Today, 1997. **37**(4): p. 367-404.
7. Muller, A. and J. Bowers, *WO Patent Application WO 99/08989*. First Chemical Corporation, 1999.
8. Bauer, K., D. Garbe, and H. Surburg, *Single Fragrance and Flavor Materials*, in *Common Fragrance and Flavor Materials*. 2001, Wiley-VCH Verlag GmbH. p. 7-165.

9. Chatterjee, M., F.Y. Zhao, and Y. Ikushima, *Effect of synthesis variables on the hydrogenation of cinnamaldehyde over Pt-MCM-48 in supercritical CO₂ medium*. Applied Catalysis A: General, 2004. **262**(1): p. 93-100.
10. Raab, C.G. and J.A. Lercher, *Activity and selectivity of NiPt/SiO₂ catalysts for hydrogenation of crotonaldehyde*. Journal of Molecular Catalysis, 1992. **75**(1): p. 71-79.
11. Waghray, A. and D.G. Blackmond, *Infrared spectroscopic studies of the adsorption and reaction of 3-methyl-2-butenal over alkali-promoted ruthenium/silica catalysts*. The Journal of Physical Chemistry, 1993. **97**(22): p. 6002-6006.
12. Chapter 11 Catalytic hydrogenation and dehydrogenation, in *Studies in Surface Science and Catalysis*, P. Vladimir and C.B. Geoffrey, Editors. 1995, Elsevier. p. 477-539.
13. Rodríguez-reinoso, F., *The role of carbon materials in heterogeneous catalysis*. Carbon, 1998. **36**(3): p. 159-175.
14. Shao, Y., J. Sui, G. Yin, and Y. Gao, *Nitrogen-doped carbon nanostructures and their composites as catalytic materials for proton exchange membrane fuel cell*. Applied Catalysis B: Environmental, 2008. **79**(1): p. 89-99.
15. Wright, W.P., V.D. Marsicano, J.M. Kearthland, R.M. Erasmus, S.M.A. Dube, and N.J. Coville, *The electrical transport properties of nitrogen doped carbon microspheres*. Materials Chemistry and Physics, 2014. **147**(3): p. 908-914.
16. Kente, T., S.M.A. Dube, N.J. Coville, and S.D. Mhlanga, *Application of Gallium Nitride Nanostructures and Nitrogen Doped Carbon Spheres as Supports for the Hydrogenation of Cinnamaldehyde*. Journal of Nanoscience and Nanotechnology, 2013. **13**(7): p. 4990-4995.
17. Xiong, H., M. Moyo, M.A. Motchelaho, Z.N. Tetana, S.M.A. Dube, L.L. Jewell, and N.J. Coville, *Fischer–Tropsch synthesis: Iron catalysts supported on N-doped carbon spheres prepared by chemical vapor deposition and hydrothermal approaches*. Journal of Catalysis, 2014. **311**(0): p. 80-87.

CHAPTER 2

LITERATURE REVIEW

2.1 Carbon materials as catalyst supports

Carbon materials have been used for decades as catalyst supports in heterogeneous catalysis owing to their unique properties that can be altered for use for specific needs [1]. Properties such as (i) resistance to acidic / basic media, (ii) possibility to control up to certain limits their porosity and surface chemistry, (iii) easy recovery of precious metals from a support through oxidation in an air atmosphere resulting in low environmental impact, (iv) good electrical conductivity, (v) low cost and (vi) good stability makes them ideal candidates as catalyst supports [2].

2.2 Carbon spheres

Carbon spheres (CSs) are made of graphite sheets that are not closed shells but are made of wavy flakes that follow the curvature of the sphere creating open edges at the surfaces with sp^2 hybridization [3]. CSs have found many uses as catalyst supports, in lithium batteries, as lubricants, as composites, in the removal of contaminants and in drug delivery etc. This relates to their high thermal stability, high surface area, unique electronic properties, low density and their tailored structure. CSs have been synthesized using methods used to synthesize carbon nanotubes which include arc discharge, laser ablation [4, 5], shock compression, catalytic and non - catalytic chemical vapour deposition, autoclave, supercritical fluids, mesoporous microbeads

and carbonization route methods [6]. However the non - catalytic CVD method is the most promising route for the large scale production of CSs because it is an inexpensive process, provides a degree of control over the synthesis process and is easy to scale up. Over the decades much information has been published on CSs. More recently, Deshmukh et al. [6] wrote a review on carbon spheres with detailed information on their synthesis, mechanisms of formation, chemistry, characterization techniques and their applications. This chapter will mainly discuss in detail the synthesis of one aspect of CSs, that of nitrogen doped carbon spheres (NCSs) and the use of doped and undoped carbon spheres in catalysis.

Carbon spheres can be classified in four different ways according to their:

- (i) morphology: solid, core - shell or hollow [7],
- (ii) arrangement of the carbon layers: concentric, radial or random layers [8, 9],
- (iii) according to their particle sizes, Serp et al. [10] classified spherical carbon materials into: fullerenes (< 2 nm) [11], carbon onions (2 - 20 nm) [12], carbon spheres (50 - 1000 nm) [10, 13, 14] and carbon beads (above 1 μm) [15-17] and lastly
- (iv) their synthesis methods [6].

2.2.1 Modification of carbon nanomaterials

Due to the inertness and hydrophobicity of carbon materials, and in particular carbon spheres, it is necessary to modify the surface of these carbon supports using (i) covalent and non - covalent modification methods and (ii) doping methods with elements (mainly nitrogen, boron or sulphur) that activate their surfaces. Covalent surface modification of carbon nanomaterials involves an irreversible change to the

functionalized carbon surface by introducing reactive groups which form a covalent bond with other molecules [18, 19]. Non - covalent surface modification involves the attachment of chemical molecules without affecting the chemical / electronic network of the carbon nanomaterials [20, 21]. Different types of polymers [22, 23], polynuclear aromatic compounds [24], surfactants [25, 26] and biomolecules [27] can bind to the surfaces of carbon materials by making use of interactions with the carbon surface such as van der Waals forces, electrostatic forces, hydrogen bonding and other attractive forces to mention a few [28].

2.2.1.1 Functionalization

When comparing the different methods that have been used for the modification of carbon nanostructure surfaces, functionalization using reagents is the most popular method used because of its versatility, efficiency and potential to scale - up [29]. The main purpose of functionalization is (i) to improve the carbon nanomaterial interaction with solvents and dispersion, (ii) to allow the attachment of metal nanoparticles, (iii) to modify the carbon nanomaterials adsorption properties, and (iv) to allow further chemical treatment on the carbon nanomaterials [18, 19, 30]. The most common reagents include HNO_3 , H_2SO_4 , KMnO_4 , $\text{K}_2\text{Cr}_2\text{O}_7$, polyphosphoric acid and H_2O_2 [31-35]. These have been used to oxidize carbon nanomaterial surfaces. Functionalization generally leads to the production of hydroxyl (-OH), carboxyl (-COOH) and carbonyl (-C=O) oxygenated surface functional groups. However one of the disadvantages of acid oxidation methods is the generation of carbon nanomaterial fragmentation and defects in the graphite network [32, 35].

2.2.1.2 Doping

2.2.1.2.1 Nitrogen doping of carbon spheres

Nitrogen doping of carbon spheres can be carried out using two methods [36]: (i) doping directly during the synthesis of the carbon spheres, which is called in - situ doping, (ii) post - treatment of already synthesized carbon spheres with nitrogen containing precursors which is called post - doping. The in-situ doping of carbon spheres is the most commonly used method for synthesizing NCSs. Several methods have been employed to synthesize undoped carbon spheres [6] and these methods can also be used on nitrogen doped carbon spheres. Methods which have been used include chemical vapour deposition (non - catalytic and catalytic), polymerization reactions, hydrothermal methods and carbonization methods just to mention a few (see Table 2.1). Different nitrogen sources have been used to modify carbon sphere surfaces and these include acetonitrile [37-40], ammonia [37, 41, 42], urea [39, 42], melamine [43-45], aniline [46], acrylonitrile [47], pyrrole [48, 49], ethylenediamine [50], phenylenediamine [51] and cyanuric chloride [47]. The types of nitrogen species which can be incorporated into carbon nanomaterials after doping with nitrogen are pyridinic N: a sp^2 hybridized nitrogen atom bonded to two C atoms in which N donates one p electron to the aromatic Π system, pyrrolic N: the N is sp^3 hybridized in a five membered ring, quaternary N: a N atom replaces a C atom within the graphite plane and is bonded to three C atoms, molecular N: nitrogen atoms adsorbed / intercalated in the carbon walls or trapped in compartments, and nitrogen oxides: oxidised pyridinic nitrogen which is bonded to two carbon atoms and one oxygen atom [52, 53]. These are shown in Figure 2.1.

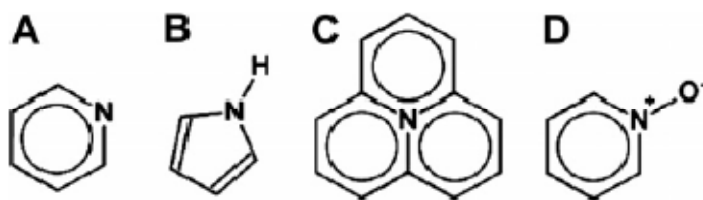


Figure 2.1. The types of nitrogen species that can be incorporated in nitrogen doped carbon nanomaterials: (A) pyridinic N, (B) pyrrolic N, (C) quaternary N and (D) nitrogen oxides [53].

2.3 Synthesis of NCSs

Table 2.1. Doping of nitrogen doped carbon spheres (NCSs)

C and N source	NCSs synthesis conditions	Properties of NCSs formed and summary	Reference
Acetonitrile	<p>Nitrogen doped hollow carbon spheres (NHCSs) were prepared by CVD. Si spheres of a given diameter were placed in a quartz tube and heated to 900 or 1000 °C with a heating rate of 5 °C min⁻¹ under N₂ (g) (30 ml / min). Another N flow of 30 ml / min containing 5 wt % CH₃CN vapor was passed through the silica spheres for 4h.</p>	<p>NHCSs produced at 1000 °C had a N content of 6.6 wt %. The diameter of the silica sphere determined the diameters of the final NHCSs products formed e.g. 1600 nm silica sphere templates, gave NHCSs with an external diameter of around 1760 nm and a shell thickness of around 120 nm. Doping of N into the HCSs enhanced the crystallinity of the hollow carbon spheres (HCSs). The cyclability of the NHCSs employed as anode materials in rechargeable lithium ion batteries at high current were found to be better than that of undoped HCSs which is due to the higher crystallinity and presence of N in the graphene sheets.</p>	[38]

Acetylene and CH ₃ CN	NCSs were prepared by a non - catalytic CVD method using acetylene as carbon source, acetonitrile as N source and N ₂ as the carrier gas. The flow rates of both gases were set at 100 ml / min, and the pyrolysis temperature and time were 950 °C and 90 minutes respectively.	NCSs were synthesized with an average diameter of 450 nm, BET surface area of 1.51 m ² / g, pore volume of 0.003 m ³ / g. NCSs were used as supports for Pd metal and resultant catalysts was compared its performance with Pd loaded on gallium nitride supports for the hydrogenation of cinnamaldehyde.	[40]
Acetylene and CH ₃ CN	NCSs were prepared by the non - catalytic horizontal CVD method using C ₂ H ₂ (100 ml / min) as a carbon source, CH ₃ CN (80 °C) as the N source and either N ₂ or Ar (100 ml / min) as the carrier gases. The carbonization temperature and time were 900 °C and 120 minutes respectively. NCSs formed were collected at different positions in the quartz tube.	NCSs synthesized using Ar as the carrier gas and collected in the quartz boat and the end of the quartz tube had nitrogen contents of 1.7 % each. NCSs synthesized using N ₂ as the carrier gas and collected in the middle of quartz tube and in the quartz boat each had N contents of 3.4 %. The N contents were determined using electron paramagnetic resonance spectroscopy. Collecting NCSs at different positions in the quartz tube did not change the N content while cooling under gases nitrogen or argon had an effect on the N	[54]

Acetylene and NH ₃	NCSs were prepared by CVD through the pyrolysis of C ₂ H ₂ (g) (100 ml / min) and NH ₃ at 900 °C for 1 h.	<p>content. Electrical transport measurements were performed on the NCSs and it was found out that two samples showed semiconducting behavior. The other two samples showed a transition from metallic to semiconducting behavior.</p> <p>This synthesis gave smooth, round CSs with a uniform diameter (approximately 700 nm, BET surface area of 3.4 m² / g and N content approximately 2 wt %). The NCSs were used as supports to load cobalt catalysts and this was used for the Fischer - Tropsch synthesis reaction.</p>	[41]
Acetylene, ammonia and acetonitrile	<p>N₂ (g) was flowed through the quartz tube from 25 °C to 900 °C.</p> <p>C₂H₂ (g) was then bubbled through warm NH₃ or CH₃CN solutions for 2 hours at 900 °C.</p> <p>The flow rates of both gases were 100 ml / min.</p>	<p>NCSs were produced with diameters ranging from 400 to 750 nm and were accreted. They had a N content of 1 - 1.5 wt %. They found that doped CSs gave uniform distribution of metal nanoparticles due to enhanced anchoring.</p>	[37]

1. Acetonitrile and acetylene	NCSs prepared in a vertically aligned CVD (NCS _{ver}), the conditions were as follows: Ar (300 ml / min) and C ₂ H ₂ (200 ml / min) were bubbled through CH ₃ CN for 30 mins at 900 °C. NCSs prepared using a horizontal CVD (NCS _{hor}) had the following reaction conditions: C ₂ H ₂ (100 ml / min) were bubbled through CH ₃ CN for 2 hours at 950 °C.	The 3 supports had different physical and chemical properties. NCS _{ver} exhibited the smallest diameters, highest surface area and N content of 200 nm, 6.8 m ² / g and 3.1 % N respectively. NCS _{hyd} had the largest diameter, lowest surface area and lowest N content of values of 1200 nm, 1.8 m ² / g and 1.5 % N respectively. NCS _{hor} had surface area, average diameters and N content values of 3.9 m ² / g, 350 nm and 2.4 % N respectively. The I _D / I _G ratios of three NCSs supports followed the order: NCS _{ver} > NCS _{hor} > NCS _{hyd} . NCS _{ver} contained the largest amount of defective sites within its structure.	[39]
2. Sucrose solution and urea	The hydrothermal method was also used to synthesize NCSs (NCS _{hyd}). Sucrose solution and Urea were heated to 190 °C in an autoclave for 4 hours.		
Benzene, aniline and nitrobenzene	CSs and NCSs were synthesized at 950 °C using a 1:4 (v/v) ratio of aromatic precursor to helium gas with a flow rate of 150 ml / min. C growth was monitored at 15,	CSs and NCSs were produced. The N content of the NCSs ranged from 2.1 - 3.4 mol %. N incorporation was favored at extended reaction times as well as for the more reactive aniline. N inclusion resulted in an enhanced	[46]

Copolymer of vinylidene chloride and acrylonitrile	<p>30, 60 and 120 minutes using CVD.</p> <p>Carbon microspheres were produced by the carbonization of a copolymer of vinylidene chloride and acrylonitrile in the presence of bentonite as template. After template removal (170 °C for 12 h and 300 °C for 1 h), carbonization (600 °C for 2 h) was performed in a quartz tube.</p>	<p>curvature of the grapheme layers, as well as the incorporation of lattice defects, resulting in a less crystalline material.</p> <p>Carbon microspheres were produced with uniform size distribution (125 - 150 µm), 1 - 10 wt %. N content and BET surface area of 692 m² / g. The NCSs contained 4 types of N: N-oxide, quaternary nitrogen, pyrrolic nitrogen and pyridinic nitrogen. They found that Ni nanoparticles were well dispersed on the nitrogen doped carbon microspheres support.</p>	[47]
Cyanuric chloride (C ₃ N ₃ Cl ₃)	<p>Nitrogen enriched CSs were synthesized using Mg powder as a catalyst and C₃N₃Cl₃ as a C and N source in a stainless steel autoclave at 400 °C for 2 h.</p>	<p>Uniform spheres with mean size of about 250 nm in diameter were obtained. Ni nanoparticles were encapsulated in the CSs. The N content of the Ni encapsulated CSs was 15.07 wt %.</p>	[55]
Iron doped polypyrrole	<p>Nitrogen doped magnetic carbon nanoparticles (NMCNPs) with spherical morphology were prepared using iron doped</p>	<p>NMCNPs had a N content and diameter of approximately 4 - 5 wt % and 50 nm respectively. The NMCNPs were deposited with Pd nanoparticles and their catalytic</p>	[48]

Melamine and formaldehyde	<p>polypyrrole nanoparticles as the carbon precursor and carbonized at 800 °C.</p> <p>A templating method was used to make the mesoporous carbon spheres (MCSs). The MCSs were prepared by the carbonization of melamine-formaldehyde resin / silica nanocomposites at 1000 °C for 2 h under N atmosphere, followed by etching with hydrofluoric acid to remove silica.</p>	<p>performance investigated for Heck, Suzuki and Sonogashira reactions. The Pd/NMCNPs displayed high catalytic activities for the 3 coupling reactions. This was attributed to the nitrogenated sites providing strong metal-support interactions.</p> <p>The MCSs produced showed excellent electrochemical properties which could be associated with the following characters: high specific surface area (around 1460 m² / g) for charge storage, suitable surface functional groups of N (6 %) which enhanced wettability and very large pore size (around 31 nm).</p>	[43]
Melamine - formaldehyde	<p>Nitrogen doped hollow graphitic carbon spheres (NHGCSs) were synthesized by the carbonization of melamine - formaldehyde (MF) resin spheres at 800 °C for 5 hours under a nitrogen atmosphere. MF</p>	<p>NHGCSs produced had the following properties: diameters in the range of 4.8 - 5.5 μm, were monodisperse, N content approximately 6.02 wt % and BET surface area of 753 cm³ / g which indicated good porosity. The NHGCSs showed very good</p>	[44]

Melamine and formaldehyde	<p>resin was produced by hydrothermal treatment of the melamine and formaldehyde aqueous solution at 180 °C for 6 hours followed by centrifugation to collect the white precipitate.</p> <p>Nitrogen doped carbon spheres containing Si nanoparticles (Si@NCSs) were synthesized using a two stage process, a condensation step followed by annealing step. A mixture of melamine - formaldehyde (MF) resin, Pluronic F127 surfactant and silica nanoparticles (Si NPs) were stirred in deionized water at 100 °C during the condensation step. The Si NPs embedded in MF spheres were then annealed at different temperatures to produce</p>	<p>capacitance performance , the specific capacitance reached 306 F g⁻¹ at a current density of 0.1 A g⁻¹ (in 2M H₂SO₄) and remains as high as 230 F g⁻¹ even at high current density of 3A g⁻¹ which showed good prospects for using these materials as supercapacitor electrode materials.</p> <p>The average diameters of NCSs and Si@NCSs were 1.5 μm and 0.7 μm respectively. The reduced sphere size was due to the smaller spheres efficiently relaxing the stress that was created by the incorporation of Si NPs in NCSs. The nitrogen contents of NCSs and Si@NCSs were 8.03 and 7.78 % respectively.</p>	[45]
---------------------------	---	---	------

O-phenylenediamine and ammonium persulfate	Si@NCSs. NHCSs were synthesized via two steps, the polymerization of <i>o</i> -phenylenediamine (OPD) and ammonium persulfate in aqueous phase to obtain poly(<i>o</i> -phenylenediamine) (PoPD) followed by the annealing of PoPD at 750 °C under a nitrogen atmosphere for 4 hours to obtain NHCSs.	NHCSs were obtained with average diameters between 400 and 700 nm. The N-HCSs contained pyridinic and pyrrolic nitrogen. The NHCSs were successfully used for the immobilization and biosensing of proteins.	[51]
Pyrrole	NHCSs were synthesized via a 3 stage process. Firstly polypyrrole (PPy)/SiO ₂ core shell particles were synthesized by using a hydrothermal method. Secondly the PPy/SiO ₂ core shells were then pyrolysed in a nitrogen atmosphere at 850 °C for 1 hour to obtain N doped carbon / SiO ₂ spheres. Finally NHCSs were	NHCSs were obtained with an average diameter of 370 nm, shell thickness of approximately of 15 nm, BET surface area of 759.1 m ² / g, pore size distribution below 2 nm and N content of 8.66 wt %.	[49]

Resorcinol, formaldehyde, urea, ammonia aqueous solution and ammonia gas.	<p>obtained by removal of the SiO₂ core shell in N doped carbon / SiO₂ spheres by treatment in 2M HF + 8M NH₄F.</p> <p>CSs were first synthesized by the hydrothermal method followed by carbonization by using resorcinol and formaldehyde as precursors. The CSs were modified with urea, ammonia aqueous solution and NH₃ were named U-CS, NH₂-CS and N-CS respectively.</p>	<p>The CSs, U-CS, NH₂-CS and N-CS had surface areas of 323.7, 225.4, 263.5 and 122.9 m² / g respectively. The CSs had a nitrogen content of 0.97 % which was lower than that of NH₂-CS (1.28 %), N-CS (1.42 %) and U-CS (2.02 %) determined from elemental analysis. All the modified carbon spheres had nearly the same amounts of nitrogen species namely pyridinic nitrogen, quaternary nitrogen and pyridine - N - oxide species. The unmodified CSs sample had the highest proportion of quaternary nitrogen.</p>	[42]
Xylene and ethylenediamine	<p>NCS were synthesized using a non catalytic spray pyrolysis method where a mixture of xylene and ethylenediamine were nebulized into a quartz tube</p>	<p>NCS were obtained with the following physical parameters: diameters ranging between 130 - 230 nm, BET specific surface areas ranging between 11.5 - 12.8 m² / g and N contents ranging between 2.1 - 6.2 wt %.</p>	[50]

	<p>heated at 1000 °C using argon as the carrier gas.</p>	<p>These were dependant on reaction conditions employed such as ratio of xylene and ethylenediamine and reaction time. The NCSs had higher catalytic activity towards the oxygen reduction reaction (ORR), had long term stability and had high methanol tolerance in alkaline media compared to undoped carbon spheres and Pt carbon catalysts. This was attributed to the presence of nitrogen in the NCSs.</p>	
--	--	---	--

2.4 Catalyst preparation methods

Catalyst synthesis techniques are an important area of study because they strongly determine the metal nanoparticle size, distribution and dispersion on the carbon support, thus ultimately controlling the activity and durability of the catalyst. There are three main methods that are used for the preparation of carbon - supported catalysts:

1. impregnation method,
2. colloidal method and
3. microemulsion method.

The three methods listed above all include a reduction step in the synthesis of nanoparticles and a deposition step for dispersing the metal catalyst on the carbon support. In this thesis two types of impregnation steps were used to synthesize the catalysts so these will be the ones discussed in detail.

2.4.1 Impregnation method

Impregnation means the penetration and soaking up of a dissolved metal catalyst precursor into a support before its reduction to metallic nanoparticles. During the impregnation step, the metal catalyst precursor solution is mixed with the carbon support which is porous and possibly has nanostructure, and it then penetrates into its pores. The reduction step can be either chemical or electrochemical and can be done in the liquid phase or gas phase. The most common reducing agents used in liquid phase reduction are Na_2SO_3 , $\text{Na}_4\text{S}_2\text{O}_5$, N_2H_4 , NaBH_4 , HCOOH , ethylene glycol and formaldehyde [56]. Flowing H_2 at high temperatures ($> 300\text{ }^\circ\text{C}$) is used during gas phase reduction.

The liquid phase reduction method (LPRM) can be conducted using either of two methods of heating, the conventional oil bathing heating method or a microwave irradiation method.

2.4.1.1 Incipient wetness impregnation method

Incipient wetness impregnation (IWI) is one of the easiest and most used methods to prepare catalysts. It has been used for the preparation of different catalysts supported on various carbon nanostructures which include CNTs, CNFs, CSs, activated carbon (AC), structured carbons etc [41, 57-63]. Yoon et al. prepared palladium catalysts loaded on nitrogen doped magnetic carbon nanoparticles (Pd / N-MCNPs) using the IWI method [48]. Three different catalyst preparation methods (impregnation, precipitation and colloidal) were used for the deposition of Pt nanoparticles on CNTs and the colloidal method was found to be the most effective method for the preparation of highly dispersed Pt nanoparticles [64]. Jung et al. [65] prepared Pt and Pd catalysts supported on CNFs and CNTs using various catalyst preparation methods including IWI for the hydrogenation of CALD and 1-octyne. Pd nanoparticles were also introduced inside MWCNTs via the IWI method using palladium nitrate as a precursor [66]. The resultant Pd / MWCNT catalyst had a high catalytic activity and high selectivity towards the C=C bond hydrogenation of CALD. Palladium catalysts deposited on CNF and CNT supports were also prepared using the IWI method and their catalytic activity was compared with Pd loaded on AC [67-69]. Chizari et al. also used the IWI method to prepare Pd catalysts supported on NCNT and CNT support materials and the catalysts were tested for the hydrogenation of CALD [70].

2.4.1.2 The liquid phase reduction method / polyol process

The liquid phase reduction method has been receiving a lot of attention in catalyst preparation methods because it provides an easy control of PGM particle sizes and distribution without the use of stabilizers [71]. It has low costs associated with the method, low processing temperatures and has the potential for large scale production. The most common used polyols are ethylene glycol (EG), di(ethylene glycol) (DEG) and poly(ethylene glycol) (PEG) which are organic compounds with two or more hydroxyl groups, and these act as both a solvent and a reducing agent. The microwave polyol method has also become a more important process because microwave irradiation allows uniform heating of a metal precursor to high temperatures in a short space of time resulting in shorter crystallization times and more homogeneous nucleation when compared to the conventional oil bath heating method [72]. Although the conventional oil bath heating polyol method has disadvantages of uneven temperature distribution during heating, it was the method used to activate EG in this thesis. This is because there are other advantages associated with the method such as the simplicity of the procedure used.

A schematic illustration of the mechanism of the polyol process is shown in Figure 2.2. During this method a polyol (most commonly EG) solution containing a metal precursor solution is refluxed at a specific temperature, where the polyol decomposes homogeneously to release the reducing agent for the metal reduction process [73]. A carbon nanomaterial support then captures the depositing metal nanoparticles. Variava et al. wrote a very informative review on the polyol process which describes the mechanism in detail [74].

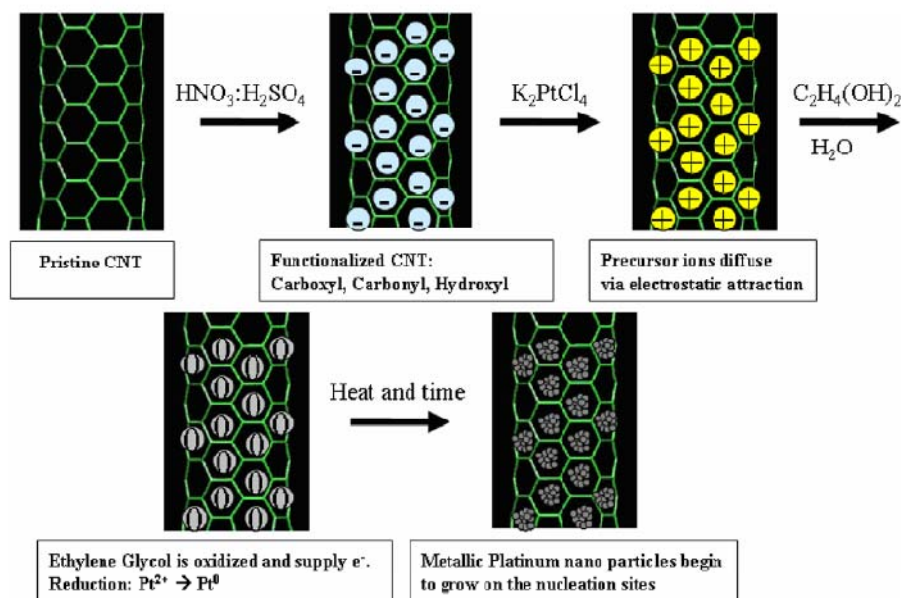


Figure 2.2. An example of the schematic illustration of the mechanism of the polyol method [72].

Harada et al. prepared highly dispersed palladium catalysts supported on various carbon supports using the liquid phase reduction of aqueous Pd complexes with KBH_4 as solvent and reductant [75]. Knupp et al. studied the effect of various experimental parameters on the synthesis of Pt catalysts loaded on CNT and CNF supports using the conventional and microwave irradiated polyol method [72]. They found out that the Pt particle size of the 10 wt % Pt / CNT catalysts did not differ that much using conventional and microwave heating. Uniform platinum nanoparticles with an average diameter of 3 nm and well dispersed on CNT supports were prepared using the microwave heating polyol method [73]. Guo et al. prepared Pt based bimetallic catalysts supported on MWCNTs using the microwave assisted polyol method and these were compared with identical catalysts prepared using the IWI method [76]. The Pt based bimetallic catalysts supported on MWCNTs had higher catalytic activity for the hydrogenation of CALD and higher selectivities to CA compared to the catalysts prepared using the IWI method [76]. Higgins et al. used the

conventional polyol method for preparing Pt nanoparticles supported on NCNT synthesized using ethylenediamine (ED-CNTs) and pyridine (Py-CNTs) nitrogen precursors [77]. The performance of Pt / NCNT catalysts were compared with nitrogen free Pt / CNT catalysts for the oxygen reduction method (ORR). The Pt / ED-CNT (4.74 at % N) catalyst displayed significantly higher electrocatalytic activity toward ORR when compared with Pt / Py-CNT (2.35 at % N) and Pt / CNT catalysts. Pt nanoparticles (30 wt %) were deposited on undoped and N doped CNTs using ethylene glycol solution as the solvent and reductant [78]. The resulting Pt catalysts with different N contents were tested in proton - exchange membrane fuel cells (PEMFC). Pt / NCNT catalysts exhibited higher stabilities than the undoped Pt / CNT catalysts and the Pt stability increased with the increase in N content of the Pt / NCNT catalysts.

2.5 Carbon spheres used as supports in various catalysis reactions

There have been a number of reports in the literature which have described the use of doped carbon spheres (mainly N or B) as supports in catalytic reactions. The few studies that have been investigated are discussed below.

2.5.1 Undoped carbon sphere supports

A comparison study of using CSs and CNTs as supports in FTS synthesis was done by Xiong et al. [58]. They investigated the effect of different Co / CS and Co / CNT catalyst preparation methods on FT activity. Different Co precursors were used to see if there would be an effect on FT performance. The Co catalysts supported on CSs and CNTs were autoreduced by the carbon supports in an inert atmosphere at approximately 480 °C. The Co catalysts deposited on the two supports which were

autoreduced in an inert atmosphere showed better FT performance than those which were reduced in H₂. Co / CNT and Co / CS catalysts prepared using a cobalt nitrate precursor showed better FTS activity than those prepared using cobalt acetate. The larger the Co particle sizes the higher the C₅₊ selectivity. Xiong et al. observed that the cobalt time yield, turnover frequency and C₅₊ selectivity were dependant on Co particle size.

In another study Xiong et al. investigated on the use of Fe / CS catalysts prepared using different methods of functionalization, different iron precursors, preparation methods and promoters (Mn, K and Cu) on FTS performance [60]. They observed that the iron catalysts synthesized from CSs functionalized at high temperatures (90 °C) in nitric acid had higher catalytic activity than those made at lower temperatures. The Fe / CS catalysts prepared using iron acetate as precursor showed a higher metal time yield than the catalyst prepared using iron nitrate solution. The Fe / CS catalysts prepared using deposition precipitation showed a higher metal time yield than the Fe / CS catalysts prepared using the impregnation method. The results observed above were attributed to the Fe dispersion and the small Fe particle sizes. When comparing Fe / CS catalysts prepared by functionalization with nitric acid, Fe / CS catalysts prepared by functionalization with KMnO₄ solution showed comparable catalytic activity and higher C₅₊ long chain hydrocarbon selectivity. This was attributed to the presence of residual manganese oxide deposited in the process of functionalization which enhanced the formation of olefins and the chain growth of hydrocarbons during FTS. Addition of K (0.05 to 1 %) to the Fe / CS catalysts inhibited the reduction of the catalysts and this resulted in a decreased catalytic activity but an increased olefin selectivity leading to higher long chain hydrocarbon selectivity. The addition of Cu into the Fe / CS catalysts improved the reduction of the catalysts but lowered the gasification of carbon spheres supports, decreased the CH₄ selectivity and had no significant effect on the FTS activity.

Nieto-Marquez et al. studied the effect of using different carbon supported Ni catalysts (Ni / AC, Ni / CSs and Ni / CNF) for the gas phase hydrogenation of nitrobenzene [79]. The Ni loading was fixed at 1 % w/w for all the catalysts. The average Ni particle sizes for Ni / AC, Ni / CNF and Ni / CS catalysts were 8.8, 7.7 and 10.4 nm respectively. After acid treatment the order of increasing surface acidity of the 3 supports was CNF < CS < AC. The selectivity to aniline for all the 3 catalysts was 100 %. The hydrogenation activity of the catalysts increased in the following order: Ni / CNF < Ni / CS < Ni / AC. The hydrogenation of nitrobenzene was not dependant on Ni particle size but was strongly dependant on the surface acid sites.

Moyo et al. investigated the effect of using K and Mn promoters on Co / carbon sphere catalysts in the Fischer Tropsch synthesis reaction [80]. Functional groups were introduced onto the carbon sphere supports by functionalizing with either HNO₃ or KMnO₄. The 5 % Co / CS KMnO₄ functionalized catalyst showed lower CH₄ and C₂ - C₄ selectivity but higher C₅₊ selectivity compared to the 5 % Co / CS HNO₃ functionalized catalyst. The 5 % Co / CS HNO₃ functionalized catalyst was used to study the effect of addition of K⁺ and MnO₄⁻ promoters on the FTS reaction (0.05 wt% Mn and K were added to 5 % Co / CS catalysts). The presence of K in the HNO₃ functionalized catalysts increased C₂ - C₄ selectivity and decreased the % CO conversion. The addition of MnO₄⁻ ions to the 5 % Co / CS HNO₃ functionalized catalyst increased the C₅₊ selectivity. They concluded that the MnO₄⁻ ions in the 5 % Co / CS KMnO₄ functionalized catalyst were responsible for the increased olefin / paraffin selectivity.

Liu et al. used mesocarbon microbeads (MCMB) made using different pretreatment conditions to support Pt catalysts in the methanol electro - oxidation reaction [81]. The average Pt particle size was in the range between 3 and 5 nm for the Pt / MCMB catalyst. Pretreatment conditions for the MCMB supports played a very important

role in determining the catalysts performance in the methanol electro - oxidation. The catalyst which had the MCMB support pretreated in boiling KOH (1 hour) exhibited a high catalytic activity during the electro - oxidation of methanol.

2.5.2 Doped carbon sphere supports

Xiong et al. reported the use of iron catalysts supported on three different nitrogen doped carbon sphere supports (NCSs) in the Fischer - Tropsch synthesis (FTS) [39]. The NCS supports were prepared using three different synthesis methods: horizontal CVD (NCS_{hor}), vertical CVD (NCS_{ver}) and the hydrothermal method (NCS_{hyd}). The supports had different physical and chemical properties. The three catalysts Fe / NCS_{ver}, Fe / NCS_{hyd} and Fe / NCS_{hor} had average Fe₃O₄ particle sizes of 15, 18 and 26 nm respectively, determined using TEM analysis. The N contents determined from C, H and N elemental analysis of NCS_{ver}, NCS_{hor} and NCS_{hyd} were 3.1, 2.4 and 1.5 % respectively. XPS analysis of the supports revealed that the N supports contained different amounts of N species: NCS_{ver} (62 % pyridinic and 38 % pyrrolic N), NCS_{hor} (50 % pyridinic and 50 % quaternary N) and NCS_{hyd} (100 % pyrrolic N). The quaternary N atoms in NCS_{hor} were found not to play a role in providing anchoring sites for the Fe particles. The pyridinic and pyrrolic sites acted as anchoring sites for metal deposition. The difference in Fe particle sizes was due to the different surface areas of the supports as well as the amount of surface defect sites and type of N species. All these variables affected the anchoring of the metal precursor onto the support. The NCS_{hyd} had additional oxygenated sites coming from sucrose used in its synthesis. The 3 different Fe / NCS catalysts exhibited different FTS results and the CO conversion of the catalysts was in the order Fe / NCS_{ver} > Fe / NCS_{hyd} > Fe / NCS_{hor}. The authors found that the Fe particle sizes, the N content in the support, the type of N species in the support as well as the defect sites played an important role in the FTS activity.

In another study Xiong et al. reported on the autoreduction of Co_3O_4 to Co metal under an inert atmosphere of Ar when supported on NCSs and CSs [41]. FTS studies were performed on the as-synthesized 2.3 wt.% Co / NCSs catalysts after pretreatment in both high purity Ar and H_2 . A 1.1 wt % Co / CSs catalyst was also used for comparison. The 2.3 wt % Co / NCS catalyst pretreated in Ar showed better FTS performance in terms of CO conversion and selectivity to C_{4+} hydrocarbons than the other catalyst pretreated in H_2 . Their result proved that pre-reduction of catalysts in H_2 is an unnecessary step. Cobalt oxide supported on NCSs could be autoreduced completely by the NCS support under an inert atmosphere of argon gas. The 1.1 wt % Co / CS catalyst reduced under an Ar atmosphere showed similar results of improved FTS performance when compared to the catalyst reduced using H_2 . The high CO activity in the 2.3 wt % Co / NCSs catalyst was attributed to the high dispersion of Co particles. The autoreduction of Co by carbon produced stable Co / NCS catalysts due to Co particles being trapped inside the cavities of the carbon surface.

Yoon and co-workers investigated the synthesis of palladium nanoparticles supported on nitrogen doped magnetic carbon nanoparticles (N-MCNPs) and their catalytic activity was tested for Heck, Suzuki and Sonogashira coupling reactions [48]. Well dispersed palladium nanoparticles were deposited on the N-MCNPs with an average diameter of 3.8 nm using a simple impregnation method. The Pd / N-MCNP catalyst showed high catalytic activity for the three reactions with conversion yields above 90 %. The catalyst was reused in three recycling reactions and showed no loss in catalytic activity in the three coupling reactions and the catalysts were easy to recover through magnetic separation. The high catalytic activities were attributed to the high dispersion of the palladium nanoparticles on the N-MCNPs. Nitrogen doping contributed to the uniform anchoring of the Pd nanoparticles. The strong interaction between Pd nanoparticles and the support also played a significant role in the catalytic activity.

The use of nitrogen doped hollow carbon spheres (N-HCS) as supports for Co catalysts in the aerobic oxidation of styrene was investigated by Nongwe et al. [82]. They calcined their catalysts at different temperatures. A 300 °C calcination temperature for 3 hours was found to be the temperature that produced the best catalytic results. The undoped Co / HCS300 catalyst gave a 90 % styrene conversion and a 79 % styrene oxide selectivity while the doped Co / N-HCS300 catalyst gave 99 % styrene conversion and 86 % styrene oxide selectivity. These reactions were performed using pure O₂ gas. The good catalytic results for the Co / N-HCS300 catalyst were due to the presence of N which promoted good Co dispersion. At the 6th recycling test, the conversion of styrene decreased from 99 % to 87 % and the selectivity to styrene oxide remained constant at 85 % for the Co / N-HCS300 catalyst. This showed that there was very minimal leaching of Co from the support as evidenced by ICP analysis with only 7 % of the Co detected in filtrate after three catalytic runs. There was a strong interaction between the doped N-HCS support and the Co metal. The Co / HCS300 catalyst gave a selectivity to styrene oxide of 75 % and a conversion of styrene of 41 % after the 6th recycling test showing the poor interaction between the HCS300 support and the Co metal. The oxidation of styrene using a Co / N-HCS300 catalyst was performed using different oxidants. The best oxidant was O₂ in dry air. The order of oxidants according to catalytic performance was shown to be: O₂ from dry air > O₂ > H₂O₂ > TBHP. It was also observed that substituted styrenes could be oxidized by dry air to their corresponding epoxides with good selectivities and conversion in the presence of DMF as solvent.

Palladium supported on boron doped hollow carbon spheres (Pd / B-HCS) were used as catalysts for the solvent free oxidation of alcohols by Ravat et al. [83]. The thermal stability of B-HCSs was higher than that of the undoped HCSs. The Pd / B-HCS catalysts were calcined at different temperatures in air. Pd / B-HCS120, Pd / B-HCS200 and Pd / B-HCS300 catalysts gave a 100 % conversion benzyl alcohol and 99 % selectivity to benzaldehyde (120, 200 and 300 stand for calcination

temperatures) using O₂ as oxidant. However after five recycling catalytic reactions the Pd / B-HCS120 catalyst showed a decrease in conversion of benzyl alcohol from 100 % to 61 % but the selectivity to benzyl aldehydes remained the same at 99 %. The decrease in catalytic activity was due to leaching and decomposition of the pyridine complex during the reaction. The Pd / B-HCS300 catalyst did not show any significant changes in conversion and selectivity to benzaldehyde after the 6th recycling test. The Pd / B-HCS300 catalyst was tested for the solvent free oxidation of substituted benzyl alcohols (*p*-XC₆H₅OH (X=OH, Br, Cl, NO₂), cinnamyl alcohol and prenol. The authors found that the catalytic activity was dependant on the substituent attached to the benzyl alcohol. The substituted benzyl alcohols showed good selectivity and conversion when oxidized by O₂. It was reported that B assisted in providing strong metal support interactions and enhanced the stability of the resultant Pd / B-HCS catalysts.

In another study Ravat et al. compared the impact of B doping on two different supports (HCSs and CNTs) [84]. They varied the Pd particle sizes of catalysts (Pd / B-HCSs and Pd / B-CNTs) by varying the catalyst preparation method, Pd loading and calcination temperature. The Pd-catalyzed benzyl alcohol to benzaldehyde reaction was chosen as the test reaction to evaluate the effects of the different Pd / B-HCSs and Pd / B-CNTs catalysts. For the Pd / B-HCS catalysts, the Pd particle sizes increased with increase in calcination temperature [0 °C (2.4 nm), 200 °C (2.3 nm), 300 °C (2.4 nm), 400 °C (3.7 nm), 450 °C (4.5 nm), 500 °C (5.5 nm) and 550 °C (11.7 nm)]. The selectivity to benzaldehyde at calcination temperatures between 0 to 550 °C remained constant at 98 +/- 1 %. The conversion of benzyl alcohol remained constant at 100 % for Pd / B-HCS catalysts calcined at temperatures of 0, 120 and 300 °C. However increasing the calcination temperature from 400 to 550 °C for the Pd / B-HCS catalysts had the effect of decreasing the conversion of benzyl alcohol. A comparison was made between carbon and silica sphere supported Pd catalysts. Pd catalysts prepared using silica spheres were named Pd / Sis. For Pd / Sis catalysts, the

Pd particle sizes increased with increase in calcination temperature [300 °C (8.9 nm), 400 °C (10.5 nm) and 500 °C (11.7 nm)]. The same trend applied to Pd / B-CNT calcined at different temperatures [300 °C (4.2 nm), 400 °C (5.4 nm), 450 °C (6.0 nm) and 500 °C (6.8 nm)]. Increasing the calcination temperature of Pd / Sis catalysts had the effect of decreasing the conversion of benzyl alcohol and the selectivity to benzaldehyde. However increasing the calcination temperature of Pd / B-CNTs catalysts had the effect of decreasing the conversion of benzyl alcohol while the selectivity to benzaldehyde remained constant at 99 %. An increase in the Pd loadings (1, 2, 2.5 and 3 wt%) on Pd / B-HCSs catalysts had the effect of increasing the conversion of benzyl alcohol and the selectivity to benzaldehyde remained constant at 99 %. The oxidation of benzyl alcohol to benzaldehyde using O₂ as the oxidant was shown to depend on the mean Pd particle size which was influenced by the B-Pd-C interaction. A calcination temperature of 300 °C for the Pd / B-HCSs catalysts was the best temperature and it gave complete conversion of benzyl alcohol (100 %) and a benzaldehyde selectivity of 99 %.

NCSs were used in the nickel catalyzed hydrogenation of butyronitrile (BTN) [85]. The carbon sphere supports were synthesized with different C and or N precursors i.e. benzene (CNS_B), aniline (CNS_A) and nitrobenzene (CNS_N) and gave NCSs with N contents of 0, 3.5 and 2.7 at % respectively. The three catalysts were synthesized using a deposition precipitation method (Ni/CNS_B, Ni/CNS_A and Ni/CNS_N) had Ni loadings of 2.5, 1.8 and 1.8 % w/w respectively. The particle sizes of the Ni nanoparticles were 10.5, 13.1 and 18.2 nm for the Ni/CNS_B, Ni/CNS_A and Ni/CNS_N catalysts respectively. The conversion of BTN followed the following sequence of increasing activity: Ni/CNS_B < Ni/CNS_A < Ni/CNS_N. Catalysts with the larger particle sizes led to higher reaction rates. This is due to the weakening of the adsorption strength of the cyano group (C≡N) which made it easier to hydrogenate this functionality. The C≡N bond adsorbs more strongly on smaller particles hence hydrogenation becomes more difficult. The selectivity to the primary amine in all the

three catalysts was close to 100 %. When the catalyst was physically mixed with the supports, the order of increasing activity was as follows: $\text{Ni} + \text{CNS}_\text{B} < \text{Ni} + \text{CNS}_\text{A} < \text{Ni} + \text{CNS}_\text{N}$. The authors reported that the presence of nitrogen in the quaternary form played an important role in the catalytic activity.

Ru and Pd catalysts supported on NCSs were investigated for the chemoselective hydrogenation of diketones, Heck and Suzuki carbon - carbon coupling reactions and the oxidation of styrene [37]. The hydrogenation of diketones to ketols was carried out using very mild reaction conditions. Using Ru / NCSs catalysts, high conversions (< 99 %) were obtained and a 100 % selectivity to hydroxyketones was achieved. The conversion of diketones remained very high at 97 % after the catalyst was recycled 10 times. There was no leaching of Ru under the reaction conditions employed in this study which showed the strong binding of Ru nanoparticles to the NCSs support. It also indicated the absence of sintering of Ru particles after long reaction times. The catalytic activity of the 3 wt % Pd / NCS catalyst was tested for the Heck coupling of iodobenzene and methyl acrylate. The conversion to the coupled product was 98 % (120 °C and 24 hours). The conversions were also very high when halide substituted benzenes were also used in the reaction. The catalyst was recycled three times and the conversion remained very high at 95 %. The 3 wt % Pd / NCS catalyst was also tested for the Suzuki coupling reaction. The reaction of iodobenzene and phenylboronic acid produced biphenyl in good yields (92%). Use of bromo and chlorobenzene produced biphenyl in good yields of above 80 %. The catalyst remained active after being recycled three times. Lastly the authors used 3 wt % V / NCS catalysts for the oxidation of styrene using hydrogen peroxide as oxidant. They observed that an increase in vanadium loading up to 3 wt % resulted in an increase in conversion and selectivity.

2.6 Hydrogenation reactions of α,β -unsaturated aldehydes

The selectivities to hydrocinnamaldehyde and cinnamyl alcohol are dependent upon a lot of factors which include the method of preparation of the catalyst and activation methods, the type of support and metal used, metal precursor and the selection of reaction conditions [86].

2.6.1 Mechanism of hydrogenation reaction of cinnamaldehyde

The hydrogenation of cinnamaldehyde over supported metal catalysts generally occurs in 7 different steps: (i) external diffusion of reagents, (ii) internal pore diffusion of reagents, (iii) adsorption of reactants, (iv) chemical reaction on the surface, (v) desorption, (iv) internal diffusion of products and lastly (vii) external diffusion of products [87]. Each of the above mentioned steps influences the reaction rate and selectivity.

There are two possible ways in which heterogeneous catalysis proceeds at a surface: the Langmuir - Hinshelwood (LH) mechanism and the Rideal - Eley (RE) mechanism. In the LH mechanism, the rate of a heterogeneous reaction is controlled by the reaction of the adsorbed molecules and it is assumed that all adsorption and desorption pressure are at equilibrium. In contrast, in the RE mechanism, the reaction occurs between a reactant molecule in the gas or liquid phase and one that is adsorbed on the surface. The LH mechanism is considered as a good approximation to explain cinnamaldehyde hydrogenation kinetics [88-91]. The kinetic models may take into account the following assumptions: (i) one or two different types of adsorption sites for CALD or H_2 , (ii) competitive or non - competitive adsorption steps and (iii) dissociative or non - dissociative adsorption of H_2 . The model can become more complicated if the by-product multiple reactions are included.

According to Delbecq and Sautet, the adsorption states possible on metal surfaces for α,β - unsaturated aldehydes are shown in Figure 2.3 [92]. For adsorption through the C=O double bond, resulting in the formation of CA, different geometries are possible: on top, di - σ_{CO} and Π_{CO} . For the formation of HCALD, resulting from the adsorption through the C=C double bond, the geometries are di - σ_{CC} and Π_{CC} . For the formation of the enol as the intermediate product or the formation of the unsaturated alcohol 3-phenyl-1-propanol as the primary product, the adsorption involves both the C=C and C=O double bonds with a geometry of the quasi-planar type (η_4). In the process the enol isomerises to HCALD. The adsorption mode of α,β - unsaturated aldehydes on metal surfaces is also dependant on the nature of the metal and the type of the exposed crystal surface [92].

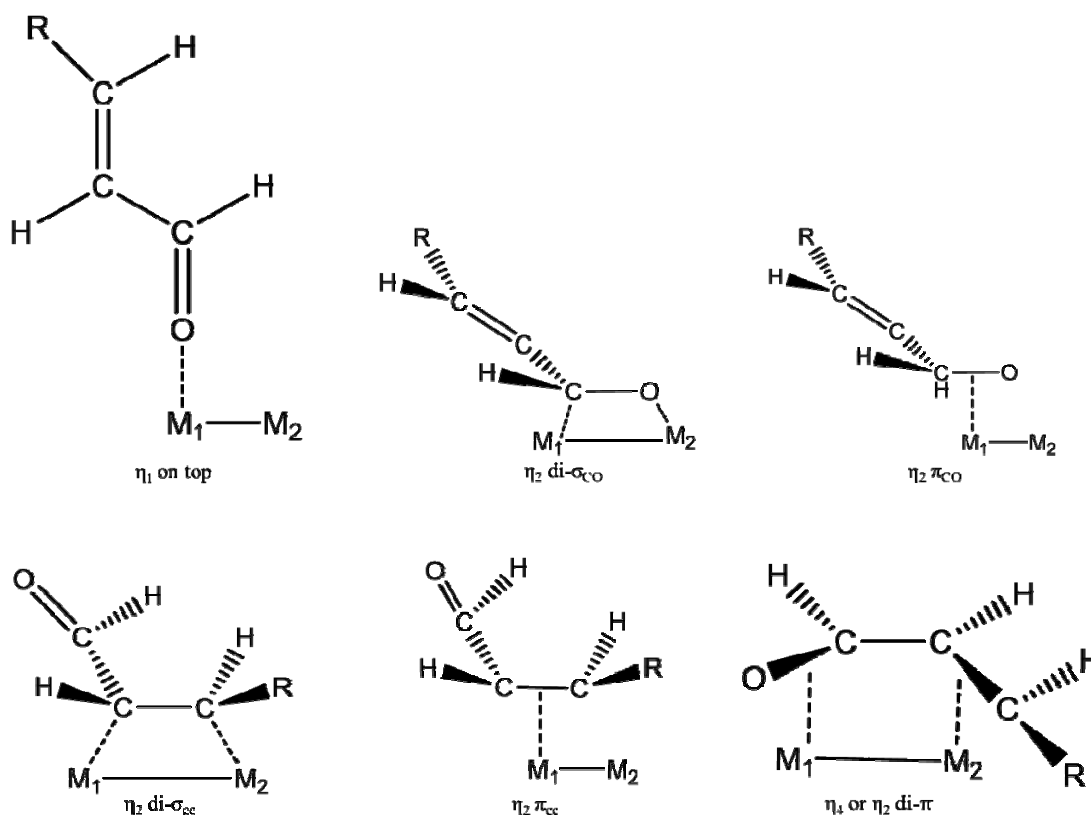


Figure 2.3. The various adsorption modes of cinnamaldehyde [90, 91, 93].

2.7 Doped and undoped carbon nanomaterials used as supports for the hydrogenation of CALD

2.7.1 Undoped carbon nanomaterials

2.7.1.1 Pd catalysts supported on undoped carbon nanomaterials for the hydrogenation of CALD

Tessonnier et al. deposited palladium nanoparticles inside multiwalled carbon nanotubes channels by using a simple impregnation method [66]. The Pd catalysts were tested for the selective hydrogenation of cinnamaldehyde into hydrocinnamaldehyde and the results obtained were compared of a commercial catalyst supported on a high surface area AC. The Pd / MWCNT catalyst attained 100 % conversion after 25 hours and the Pd / AC catalyst attained 100 % conversion after 27 hours. The selectivities were different for the 2 catalysts. The Pd / MWCNT catalyst was selective towards HCALD (90 %) and 3P1P (10 %). The Pd / AC catalyst gave HCALD and 3P1P in equal quantities. The high selectivities of the Pd / MWCNTs were attributed to the absence of micropores. A low concentration of oxygen surface groups on the MWCNT surface and a strong metal - support interaction.

Comparison studies have been conducted on carbon nanofibre (CNF) and activated charcoal (AC) supported palladium catalysts for the hydrogenation of cinnamaldehyde [67, 68]. Pd / CNF based catalysts exhibited higher hydrogenation activity compared with that observed on Pd / AC based catalysts under similar reaction conditions. The absence of microporosity and the high mass transfer rate in the CNT based catalysts were responsible for the improved C=C bond hydrogenation

selectivity results. The Pd / AC catalysts produced HCALD, CA and 3P1P as products which could be explained by the presence of microporosity and residual acidity on the activated charcoal surface which could hydrogenate the C=O bond in CALD.

2.7.1.2 Other PGM catalysts excluding Pd supported on undoped carbon nanomaterials for the hydrogenation of CALD

The hydrogenation of CALD using different metals (Pt, Ru, Ir, Os) supported on different carbon nanostructures (CNTs, CNFs) is well documented in the literature. A few representative examples are shown in Table 2.2.

Table 2.2. Selected examples of the hydrogenation of cinnamaldehyde using undoped carbon nanostructures.

Catalyst	Hydrogenation conditions	Hydrogenation results summary	References
0.2 wt % Ru / nanotube	Ru / nanotubes catalyst (0.26 g), 2-propanol (40 cm ³), T = 110 °C, 4.5 MPa H ₂ pressure, 2 hours	80 % conversion and selectivity to cinnamyl alcohol of 92 %.	[94]
5 wt % Pd / CNF 5 wt % Pd / activated charcoal (AC)	T = 80 °C, 40 ml of dioxane, 10 ml of CALD, 0.00105 g Pd, stirring speed 400 rpm. Atmospheric pressure.	98 % HCALD selectivity and 2 % 3P1P selectivity for the Pd / CNF catalyst. The commercial catalyst had low selectivities of a mixture of HCALD, 3P1P and CA.	[67]
Pt / herring bone nanofibres (HB-CNF) Pt / platelet nanofibres (PL-CNF) Pt / multiwalled nanotubes (MWCNT) and Pt / AC	T = 110 °C, Tetrahydrofuran, 0.15 MPa H ₂ pressure	Pt / HB-CNF catalyst prepared using the microwave assisted polyol method had the highest catalyst activity and selectivity to CA when compared to the same catalysts prepared using other methods.	[65]

5 wt% Ru / CNF and 5 wt% Ru / CNF catalysts annealed at different temperatures of 573, 773 and 973K.	Ru / CNF catalyst (0.5-1 g), CALD (9 g), isopropanol (100 ml), T = 383 K, H ₂ = 4.5 MPa, time = 50 minutes.	Activity of 5 wt% Ru / CNF973 catalyst increased by a factor of 22 fold when compared to 5 w% Ru / CNF catalyst. This was attributed to the low concentration of oxygenated sites in the Ru / CNF973 catalyst.	[95]
--	--	---	------

2.7.2 Nitrogen doped carbon nanomaterials

There have been very few reports in the worldwide literature on the use of nitrogen doped carbon nanostructures as supports in the hydrogenation of cinnamaldehyde. The few reports that are available are discussed below.

Chizari et al. reported on the use of undoped and nitrogen doped CNTs supported Pd catalysts in the hydrogenation of CALD [70]. There were two types of NCNT supports used, both with N contents of approximately 3 at %: NCNT-Nint and NCNT-Nsub which were synthesized at temperatures of 750 °C and 850 °C respectively, with an ethane in ammonia concentration of 50 %. The catalysts were prepared using an incipient wetness impregnation method using palladium nitrate as the metal precursor solution. The average particle sizes of Pd determined from TEM analysis of the Pd / CNT and Pd / NCNT (for both NCNT-Nint and NCNT-Nsub) catalysts were 10 and 3 nm respectively. The difference in average particle sizes were due to the presence of N atoms in the Pd / NCNT catalyst which act as anchoring sites for metal adsorption and decreases the chances of metal agglomeration. A higher catalytic activity was observed for the Pd / NCNT-Nsub catalyst compared with the Pd / NCNT-Nint catalyst. This was due to the differences in the amounts of N species in the two supports. The NCNT-Nsub support had higher amounts of pyridinic N and substituted nitrogen (pyrrolic + quaternary) and low amounts of intercalated and / N-oxide species. The NCNT-Nint had higher amounts of intercalated and / N-oxide species and lower amounts of pyridinic N and substituted nitrogen (pyrrolic + quaternary). The catalytic results showed that the Pd / NCNT catalysts exhibited a higher catalytic activity (expressed in terms of conversion) and C=C bond selectivity compared to the Pd / CNT catalyst. The differences in results were attributed to the difference in the average particle sizes of the Pd nanoparticles, the presence of N, the type of N species and also the high dispersion of Pd particles in the Pd / NCNT

catalyst. The high dispersion was due to the electronic interactions between the metal and support. The Pd / NCNT catalyst was also very stable for this reaction and no leaching was observed which indicated strong metal support interactions.

In another study Lepro et al. reported on an efficient method for anchoring Pt nanoparticles on undoped and nitrogen doped MWCNTs using a hydrothermal method with sodium hexachloroplatinate (IV) hexahydrate and acetic acid [96]. The resultant catalysts Pt / MWCNT-CN_x (Pt / CN_x), untreated MWCNTs-CN_x (CN_x) and undoped MWCNTs (CNT) were tested for the hydrogenation of CALD. The Pt / CN_x catalyst had a conversion of CALD which was 6 times greater than that of MWNTs-CN_x and MWCNTs catalysts. The selectivities toward CA for the Pt / CN_x and MWNTs-CN_x catalyst were 50 and approximately 15 % respectively. The good performance of the Pt / CN_x catalyst was due to the N rich sites in the bamboo compartments of the MWNTs-CN_x supports which created anchor sites for Pt particles.

Amadou et al. used N doped CNTs as catalyst supports for palladium in the liquid phase hydrogenation of CALD [97]. They compared the catalytic activity of Pd supported on 3 different supports namely nitrogen doped carbon nanotubes (NCNTs), undoped carbon nanotubes (CNTs) and activated charcoal (AC). The Pd / AC catalyst produced the best results in terms of catalyst activity and this was due to the high specific surface area of the activated carbon which improved the adsorption process. The HCALD selectivities were 80 % and 60 % for Pd / CNT and Pd / NCNT catalysts whereas for Pd / AC decreased from 60 to 20 % with time on line. The high selectivity of the Pd / NCNT catalyst was due to the increased electron density due to the electron pairs on the nitrogen atoms. The activated carbon had low HCALD selectivities due to the presence of acidic sites and its microporosity.

Kente et al. reported on a comparison study of using gallium nitride (GaN) and NCSs as supports for the hydrogenation of cinnamaldehyde [40]. Their study was the first one available in the literature on the use of the two supports for this reaction. The GaN and NCS supports were synthesized using double stage and single stage CVD methods respectively. The Pd / GaN and Pd / NCSs catalysts were synthesized using the conventional polyol method which uses ethylene glycol as the both the solvent and reductant. The loadings were fixed at 1 and 3 wt % Pd. The Pd nanoparticles were well dispersed on both supports although the Pd / NCS catalysts had larger average Pd particle sizes compared to Pd / GaN supports. The catalysts were tested for the hydrogenation of CALD at reaction temperatures of 40 and 60 °C and the CALD conversion of the catalysts was found to be in the following order 3% Pd / GaN > 3 % Pd / NCSs > 1 % Pd / NCSs > 1 % Pd / GaN. This study has shown that GaN and NCSs can be used as supports in hydrogenation reactions.

2.8 Summary

From the literature cited in this section, it can be seen that there is an increasing interest in the use of nitrogen doped carbon spheres in various catalytic reactions which include FTS reaction, Heck and Suzuki reactions just to mention a few. The synthesis of nitrogen doped carbon spheres has been done using various methods which include chemical vapour deposition (non - catalytic and catalytic), polymerization reactions, hydrothermal methods and carbonization methods. Recent literature on the selective hydrogenation of unsaturated aldehydes to unsaturated alcohols over heterogeneous catalysts is overviewed. The main challenge in chemoselective hydrogenation is to develop a catalyst which is stable, active and selective. Often there is an inverse relationship between activity and selectivity in catalysis. The work in this thesis aims to address this issue by focusing mainly on the properties of nitrogen doped carbon sphere support and the methods of catalyst preparation.

2.9 References

1. Auer, E., A. Freund, J. Pietsch, and T. Tacke, *Carbons as supports for industrial precious metal catalysts*. Applied Catalysis A: General, 1998. **173**(2): p. 259-271.
2. Shao, Y., J. Sui, G. Yin, and Y. Gao, *Nitrogen-doped carbon nanostructures and their composites as catalytic materials for proton exchange membrane fuel cell*. Applied Catalysis B: Environmental, 2008. **79**(1): p. 89-99.
3. Kang, Z.C. and Z.L. Wang, *Chemical activities of graphitic carbon spheres*. Journal of Molecular Catalysis A: Chemical, 1997. **118**(2): p. 215-222.
4. Glerup, M., J. Steinmetz, D. Samaille, O. Stephan, S. Enouz, A. Loiseau, S. Roth, and P. Bernier, *Synthesis of N-doped SWNT using the arc-discharge procedure*. Chemical Physics Letters, 2004. **387**(1-3): p. 193-197.
5. Zhang, Y., H. Gu, K. Suenaga, and S. Iijima, *Heterogeneous growth of B C N nanotubes by laser ablation*. Chemical Physics Letters, 1997. **279**(5-6): p. 264-269.
6. Deshmukh, A.A., S.D. Mhlanga, and N.J. Coville, *Carbon spheres*. Materials Science and Engineering: R: Reports, 2010. **70**(1-2): p. 1-28.
7. Xia, Y., B. Gates, Y. Yin, and Y. Lu, *Monodispersed Colloidal Spheres: Old Materials with New Applications*. Advanced Materials, 2000. **12**(10): p. 693-713.
8. Inagaki, M., *Carbon materials Structure, texture and intercalation*. Solid State Ionics, 1996. **86-88, Part 2**(0): p. 833-839.
9. Inagaki, M., *Discussion of the formation of nanometric texture in spherical carbon bodies*. Carbon, 1997. **35**(5): p. 711-713.
10. Serp, P., R. Feurer, P. Kalck, Y. Kihn, J.L. Faria, and J.L. Figueiredo, *A chemical vapour deposition process for the production of carbon nanospheres*. Carbon, 2001. **39**(4): p. 621-626.

11. Kroto, H.W., J.R. Heath, S.C. O'Brien, R.F. Curl, and R.E. Smalley, *C 60: buckminsterfullerene*. Nature, 1985. **318**(6042): p. 162-163.
12. Iijima, S., *Direct observation of the tetrahedral bonding in graphitized carbon black by high resolution electron microscopy*. Journal of Crystal Growth, 1980. **50**(3): p. 675-683.
13. Kang, Z.C. and Z.L. Wang, *On Accretion of Nanosize Carbon Spheres*. The Journal of Physical Chemistry, 1996. **100**(13): p. 5163-5165.
14. Qian, H.-s., F.-m. Han, B. Zhang, Y.-c. Guo, J. Yue, and B.-x. Peng, *Non-catalytic CVD preparation of carbon spheres with a specific size*. Carbon, 2004. **42**(4): p. 761-766.
15. Pol, V.G., M. Motiei, A. Gedanken, J. Calderon-Moreno, and M. Yoshimura, *Carbon spherules: synthesis, properties and mechanistic elucidation*. Carbon, 2004. **42**(1): p. 111-116.
16. Qiu, J., Y. Li, Y. Wang, C. Liang, T. Wang, and D. Wang, *A novel form of carbon micro-balls from coal*. Carbon, 2003. **41**(4): p. 767-772.
17. Kamegawa, K. and H. Yoshida, *Preparation and characterization of swelling porous carbon beads*. Carbon, 1997. **35**(5): p. 631-639.
18. Hirsch, A., *Functionalization of Single-Walled Carbon Nanotubes*. Angewandte Chemie International Edition, 2002. **41**(11): p. 1853-1859.
19. Tasis, D., N. Tagmatarchis, A. Bianco, and M. Prato, *Chemistry of Carbon Nanotubes*. Chemical Reviews, 2006. **106**(3): p. 1105-1136.
20. Dyke, C.A. and J.M. Tour, *Overcoming the Insolubility of Carbon Nanotubes Through High Degrees of Sidewall Functionalization*. Chemistry – A European Journal, 2004. **10**(4): p. 812-817.
21. Moghaddam, M.J., S. Taylor, M. Gao, S. Huang, L. Dai, and M.J. McCall, *Highly Efficient Binding of DNA on the Sidewalls and Tips of Carbon Nanotubes Using Photochemistry*. Nano Letters, 2003. **4**(1): p. 89-93.
22. Andrews, R., D. Jacques, D. Qian, and T. Rantell, *Multiwall Carbon Nanotubes: Synthesis and Application*. Accounts of Chemical Research, 2002. **35**(12): p. 1008-1017.

23. Wu, G., L. Li, J.-H. Li, and B.-Q. Xu, *Methanol electrooxidation on Pt particles dispersed into PANI/SWNT composite films*. Journal of Power Sources, 2006. **155**(2): p. 118-127.
24. Nakashima, N., Y. Tomonari, and H. Murakami, *Water-Soluble Single-Walled Carbon Nanotubes via Noncovalent Sidewall-Functionalization with a Pyrene-Carrying Ammonium Ion*. Chemistry Letters, 2002. **31**(6): p. 638-639.
25. Moore, V.C., M.S. Strano, E.H. Haroz, R.H. Hauge, R.E. Smalley, J. Schmidt, and Y. Talmon, *Individually Suspended Single-Walled Carbon Nanotubes in Various Surfactants*. Nano Letters, 2003. **3**(10): p. 1379-1382.
26. Matarredona, O., H. Rhoads, Z. Li, J.H. Harwell, L. Balzano, and D.E. Resasco, *Dispersion of Single-Walled Carbon Nanotubes in Aqueous Solutions of the Anionic Surfactant NaDDBS*. The Journal of Physical Chemistry B, 2003. **107**(48): p. 13357-13367.
27. Katz, E. and I. Willner, *Biomolecule-Functionalized Carbon Nanotubes: Applications in Nanobioelectronics*. ChemPhysChem, 2004. **5**(8): p. 1084-1104.
28. Lin, Y., S. Taylor, H. Li, K.A.S. Fernando, L. Qu, W. Wang, L. Gu, B. Zhou, and Y.-P. Sun, *Advances toward bioapplications of carbon nanotubes*. Journal of Materials Chemistry, 2004. **14**(4): p. 527-541.
29. Ebbesen, T.W., H. Hiura, M.E. Bisher, M.M.J. Treacy, J.L. Shreeve-Keyer, and R.C. Haushalter, *Decoration of carbon nanotubes*. Advanced Materials, 1996. **8**(2): p. 155-157.
30. Wildgoose, G.G., C. E. Banks, and R. G. Compton, *Metal Nanoparticles and Related Materials Supported on Carbon Nanotubes: Methods and Applications*. Small, 2006. **2**(2): p. 182-193.
31. Hou, P.X., C. Liu, and H. M. Cheng,, *Purification of carbon nanotubes*. Carbon, 2008. **46**(15): p. 2003-2025.
32. Balasubramanian, K., and M. Burghard, *Chemically Functionalized Carbon Nanotubes*. Small, 2005. **1**(2): p. 180-192.

33. Gojny, F.H., J. Nastalczyk, Z. Roslaniec, and K. Schulte, , *Surface modified multi-walled carbon nanotubes in CNT / epoxy-composites*. Chemical Physics Letters, 2003. **370**(5): p. 820-824.
34. Liu, L., Y. Qin, Z. X. Guo, and D. Zhu, , *Reduction of solubilized multi-walled carbon nanotubes*. Carbon, 2003. **41**(2): p. 331-335.
35. Saha, M.S., and A. Kundu, *Functionalizing carbon nanotubes for proton exchange membrane fuel cells electrode*. Journal of Power Sources, 2010. **195**(19): p. 6255-6261.
36. Ewels, C. and M. Glerup, *Nitrogen doping in carbon nanotubes*. Journal of nanoscience and nanotechnology, 2005. **5**(9): p. 1345-1363.
37. Deshmukh, A.A., R. Ul Islam, M.J. Witcomb, W.A.L. van Otterlo, and N.J. Coville, *Catalytic Activity of Metal Nanoparticles Supported on Nitrogen-Doped Carbon Spheres*. ChemCatChem, 2010. **2**(1): p. 51-54.
38. Su, F., X.S. Zhao, Y. Wang, L. Wang, and J.Y. Lee, *Hollow carbon spheres with a controllable shell structure*. Journal of Materials Chemistry, 2006. **16**(45): p. 4413-4419.
39. Xiong, H., M. Moyo, M.A. Motchelaho, Z.N. Tetana, S.M.A. Dube, L.L. Jewell, and N.J. Coville, *Fischer–Tropsch synthesis: Iron catalysts supported on N-doped carbon spheres prepared by chemical vapor deposition and hydrothermal approaches*. Journal of Catalysis, 2014. **311**(0): p. 80-87.
40. Kente, T., S. Dube, N.J. Coville, and S.D. Mhlanga, *Application of Gallium Nitride Nanostructures and Nitrogen Doped Carbon Spheres as Supports for the Hydrogenation of Cinnamaldehyde*. Journal of nanoscience and nanotechnology, 2013. **13**(7): p. 4990-4995.
41. Xiong, H., M. Moyo, M.K. Rayner, L.L. Jewell, D.G. Billing, and N.J. Coville, *Autoreduction and Catalytic Performance of a Cobalt Fischer–Tropsch Synthesis Catalyst Supported on Nitrogen-Doped Carbon Spheres*. ChemCatChem, 2010. **2**(5): p. 514-518.

42. Feng, Y., W. Yang, N. Wang, W. Chu, and D. Liu, *Effect of nitrogen-containing groups on methane adsorption behaviors of carbon spheres*. Journal of Analytical and Applied Pyrolysis, 2014. **107**(0): p. 204-210.
43. Li, W., D. Chen, Z. Li, Y. Shi, Y. Wan, G. Wang, Z. Jiang, and D. Zhao, *Nitrogen-containing carbon spheres with very large uniform mesopores: The superior electrode materials for EDLC in organic electrolyte*. Carbon, 2007. **45**(9): p. 1757-1763.
44. Ma, F., H. Zhao, L. Sun, Q. Li, L. Huo, T. Xia, S. Gao, G. Pang, Z. Shi, and S. Feng, *A facile route for nitrogen-doped hollow graphitic carbon spheres with superior performance in supercapacitors*. Journal of Materials Chemistry, 2012. **22**(27): p. 13464-13468.
45. Jeong, H.M., S.Y. Lee, W.H. Shin, J.H. Kwon, A. Shakoor, T.H. Hwang, S.Y. Kim, B.-S. Kong, J.-S. Seo, Y.M. Lee, J.K. Kang, and J.W. Choi, *Silicon@porous nitrogen-doped carbon spheres through a bottom-up approach are highly robust lithium-ion battery anodes*. RSC Advances, 2012. **2**(10): p. 4311-4317.
46. Nieto-Márquez, A., I. Espartero, J.C. Lazo, A. Romero, and J.L. Valverde, *Direct synthesis of carbon and nitrogen-carbon nanospheres from aromatic hydrocarbons*. Chemical Engineering Journal, 2009. **153**(1-3): p. 211-216.
47. Li, F., Q. Qian, F. Yan, and G. Yuan, *Nitrogen-doped porous carbon microspherules as supports for preparing monodisperse nickel nanoparticles*. Carbon, 2006. **44**(1): p. 128-132.
48. Yoon, H., S. Ko, and J. Jang, *Nitrogen-doped magnetic carbon nanoparticles as catalyst supports for efficient recovery and recycling*. Chemical Communications, 2007(14): p. 1468-1470.
49. Liao, Y., L. Gao, X. Zhang, and J. Chen, *Nitrogen-doped hollow carbon spheres with enhanced electrochemical capacitive properties*. Materials Research Bulletin, 2012. **47**(7): p. 1625-1629.
50. Zhou, X., Z. Yang, H. Nie, Z. Yao, L. Zhang, and S. Huang, *Catalyst-free growth of large scale nitrogen-doped carbon spheres as efficient*

- electrocatalysts for oxygen reduction in alkaline medium*. Journal of Power Sources, 2011. **196**(23): p. 9970-9974.
51. Zhang, Z., R. Zhang, C. Li, L. Yuan, P. Li, L. Yao, and S. Liu, *Nitrogen-Doped Carbon Hollow Spheres for Immobilization, Direct Electrochemistry, and Biosensing of Protein*. Electroanalysis, 2012. **24**(6): p. 1424-1430.
 52. Chen, Y., J. Wang, H. Liu, M. N. Banis, R. Li, X. Sun. T. S. Sham, S. Ye, and S. Knights, *Nitrogen Doping Effects on Carbon Nanotubes and the Origin of the Enhanced Electrocatalytic Activity of Supported Pt for Proton-Exchange Membrane Fuel Cells*. The Journal of Physical Chemistry C, 2011. **115**(9): p. 3769-3776.
 53. van Dommele, S., A. Romero-Izquierdo, R. Brydson, K.P. de Jong, and J.H. Bitter, *Tuning nitrogen functionalities in catalytically grown nitrogen-containing carbon nanotubes*. Carbon, 2008. **46**(1): p. 138-148.
 54. Wright, W.P., V.D. Marsicano, J.M. Keartland, R.M. Erasmus, S.M.A. Dube, and N.J. Coville, *The electrical transport properties of nitrogen doped carbon microspheres*. Materials Chemistry and Physics, 2014. **147**(3): p. 908-914.
 55. Li, X., X. Tian, D. Zhang, X. Chen, and D. Liu, *Solvothermal synthesis and characterization of nitrogen-enriched carbon-encapsulated nickel nanospheres*. Materials Science and Engineering: B, 2008. **151**(3): p. 220-223.
 56. Yoon, S.B., B. Fang, M. Kim, J. H. Kim, and J. S. Yu, *Nanostructured Supported Catalysts for Low - Temperature Fuel Cells*, in *Frontiers of Nanoscience*. 2009, Elsevier. p. 173-231.
 57. Yang, Y., K. Chiang, and N. Burke, *Porous carbon-supported catalysts for energy and environmental applications: A short review*. Catalysis Today, 2011. **178**(1): p. 197-205.
 58. Xiong, H., M.A.M. Motchelaho, M. Moyo, L.L. Jewell, and N.J. Coville, *Correlating the preparation and performance of cobalt catalysts supported on carbon nanotubes and carbon spheres in the Fischer–Tropsch synthesis*. Journal of Catalysis, 2011. **278**(1): p. 26-40.

59. Malek, R.M., J. Soltan, and A. K. Dalai, *Effects of nanotubes pore size on the catalytic performances of iron catalysts supported on carbon nanotubes for Fischer-Tropsch synthesis*. Applied Catalysis A: General, 2010. **379**(1-2): p. 129-134.
60. Xiong, H., M. Moyo, M.A.M. Motchelaho, L.L. Jewell, and N.J. Coville, *Fischer-Tropsch synthesis over model iron catalysts supported on carbon spheres: The effect of iron precursor, support pretreatment, catalyst preparation method and promoters*. Applied Catalysis A: General, 2010. **388**(1-2): p. 168-178.
61. Zhang, H., W. Chu, C. Zou, Z. Huang, Z. Ye, and L. Zhu, *Promotion Effects of Platinum and Ruthenium on Carbon Nanotube Supported Cobalt Catalysts for Fischer-Tropsch Synthesis*. Catalysis Letters, 2011. **141**(3): p. 438-444.
62. Zhang, S., L. Chen, S. Zhou, D. Zhao, and L. Wu, *Facile Synthesis of Hierarchically Ordered Porous Carbon via in Situ Self Assembly of Colloidal Polymer and Silica Spheres and Its Use as a Catalyst Support*. Chemistry of Materials, 2010. **22**(11): p. 3433-3440.
63. van Steen, E., and M. Claeys, *Fischer-Tropsch Catalysts for the Biomass-to-Liquid (BTL)-Process*. Chemical Engineering and Technology, 2008. **31**(5): p. 655-666.
64. Li, X., and I. Ming Hsing, *The effect of the Pt deposition method and the support on Pt dispersion on carbon nanotubes*. Electrochimica Acta, 2006. **51**(25): p. 5250-5258.
65. Jung, A., A. Jess, T. Schubert, and W. Schütz, *Performance of carbon nanomaterial (nanotubes and nanofibres) supported platinum and palladium catalysts for the hydrogenation of cinnamaldehyde and of 1-octyne*. Applied Catalysis A: General, 2009. **362**(1-2): p. 95-105.
66. Tessonnier, J.-P., L. Pesant, G. Ehret, M.J. Ledoux, and C. Pham-Huu, *Pd nanoparticles introduced inside multi-walled carbon nanotubes for selective hydrogenation of cinnamaldehyde into hydrocinnamaldehyde*. Applied Catalysis A: General, 2005. **288**(1-2): p. 203-210.

67. Pham-Huu, C., N. Keller, L.J. Charbonniere, R. Ziessel, and M.J. Ledoux, *Carbon nanofiber supported palladium catalyst for liquid-phase reactions. An active and selective catalyst for hydrogenation of C=C bonds*. Chemical Communications, 2000(19): p. 1871-1872.
68. Pham-Huu, C., N. Keller, G. Ehret, L.J. Charbonniere, R. Ziessel, and M.J. Ledoux, *Carbon nanofiber supported palladium catalyst for liquid-phase reactions: An active and selective catalyst for hydrogenation of cinnamaldehyde into hydrocinnamaldehyde*. Journal of Molecular Catalysis A: Chemical, 2001. **170**(1–2): p. 155-163.
69. Nhut, J.M., R. Vieira, L. Pesant, J. P. Tessonnier, N. Keller, G. Ehret, C. Pham-Huu, and M. J. Ledoux, *Synthesis and catalytic uses of carbon and silicon carbide nanostructures*. Catalysis Today, 2002. **76**(1): p. 11-32.
70. Chizari, K., I. Janowska, M. Houllé, I. Florea, O. Ersen, T. Romero, P. Bernhardt, M.J. Ledoux, and C. Pham-Huu, *Tuning of nitrogen-doped carbon nanotubes as catalyst support for liquid-phase reaction*. Applied Catalysis A: General, 2010. **380**(1–2): p. 72-80.
71. Zhu, Y.J., and X. L. Hu, *Preparation of powders of selenium nanorods and nanowires by microwave-polyol method*. Materials Letters, 2004. **58**(7-8): p. 1234-1236.
72. Knupp, S.L., W. Li, O. Paschos, T. M. Murray, J. Snyder, and P. Haldar, *The effect of experimental parameters on the synthesis of carbon nanotube / carbon nanofiber supported platinum by polyol processing techniques*. Carbon, 2008. **46**(10): p. 1276-1284.
73. Chen, W., J. Zhao, J. Y. Lee, and Z. Liu, *Microwave heated polyol synthesis of carbon nanotubes supported Pt nanoparticles for methanol electrooxidation*. Materials Chemistry and Physics, 2005. **91**(1): p. 124-129.
74. Variava, M.F., T.L. Church, A.T. Harris, and A.I. Minett, *Polyol-assisted functionalization of carbon nanotubes-a perspective*. Journal of Materials Chemistry A, 2013. **1**(30): p. 8509-8520.

75. Harada, T., S. Ikeda, M. Miyazaki, T. Sakata, H. Mori, and M. Matsumura, *A simple method for preparing highly active palladium catalysts on various supports for liquid-phase oxidation and hydrogenation reactions*. Journal of Molecular Catalysis A: Chemical, 2007. **268**(1): p. 59-64.
76. Guo, Z., Y. Chen, L. Li, X. Wang, G.L. Haller, and Y. Yang, *Carbon nanotube-supported Pt-based bimetallic catalysts prepared by a microwave-assisted polyol reduction method and their catalytic applications in the selective hydrogenation*. Journal of Catalysis, 2010. **276**(2): p. 314-326.
77. Higgins, D.C., D. Meza, and Z. Chen, *Nitrogen-Doped Carbon Nanotubes as Platinum Catalyst Supports for Oxygen Reduction Reaction in Proton Exchange Membrane Fuel Cells*. Journal of Physical Chemistry C, 2010. **114**(50): p. 21982-21988.
78. Chen., Y., J. Wang, H. Liu, R. Li, X. Sun, S. Ye, and S. Knights, *Enhanced stability of Pt electrocatalysts by nitrogen doping in CNTs for PEM*. Electrochemistry Communications, 2009. **11**(10): p. 2071-2076.
79. Nieto-Márquez, A., S. Gil, A. Romero, J.L. Valverde, S. Gómez-Quero, and M.A. Keane, *Gas phase hydrogenation of nitrobenzene over acid treated structured and amorphous carbon supported Ni catalysts*. Applied Catalysis A: General, 2009. **363**(1-2): p. 188-198.
80. Moyo, M., M.A.M. Motchelaho, H. Xiong, L.L. Jewell, and N.J. Coville, *Promotion of Co/carbon sphere Fischer–Tropsch catalysts by residual K and Mn from carbon oxidation by KMnO₄*. Applied Catalysis A: General, 2012. **413–414**(0): p. 223-229.
81. Liu, Y.C., X.P. Qiu, Y.Q. Huang, and W.T. Zhu, *Methanol electro-oxidation on mesocarbon microbead supported Pt catalysts*. Carbon, 2002. **40**(13): p. 2375-2380.
82. Nongwe, I., V. Ravat, R. Meijboom, and N.J. Coville, *Efficient and reusable Co/nitrogen doped hollow carbon sphere catalysts for the aerobic oxidation of styrene*. Applied Catalysis A: General, 2013. **466**(0): p. 1-8.

83. Ravat, V., I. Nongwe, and N.J. Coville, *Palladium-Supported Boron-Doped Hollow Carbon Spheres as Catalysts for the Solvent-free Aerobic Oxidation of Alcohols*. ChemCatChem, 2012. **4**(12): p. 1930-1934.
84. Ravat, V., I. Nongwe, R. Meijboom, G. Bepete, and N.J. Coville, *Pd on boron-doped hollow carbon spheres – PdO particle size and support effects*. Journal of Catalysis, 2013. **305**(0): p. 36-45.
85. Nieto-Márquez, A., D. Toledano, P. Sánchez, A. Romero, and J.L. Valverde, *Impact of nitrogen doping of carbon nanospheres on the nickel-catalyzed hydrogenation of butyronitrile*. Journal of Catalysis, 2010. **269**(1): p. 242-251.
86. Maki-Arvela, P., J. Hajek, T. Salmi, D. Y. Murzin, *Chemoselective hydrogenation of carbonyl compounds over heterogeneous catalysts*. Applied Catalysis A: General, 2005. **292**: p. 1-49.
87. Santacesaria, E., *Kinetics and transport phenomena*. Catalysis Today, 1997. **34**(3–4): p. 393-400.
88. Toebes, M.L., T. Alexander Nijhuis, J. Hájek, J.H. Bitter, A. Jos van Dillen, D.Y. Murzin, and K.P. de Jong, *Support effects in hydrogenation of cinnamaldehyde over carbon nanofiber-supported platinum catalysts: Kinetic modeling*. Chemical Engineering Science, 2005. **60**(21): p. 5682-5695.
89. Neri, G., L. Bonaccorsi, and S. Galvagno, *Kinetic Analysis of Cinnamaldehyde Hydrogenation over Alumina-Supported Ruthenium Catalysts*. Industrial & Engineering Chemistry Research, 1997. **36**(9): p. 3554-3562.
90. Vergunst, T., F. Kapteijn, and J.A. Moulijn, *Kinetics of cinnamaldehyde hydrogenation–concentration dependent selectivity*. Catalysis Today, 2001. **66**(2–4): p. 381-387.
91. Marchi, A.J., J.F. Paris, N.M. Bertero, and C.R. Apesteguía, *Kinetic Modeling of the Liquid-Phase Hydrogenation of Cinnamaldehyde on Copper-Based Catalysts*. Industrial & Engineering Chemistry Research, 2007. **46**(23): p. 7657-7666.

92. Delbecq, F. and P. Sautet, *Competitive C \equiv C and C \equiv O Adsorption of α - β -Unsaturated Aldehydes on Pt and Pd Surfaces in Relation with the Selectivity of Hydrogenation Reactions: A Theoretical Approach*. Journal of Catalysis, 1995. **152**(2): p. 217-236.
93. Ponec, V., *On the role of promoters in hydrogenations on metals; α , β -unsaturated aldehydes and ketones*. Applied Catalysis A: General, 1997. **149**(1): p. 27-48.
94. Planeix, J.M., N. Coustel, B. Coq, V. Brotons, P.S. Kumbhar, R. Dutartre, P. Geneste, P. Bernier, and P.M. Ajayan, *Application of Carbon Nanotubes as Supports in Heterogeneous Catalysis*. Journal of the American Chemical Society, 1994. **116**(17): p. 7935-7936.
95. Toebe, M.L., F.F. Prinsloo, J.H. Bitter, A.J. van Dillen, and K.P. de Jong, *Influence of oxygen-containing surface groups on the activity and selectivity of carbon nanofiber-supported ruthenium catalysts in the hydrogenation of cinnamaldehyde*. Journal of Catalysis, 2003. **214**(1): p. 78-87.
96. Lepró, X., E. Terrés, Y. Vega-Cantú, F.J. Rodríguez-Macías, H. Muramatsu, Y.A. Kim, T. Hayahsi, M. Endo, M. Torres R, and M. Terrones, *Efficient anchorage of Pt clusters on N-doped carbon nanotubes and their catalytic activity*. Chemical Physics Letters, 2008. **463**(1-3): p. 124-129.
97. Amadou, J., K. Chizari, M. Houllé, I. Janowska, O. Ersen, D. Bégin, and C. Pham-Huu, *N-doped carbon nanotubes for liquid-phase CC bond hydrogenation*. Catalysis Today, 2008. **138**(1-2): p. 62-68.

CHAPTER 3

The synthesis of nitrogen doped carbon spheres by non - catalytic chemical vapour deposition.*

3.1 Introduction

The discovery of buckminsterfullerenes in 1985 prompted increased research interest into spherical carbon structures in the scientific community [1]. These fullerenes are single walled hollow spheres made with a continuous carbon layer. The other well known type of carbon spheres (CSs) is made with a discontinuous carbon layer. These latter types of CSs have been of particular interest because they possess the following properties: light weight, high surface area, high thermal stability, high strength and unique electronic properties. This makes them useful in many fields of science and technology to develop electronic devices, catalyst support materials, high strength composites, lubricants just to mention a few [2]. CSs can be classified as solid, core - shell or hollow [3]. Inagaki classified spherical carbon structures according to the arrangement of carbon layers as being concentric, radial or random [4]. Serp *et al* classified spherical carbon materials according to size: fullerenes C_n (less than 2 nm), carbon onions (2 - 20 nm), CSs (50 - 1000 nm) and carbon beads (above 1 μ m) [5]. Lastly carbon spheres can be classified according to the synthesis method employed to make them.

The addition of nitrogen into carbon nanomaterials is widely used to modify the structural, chemical and electronic properties of the resulting doped carbon materials. Doping of carbonaceous materials can be done by either in situ doping (the N is added to the carbon structure during its synthesis) or post synthesis doping (carbon

material is first made then the doping element is incorporated). The incorporation of nitrogen in carbon nanotubes results in improved conductivity, polarity and basicity, while modifying the surface hydrophilicity [6]. Nitrogen is an n-type dopant with an extra electron which can be donated when replacing carbon in the carbon matrix.

There are various methods which have been employed to produce nitrogen doped carbon spheres and these include chemical vapour deposition (CVD) methods in the absence of catalyst or template [7-10], combination of a CVD template synthesis method [11, 12] and pyrolysis and / or polymerization reactions [13-15]. There are very few reports which are cited in literature on the synthesis of NCSs using the CVD method in the absence of a catalyst or template. Deshmukh et al. managed to synthesize NCSs using a non - catalytic CVD method using acetylene as the C source and ammonium hydroxide or acetonitrile solutions as the N sources at carbonization temperatures and times of 900 °C and 2 hours respectively [7]. The NCSs had diameters ranging from 400 - 750 nm and 1 - 1.5 wt. % nitrogen content. Zhou *et al* made NCSs by introducing a nebulized solution of different ratios of ethylenediamine and xylene into a quartz tube heated at 1000 °C with no catalyst present [9]. It was found that the N content (0 - 6.2 wt. %) and sphere size (130 - 500 nm) for the NCSs could be controlled by varying the ratios of ethylenediamine and xylene and the reaction times. Nieto - Marquez et al. reported on the controlled production of NCSs via pyrolysis of aniline and nitrobenzene at 950 °C using a CVD method [10]. It was observed that the N incorporation increased with increased reaction times and also the nature of the feed. NCSs with uniform diameters of approximately 700 nm, BET surface areas of 3.4 m² / g and 2 wt. % N were successfully synthesized using CVD method at 900 °C for 1 hour with acetylene and an ammonia solution as C and N sources [8].

There are a very few systematic reports cited in literature which have investigated different parameters such as the nature or type of N source [7, 9, 10], reaction temperature, reaction time [9, 10], to see their effects on the resultant nitrogen doped carbon spheres synthesized. In this chapter, we report on the synthesis of NCSs using a CVD method in the absence of a catalyst or template. The effects of varying experimental parameters (pyrolysis time, pyrolysis temperature and different flow rates of gases during pyrolysis step) are studied in depth. The physical and chemical properties and nitrogen incorporation in the carbon nanostructures are discussed.

3.2 Experimental

3.2.1 Synthesis of NCSs

The synthesis of NCSs was performed according to the procedure reported by Deshmukh et al. [7] with a few modifications. NCSs were synthesized using a non-catalytic chemical vapor deposition (CVD) method where acetylene (C_2H_2) was used as a carbon source and acetonitrile (CH_3CN) was the N source. N_2 was first flowed through a quartz tube at 100 ml / min while the furnace was heated from room temperature to the desired temperature at a heating rate of 10 $^{\circ}C$ / min to create an inert atmosphere. Once the desired temperature was reached the N_2 flow was switched off and C_2H_2 was bubbled through CH_3CN (80 $^{\circ}C$) at a flow rate of 100 ml / min for the required carbonization time. After the required carbonization time, the C_2H_2 flow was switched off and N_2 was flowed through the system at 100 ml / min until the furnace had cooled down to room temperature. NCSs were then collected from the walls of the quartz tube and weighed. The volume of CH_3CN used in the reaction was also recorded. Summary of experimental conditions are shown in Table 3.1. For more details see Appendix.

Table 3.1. CVD experimental conditions ^a.

Experiment number	Carbonization temperature (°C)	Carbonization time (minutes)	Flow rate of gases during carbonization step (ml / min)	
			C ₂ H ₂	N ₂
Experiment 1	800	120	100	100
	850			
	900			
	950			
	1000			
Experiment 2	950	5	100	0
		10		
		30		
		60		
		90		
		120		
		150		
		180		
		240		
Experiment 3	950	90	50	50
			80	20
			100	0
			200	0

^a Heating rate of 10 °C / min, CH₃CN heated to 80 °C and 100 ml / min N₂ used during the heating up and cooling of the furnace were all kept constant.

3.2.2 Characterization techniques

The morphology of the NCSs was characterized by transmission electron microscopy (TEM). A spatula tip of the sample was mixed with methanol and the mixture was sonicated for 1 minute. A drop of the suspension was transferred onto a SPI carbon coated copper grid and allowed to dry before analysis. TEM examinations were conducted using a FEI Technai G² Spirit electron microscope operated at 120 kV. The composition of carbon and nitrogen in the NCSs was determined by CN elemental analysis using a Carlo Erba NA1500 Nitrogen Carbon Sulphur analyzer. Approximately 1.0 - 1.5 mg of sample was used for the analysis, a GC equipped with a thermal conductivity detector (TCD) was used to separate the gases produced. Scanning X-ray photoelectron spectroscopy (XPS) was used to determine the elemental composition in the carbon spheres. The binding energy was recorded on a Physical Electronics Quantum2000 instrument using AlK α X-rays at a power of 20 W. The beam diameter was 100 μ m. Raman spectra were recorded using a Jobin - Yvon T6400 micro - Raman spectrometer equipped with a liquid nitrogen cooled charge coupled device detector. The thermal stability of the NCSs was determined by thermogravimetric analysis (TGA) using a Perkin Elmer Pyris 1 TGA. Approximately 10 mg of sample was used for the analysis and the samples were heated from room temperature up to 950 °C at a heating rate of 5 °C / min in air atmosphere (20 ml / min). For more details see Appendix.

3.3 Results and Discussion

A detailed description on the effect of temperature, time and flow rates of gases during the carbonization step was investigated. The product morphology, size, composition, thermal stability and the degree of crystallinity of the carbon products produced is discussed below.

3.3.1 Variation of carbonization temperature

TEM was used to study the morphology and particle size of the carbon sphere products formed at various temperatures. The effects of carbonization temperature on the physical and chemical characteristics of NCSs were studied. The temperatures used were 700, 800, 850, 900, 950 and 1000 °C. TEM images of NCSs produced at the different temperatures and their corresponding particle size distribution graphs are shown in Figures 3.1 and 3.2 respectively. At 700 °C, a mixture of carbon spheres and amorphous carbon was produced. The size distribution of the spheres produced was not obtained because their yield was very low. Further, the presence of amorphous carbon is a disadvantage since only carbon spheres were required. No further characterization techniques were done for samples produced at 700 °C. Table 3.2 gives a summary of the morphology and particle size distribution of carbon spheres produced at different temperatures. Figure 3.3 shows the average diameter of the NCSs as a function of temperature. Increasing the carbonization temperature between 800 and 900 °C did not have a significant effect on the CS diameters. They remained nearly the same. However increasing the temperature between 950 and 1000 °C, the CS diameters did decrease. Jin and co - workers have also reported that increasing the pyrolysis temperatures and keeping reaction times constant did not affect the CS diameters significantly [16].

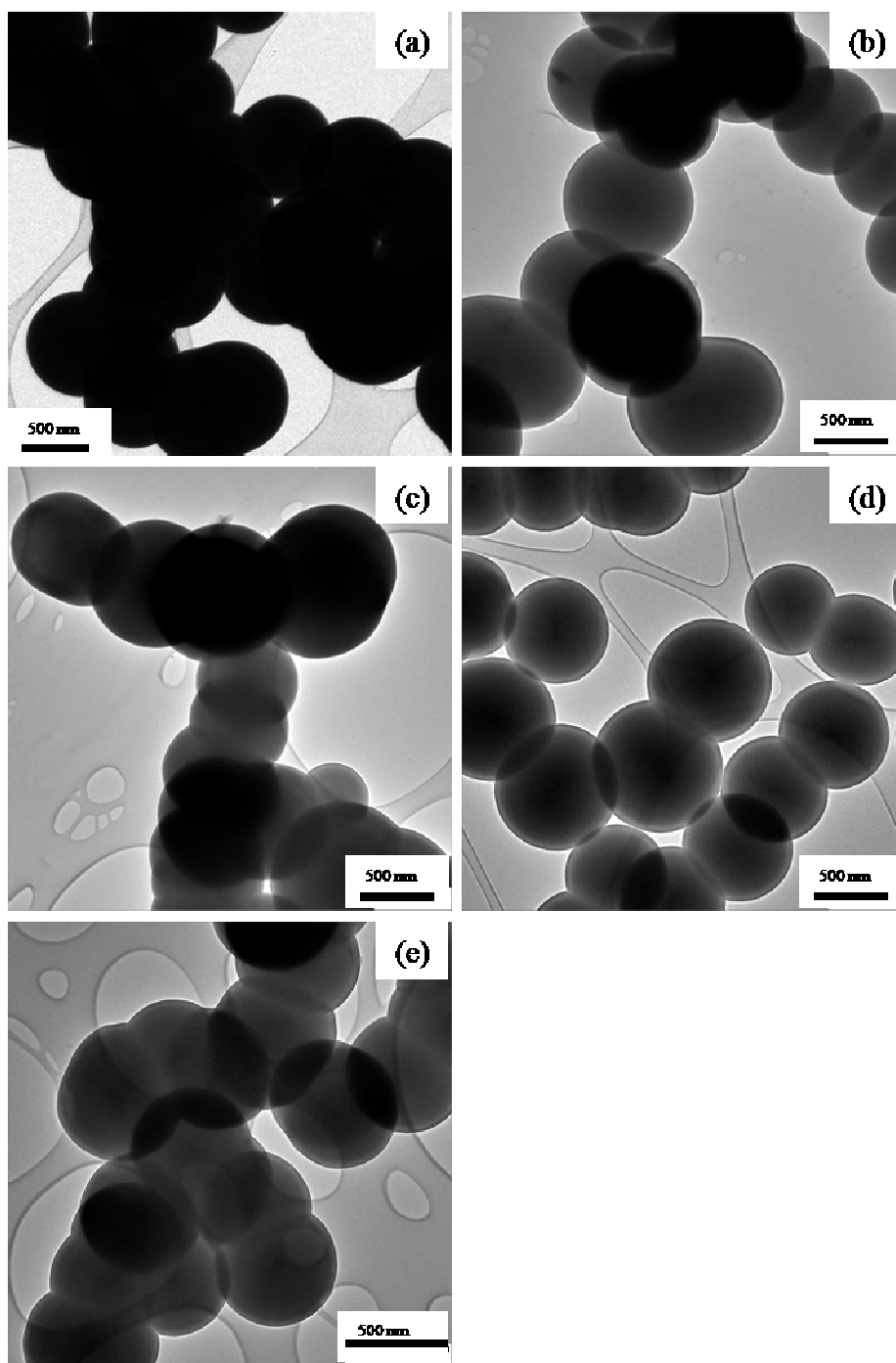


Figure 3.1. TEM images and the corresponding size distribution graphs of NCSs synthesized at (a) 800 °C, (b) 850 °C, (c) 900 °C, (d) 950 °C and (e) 1000 °C using C_2H_2 as a carbon source (100 ml / min), CH_3CN (80 °C) as a nitrogen source and a carbonization time of 120 minutes.

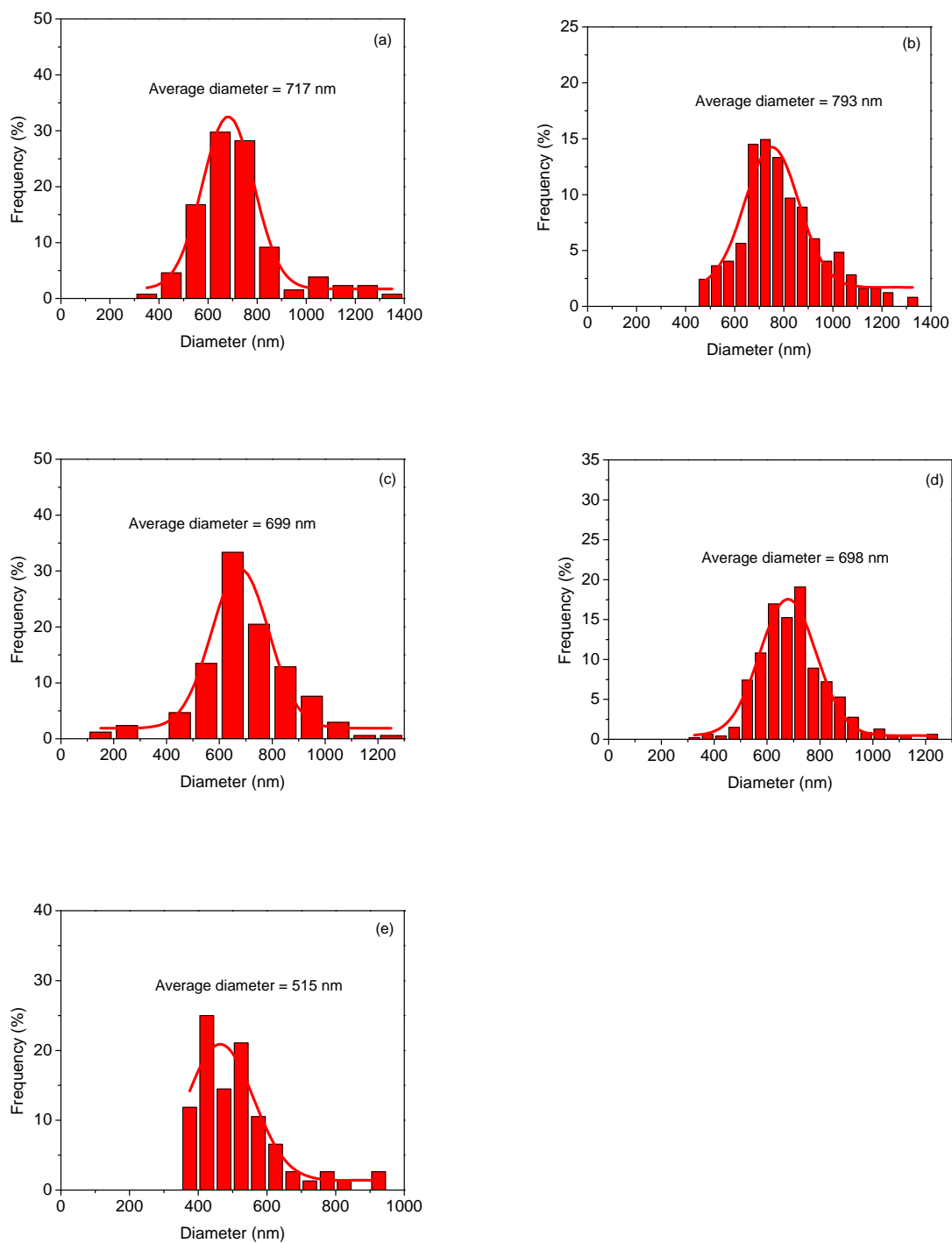


Figure 3.2. TEM images and the corresponding size distribution graphs of NCSs synthesized at (a) 800 °C, (b) 850 °C, (c) 900 °C, (d) 950 °C and (e) 1000 °C.

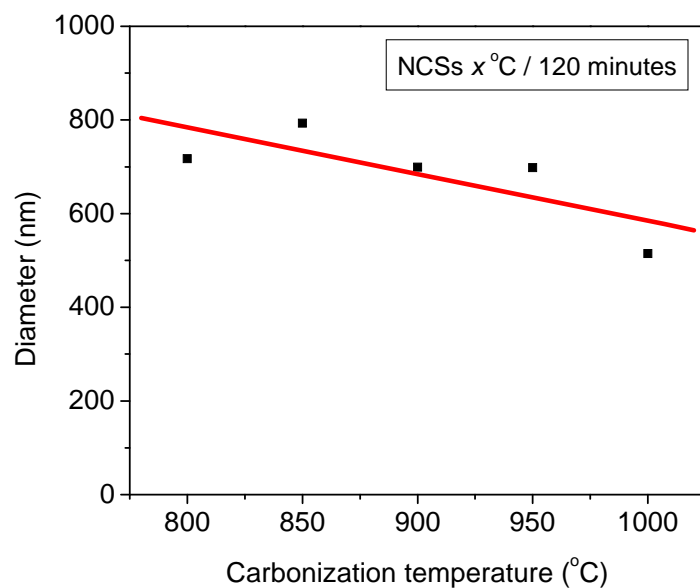


Figure 3.3. Graph showing average diameter of NCSs as a function of carbonization temperature.

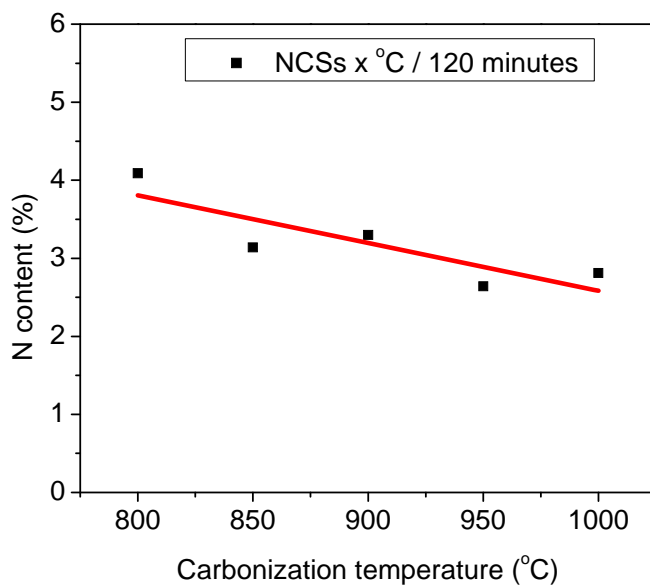


Figure 3.4. N content as a function of carbonization temperature.

C and N elemental analysis was used to show the incorporation of nitrogen in the carbon sphere matrixes synthesized at various carbonization temperatures. The NCSs produced at 800, 850, 900, 950 and 1000 °C had N concentrations of 4.09, 3.14, 3.30, 2.64 and 2.81 wt. % N respectively. Figure 3.4 shows the effect of variation of carbonization temperature on the N content of the NCSs formed. The N concentration of the NCSs decreased linearly as the carbonization temperature was increased. These results were similar to those reported previously by Bepete et al., Yadav et al. and van Dommele et al. where the N content in N - CNTs decreased with increasing CVD temperature [17-19]. It has been suggested that at higher carbonization temperatures N forms radicals which do not bond with carbon, hence the decrease in N concentration as the carbonization temperature was increased. Maldonado and co-workers studied the formation of N - CNTs using NH₃ gas as the N source and pyridine as the C source [20]. They showed that at higher temperatures the decomposition of NH₃ in the presence of carbon containing materials produced free radicals such as NH₂. At low temperatures, N incorporation in CNT structures is done with the free radicals and at high temperature levels the radicals attack the graphitic carbon and enhance the gasification to methane and cyanogen species. Carroll and co-workers found that at low synthesis temperatures, there was a higher incorporation of nitrogen in CNTs compared to higher temperature synthesis and this in turn led to a higher number of defects in the CNT structures which provided nitrogen insertion sites [21]. Their explanation was that at higher temperatures the C - C bonds have higher bond dissociation energies compared to C - N bonds. This in turn favours the formation of C - C bonds and N₂, so there is no incorporation of N in CNTs at higher temperatures. These authors' explanations could also be used to explain the decrease of N content as the carbonization temperature was increased as found in this study.

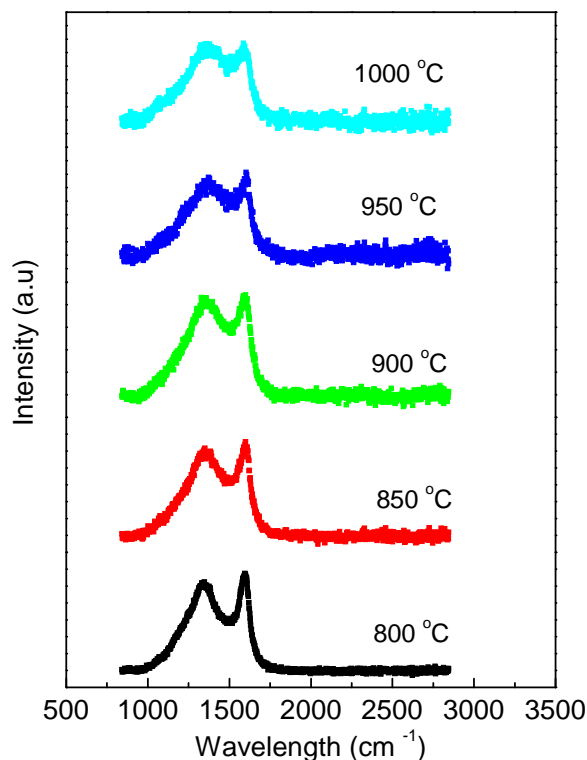


Figure 3.5. Raman spectra of NCSs synthesized at different carbonization temperature. Carbonization time was kept constant at 120 minutes. C_2H_2 was bubbled through CH_3CN at 80 °C.

Raman spectroscopy was used in this study to gain information about the degree of order in the carbon nanomaterials. The Raman spectra of NCSs synthesized at different carbonization temperatures are shown in Figure 3.5. All the Raman spectra showed two characteristic peaks at 1350 - 1382 nm and 1593 - 1600 nm which correspond to the D and the G bands respectively. The D band is attributed to the presence of disordered amorphous carbon and double resonance effects in sp^2 carbon, while the G band is attributed to the E_{2G} vibration mode that is present due to the sp^2 bonded graphitic carbon [22, 23]. The D band to G band intensity ratio (I_D / I_G) is used to measure the degree of defects in the NCSs. The Raman data and I_D / I_G ratios

of the NCSs are shown in Table 3.2. The I_D / I_G ratios increased as the carbonization temperature was increased. This however is not in agreement with TGA results and CN elemental results. Ordinarily the I_D / I_G ratios should decrease with increasing CVD temperature as the N introduced into the carbon matrixes decreased which means there are less N type defects in the samples.

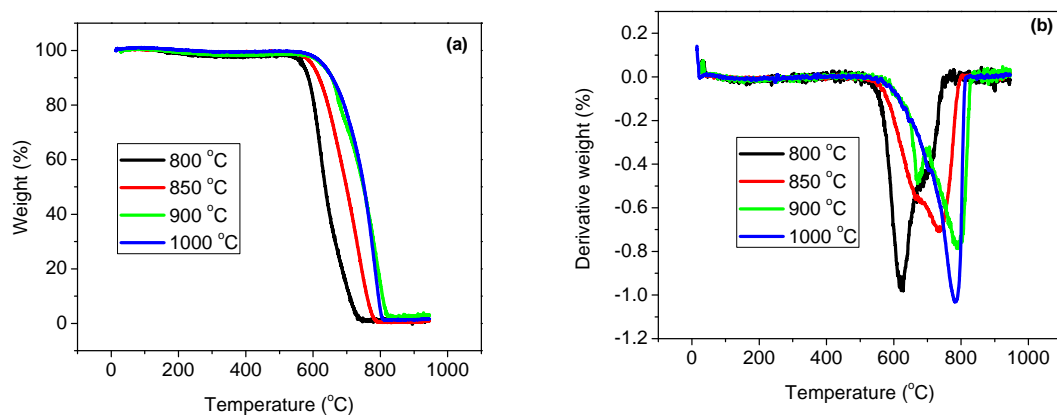


Figure 3.6. (a) TGA and (b) corresponding derivative weight loss graphs of NCSs synthesized at different carbonization temperatures. Carbonization time was kept constant at 120 minutes. C_2H_2 was bubbled through CH_3CN at 80 °C.

Thermogravimetric analysis (TGA) was used to study the thermal stability of the NCSs. The TGA graphs and the corresponding derivative weight graphs of NCSs synthesized at different carbonization temperatures are shown in Figure 3.6. For all samples made at the different pyrolysis temperatures, no weight loss was observed at temperatures below 500 °C confirming the TEM findings that no amorphous carbon was present in the samples. Landi and co - workers reported that amorphous carbon normally burns off in air between 300 and 400 °C in single walled carbon nanotubes (SWNTs) samples [24]. NCSs synthesized using differing furnace temperatures showed increasing stability with respect to thermal oxidation as the synthesis

temperature increased from 800 to 1000 °C. Two decomposition peaks are observed in each of the derivative weight graphs which occur in the temperature ranges of approximately 621 - 701 °C and 708 - 785 °C respectively. The two decomposition peaks can be assigned to the oxidation of carbon in the NCSs and oxidation of graphite. McKee and Vecchio studied the thermogravimetric analysis data of a sample containing a mixture of carbon nanotubes and graphite and saw two weight loss peaks corresponding to nanotube burn off and graphite burn off at 570 and 760 °C respectively [25]. As the synthesis temperature increased from 800 to 1000 °C, the burn off temperature of the two peaks shifted to higher temperatures, indicating increased formation of more stable or less defected NCSs and lower N incorporation into the carbon nanostructures (data in Table 3.2). CN elemental analysis results supports the TGA results for samples synthesized at pyrolysis temperatures of 800, 850, 900, 950 and 1000 °C. The nitrogen content in the spheres decreased with an increase in carbonization temperature from 800 to 1000 °C. As the N content increased the thermal stability decreased.

Table 3.2. NCSs diameter range, elemental (CN) composition, D, G bands and I_D / I_G ratios and gasification temperature of NCSs synthesized at different temperatures. Carbonization time was kept constant at 120 minutes. C_2H_2 was bubbled through CH_3CN at 80 °C.

Carbonization temperature (°C)	Diameter range (average) (nm)	C (%)	N (%)	D - band (cm^{-1})	G - band (cm^{-1})	I_D / I_G	Decomposition temperature (°C)
800	360 - 1342 (721)	94.46	4.09	1356	1593	1.03	621, 708
850	455 - 1097 (714)	93.26	3.14	1366	1597	1.24	664, 738
900	432 - 1103 (678)	96.58	3.30	1370	1596	1.37	671, 789
950	342 - 1220 (698)	97.22	2.64	1382	1600	1.51	
1000	273 - 723 (451)	98.12	2.81	1379	1594	1.68	701, 785

3.3.2 Variation of carbonization time

The pyrolysis of C_2H_2 and CH_3CN for different times (5 - 240 minutes) was investigated. Figures 3.7, 3.8 and 3.9 shows the TEM images and corresponding sphere size distribution graphs of the black carbon soot produced in the experiments. All the TEM images of the products produced from the pyrolysis of acetylene and acetonitrile at different times consisted of 100 % carbon spheres with smooth surfaces. The carbon spheres appear as chains of bead like accretions at all the carbonization times. For pyrolysis times 5 - 60 minutes, the texture of the carbon soot produced was soft, light and was in the form of cotton like particles. However as the carbonization time was increased from 90 - 240 minutes, the carbon soot produced contained a mixture of the soft, light and cotton like carbon soot and hard, solid sand - like particles of carbon soot. Jin et al. and Miao et al. observed similar results of hard sand like particles being produced at longer pyrolysis times [16, 26]. The hard, solid, sand - like particles were found to be caused by long periods of annealing of the carbon spheres at high temperatures under a continuous flow of the carbon source.

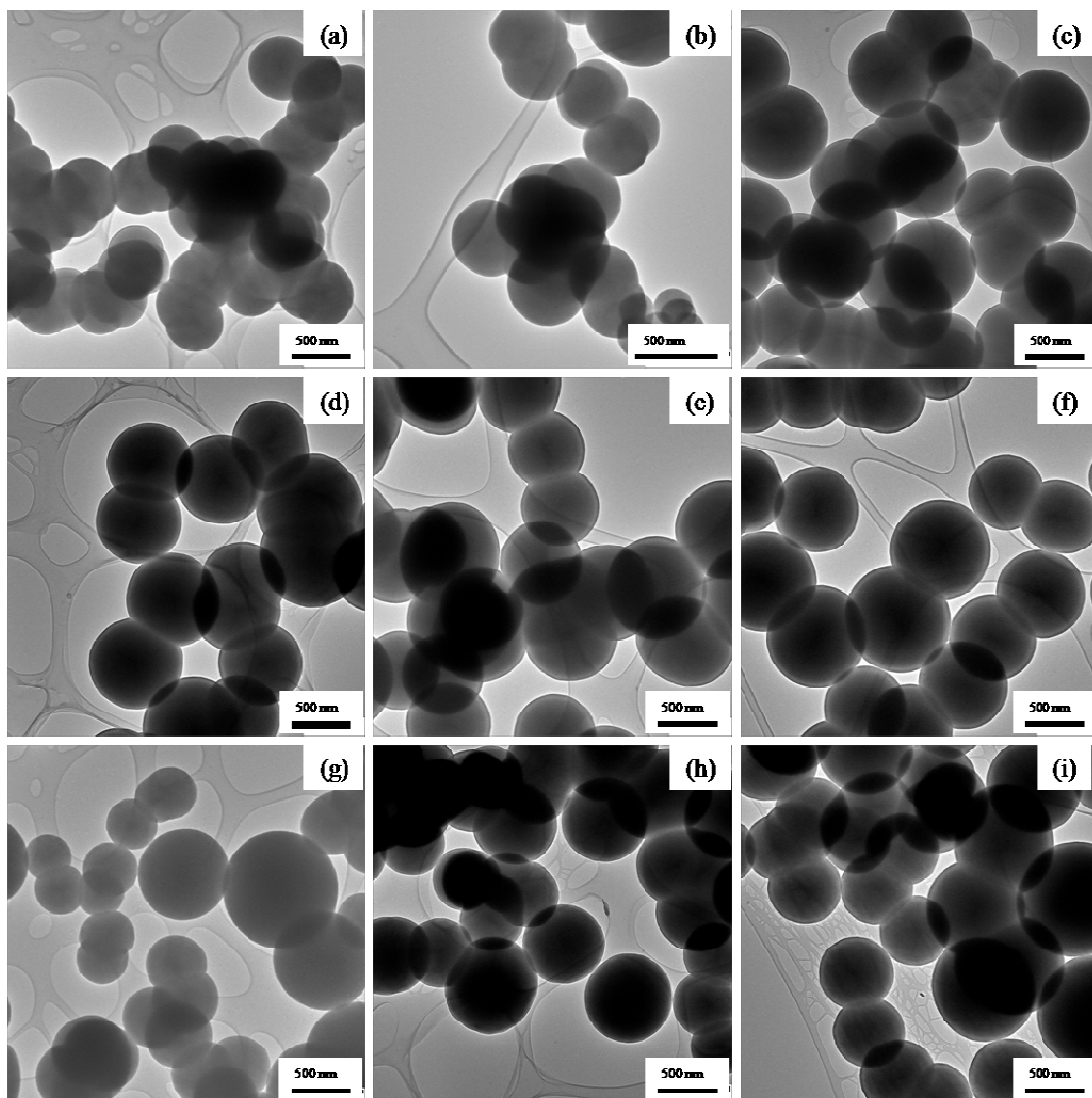


Figure 3.7. TEM images of NCSs synthesized at (a) 5 minutes, (c) 30 minutes, (d) 60 minutes, (e) 90 minutes, (f) 120 minutes, (g) 150 minutes, (h) 180 minutes and (i) 240 minutes using C_2H_2 as a carbon source (100 ml / min), CH_3CN (80 °C) as a nitrogen source and carbonization temperature of 950 °C.

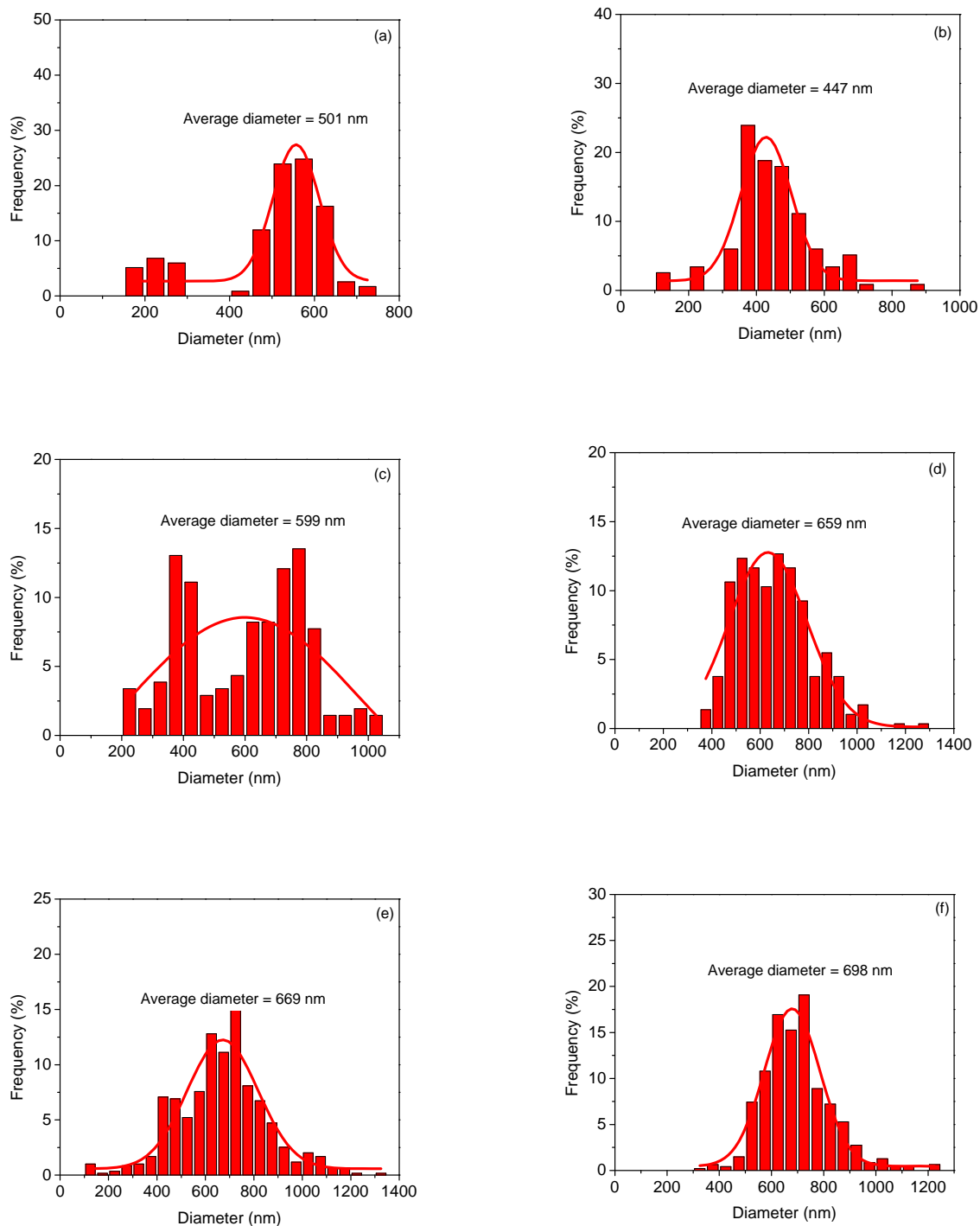


Figure 3.8. Particle size distribution graphs of (a) NCSs 950 °C / 5 minutes, (b) NCSs 950 °C / 10 minutes, (c) NCSs 950 °C / 30 minutes, (d) NCSs 950 °C / 60 minutes, (e)

NCSs 950 °C / 90 minutes and (f) NCSs 950 °C / 120 minutes. C source = C₂H₂ (100 ml / min), N source = CH₃CN (80 °C) and T = 950 °C.

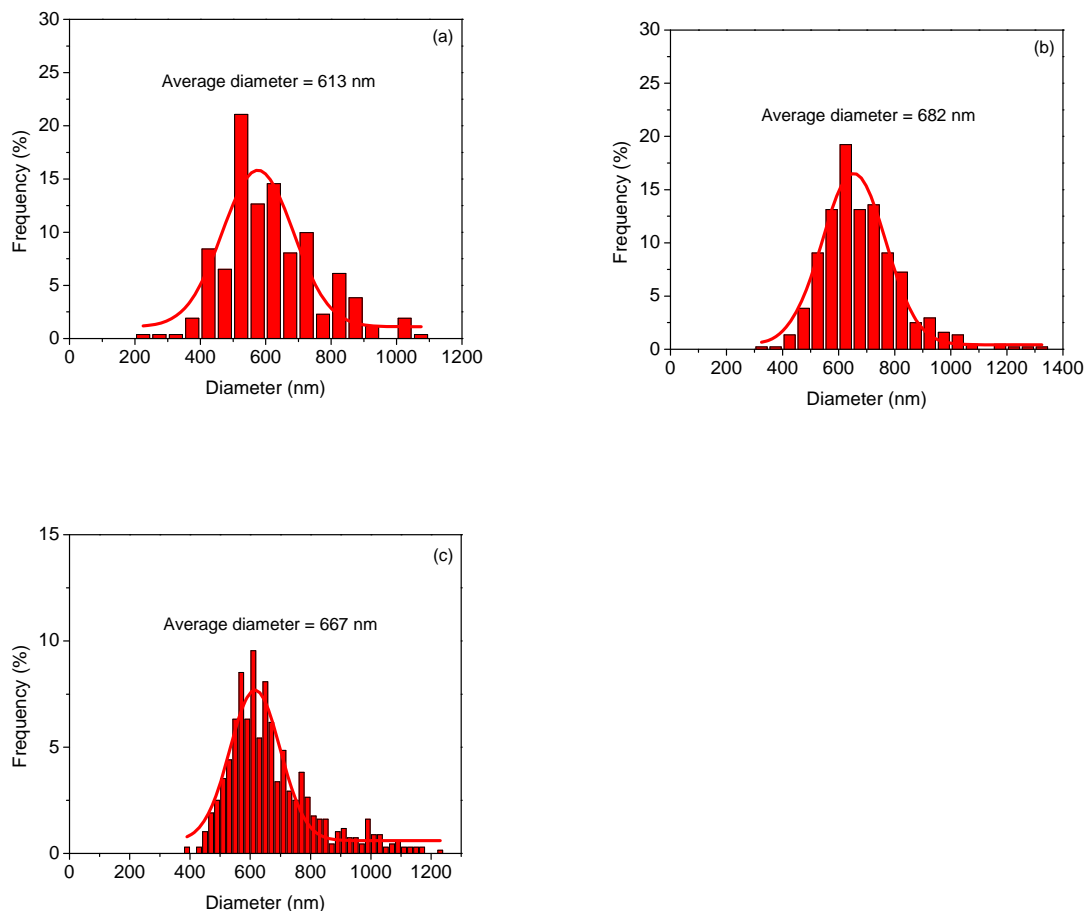


Figure 3.9. Particle size distribution graphs of (a) NCSs 950 °C / 150 minutes, (b) NCSs 950 °C / 180 minutes and (c) NCSs 950 °C / 240 minutes. C source = C₂H₂ (100 ml / min), N source = CH₃CN (80 °C) and T = 950 °C.

Table 3.3 shows the NCS diameter range, elemental (CN) composition, D, G bands and I_D / I_G ratios, gasification temperature and BET surface areas and pore volumes of

NCSs synthesized at different times. The average diameter of the NCSs increased with an increase in carbonization time (Table 3.3 and Figures 3.8 and 3.9). The increase in the average diameter of the spheres with increase in time is caused by long periods of annealing of the spheres at high temperatures at the same positions along the quartz tube with continuous carbon and nitrogen supply flowing through the system. The carbon and nitrogen precursors are pyrolysed at a faster rate at high temperatures which allows for more carbon to be deposited on the spheres enabling them to become bigger in size. Similar results were obtained by Jin and co - workers, they found that increasing the feed time of styrene from 2 to 5 minutes at 1100 °C led to larger spheres with diameters increasing from 300 - 400 nm to 600 - 700 nm [16]. The variation of carbonization time plays a key role in controlling the diameters of carbon spheres produced.

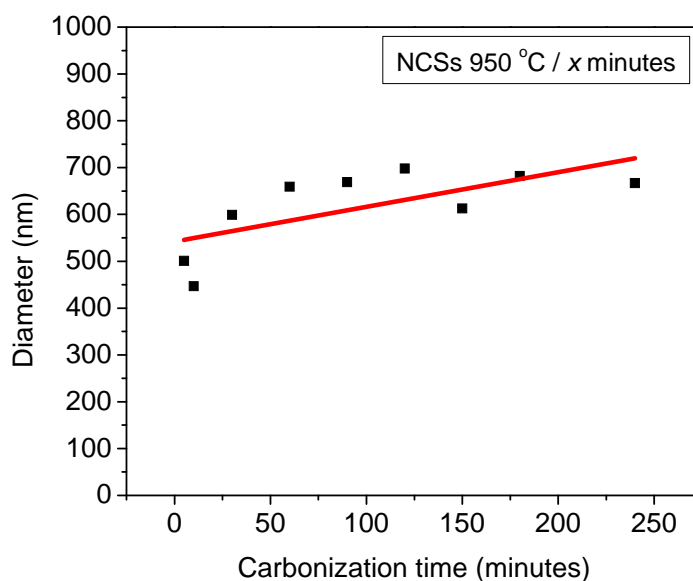


Figure 3.10. Graph showing average diameter of NCSs as a function of carbonization time.

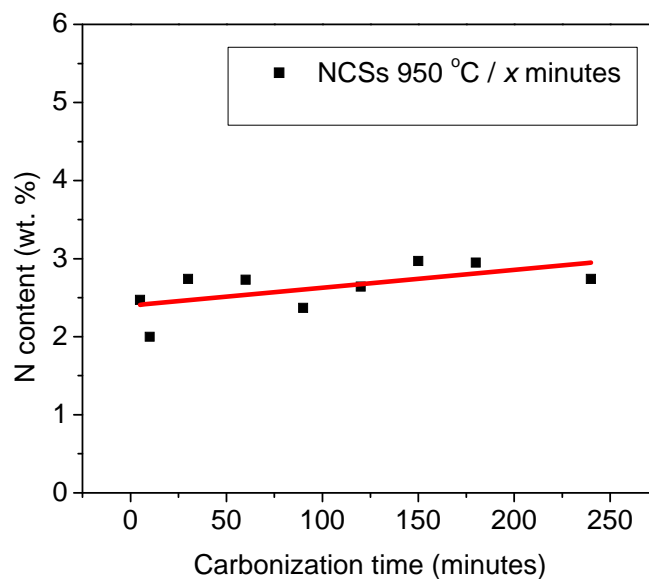


Figure 3.11. Graph showing N content as a function of carbonization time.

The effect of variation of carbonization time on the N content of the NCSs formed was investigated (Figure 3.11). Variation of carbonization time had a small effect on the N concentration of the NCSs. The N concentration between 5 - 240 minutes varied between 2.00 and 2.97 wt. % (Table 3.3). The N content increased slightly as the carbonization time was increased.

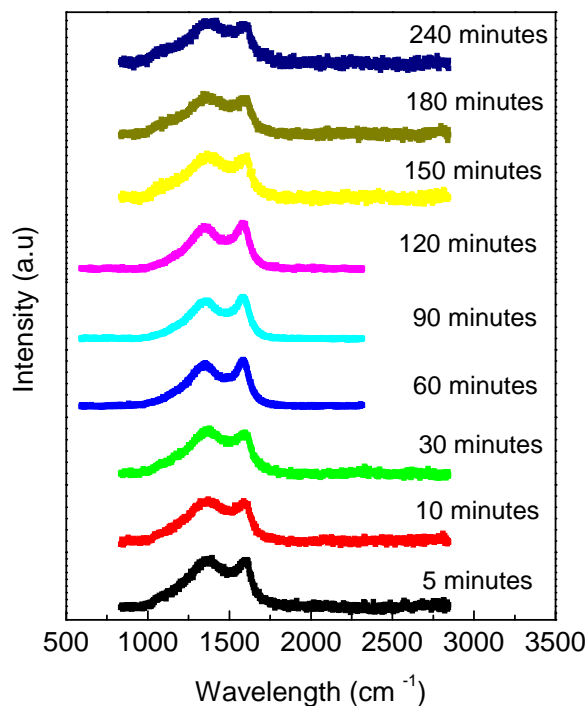


Figure 3.12. Raman graphs of NCSs synthesized at different carbonization times. Carbonization temperature was kept constant at 950 °C. C₂H₂ was bubbled through CH₃CN at 80 °C.

The graphitic nature as well as the disorder of the NCSs synthesized using different carbonization times was investigated by the use of Raman spectroscopy studies. The Raman spectra of NCSs synthesized at different carbonization times are shown in Figure 3.12. All the Raman spectra showed two characteristic peaks at 1349 - 1386 nm and 1588 - 1598 nm which correspond to the D and the G band respectively. The D band to G band intensity ratio (I_D / I_G) is used to measure the degree of defects in the NCSs. The Raman data and I_D / I_G ratios of the NCSs are shown in Table 3.3. The I_D / I_G ratios remained nearly constant with increase in carbonization time. There was a slight increase of the I_D / I_G ratio with increase in carbonization time suggesting that

the relative degree of order in the NCSs decreased with an increase in CVD time. This is also consistent with the N content studies: more nitrogen was incorporated into the carbon sphere matrix with increasing carbonization time.

Thermogravimetric analysis was used to study the crystallinity of the NCSs produced at different carbonization times. Less ordered materials react with the oxidant (air) and lose weight at lower temperatures during gasification. Figure 3.13 shows the TGA profiles and the corresponding derivative weight curves of NCSs synthesized at different pyrolysis times. For all samples made at the different pyrolysis times, no weight loss was observed at temperatures below 500 °C confirming findings from TEM that no amorphous carbon had been formed in the reaction. The derivative weight loss graphs for NCSs synthesized at 5, 10 and 30 minutes pyrolysis time show one sharp oxidation peak which has a shoulder peak. The sharp and shoulder peaks which occur in the temperature ranges of 654 - 763 °C are due to the oxidation of the carbon in the NCSs and undoped CSs (Table 3.3). The derivative weight loss graphs for NCSs synthesized at 60, 90, 120, 150, 180 and 240 minutes show two sharp peaks. The first and second peaks occur in the temperature ranges of 597 - 618 °C and 768 - 808 °C respectively and they correspond to the oxidation of the NCSs and of graphite and or undoped CSs. The mass loss maximum of the first sharp peaks obtained from the derivative weight loss curves were seen to decrease from approximately 695 to 597 °C with increasing pyrolysis time. This is due to the increase in nitrogen content of the NCSs as the pyrolysis time is increased which suggests that more defects and disorder were present (Table 3.3 and Figure 3.11). The TGA results further confirmed the findings obtained from CN elemental analysis and RAMAN spectroscopy.

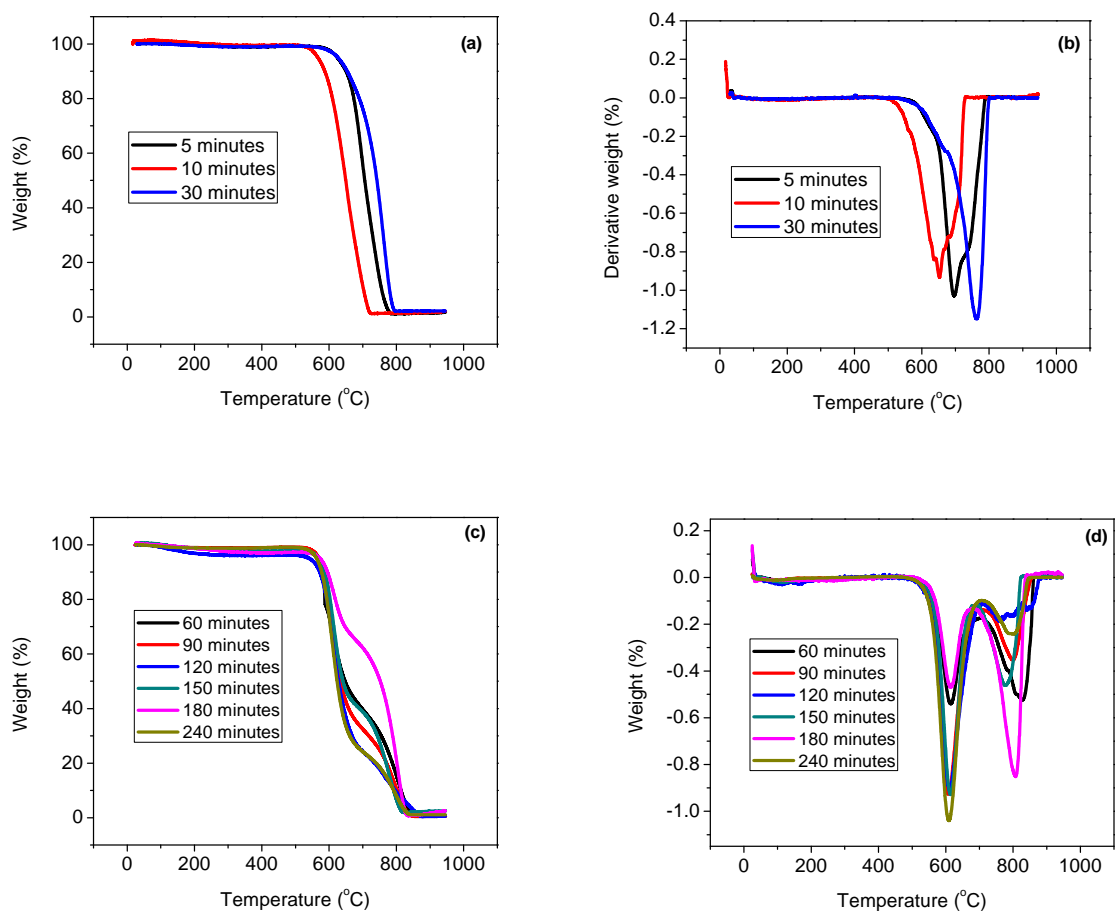


Figure 3.13. TGA and corresponding derivative weight loss graphs of NCSs synthesized at different carbonization times. Carbonization temperature was kept constant at 950 °C. C_2H_2 was bubbled through CH_3CN at 80 °C.

Table 3.3. NCSs diameter range, elemental (CN) composition, D, G bands and I_D / I_G ratios and gasification temperature of NCSs synthesized at different times. Carbonization temperature was kept constant at 950 °C. C_2H_2 was bubbled through CH_3CN at 80 °C.

Carbonization time (minutes)	Diameter range (average) (nm)	C (%)	N (%)	D - band (cm⁻¹)	G - band (cm⁻¹)	I_D / I_G	Decomposition temperature (°C)
5	167 - 726 (501)	97.47	2.47	1384	1598	1.64	695, 738
10	114 - 869 (447)	97.77	2.00	1379	1594	1.67	654, 685
30	206 - 1012 (599)	96.96	2.74	1386	1595	1.83	661, 763
60	370 - 1268 (659)	92.47	2.73	1349	1589	1.23	618, 808
90	118 - 1349 (669)	95.54	2.37	1357	1590	1.38	607, 802
120	342 - 1220 (698)	97.22	2.64	1355	1590	1.51	607, 761
150	242 - 1067 (613)	96.61	2.97	1380	1595	1.70	597, 812
180	333 - 1301 (682)	97.57	2.95	1379	1595	1.81	608, 768
240	383 - 1226 (667)	97.62	2.74	1370	1588	1.60	611, 798

3.3.3 Variation of flow rates of gases

Use of different flow rates of acetylene and nitrogen gases during the carbonization step was investigated to see if this had an effect on the properties of NCSs produced. All other experimental parameters such as carbonization temperature (950 °C), time (90 minutes) and the source of N (CH₃CN, 80 °C) were kept constant. The notations used for samples under investigation are noted below:

FR 50 + 50: 50 ml / min C₂H₂ + 50 ml / min N₂

FR 80 + 20: 80 ml / min C₂H₂ + 20 ml / min N₂

FR 100 + 0: 100 ml / min C₂H₂ + 0 ml / min N₂

FR 200 + 0: 200 ml / min C₂H₂ + 0 ml / min N₂

The TEM images and corresponding particle size distribution graphs of FR 50 + 50, FR 80 + 20, FR 100 + 0 and FR 200 + 0 samples are shown in Figure 3.14. All samples formed using different flow rates of gases during the pyrolysis step were of perfect spherical morphology. The average diameters of spheres were 653, 629, 669 and 236 nm for the samples FR 50 + 50, FR 80 + 20, FR 100 + 0 and FR 200 + 0 respectively. Increasing the acetylene flow rate and decreasing the nitrogen flow rates had little effect of on the average diameter of the NCSs formed. Samples FR 80 + 20 and FR 50 + 50 had average diameters of 629 and 653 nm respectively. However increasing the acetylene flow rate and eliminating the nitrogen gas introduced during the pyrolysis step had a huge effect on the average diameters of the NCSs formed. This was shown by FR 100 + 0 and FR 200 + 0 samples which had average diameters of 669 and 236 nm. The decrease in the average diameters of the NCSs when higher flow rates of acetylene were used could be due to the short residence time of the spheres in the hot region of the quartz tube. The NCSs are

pushed to the outer end of the tube as they are being formed so there is very little time for them to be continuously heated or annealed and become bigger.

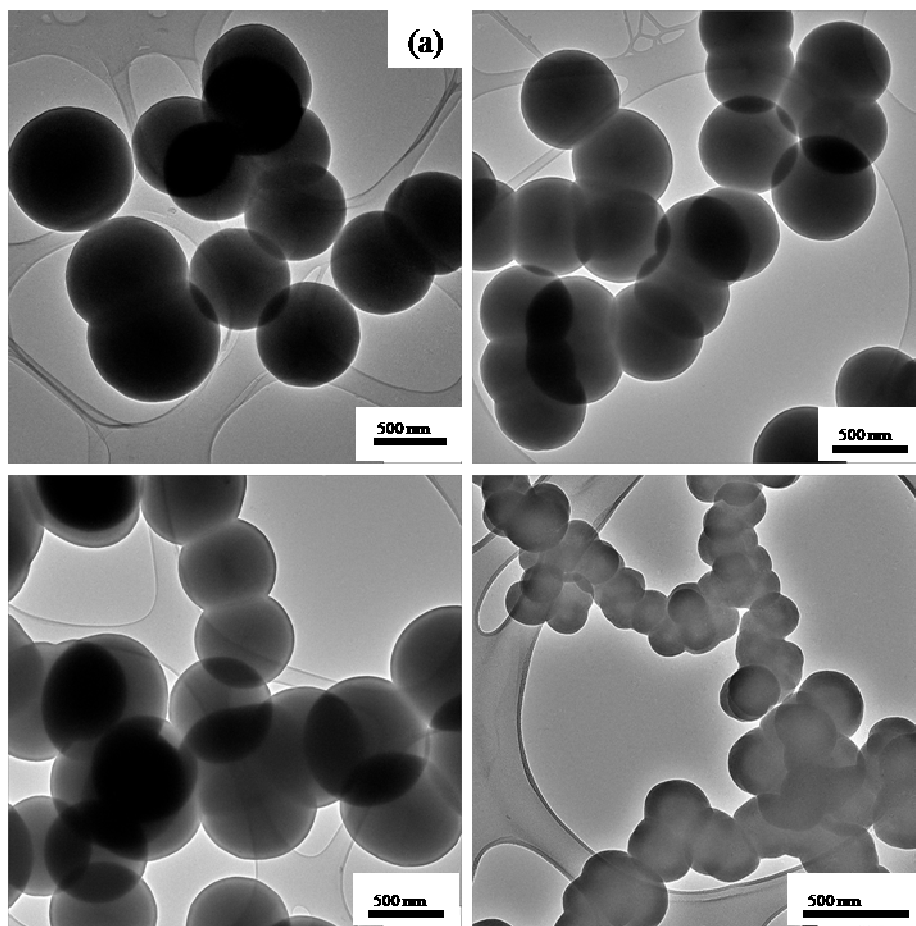


Figure 3.14. TEM images of NCSs synthesized using different flow rates of acetylene and nitrogen gases during the carbonization step a) NCSs 50 + 50, b) NCSs 80 + 20, c) NCSs 100 + 0 and NCSs 200 + 0.

The N content of the NCSs produced using different flow rates of acetylene and nitrogen gases were determined by CN elemental analysis and XPS analysis (Table 3.5). The N contents determined from CN elemental analysis of FR 50 + 50, FR 80 + 20, FR 100 + 0 and FR 200 + 0 samples were 3.03, 3.43, 2.39 and 3.84 %

respectively. Increasing the acetylene flow rate and decreasing the nitrogen flow rates had little effect on the N content of the resultant NCSs formed. This was seen with samples FR 80 + 20 and FR 50 + 50 samples which had N contents of 3.43 and 3.03 % respectively. Increasing the flow rates of C₂H₂ from 100 ml / min to 200 ml / min with no nitrogen gas available during the pyrolysis step had a small effect of increasing the N content of the resultant NCSs formed. FR 100 + 0 and FR 200 + 0 samples had N contents of 2.39 and 3.84 % respectively.

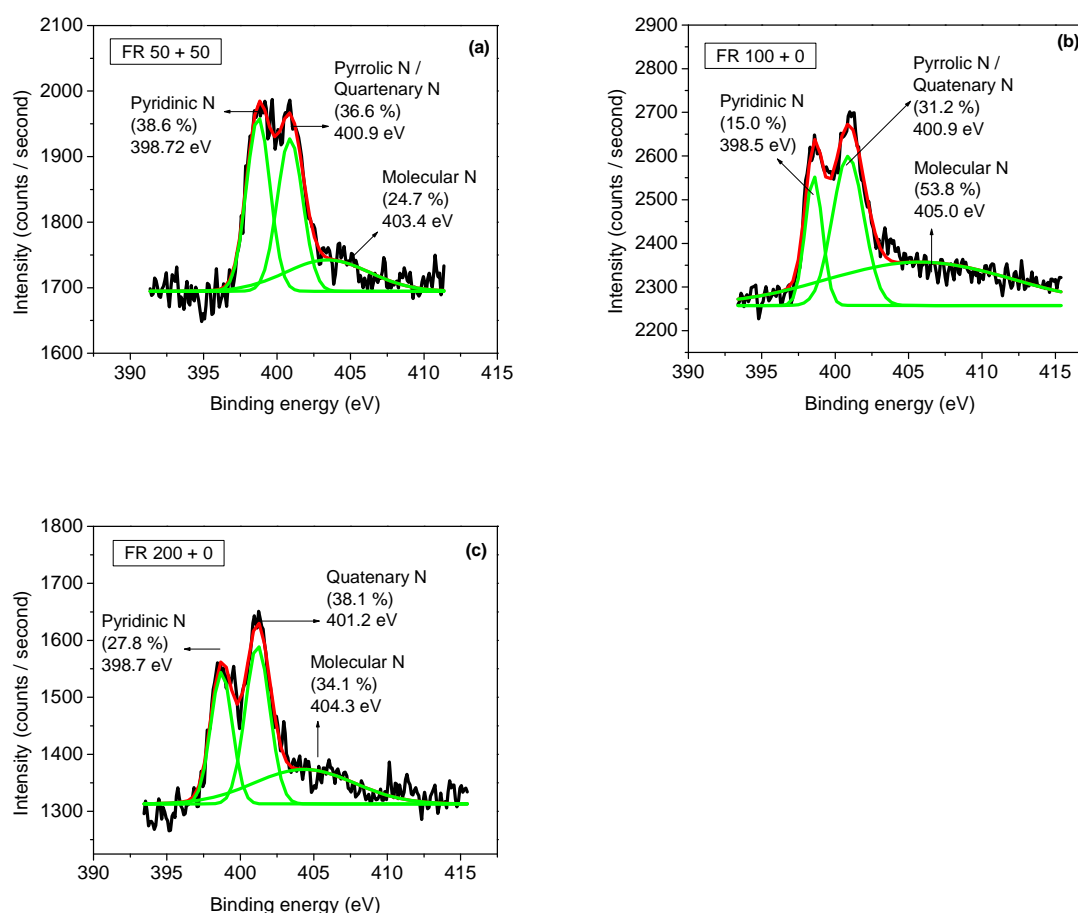


Figure 3.15. XPS N1s spectra of NCSs produced using different flow rates of C₂H₂ and N₂ gases during the carbonization step: (a) FR 50 + 50, (b) FR 100 + 0 and (c) FR 200 + 0. C₂H₂ and or N₂ was bubbled through CH₃CN at 80 °C.

XPS analysis was conducted on selected samples (FR 50 + 50, FR 100 + 0 and FR 200 + 0). The atomic percentages of nitrogen determined using XPS analysis of FR 50 + 50, FR 100 + 0 and FR 200 + 0 samples were 3.00, 3.00 and 5.00 at.% respectively. The N content results determined from CN elemental analysis were lower than those obtained from XPS analysis. This is due to XPS being a surface sensitive technique while CN elemental analysis measures the whole sample. The N1s XPS spectra of the samples are shown in Figure 3.15. After deconvolution of the N1s peaks, at least three different signals were fitted, showing the presence of different types of nitrogen functionalities and their relative amounts (Table 3.4). The amount of contributing species was calculated based on the areas of the peaks. Nitrogen functionalities in nitrogen doped carbons can be assigned to pyridinic N (398.4 - 399.0 eV), pyrrolic N (400.0 - 400.6 eV), quaternary N (401.1 - 401.7 eV), adsorbed nitrogen, nitrogen oxides or $\pi - \pi^*$ shake - up satellite peak (402.0 - 405.0 eV) according to literature [18, 27, 28]. The N1s peak from the FR 50 + 50 sample exhibited three contributions with relative nitrogen amounts of 38.6, 36.6 and 24.7 % corresponding to pyridinic N, pyrrolic N / quaternary N and molecular N / N - oxide respectively. For the FR 100 + 0 sample, the N1s peak showed three different types of nitrogen corresponding to pyridinic N, pyrrolic N / quaternary N and molecular N / N - oxide with relative nitrogen amounts of 15.0, 31.2 and 53.8 % respectively. However the FR 200 + 0 sample's N1s peak exhibited three contributions with relative nitrogen amounts of 27.8, 38.1 and 34.1 % corresponding to pyridinic N, quaternary N and molecular N / N - oxide respectively. Increasing the flow rate of C₂H₂ from 100 ml / min to 200 ml / min during the carbonization step had an effect of increasing the amount of pyridinic N, decreasing the molecular N / N - oxide content and changing the pyrrolic N or quaternary N to quaternary N in the samples. XPS results relating to N content is in good agreement with CN elemental analysis, they both confirm that increasing the flow rate of C₂H₂ from 100 ml / min to 200 ml / min during the carbonization step for samples FR 100 + 0 and FR 200 + 0 led to higher nitrogen inclusion in the NCSs.

Table 3. 4. The nitrogen contents and related detailed breakdown of nitrogen species of NCSs synthesized using different flow rates of acetylene and nitrogen during carbonization step.

Sample name	Nitrogen content (at. %)	Pyridinic N (%)	Pyrrolic N / Quaternary N (%)	Quaternary N (%)	Molecular N / N - oxide (%)
FR 50 + 50	3.00	38.6	36.6	-	24.7
FR 100 + 0	3.00	15.0	31.2	-	53.8
FR 200 + 0	5.00	27.8	-	38.1	34.1

Carbonization temperature and time were kept constant at 950 °C and 90 minutes respectively. C₂H₂ and or N₂ were bubbled through CH₃CN at 80 °C.

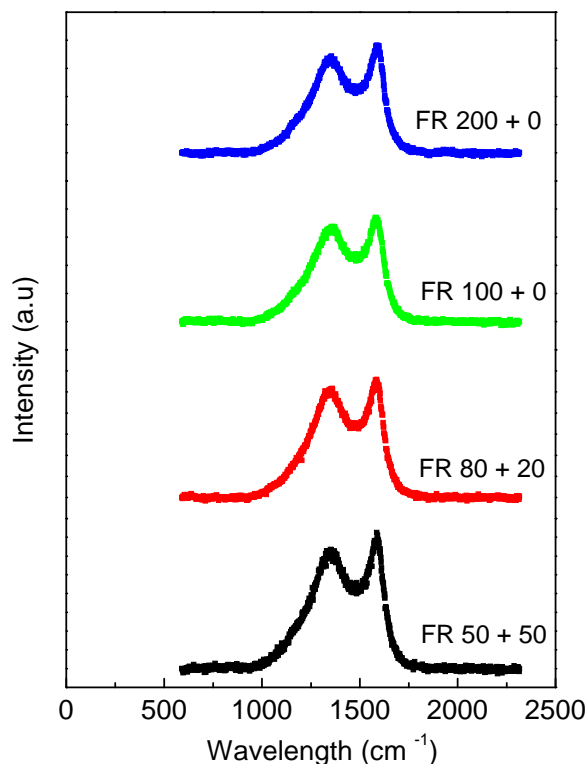


Figure 3.16. Raman graphs of NCSs synthesized at different flow rates of gases. Carbonization temperature and time were kept constant at 950 °C and 90 minutes respectively. C₂H₂ and or N₂ were bubbled through CH₃CN at 80 °C.

The Raman spectra of NCSs synthesized using different flow rates of C₂H₂ and N₂ gases during the pyrolysis step are shown in Figure 3.16. Carbonization temperature and time were kept constant at 950 °C and 90 minutes respectively. CH₃CN was heated to 80 °C. All the spectra show two resonance peaks at approximately 1348 - 1352 cm⁻¹ and 1577 - 1582 cm⁻¹ corresponding to the D and G bands respectively. The I_D / I_G ratios of FR 50 + 50, FR 80 + 20, FR 100 + 0 and FR 200 + 0 samples are 1.04, 1.07, 1.05 and 1.01 respectively. The I_D / I_G ratios did not correlate with the N contents of the NCSs. We would expect that as the C₂H₂ flow rate increased from 100 to 200 ml / min, the values of the I_D / I_G would increase. This is because the N content

of the FR100 + 0 and FR 200 + 0 samples increased according to both CN elemental analysis and XPS analysis results. The increased N doping is expected to introduce more defects into the carbon sphere structures and thereby increase the I_D / I_G ratio.

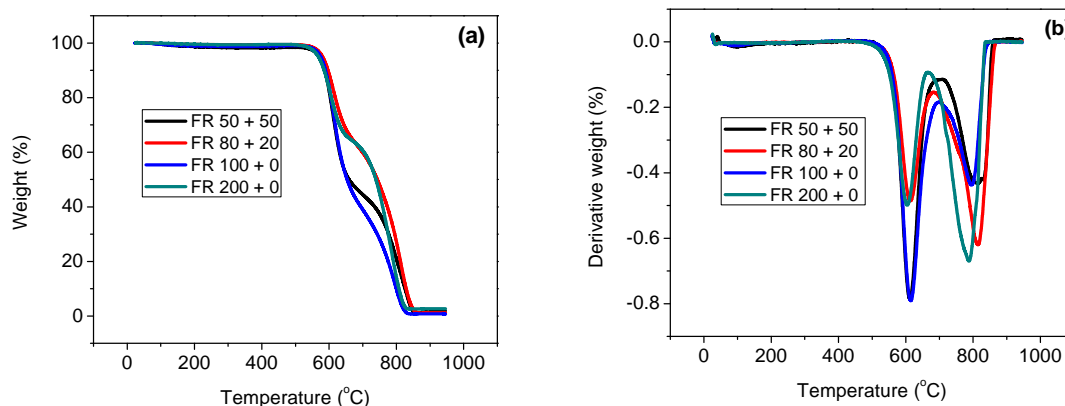


Figure 3.17. TGA and corresponding derivative weight graphs of NCSs synthesized at different flow rates of gases. Carbonization temperature and time were kept constant at 950 °C and 90 minutes respectively. C_2H_2 and or N_2 were bubbled through CH_3CN at 80 °C.

Thermogravimetric analysis was investigated to determine if the variation of flow rates of acetylene and nitrogen gases during the carbonization step had an effect on the thermal stability of the NCSs formed. Figure 3.17 shows the TGA graphs and the corresponding derivative weight loss graphs. There was no amorphous carbon present in all samples as indicated by the absence of weight losses below 500 °C. The derivative weight loss graphs of all samples showed two characteristic weight loss peaks in the temperature ranges of 604 - 614 and 789 - 815 °C corresponding to the oxidation of carbon and graphite respectively. Increasing the flow rate of C_2H_2 from 100 ml / in to 200 ml / min had an effect of increasing the N content of the FR 100 + 0 and FR 200 + 0 samples from 2.39 to 3.84 % respectively according to CN

elemental analysis and the thermal stability of the samples also decreased marginally from 607 to 604 °C respectively. Higher N incorporation has an effect of introducing lattice defects within the carbon matrix framework thereby making the samples less thermally stable. Increasing the acetylene flow rate and decreasing the nitrogen flow rates had an effect of increasing the N content of the resultant NCSs formed. This was evidenced with samples FR 80 + 20 and FR 50 + 50 samples. They had N contents of 3.43 and 3.03 % respectively according to CN elemental analysis. However there was not much of a difference in the thermal stability of the samples as the temperatures of oxidation of carbon and graphite were 614 and 815 °C for FR 80 + 20 sample and 611 and 812 °C for FR 50 + 50 sample.

Table 3. 5. NCSs diameter range, elemental (CN) composition, XPS analysis results, D, G bands and I_D / I_G ratios and gasification temperatures of NCSs synthesized using different flow rates of C_2H_2 and N_2 gases during the carbonization step.

Sample name	Diameter range (average) (nm)	CN elemental analysis (%)		XPS - Atomic concentration (%)			D - band (cm^{-1})	G - band (cm^{-1})	I_D / I_G	Decomposition temperature ($^{\circ}C$)
		C	N	C	N	O				
FR 50 + 50	444 - 1110 (653)	93.05	3.03	93.00	3.00	4.00	1351	1580	1.04	611, 812
FR 80 + 20	387 - 1083 (629)	92.42	3.43	Not analysed	Not analysed	Not analysed	1348	1577	1.07	614, 815
FR 100 + 0	118 - 1349 (669)	93.90	2.39	93.00	3.00	4.00	1352	1578	1.05	607, 802
FR 200 + 0	148 - 538 (236)	94.44	3.84	92.00	5.00	3.00	1351	1582	1.01	604, 788

Carbonization temperature and time were kept constant at 950 $^{\circ}C$ and 90 minutes respectively. C_2H_2 and or N_2 were bubbled through CH_3CN at 80 $^{\circ}C$.

3.4 Conclusion

Nitrogen containing carbon spheres were successfully prepared by a non - catalytic CVD method using acetonitrile as the N source and acetylene gas as the C source. The influence of synthesis parameters, i.e., temperature, time and flow rate of gases on the product morphology, size, N composition, thermal stability and the degree of crystallinity of the carbon products was studied. The variation of synthesis parameters were found to have an effect on the physical and chemical properties of the NCSs formed. In summary the following reaction parameters had the following effects on the resultant NCSs produced:

1) Increasing pyrolysis temperature

- The average diameter of the NCSs did not change significantly
- N content decreased
- I_D / I_G ratios surprisingly increased
- Thermal stability increased.

2) Increasing pyrolysis time

- The average diameter of the NCSs increased
- N content slightly increased
- I_D / I_G ratios increased
- Thermal stability decreased

3) Variation of flow rate of gases

a) Increasing C_2H_2 flow rate and eliminating the N_2 introduced during pyrolysis stage

- The average diameter of the NCSs decreased
- N content increased
- I_D / I_G ratios increased
- Thermal stability decreased

b) Increasing C_2H_2 flow rate and decreasing N flow rate

- The average diameter of the NCSs remained nearly constant

- N content increased
- I_D / I_G ratios increased
- Thermal stability remained nearly constant

3.5 References

1. Smalley, R.E., H. Kroto, and J. Heath, *C60: Buckminsterfullerene*. Nature, 1985. **318**(6042): p. 162-163.
2. Deshmukh, A.A., S.D. Mhlanga, and N.J. Coville, *Carbon spheres*. Materials Science and Engineering: R: Reports, 2010. **70**(1–2): p. 1-28.
3. Xia, Y., B. Gates, Y. Yin, and Y. Lu, *Monodispersed Colloidal Spheres: Old Materials with New Applications*. Advanced Materials, 2000. **12**(10): p. 693-713.
4. Inagaki, M., *Discussion of the formation of nanometric texture in spherical carbon bodies*. Carbon, 1997. **35**(5): p. 711-713.
5. Serp, P., R. Feurer, P. Kalck, Y. Kihn, J.L. Faria, and J.L. Figueiredo, *A chemical vapour deposition process for the production of carbon nanospheres*. Carbon, 2001. **39**(4): p. 621-626.
6. Maiyalagan, T. and B. Viswanathan, *Template synthesis and characterization of well-aligned nitrogen containing carbon nanotubes*. Materials Chemistry and Physics, 2005. **93**(2–3): p. 291-295.
7. Deshmukh, A.A., R. Ul-Islam, M.J. Witcomb, W.A.L. van Otterlo, and N.J. Coville, *Catalytic Activity of Metal Nanoparticles Supported on Nitrogen-Doped Carbon Spheres*. ChemCatChem, 2010. **2**(1): p. 51-54.
8. Xiong, H., M. Moyo, M.K. Rayner, L.L. Jewell, D.G. Billing, and N.J. Coville, *Autoreduction and Catalytic Performance of a Cobalt Fischer–Tropsch Synthesis Catalyst Supported on Nitrogen-Doped Carbon Spheres*. ChemCatChem, 2010. **2**(5): p. 514-518.

9. Zhou, X., Z. Yang, H. Nie, Z. Yao, L. Zhang, and S. Huang, *Catalyst-free growth of large scale nitrogen-doped carbon spheres as efficient electrocatalysts for oxygen reduction in alkaline medium*. Journal of Power Sources, 2011. **196**(23): p. 9970-9974.
10. Nieto-Márquez, A., I. Espartero, J.C. Lazo, A. Romero, and J.L. Valverde, *Direct synthesis of carbon and nitrogen-carbon nanospheres from aromatic hydrocarbons*. Chemical Engineering Journal, 2009. **153**(1-3): p. 211-216.
11. Su, F., X.S. Zhao, Y. Wang, L. Wang, and J.Y. Lee, *Hollow carbon spheres with a controllable shell structure*. Journal of Materials Chemistry, 2006. **16**(45): p. 4413-4419.
12. Jeong, H.M., S.Y. Lee, W.H. Shin, J.H. Kwon, A. Shakoar, T.H. Hwang, S.Y. Kim, B.-S. Kong, J.-S. Seo, Y.M. Lee, J.K. Kang, and J.W. Choi, *Silicon@porous nitrogen-doped carbon spheres through a bottom-up approach are highly robust lithium-ion battery anodes*. RSC Advances, 2012. **2**(10): p. 4311-4317.
13. Ma, F., H. Zhao, L. Sun, Q. Li, L. Huo, T. Xia, S. Gao, G. Pang, Z. Shi, and S. Feng, *A facile route for nitrogen-doped hollow graphitic carbon spheres with superior performance in supercapacitors*. Journal of Materials Chemistry, 2012. **22**(27): p. 13464-13468.
14. Zhang, Z., R. Zhang, C. Li, L. Yuan, P. Li, L. Yao, and S. Liu, *Nitrogen-Doped Carbon Hollow Spheres for Immobilization, Direct Electrochemistry, and Biosensing of Protein*. Electroanalysis, 2012. **24**(6): p. 1424-1430.
15. Li, W., D. Chen, Z. Li, Y. Shi, Y. Wan, G. Wang, Z. Jiang, and D. Zhao, *Nitrogen-containing carbon spheres with very large uniform mesopores: The superior electrode materials for EDLC in organic electrolyte*. Carbon, 2007. **45**(9): p. 1757-1763.
16. Jin, Y.Z., C. Gao, W.K. Hsu, Y. Zhu, A. Huczko, M. Bystrzejewski, M. Roe, C.Y. Lee, S. Acquah, H. Kroto, and D.R.M. Walton, *Large-scale synthesis and characterization of carbon spheres prepared by direct pyrolysis of hydrocarbons*. Carbon, 2005. **43**(9): p. 1944-1953.

17. Bepete, G., Z.N. Tetana, S. Lindner, M.H. Rummeli, Z. Chiguvare, and N.J. Coville, *The use of aliphatic alcohol chain length to control the nitrogen type and content in nitrogen doped carbon nanotubes*. Carbon, 2013. **52**(0): p. 316-325.
18. van Dommele, S., A. Romero-Izquierdo, R. Brydson, K.P. de Jong, and J.H. Bitter, *Tuning nitrogen functionalities in catalytically grown nitrogen-containing carbon nanotubes*. Carbon, 2008. **46**(1): p. 138-148.
19. Yadav, R., P. Dobal, T. Shripathi, R.S. Katiyar, and O.N. Srivastava, *Effect of Growth Temperature on Bamboo-shaped Carbon–Nitrogen (C–N) Nanotubes Synthesized Using Ferrocene Acetonitrile Precursor*. Nanoscale Research Letters, 2009. **4**(3): p. 197-203.
20. Maldonado, S., S. Morin, and K.J. Stevenson, *Structure, composition, and chemical reactivity of carbon nanotubes by selective nitrogen doping*. Carbon, 2006. **44**(8): p. 1429-1437.
21. Liu, J., S. Webster, and D.L. Carroll, *Temperature and Flow Rate of NH₃ Effects on Nitrogen Content and Doping Environments of Carbon Nanotubes Grown by Injection CVD Method*. The Journal of Physical Chemistry B, 2005. **109**(33): p. 15769-15774.
22. Higgins, D., Z. Chen, and Z. Chen, *Nitrogen doped carbon nanotubes synthesized from aliphatic diamines for oxygen reduction reaction*. Electrochimica Acta, 2011. **56**(3): p. 1570-1575.
23. Lin, Y.G., Y.K. Hsu, C.T. Wu, S.Y. Chen, K.H. Chen, and L.C. Chen, *Effects of nitrogen-doping on the microstructure, bonding and electrochemical activity of carbon nanotubes*. Diamond and Related Materials, 2009. **18**(2–3): p. 433-437.
24. Landi, B.J., C.D. Cress, C.M. Evans, and R.P. Raffaele, *Thermal Oxidation Profiling of Single-Walled Carbon Nanotubes*. Chemistry of Materials, 2005. **17**(26): p. 6819-6834.

25. McKee, G.S.B. and K.S. Vecchio, *Thermogravimetric Analysis of Synthesis Variation Effects on CVD Generated Multiwalled Carbon Nanotubes*. The Journal of Physical Chemistry B, 2005. **110**(3): p. 1179-1186.
26. Miao, J.-Y., D.W. Hwang, K.V. Narasimhulu, P.-I. Lin, Y.-T. Chen, S.-H. Lin, and L.-P. Hwang, *Synthesis and properties of carbon nanospheres grown by CVD using Kaolin supported transition metal catalysts*. Carbon, 2004. **42**(4): p. 813-822.
27. Amadou, J., K. Chizari, M. Houllé, I. Janowska, O. Ersen, D. Bégin, and C. Pham-Huu, *N-doped carbon nanotubes for liquid-phase CC bond hydrogenation*. Catalysis Today, 2008. **138**(1–2): p. 62-68.
28. Pels, J.R., F. Kapteijn, J.A. Moulijn, Q. Zhu, and K.M. Thomas, *Evolution of nitrogen functionalities in carbonaceous materials during pyrolysis*. Carbon, 1995. **33**(11): p. 1641-1653.

CHAPTER 4

Nitrogen doped carbon spheres as a catalyst support for the hydrogenation of cinnamaldehyde. The effect of support characteristics on the reaction.

4.1 Introduction

The use of catalyst supports provides a means of facilitating the separation of the reaction product/s and the catalyst [1-3]. Of the wide range of catalyst supports, carbon materials have been extensively used in heterogeneous catalysis due to their features such as chemical inertness, good mechanical stability, and electrical conductivity [4, 5]. The different types of carbon supports used in heterogeneous catalysis include carbon nanotubes (CNTs) and carbon nanofibres (CNFs), more recently carbon spheres (CSs) have attracted a growing interest because of their (i) uncomplicated synthesis without the use of catalysts, (ii) high yields of pure material, (iii) ability to control their physical and chemical properties [6-8] and (iv) unclosed graphitic flakes in a spherical structure which provides reactive dangling bonds [9, 10].

Because the surfaces of CSs are chemically inert, it is necessary to activate them. Functionalization and doping are the two methods normally used to modify the wettability of the carbon sphere surface. Functionalization using different acids or oxidizing treatments creates carboxylic, carbonyl and hydroxyl groups that act as anchoring sites on the carbon sphere surface and bond covalently to the metal

precursor solution. The most common acids used during functionalization of CSs are concentrated nitric acid (HNO_3) [11, 12] or sulphuric acid (H_2SO_4) / HNO_3 [13] mixtures. Other oxidants that have also been used include hydrogen peroxide and potassium permanganate [11, 12] just to mention a few. Doping of the carbon spheres alters its chemistry by allowing the addition of elements such as N into the sphere structure. N is the common element used to dope carbon nanostructures and this can be done either by doping during carbon nanostructure synthesis or post addition of a N source after the carbon structures have already been made [14, 15]. Nitrogen doped carbon spheres (NCSs) contain N sites that are chemically active and allow for the attachment of metal precursors onto the surface of carbon spheres. Since the supports can strongly affect catalyst activity, it is necessary to modify the carbon supports in an effort to improve catalyst performance.

The selective catalytic hydrogenation of α,β -unsaturated aldehydes is a very important reaction from an industrial and research point of view [16-19]. Cinnamaldehyde (CALD) is a member of the α,β -unsaturated aldehydes. The hydrogenation of CALD may proceed through different reaction pathways (Figure 4.1). The reduction of the carbonyl ($\text{C}=\text{O}$) bond in CALD leads to the production of cinnamyl alcohol (CA). The reduction of the olefinic ($\text{C}=\text{C}$) bond leads to the production of hydrocinnamaldehyde (HCALD). Both CA and HCALD can be further hydrogenated to produce the fully saturated alcohol, 3-phenyl-1-propanol (3P1P). Cinnamyl alcohol is a valuable intermediate for the synthesis of perfumes, flavoring additives, pharmaceuticals and agrochemicals [20]. It is a challenge to selectively hydrogenate the carbonyl group to produce cinnamyl alcohol because thermodynamics favours the hydrogenation of the $\text{C}=\text{C}$ bond over the $\text{C}=\text{O}$ bond by about 35 kJmol^{-1} and also kinetically the reactivity of the $\text{C}=\text{C}$ bond is higher than that of the $\text{C}=\text{O}$ bond [21]. Hydrocinnamaldehyde has been found to be an important intermediate in the manufacture of pharmaceutical products used in the treatment of

HIV [22]. Catalysts are now required which can selectively hydrogenate either the C=C bond or C=O bond leaving the other one intact.

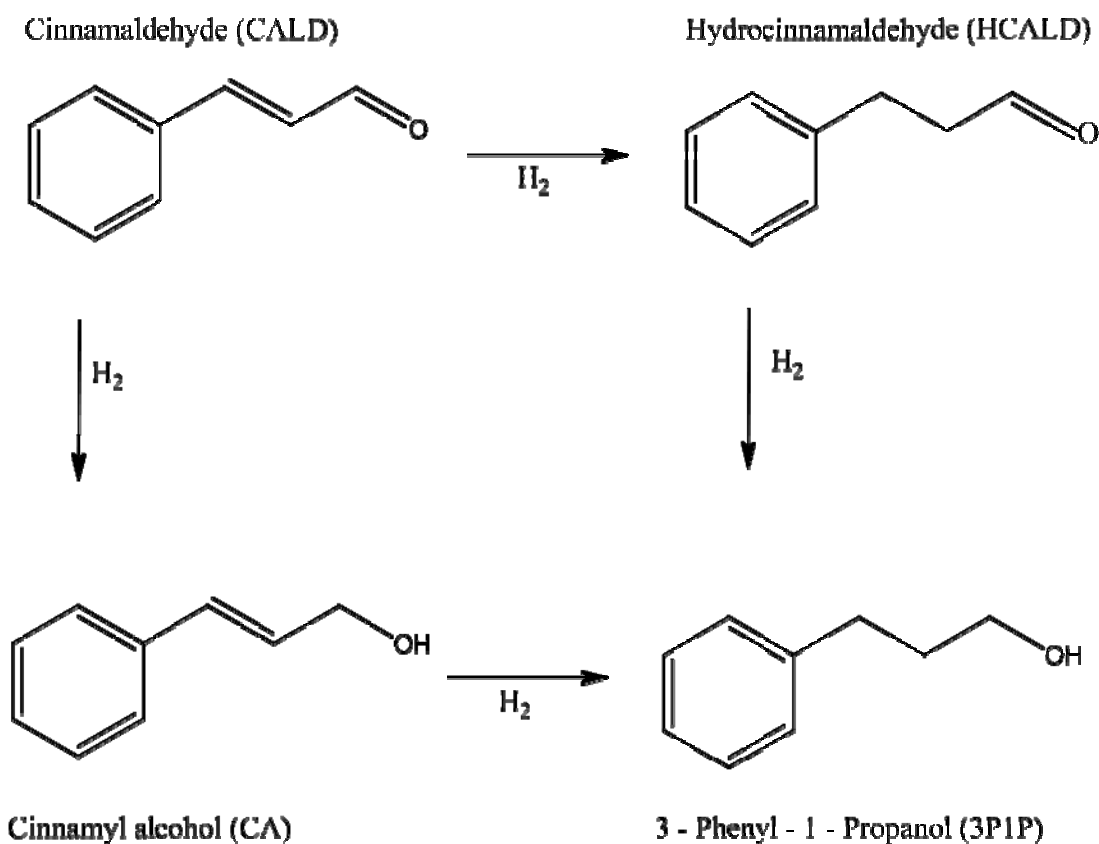


Figure 4.1. Reaction pathway for the selective hydrogenation of cinnamaldehyde.

In general, noble metals (Pt, Os, Ir, Pd, Rh and Ru) have been used for the hydrogenation of CALD leading to differences in selectivities and activity. Palladium catalysts are well known in literature to be the most effective catalysts for the catalytic selective hydrogenation of α,β -unsaturated aldehydes to saturated aldehydes [23].

The influence of oxygenated surface groups in carbon supported catalysts for α,β -unsaturated aldehyde hydrogenation reactions has been receiving a lot of research interest over the past few years [24-32]. In terms of carbon supports, the reaction has mainly been studied on carbon nanotube (CNT) and carbon nanofibre (CNF) supports using ruthenium, iridium and platinum as catalysts. It has been reported that for the α,β -unsaturated aldehyde hydrogenation by monometallic catalysts, the removal of oxygen surface groups is important. Depending on the amount of surface groups, the metal and the type of carbon support, the outcome of the reaction can be modified by changing the hydrogenation pathway. The amount of oxygen surface groups on a carbon nanostructure surface can be tuned by treatment in an inert atmosphere at various temperatures, which partly removes the surface groups. Researchers have attributed the high catalytic activity and selectivity after oxygen surface group removal as due to the enhanced cinnamaldehyde adsorption via the phenyl ring. The catalyst surface becomes less polar [32].

In this work we selected the selective hydrogenation of cinnamaldehyde to hydrocinnamaldehyde to test the performance of our new catalysts. Several investigators have already demonstrated the great potential of nitrogen doped carbon spheres (NCSs) and CSs as support materials. Kente et al. reported on a study where they compared using GaN and NCSs supports for the hydrogenation of CALD [33]. NCSs have been used as supports in various catalytic reactions [12, 13, 34-38].

The only available literature on the use of nitrogen doped carbon supports in the hydrogenation of CALD is that which is available on nitrogen doped carbon nanotubes (NCNTs). Even here the information is very limited. Lepro et al. reported on a hydrothermal treatment method of depositing Pt clusters on nitrogen doped multi walled carbon nanotubes (N-MWCNTs) which did not require prior functionalization of the support and the use of additional reducing agents other than acetic acid used

during catalyst synthesis [39]. They compared the activities of the catalysts, Pt on nitrogen doped MWCNTs and Pt on undoped MWCNTs. They also studied the effect of Pt on nitrogen doped MWCNTs using different hydrogen pressures. They found that the conversion to CALD using Pt / N-MWCNTs increased 6 times with respect to the values obtained for Pt / MWCNTs and MWCNTs at 2.5 MPa of hydrogen pressure and 300 minutes reaction time. Selectivities to cinnamyl alcohol were 50 % and ~ 15 % for the Pt / MWCNTs and MWCNTs catalysts respectively. They attributed the high conversion of CALD and the higher selectivities to CA of the Pt / N-MWCNTs when compared to Pt / MWCNTs being due to differences in deposition conditions and the presence of N in the supports.

Amadou et al. compared the catalytic results for the hydrogenation of CALD into HCALD using palladium catalysts supported on 3 different supports namely nitrogen doped CNTs, undoped CNTs and activated charcoal (AC) supports [40]. The increasing order of catalytic activity (in terms of conversion) of the catalysts was found to be Pd / CNTs < Pd / NCNTs < Pd / AC. The Pd / AC catalyst had the highest conversion of CALD because of the high specific surface area (1000 - 1500 m²/g) of the support which favoured the adsorption process. The Pd / NCNT catalyst had almost double the conversion of CALD compared to the Pd / CNT catalyst and this was due to the introduction of N atoms in the graphite layers of carbon which modified the metal surface adsorption thereby increasing the C=C bond hydrogenation activity.

Chizari et al. [41] obtained similar results as those found by Lepro et al. [39] and Amadou et al. [40] where they saw a higher hydrogenation activity for nitrogen doped Pd catalysts compared to undoped Pd catalysts in the hydrogenation of CALD. The higher hydrogenation activity in the nitrogen doped Pd catalysts was attributed to the higher dispersion of metals on the nitrogen doped Pd support and also to an

electronic alteration of metal particles on the carbon surface due to the insertion of nitrogen. There was no leaching of palladium nanoparticles during the hydrogenation reaction of Pd / NCNT catalysts which showed a strong interaction between the metal active phase and the support.

Besides the above studies on NCNTs, there is no literature to the best of our knowledge on the use of nitrogen doped carbon spheres as a catalyst support for the hydrogenation of cinnamaldehyde. The aim of this chapter was to bridge the gap on the use of nitrogen doped carbon spheres as catalyst supports in the hydrogenation of CALD. Support pre-treatments on catalytic activity such as different functionalization conditions were studied. The use of supports with different nitrogen contents was also tested for the hydrogenation of CALD.

4.2 Experimental

4.2.1 Synthesis of NCSs

The synthesis of NCSs was performed according to the procedure reported by Deshmukh et al. with a few modifications [13]. NCSs were synthesized using a non-catalytic chemical vapor deposition (CVD) method where acetylene (C_2H_2) was used as a carbon source and acetonitrile (CH_3CN) was the N source. N_2 was first flowed through a quartz tube at 100 ml / min while the furnace was heated up from room temperature to 950 °C at a heating rate of 10 °C / min to create an inert atmosphere. Once 950 °C was reached the N_2 flow was switched off and C_2H_2 was bubbled through CH_3CN (80 °C) at a flow rate of 100 ml / min for 90 minutes. After 90 minutes, the C_2H_2 was switched off and N_2 was again flowed through the system at 100 ml / min until the furnace had cooled down to room temperature. NCSs were then

collected from the walls of the quartz tube and weighed. The volume of CH₃CN used in the reaction was also recorded. CSs with different amounts of nitrogen were also synthesized by varying the amount of C₂H₂ and N₂ flow rates during the carbonization step. Full details of experimental conditions are shown in the Chapter 3 and the Appendix section.

4.2.1.1 Removal of polycyclic aromatic hydrocarbons (PAHs)

NCSs (1.0 g) were placed into a thimble and toluene (150 ml) was added into a round bottomed flask (250 ml). Soxhlet extraction was carried out for 6 hours. The extracted carbon material was dried in an oven overnight at 80 °C.

4.2.1.2 Functionalization of NCSs

Functionalization of the carbon material was carried out by treatment with 55 % nitric acid (HNO₃) for 24 hours while varying the temperatures (40, 60 and 80 °C). The functionalized carbon materials were then filtered using deionized water until the pH of the filtrate was 7. The functionalized carbon materials were then dried in an oven for 12 hours at 80 °C. The samples obtained were denoted as follows: fCSs 40 (functionalized CSs at 40 °C), fNCSs 40 (functionalized NCSs at 40 °C), fNCSs 60 (functionalized NCSs at 60 °C) and fNCSs 80 (functionalized NCSs at 80 °C).

4.2.2 Catalyst synthesis

The catalysts were prepared using the polyol - reduction method of a metal salt in ethylene glycol solution. The method was adopted from Chen et al. with a few

modifications [42]. Carbon supports (400 mg) were placed into a 500 ml round bottomed flask and ethylene glycol solution (150 ml) was added. The contents of the beaker were sonicated for 15 minutes followed by magnetic stirring for 30 minutes. The metal precursor solution of $\text{Pd}(\text{C}_2\text{H}_3\text{O}_3)_2$ in acetone (0.05 M) was then added drop wise to the mixture of carbon support and ethylene glycol solution. The concentrations of the precursor solutions in the ethylene glycol solutions were calculated in order to prepare catalysts with metal loadings with a fixed 1 wt % loading. The resultant solution was magnetically stirred vigorously for a further 3 hours at room temperature followed by refluxing at 195 °C in an oil bath for 3 hours. The solution was then cooled down to room temperature. The metal/carbon sphere powder in the solution was filtered and thoroughly washed first with 20 ml of acetone followed by excess distilled water. The resulting carbon supported metal catalyst was dried in air for 8 hours at 80 °C and a mortar was used to homogeneously grind the material to form a powder. The catalysts obtained were named 1 % Pd/fCSs 40, 1 % Pd/NCSs, 1 %Pd/fNCSs 40, 1 %Pd/fNCSs 60 and 1 % Pd/fNCSs 80 where 1 % means the Pd loading was 1 wt. % and the 40, 60 and 80 stand for temperature used when functionalizing the CSs and NCSs with HNO_3 . Catalysts were also prepared using supports with different N contents. These were named 1 % Pd /fCSs 40 (0.00 % N) catalyst, 1 % Pd /fNCSs 40 (0.41 % N) catalyst, 1 % Pd /fNCSs 40 (2.39 % N) catalyst and 1 % Pd /fNCSs 40 (3.84 % N) catalyst. The supports of these catalysts were functionalized at 40 °C using HNO_3 for 24 hours and had a fixed Pd metal loading of 1 wt. %. The N content was determined by CN elemental analysis.

4.2.3 Characterization techniques

The morphology of the NCSs was determined by transmission electron microscopy (TEM). A spatula tip of the sample was mixed with methanol and the mixture was sonicated for 1 minute. A drop of the suspension was transferred onto a SPI carbon

coated copper grid and allowed to dry before analysis. TEM examinations were conducted using a FEI Technai G² Spirit electron microscope operated at 120 kV. The composition of carbon and nitrogen in the NCSs was determined by CN elemental analysis using a Carlo Erba NA1500 Nitrogen Carbon Sulphur analyzer. Approximately 1.0 - 1.5 mg of sample was used for the analysis and a GC equipped with a thermal conductivity detector (TCD) was used to separate the gases produced. X-ray photoelectron spectroscopy (XPS) was used to determine the elemental composition in the carbon spheres. The binding energy was recorded on a Physical Electronics Quantum2000 instrument using AlK α X-rays at a power of 20 W. The beam diameter was 100 μ m. Raman spectroscopy was done using a Jobin - Yvon T6400 micro - Raman spectrometer equipped with a liquid nitrogen cooled charge coupled device detector. The thermal stability of the NCSs was determined by thermogravimetric analysis (TGA) using a Perkin Elmer Pyris 1 TGA. Approximately 10 mg of sample was used for the analysis and the samples were heated from room temperature up to 950 °C at a heating rate of 5 °C / min in an air atmosphere (20 ml / min). The metal weight - loading of the samples was determined using ICP-OES. The measurements were performed using a SPECTRO CIROSCCD ICP-Spectrometer. Each sample was decomposed by heating in aqua regia (1:3 mixture of HNO₃: HCl) before analysis. Zeta potentials of as - synthesized and acid functionalized undoped and doped carbon spheres were measured using a Malvern Zetasizer nano - series instrument. The as - synthesized and acid functionalized undoped and doped carbon spheres (0.5 g) were dispersed in deionized water (100 ml) at room temperature and the pH of the suspension was adjusted from 2.0 to 12.0 by adding either 0.1 M HCl or 0.1 M NaOH. By measuring the zeta potential as a function of pH the point of zero charge was determined.

4.2.4 Hydrogenation of cinnamaldehyde (CALD)

The selective hydrogenation of cinnamaldehyde was carried out at atmospheric pressure in a 250 ml three necked round bottomed flask equipped with a magnetic stirrer, reflux condenser, gas inlet and sampling port. The three necked round bottomed flask was maintained in an oil bath which was heated to a desired reaction temperature. In a typical catalytic run, the reaction mixture contained 1.26 ml of cinnamaldehyde; 100 ml of hexan-1-ol and 0.1 g of catalyst. Nitrogen gas was bubbled through the solution for 30 minutes, while the oil bath heated the reaction contents in the three necked flask from room temperature to 60 °C to remove traces of dissolved oxygen in the system. After this, hydrogen gas (H₂) was flowed at 50 ml / min and the reaction was started. Hydrogen was continuously fed into the system while the contents were stirred. The duration of each reaction was 8 hours. Chemical analysis of the reaction products was performed by taking samples of the reaction solution periodically and analyzing by gas chromatography (GC) using a flame ionization detector (FID) and a ZB-1 capillary column (30 m × 0.32 × 0.53 μm). Blank experiments using as-synthesized and functionalized nitrogen doped carbon spheres with no Pd was carried out and revealed that the CALD conversion was zero i.e. no product was detected by GC. Reactants and products were identified by GC comparison with authentic standards (GC grade). Qualitative analysis was carried out by calculating the area of the chromatographic peaks using computer packages.

The results of the catalytic reaction runs were analyzed in terms of reactant conversion and product selectivity [43]:

$$\text{Conversion (\%)} = 100 \times [\text{CALD}]_0 - [\text{CALD}]_t \div [\text{CALD}]_0 \quad (1)$$

$$\text{Selectivity (\%)} = 100 \times [X]_t \div \sum [X]_t \quad (2)$$

where $[\text{CALD}]_0$ represents the initial concentration of CALD at time 0, $[\text{CALD}]_t$ represents the concentration of CALD at a given time t and $[\text{X}]_t$ represents the concentration of all the other main identifiable hydrogenation products of CALD, namely cinnamyl alcohol, hydrocinnamaldehyde, 3 - phenyl - 1 - propanol and others at a given time t .

4.3 Results and Discussion

4.3.1. Effect of functionalization of undoped and doped carbon supports.

4.3.1.1 Support characterization

TEM was used to study the effect of using different functionalizing conditions on the morphology of the undoped and nitrogen doped carbon spheres (Figure 4.2). Undoped CSs and nitrogen doped carbon spheres (NCSs) were successfully synthesized using the CVD method. For undoped carbon spheres, nitrogen was first flowed through the system to remove oxygen then it was switched off and acetylene gas (C source) was flowed through at a flow rate of 100 ml / min for 90 minutes. The system was cooled off using nitrogen gas and the black carbon soot was collected. The yield was approximately 2.2 g. The nitrogen doped carbon spheres were synthesized using the same method as that for the undoped CSs. The only variation was that the acetylene gas was bubbled through an acetonitrile solution which was heated at 80 °C. The yield of the black soot collected was approximately 2.0 g. Typical TEM images of as - synthesized and functionalized CSs and NCSs are shown in Figure 4.2. The average diameters of as - synthesized CSs and NCSs are 751 and 729 nm respectively.

The CSs and NCSs were functionalized as described in the experimental section 4.2.1.2. Functionalization did not alter the average diameters of the undoped and doped carbon spheres. Functionalizing the CSs and NCSs using HNO_3 at 40 and 60 °C for 24 hours had little or no effect on the spherical morphology of the CSs and NCSs. However functionalizing the NCSs at 80 °C for 24 hours using 55 % HNO_3 was seen to start to introduce imperfections on the sphere surface.

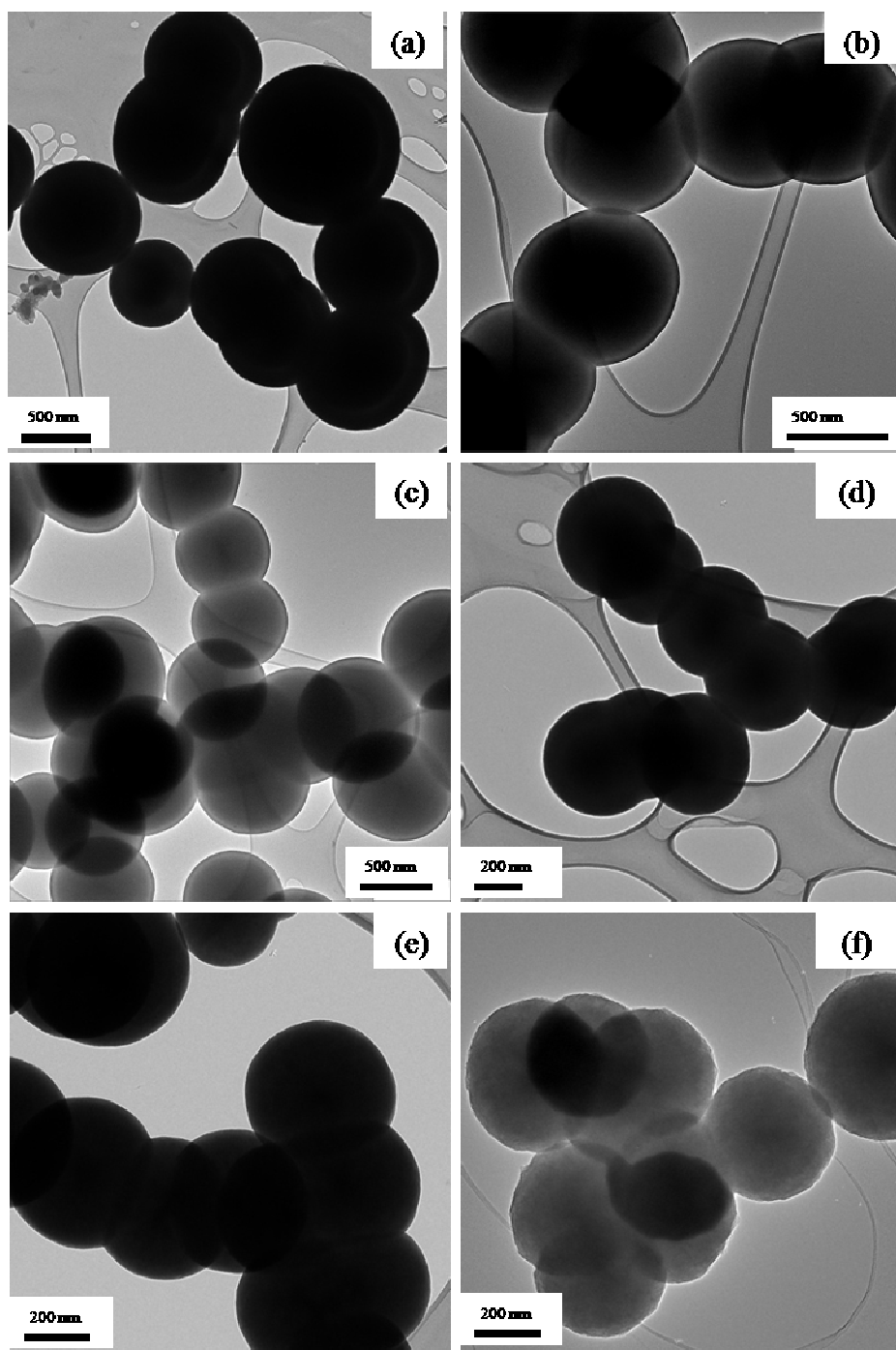


Figure 4.2. TEM images of (a) as - synthesized CSs and (b) fCSs 40 supports, (c) as - synthesized NCSs, (d) fNCSs 40, (e) fNCSs 60 and (f) fNCSs 80 supports.

Zeta potential measurements were used to evaluate the presence of oxygen surface groups on the as-synthesized and functionalized doped and undoped carbon spheres. The point of zero charge (PZC) of carbon materials is important in studying the dispersion of carbon in polymers and the adsorption of metal cations during catalyst preparation [44-46]. Figure 4.3 shows the zeta potential plots as a function of the pH for as-synthesized and acid-treated CSs and NCSs. Table 4.1 shows the PZC values of pristine and treated doped and undoped carbon spheres obtained from zeta potential measurements. Acidic groups tend to make the carbon surface more hydrophilic, and this is reflected by the increase in the negative surface charge density and the decrease in the pH of the point of zero charge (pH_{PZC}). The addition of N onto carbon supports leads to the formation of basic groups which tend to increase the value of the pH_{PZC} compared to N-free carbon supports [40]. The pH_{PZC} values of as-synthesized CSs and NCSs were 5.14 and 6.43 respectively. When N was introduced into the graphene sheets of the CSs, there was an increase in the PZC values compared to N-free CSs. After introducing functional groups into the carbon supports, the PZC was shifted to lower pH values. The pH_{PZC} values for supports fCSs 40, fNCSs 60 and fNCSs 80 were all below 0. The introduction of functional groups on the carbon supports caused a shift in the zeta plots to more negative values that was dependant on the functionalization temperature or presence or absence of N. The fNCSs 40 support had a pH_{PZC} value of 2.97. The results indicate that the pH_{PZC} is affected by the temperature of functionalization and also by the presence or absence of N in the carbon spheres. The higher the temperature of functionalization, the more surface functional groups added to the carbon which in turn increased the surface (negative) charge and hence the hydrophilicity. The addition of N on carbon supports has the opposite effect.

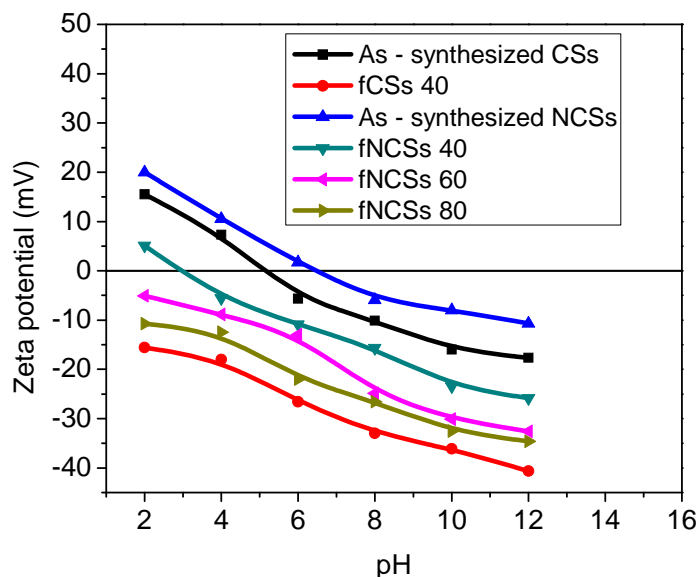


Figure 4.3. Zeta potential measurements as a function of pH for as - synthesized and functionalized supports.

Since most of the samples had $PZC < 0$, another procedure was used to determine the relative ordering of the samples. This was achieved by considering the zeta potential measurements at $pH = 2$. The zeta potential measurements at $pH = 2$ for as - synthesized CSs, fCSs 40, as-synthesized NCSs, fNCSs 40, fNCSs 60 and fNCSs 80 were 15.54, -15.81, 19.99, 5.09, -5.97 and -10.76 mV respectively (Table 4.1). From these results, it can be seen that the order of negative surface charge of the supports was in this order fCSs 40 > fNCSs 80 > fNCSs 60 > fNCSs 40 > as-synthesized CSs > as-synthesized NCSs at $pH = 2$. The addition of N had an effect of making the support more basic and decreasing the negative surface charge density.

Table 4.1. Point of zero charge (PZC) obtained from zeta potential measurements of as - synthesized and functionalized supports.

Sample	PZC (mV)	Zeta potential (mV) at pH = 2
As-synthesized CSs	5.14	15.54
fCSs 40	< 0.00	-15.81
As-synthesized NCSs	6.43	19.99
fNCSs 40	2.97	5.09
fNCSs 60	< 0.00	-5.97
fNCSs 80	< 0.00	-10.76

Figure 4.4 shows the thermogravimetric analysis (TGA) and derivative curves of weight loss (DTG) of unpurified and purified carbon supports under an air atmosphere. The peak positions of weight loss of the samples are given in Table 4.2. The relative DTG curves of all samples exhibited two weight loss peaks located in the regions 600 - 612 °C and 760 - 801 °C respectively. The two weight loss peaks observed in the derivative weight graphs of as - synthesized CSs and fCSs 40 correspond to the oxidation of carbon in the CSs and the oxidation of graphite like carbon [47]. Two oxidation peaks determined by temperature programmed oxidation (TPO) have been reported in literature for nitrogen containing carbon materials, attributed to the release of CO, CO₂ and NO_x [34, 48-50]. The first peak corresponded to the gasification of carbon with subsequent release of carbon oxides and a minor contribution of nitrogen oxides. The second peak in this study was said to be due to the presence and release of nitrogen in the char. However in our case this cannot be true as our N content was very low and two peaks were noted for the undoped CSs. Undoped carbon supports were more thermally stable than the doped carbon supports. Doped carbon supports were less thermally stable due to the introduction of nitrogen in the carbon structure which induces lattice defects in the graphene layers and makes the material easier to oxidize. Functionalized carbon supports were less thermally stable than their as-synthesized carbon support counterparts. This is a result of the

high amount of defects introduced during the nitric acid oxidation step which allows the graphite sheets to be consumed at lower temperatures.

Table 4.2. Decomposition temperatures of as - synthesized and functionalized undoped and doped CSs.

Sample name	First decomposition temperature (°C)	Second decomposition temperature (°C)	Intensity of 1st peak / Intensity of 2nd peak
As-synthesized CSs	616	799	0.33
fCSs 40	612	795	0.54
As-synthesized NCSs	612	801	0.41
fNCSs 40	610	760	1.35
fNCSs 60	612	799	0.96
fNCSs 80	606	795	1.04

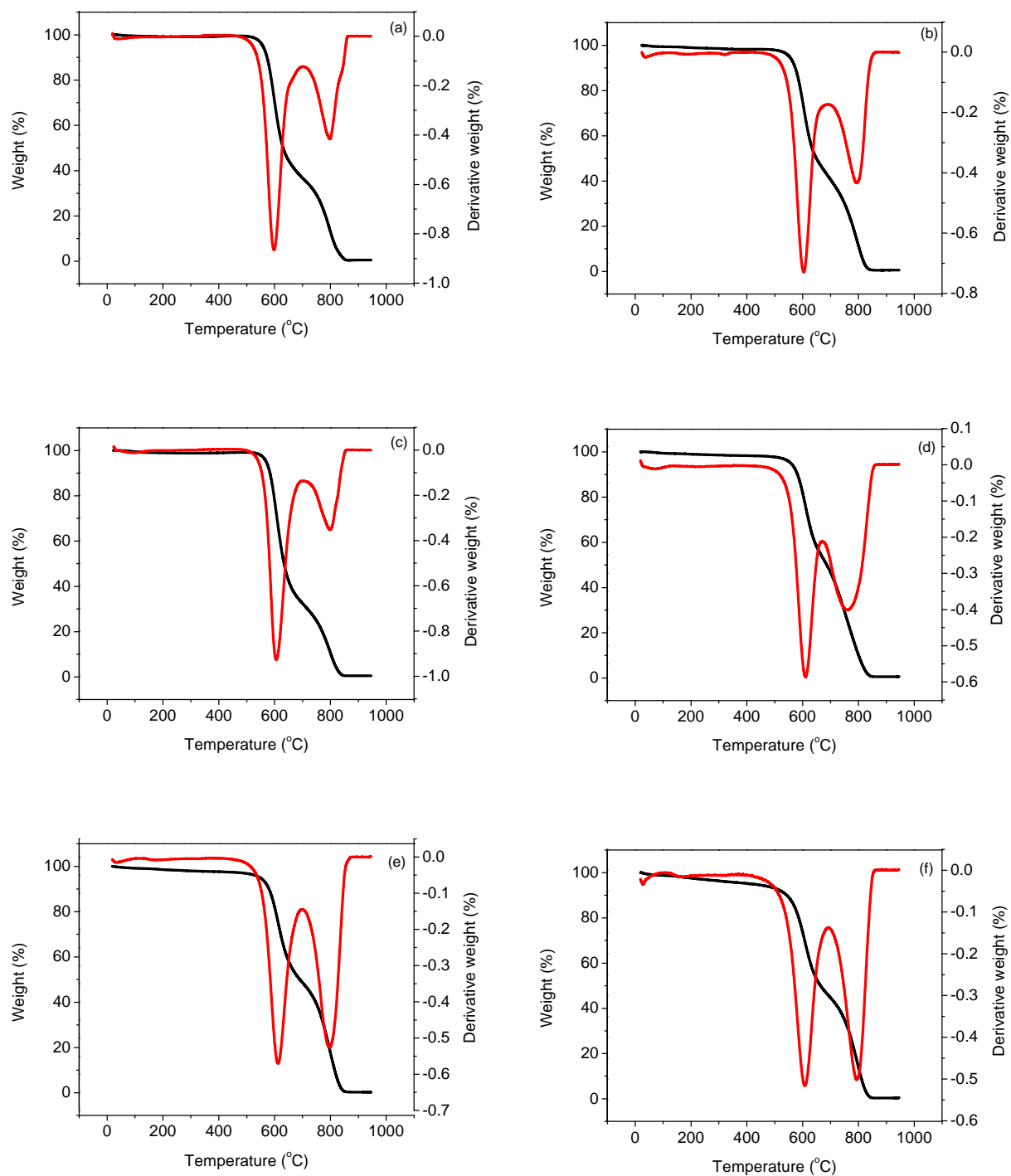


Figure 4.4. TGA and corresponding derivative weight loss graphs of (a) as - synthesized CSs and (b) fCSs 40 supports, (c) as - synthesized NCSs, (d) fNCSs 40, (e) fNCSs 60 and (f) fNCSs 80 supports.

The introduction of surface groups on carbon supports is very useful for the deposition of metals. The surface groups introduced are oxygenated and nitrogen surface groups. However functionalization and doping both damage the carbon surface structure by introducing large amounts of defects. These defects were analyzed using Raman spectroscopy (Figure 4.5 and Table 4.3) by evaluation of the intensities of the D (diamond - like sp^3 , $\sim 1350\text{ cm}^{-1}$) and the G (graphite - like sp^2 , $\sim 1590\text{ cm}^{-1}$) bands [51].

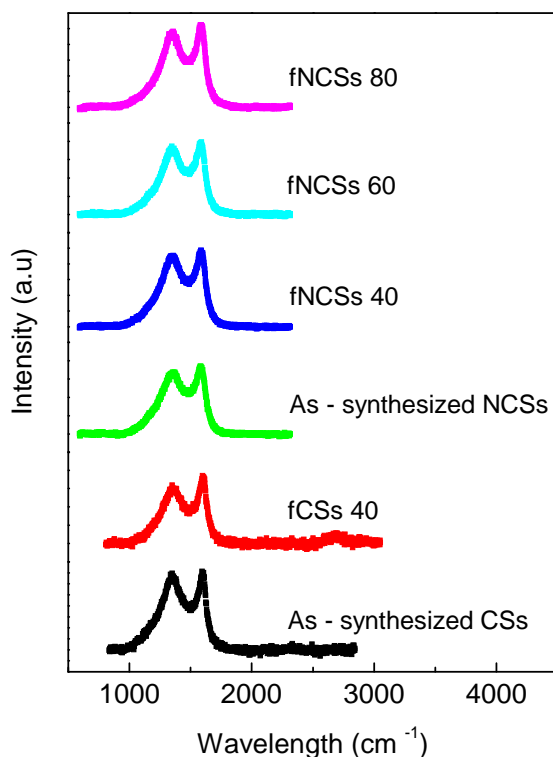


Figure 4.5. Raman graphs of as - synthesized and functionalized doped and undoped carbon spheres.

The ratio of the intensities of the two bands (I_D / I_G) shows the degree of disorder within the samples [52]. The I_D / I_G ratios of as - synthesized CSs, fCSs 40, as - synthesized NCSs, fNCSs 40, fNCSs 60 and fNCSs 80 are 2.49, 2.52, 2.62, 2.69, 2.72 and 2.75 respectively. The higher I_D / I_G ratios of NCSs compared to CSs imply a higher defectiveness of the graphite like layers by nitrogen doping. Functionalized supports had higher I_D / I_G ratios compared to their as-synthesized counterparts which showed that the introduction of oxygenated surface groups with nitric acid treatment damaged the carbon surface structures and led to the incorporation of a high amount of defects [28]. It was also observed that as the functionalization temperature increased the I_D / I_G ratio increased since the amount of oxygenated groups introduced onto the carbon surfaces also increased. The Raman results agree well with TGA and Zeta potential measurement results.

Table 4.3. Raman data for as - synthesized and functionalized CSs and NCSs.

Sample name	Peak position (cm^{-1})		I_D / I_G
	G - band	D - band	
As-synthesized CSs	1353.60	1592.90	2.49
fCSs 40	1354.11	1594.38	2.52
As-synthesized NCSs	1357.06	1589.93	2.62
fNCSs 40	1352.85	1591.05	2.69
fNCSs 60	1352.62	1588.95	2.72
fNCSs 80	1350.36	1590.52	2.75

The physical and chemical properties of as-synthesized and functionalized doped and undoped carbon spheres are shown in Table 4.4. The N content of as-synthesized NCSs, fNCSs 40, fNCSs 60 and fNCSs 80 supports are 2.50, 2.48, 2.41 and 2.47 % respectively. From CN elemental analysis results it can be seen that functionalization did not alter the N content of the carbon supports. The as - synthesized and

functionalized CSs and NCSs all had very low surface areas and pore volumes. This showed that they are non - porous support materials. The low surface areas of the as - synthesized and functionalized carbon spheres were consistent with those reported in literature [9, 11, 34, 53-55]. The low surface areas are attributed to the spherical morphology where the exposed surface areas are low. The low pore volumes are due to the open edges created by the unclosed graphitic flakes in the spheres.

Table 4.4. Physical and chemical properties of as - synthesized and functionalized CSs and NCSs supports.

Sample name	CN elemental analysis (%)		BET surface area (m^2 / g)	Pore volume (cm^3 / g)
	C	N		
As-synthesized CSs	99.34	< 0.05	1.50	0.0025
fCSs 40	99.18	< 0.05	1.53	0.0029
As-synthesized NCSs	93.90	2.50	1.51	0.0030
fNCSs 40	94.88	2.48	1.67	0.0028
fNCSs 60	91.50	2.41	1.79	0.0034
fNCSs 80	90.44	2.47	1.90	0.0044

4.3.1.2 Characterization of the Pd catalysts

The loading of Pd on the functionalized CSs and NCSs supports was done using the polyol method with ethylene glycol (EG) acting as both the solvent and reductant. Catalysts with 1 wt. % loading of Pd were prepared with CS supports functionalized at 40 °C and NCS supports functionalized at 40, 60 and 80 °C. The difference between the 4 catalysts (1 % Pd / fCSs 40, 1 % Pd / fNCSs 40, 1 % Pd / fNCSs 60

and 1 % Pd / fNCSs 80) prepared were the presence or absence of N in the support and support pretreatment conditions.

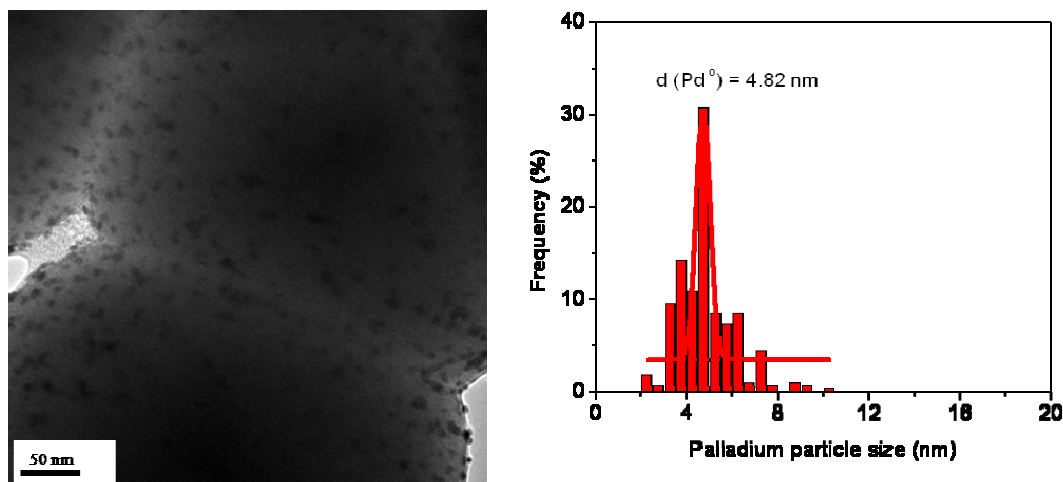


Figure 4.6. Typical TEM image and palladium particle size histogram of 1 % Pd / fCSs 40 catalyst.

The TEM images and corresponding histograms of the Pd particle size distribution graphs of 1 % Pd / fCSs 40, 1 % Pd / fNCSs 40, 1 % Pd / fNCSs 60 and 1 % Pd / fNCSs 80 catalysts are shown in Figures 4.6 - 4.9. The palladium nanoparticles sizes on the different supports were determined from the statistical analysis of TEM images of the catalysts. The average particle sizes of 1 % Pd / fCSs 40, 1 % Pd / fNCSs 40, 1 % Pd / fNCSs 60 and 1 % Pd / fNCSs 80 catalysts are 4.82, 4.68, 7.51 and 6.56 nm respectively (Table 4.5). On 1 % Pd / fNCSs 40 catalyst, the average Pd nanoparticles size is 4.68 nm, which is slightly smaller than that of 1 % Pd / fCSs 40 catalyst, 4.82 nm. Also some surfaces of the fCSs 40 support are free of Pd nanoparticles coverage while on the fNCSs 40 support, the Pd nanoparticles are homogeneously distributed. Because the deposition of Pd nanoparticles on the two supports was carried out under the same conditions, the difference in dispersion and nanoparticles size is attributed to the difference in the two supports. These results suggest that nitrogen doping on CSs

had a very small effect on the particle size and distribution of Pd during the reduction of $\text{Pd}(\text{C}_2\text{H}_3\text{O}_3)_2$ by ethylene glycol [42]. The presence of evenly distributed nitrogen species on the surfaces of doped carbon spheres provides nucleation sites and promotes a slightly higher dispersion of Pd nanoparticles. A previous study in literature has shown that Pt nanoparticles prefer to nucleate along kinks on the doped surface of CNTs, where nitrogen atoms are located [56]. It has been reported that nitrogen doping not only can facilitate a high dispersion of metal nanoparticles on the carbon surface but also results in a stronger interaction between the metal and the carbon support [14]. The oxygenated surface groups act as anchoring sites that bond covalently to the metal precursor. As the functionalization temperature was increased during the oxidative treatments, the amount of oxygen - containing groups on the NCSs supports increased. Solhy et al. have reported that the average metal particle diameter of metal nanoparticles decreases as the amount of anchoring sites of the NCNTs support increases [27]. The average particle sizes of 1 % Pd / fNCSs 40, 1 % Pd / fNCSs 60 and 1 % Pd / fNCSs 80 catalysts were found to vary. There was no direct correlation between the functionalization temperature of the NCSs support and the average particle sizes of Pd nanoparticles in the catalysts. For these 3 catalysts the nitrogen content of the supports is the same. For the 1 % Pd / fNCSs 60 and 1 % Pd / fNCSs 80 catalysts, an increase in functionalization temperature should have created more oxygen functional groups on the carbon surfaces to act as anchoring sites for metal adsorption and hence the mean particle size of Pd decreased from 7.51 nm to 6.56 nm respectively. However the mean particle diameters of the Pd nanoparticles in 1 % Pd / fNCSs 60 and 1 % Pd / fNCSs 80 catalysts were larger than that of the 1 % Pd / fNCSs 40 catalysts. The results were unexpected and no obvious explanation can be given for the increase of Pd particle size with functionalization temperature. The Pd nanoparticles were reasonably well dispersed on the NCSs supports for the 3 catalysts.

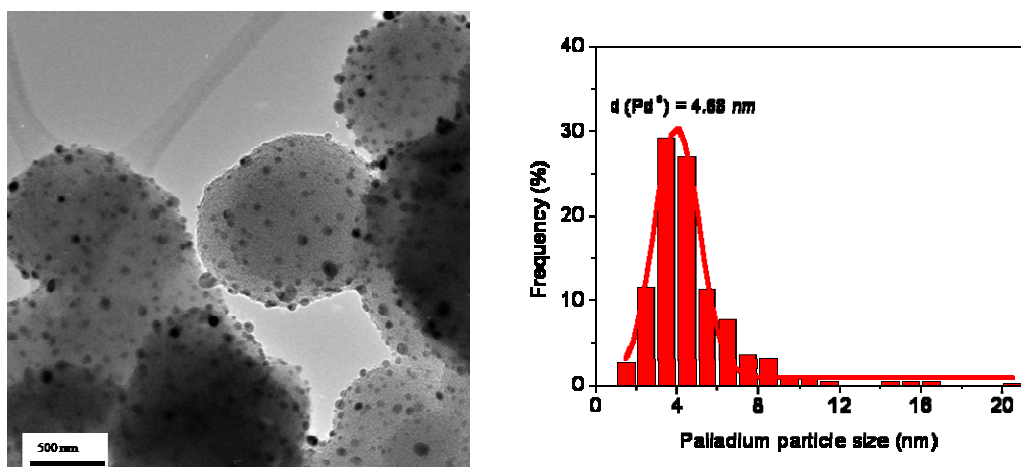


Figure 4.7. Typical TEM image and palladium particle size histogram of 1 % Pd / fNCSs 40 catalyst.

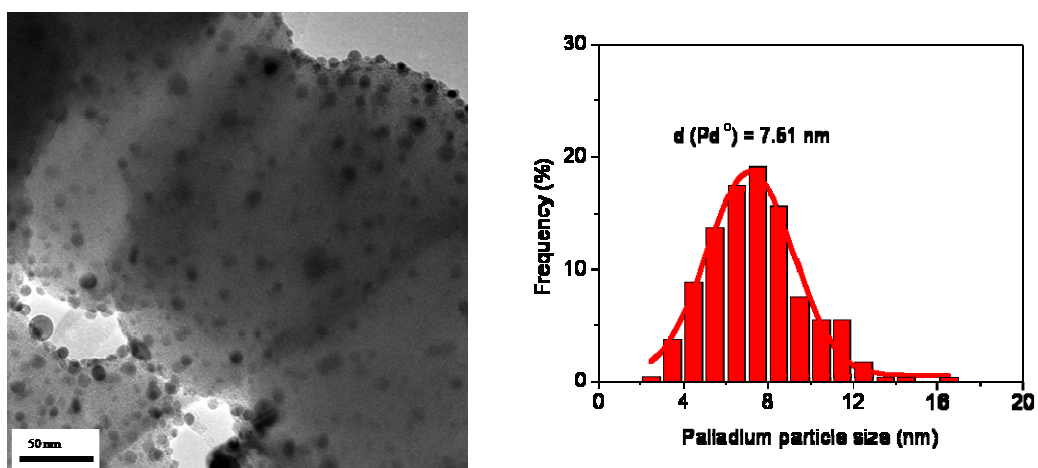


Figure 4.8. Typical TEM image and palladium particle size histogram of 1 % Pd / fNCSs 60 catalyst.

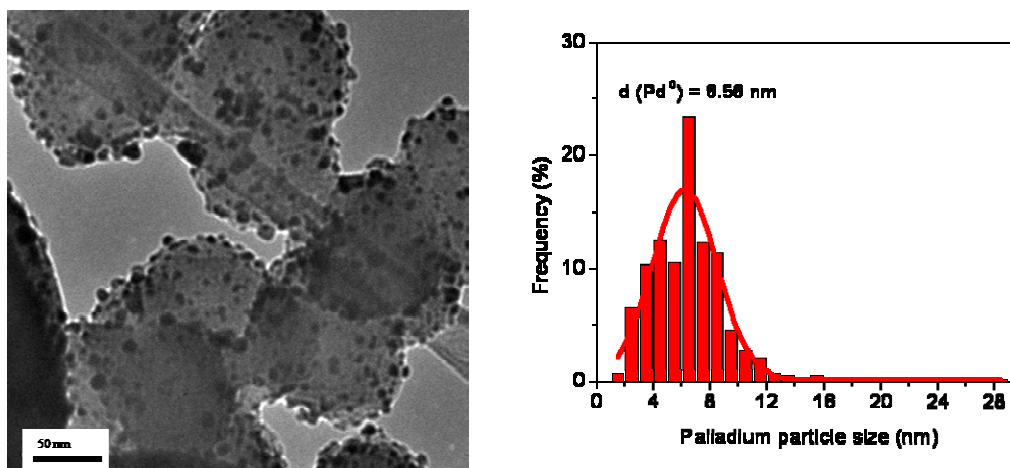


Figure 4.9. Typical TEM image and palladium particle size histogram of 1 % Pd / fNCSs 80 catalyst.

The presence of palladium was confirmed using TEM - EDX and ICP - OES. Table 4.5 shows the metal content for the four different catalysts. ICP - OES analysis showed that the palladium loadings for the catalysts were in the range 0.9 - 1.1 wt. %. ICP - OES analysis of the catalysts revealed that the metal contents obtained are fairly close to the targeted 1 wt. % loading of Pd predicted from the catalyst preparation. EDX was used to determine the elemental composition of the catalysts. A representative EDX spectrum of 1 % Pd / fNCSs 40 catalyst (Figure 4.10) illustrated that C, O and Pd elements were present in the catalyst. The presence of Cu is due to the use of Cu grids.

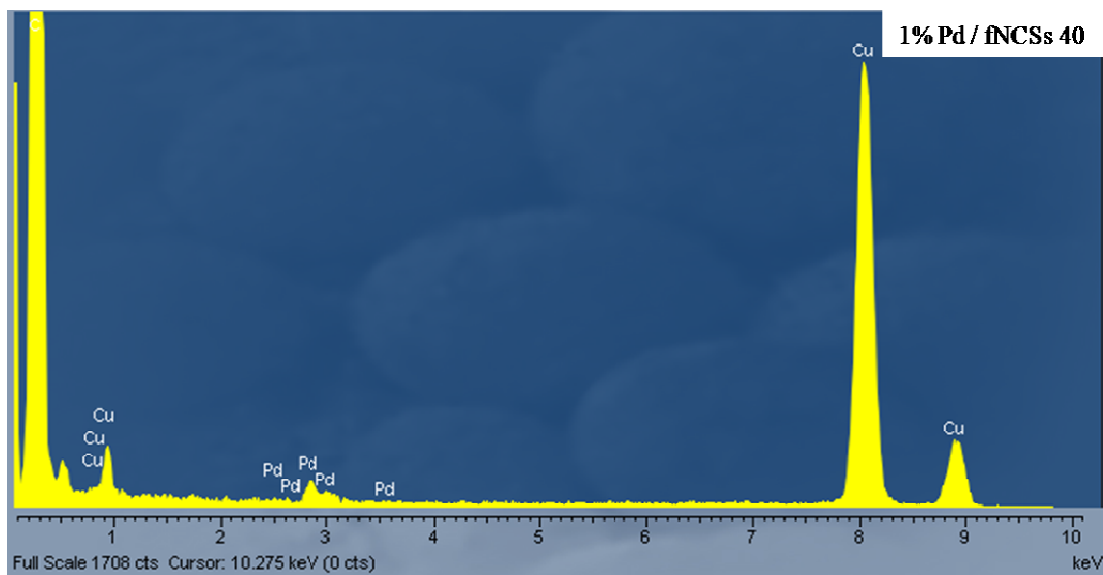


Figure 4.10. EDX spectrum showing the presence of Pd nanoparticles in the 1% Pd / fNCSs 40 catalyst.

The structural parameters of the catalysts are compiled in Table 4.5. The measured BET surface areas were $3.5 \text{ m}^2 / \text{g}$ for 1 % Pd / fNCSs 40 catalyst, $3.8 \text{ m}^2 / \text{g}$ for 1 % Pd / fNCSs 40 catalyst, $3.9 \text{ m}^2 / \text{g}$ for 1 % Pd / fNCSs 60 catalyst and $4.0 \text{ m}^2 / \text{g}$ for 1 % Pd / fNCSs 80 catalyst. The presence or absence of nitrogen and the functionalization at different temperatures with nitric acid in the carbon spheres supports did not yield any significant changes to the resultant catalyst properties.

Table 4.5. Physical properties of the catalysts.

Sample name	BET surface area (m² / g)	Pore volume (cm³ / g)	Metal loading (wt. %)^a	Average particle size (nm)^b
1 % Pd / fCSs 40	3.5	0.011	0.99	4.82
1% Pd / fNCSs 40	3.8	0.016	1.03	4.68
1 % Pd / fNCSs 60	3.9	0.022	0.96	6.56
1 % Pd / fNCSs 80	4.0	0.031	1.00	7.51

^a Determined by ICP - OES analysis, ^b Based on TEM

The TGA of the functionalized support materials and their corresponding catalysts run under an air atmosphere are shown in Figure 4.11. The peak positions of weight loss of the catalysts are shown in Table 4.6. The onset of oxidation was lowered when Pd was added to the supports (Table 4.6). This was due to the Pd metal catalyzing the oxidation of carbon [35]. The onset of oxidation for functionalized doped and undoped carbon spheres was in the temperature ranges of $\approx 606 - 612$ °C and that of the CSs containing Pd at $\approx 521 - 557$ °C. Two distinct regions for the oxidation of all catalysts were observed. The first region is due to the oxidation of doped or undoped carbon spheres functional groups directly in contact with Pd. The second region is due to the oxidation of carbon that contains no functional groups that are in contact with Pd nanoparticles present. The temperatures at which the first regions occur are 557, 544, 533 and 521 °C for 1 % Pd / fCSs 40, 1 % Pd / fNCSs 40, 1 % Pd / fNCSs 60 and 1 % Pd / fNCSs 80 catalysts respectively. The temperatures at which the second regions occur are 692, 671, 655 and 623 °C for 1 % Pd / fCSs 40, 1 % Pd / fNCSs 40, 1 % Pd / fNCSs 60 and 1 % Pd / fNCSs 80 catalysts respectively. The thermal stability of the catalysts decreased as the functionalization temperature of the supports with nitric acid was increased. This was due to the number of functional groups increasing the number of defects introduced in the oxidation step which then allowed the carbon matrix to be consumed at lower temperatures. The nitrogen doped

catalysts were less thermally stable than the undoped catalysts. This was due to the presence of defects in the graphite like layers caused by nitrogen doping which makes the doped catalysts burn at lower temperatures.

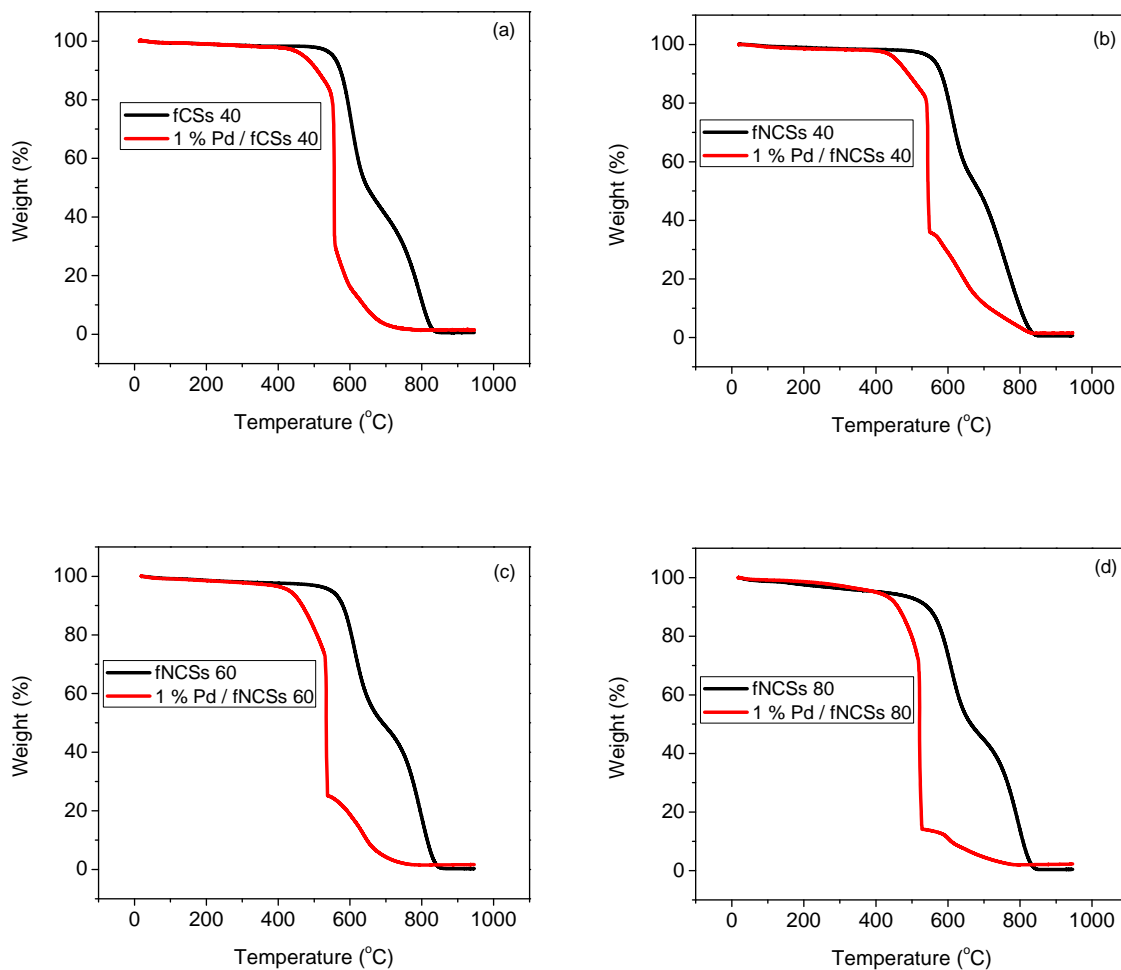


Figure 4.11. TGA profiles run in air of (a) fCSs 40 and 1 % Pd / fCSs 40 (b) fNCSs 40 and 1 % Pd / fNCSs 40, (c) fNCSs 60 and 1 % Pd / fNCSs 60 and (d) fNCSs 80 and 1 % Pd / fNCSs 80 catalysts.

Table 4.6. TGA data of functionalized carbon supports and the corresponding catalysts.

Sample name	Temperature range (°C)	
	Region I	Region II
fCSs 40	612	791
fNCSs 40	610	760
fNCSs 60	612	799
fNCSs 80	606	795
1 % Pd / fCSs 40	557	692
1 % Pd / fNCSs 40	544	671
1 % Pd / fNCSs 60	533	655
1 % Pd / fNCSs 80	521	623

XRD patterns of 1 wt. % Pd catalysts synthesized using doped and undoped carbon sphere supports functionalized at different temperatures are shown in Figure 4.12. The XRD patterns of 1 % Pd / fCSs 40, 1 % Pd / fNCSs 40, 1 % Pd / fNCSs 60 and 1 % Pd / fNCSs 80 catalysts show diffraction peaks at approximately 29.4 °, 47.0 ° and 52.0 ° which are attributed to the (002), (101) and (004) reflections of graphite [57-59]. No diffraction peaks corresponding to Pd particles were observed indicating the high dispersion of Pd nanoparticles on the surfaces of CSs and NCSs supports [60]. This was in agreement with the TEM results. The absence of diffraction peaks of Pd was also related to the low percentage loading of Pd on the catalysts.

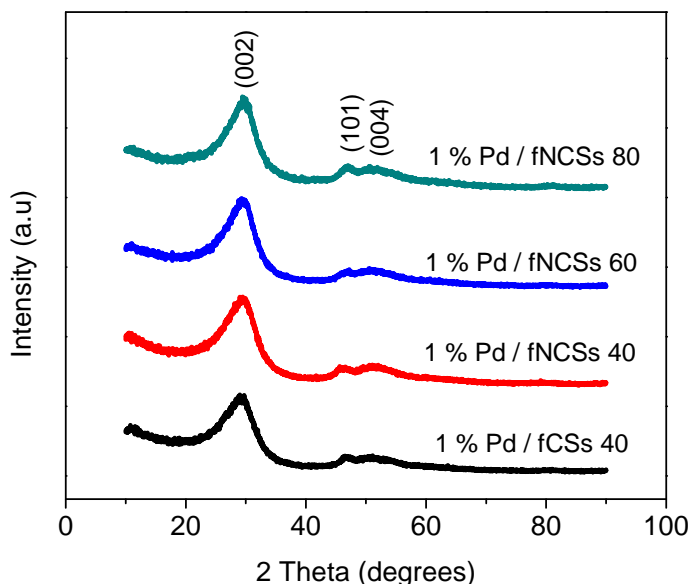


Figure 4.12. Powder XRD patterns of 1 wt. % Pd catalysts synthesized using doped and undoped carbon sphere supports functionalized at different temperatures of nitric acid.

4.3.1.3 Catalytic tests

The catalysts (1 % Pd / fCSs 40, 1 % Pd / fNCSs 40, 1 % Pd / fNCSs 60 and 1 % Pd / fNCSs 80) were tested for the cinnamaldehyde (CALD) hydrogenation reaction and the results are depicted in Figure 4.13 and Table 4.7. Blank tests carried out over the supports alone showed no catalytic activity. It is important to note that the main product of this reaction using all the 4 catalysts was hydrocinnamaldehyde (HCALD). Cinnamyl alcohol (CA) and 3-phenyl-1-propanol were not detected. The selectivities to HCALD were 100.00 % from reaction time 1 hour to 8 hours for all the 4 catalysts regardless of the presence or absence of nitrogen in the support and the different support functionalization temperatures used. The high C=C bond hydrogenation selectivity observed for all the 4 catalysts could be attributed to the small particle

sizes of Pd nanoparticles and the complete absence of micropores, which provided an efficient contact surface between reactants and the active phase in the liquid phase medium [61]. However there was a marked difference, in catalyst activity (expressed as conversion) for the 4 catalysts at reaction time of 3 hours. The conversions of CALD for 1 % Pd / fCSs 40, 1 % Pd / fNCSs 40, 1 % Pd / fNCSs 60 and 1 % Pd / fNCSs 80 catalysts were 48, 87 91 and 10 % respectively. The conversion of CALD over the 1 % Pd / fNCSs 40 catalyst almost doubled (87 % at reaction time 3 hours) when compared to that of the 1 % Pd / fCSs 40 catalyst (48 % at reaction time 3 hours). This was due to the introduction of N atoms in the graphite structure of the CS supports which improved the metal surface adsorption and resulted in higher C=C hydrogenation activity. Similar results of improved catalytic activity for the hydrogenation of CALD were observed for catalysts with N present when compared to N free catalysts [39-41]. The difference in CALD conversion was reported to be attributed to an electronic alteration of the metal particles which in turn is due to the electronic modification of the support by the incorporation of nitrogen atoms inside the carbon framework. Functionalization of the doped carbon sphere supports at 40 and 60 °C with nitric acid for 24 hours had a very small or little effect on the hydrogenation of CALD with the resultant Pd catalysts. The conversions of CALD were 87 and 91 % for the 1 % Pd / fNCSs 40 and 1 % Pd / fNCSs 60 catalysts respectively. The conversion of CALD for the 1 % Pd / fNCSs 80 catalyst was 10 %. Increasing the functionalization temperature of the NCSs supports from 60 to 80 °C, had the effect of lowering the conversion of CALD approximately 10 times. This might have been due to the high concentration of oxygen surface groups on the catalyst. The carbon support with a low concentration of oxygen is favourable for the π - π interaction between the phenyl ring of CALD and the basic sites on the carbon sphere surface [26, 31]. The local concentration of CALD on the carbon sphere surfaces could therefore increase, resulting in improved catalytic activity. Several studies have been done by other researchers where they saw that the selectivity and activity in the liquid phase hydrogenation of CALD was found to be dependent on the amount of oxygen on the CNT or CNF support [24, 25, 27, 28, 32]. The improved

catalytic activity on 1 % Pd / fNCSs40 and 1 % Pd / fNCSs60 catalysts could also be due to the lower amount of oxygen surface groups on the supports which resulted in an electron density enrichment of the palladium nanoparticles and increased metal support interaction [62]. From the results obtained, the hydrogenation of CALD is greatly affected by the surface chemistry of the doped and undoped carbon sphere supports as the metal particle sizes were kept constant.

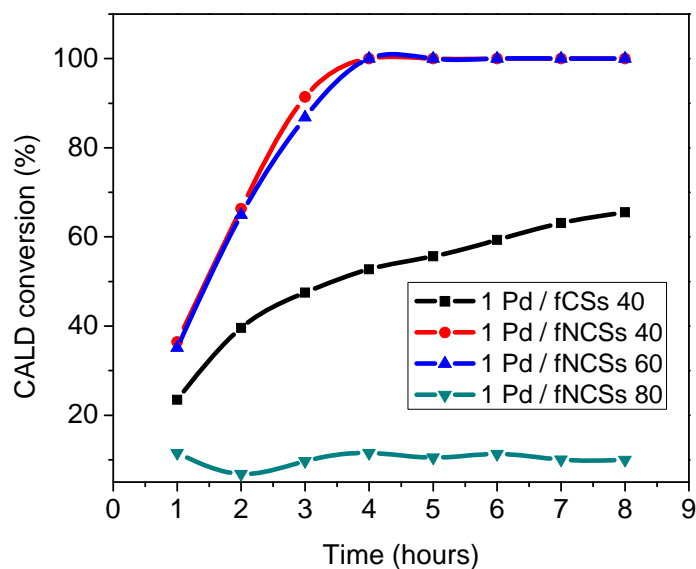


Figure 4.13. Catalytic activity, expressed in terms of conversion as a function of time for the cinnamaldehyde (CALD) hydrogenation of the different Pd - based CSs and NCSs catalysts.

Table 4.7. The effect of support pre - treatment on the hydrogenation of CALD.

Catalyst	Activity (%)	Reaction time (hours)							
		1	2	3	4	5	6	7	8
1 % Pd / fCSs 40	Conversion	24	40	48	53	56	59	63	66
	HCALD selectivity	100.0	100.0	100.0	100.0	100.0	100.0	100.0	100.0
1 % Pd / fNCSs 40	Conversion	35	65	87	100	100	100	100	100
	HCALD selectivity	100.0	100.0	100.0	100.0	100.0	100.0	100.0	100.0
1 % Pd / fNCSs 60	Conversion	37	66	91	100	100	100	100	100
	HCALD selectivity	100.0	100.0	100.0	100.0	100.0	100.0	100.0	100.0
1 % Pd / fNCSs 80	Conversion	12	7	10	11	11	11	10	10
	HCALD selectivity	100.0	100.0	100.0	100.0	100.0	100.0	100.0	100.0

No Cinnamyl alcohol and 3-phenyl-1-propanol were observed.

Reaction conditions: CALD = 1.26 ml, hexan-1-ol = 100 ml, catalyst weight = 100 mg, T = 60 °C and H₂ (g) = 50 ml / min.

4.3.2 Effect of N content of the support

4.3.2.1 Support characterization

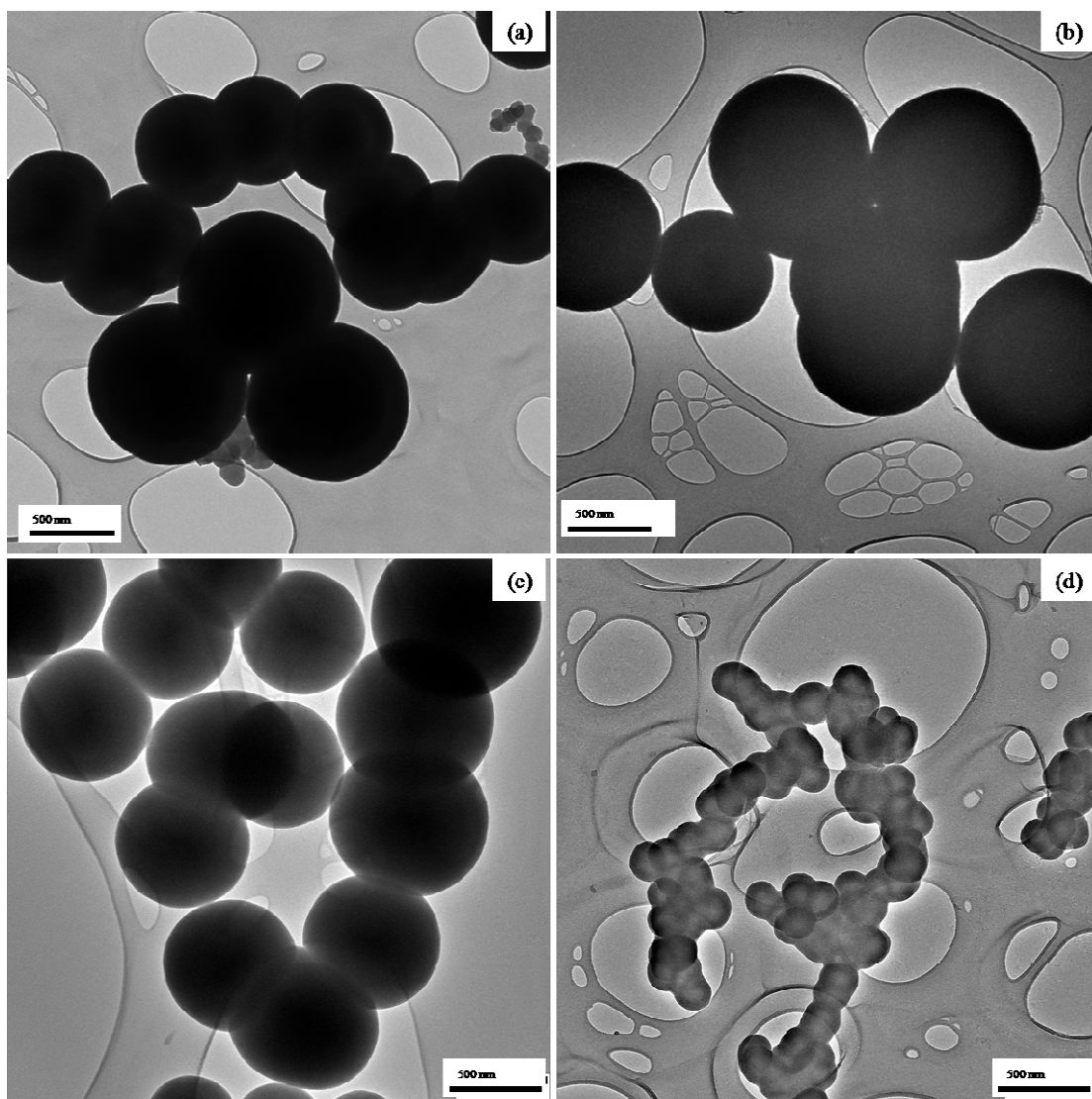


Figure 4.14. TEM images of (a) 0.00 % N support, (b) 0.41 % N support, (c) 2.39 % N support and (d) 3.84 % N support.

The CSs with different nitrogen contents were synthesized by either using acetonitrile or not and by varying the flow rates of the acetylene and nitrogen gases during the carbonization step. See Chapter 3. The TEM images of carbon spheres supports with different nitrogen contents are shown in Figure 4.14. The average diameters of 0.00 % N, 0.41 % N, 2.39 % N and 3.84 % N supports are 751 nm, 814 nm, 669 nm and 236 nm respectively. There is no direct correlation between the average diameters of carbon spheres and the nitrogen content.

The incorporation of nitrogen in the carbon sphere structures was confirmed by XPS and CN elemental analysis. The results are shown in table 4.8. CN elemental results confirmed the nitrogen contents of 0.00 % N, 0.41 % N, 2.39 % N and 3.84 % N for the different supports. XPS analysis results showed that the 0.41 % N, 2.39 % N and 3.84 % N supports had 1, 3 and 5 at. % N contents respectively. The XPS and CN elemental results were different because XPS is a surface analysis technique whereas CN elemental analysis measures the N in the whole bulk sample. The samples were named according to their N contents determined using CN elemental analysis.

The N1s XPS spectra of carbon sphere supports containing different nitrogen amounts are presented in Figure 4.15. The XPS N1s spectrum indicates the presence of at least two different nitrogen based species on the NCSs. Literature related to nitrogen doped carbon nanostructures assigns nitrogen functionalities to pyridinic nitrogen (398.4 - 399.0 eV), pyrrolic nitrogen (400.0 - 400.6 eV), quaternary nitrogen (401.1 - 401.7 eV) and to nitrogen oxide species and or intercalated nitrogen molecules (402.0 - 405.0 eV) [40, 63, 64]. The 0.41 % N support contained pyrrolic nitrogen (79.50 %) and nitrogen oxide species and or intercalated nitrogen molecules (20.50 %). The 2.39 % N support had 27.79, 56.97 and 15.24 % of pyridinic nitrogen, pyrrolic + quaternary nitrogen and nitrogen oxide species and or intercalated nitrogen molecules respectively. The 3.84 % N support contained pyridinic nitrogen,

quaternary nitrogen and nitrogen oxide species and or intercalated nitrogen molecules in percentages of 29.38, 45.06 and 25.56 % respectively.

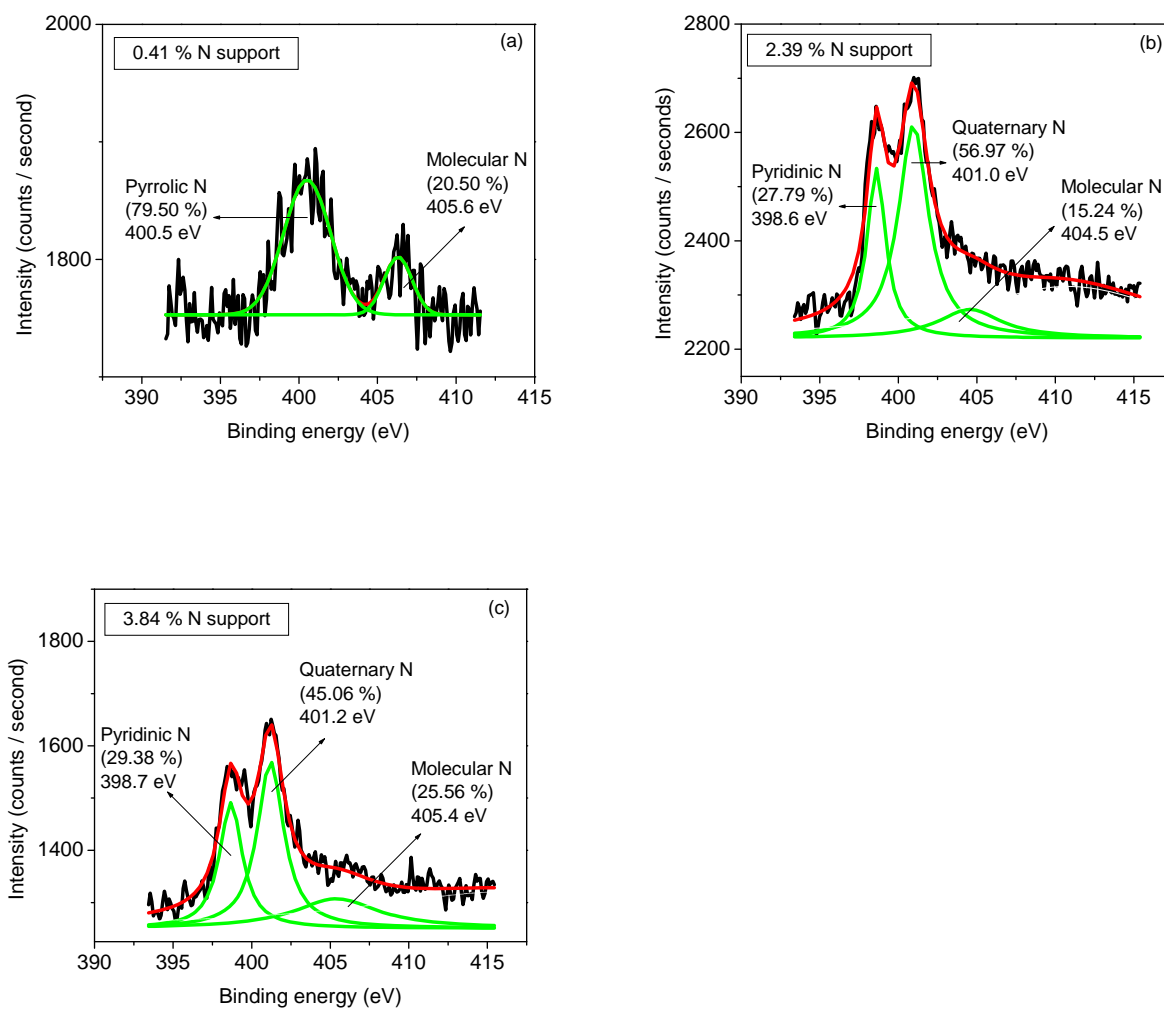


Figure 4.15. N1s spectra of a) 0.41 % N, b) 2.39 % N and c) 3.84 % N supports.

Table 4.8. CN elemental and XPS analysis results.

Support name	CN elemental analysis (%)		XPS analysis (at. %)			Nitrogen species (%) (Binding energy (eV))				
	C	N	C	N	O	Pyridinic N	Pyrrolic N	Pyrrolic + Quaternary N	Quaternary N	Molecular N or N-O-C
0.00 % N support	98.46	< 0.05	-	-	-	-	-	-	-	-
0.41 % N support	98.28	0.41	97	1	2	-	79.50 (400.5)	-	-	20.50 (405.0)
2.39 % N support	93.90	2.39	93	3	4	27.79 (398.6)	-	56.97 (401.0)	-	15.24 (404.5)
3.84 % N support	94.44	3.84	92	5	3	29.38 (398.7)	-	-	45.06 (401.2)	25.56 (405.0)

4.3.2.2 Catalyst characterization

TEM micrographs and the corresponding particle size distribution graphs of the Pd catalysts on the different N supports are presented in Figures 4.16 - 4.18. According to the TEM analysis the palladium particles were well dispersed on the NCS supports. The better dispersion of the Pd nanoparticles on NCS supports could be ascribed to higher wettability, more surface structural defects and active surface by nitrogen doping [41, 65]. The undoped carbon sphere support (0.00 % N support) had some areas where palladium nanoparticles were absent. The average metal particle sizes determined from the statistical analysis of the TEM micrographs were 4.82, 4.24, 4.68 and 4.15 nm for the 1 % Pd / fCSs 40 catalyst (0.00 % N), 1 % Pd / fNCSs 40 catalyst (0.41 % N), 1 % Pd / fNCSs 40 catalyst (2.39 % N) and 1 % Pd / fNCSs 40 catalyst (3.84 % N) respectively. The difference in the average Pd particle sizes of the 4 catalysts was due to the number of functional sites available on the surface of the support material available for palladium anchorage and nanoparticle deposition [66]. The 1 % Pd / fCSs 40 catalyst (0.00 % N) had the largest particle sizes compared to 1 % Pd / fNCSs 40 catalysts with different N contents. This was due to the presence of N in the NCSs support which increased the number of anchoring sites for the palladium particles. As the nitrogen content in the support increased, the number of anchorage sites for adsorption of metal nanoparticles also increased. Jiang et al observed that the introduction of nitrogen groups onto the surface of CNTs drastically increased the dispersion and stability of metal nanoparticles, owing to a strong - metal - nitrogen interaction [67-69]. The average particle sizes were supposed to decrease as the nitrogen content in the catalyst increased. However the 1% Pd / fNCSs 40 catalyst (2.39 % N) did not follow the trend. The 1 % Pd / fNCSs 40 catalyst (0.41 % N) and 1 % Pd / fNCSs 40 catalyst (3.84 % N) did follow the trend. The decrease in average particle sizes of palladium nanoparticles as the N content in the supports increased was due to the increase in the number of anchorage sites for the adsorption of the active phase on the support. The effect was very small.

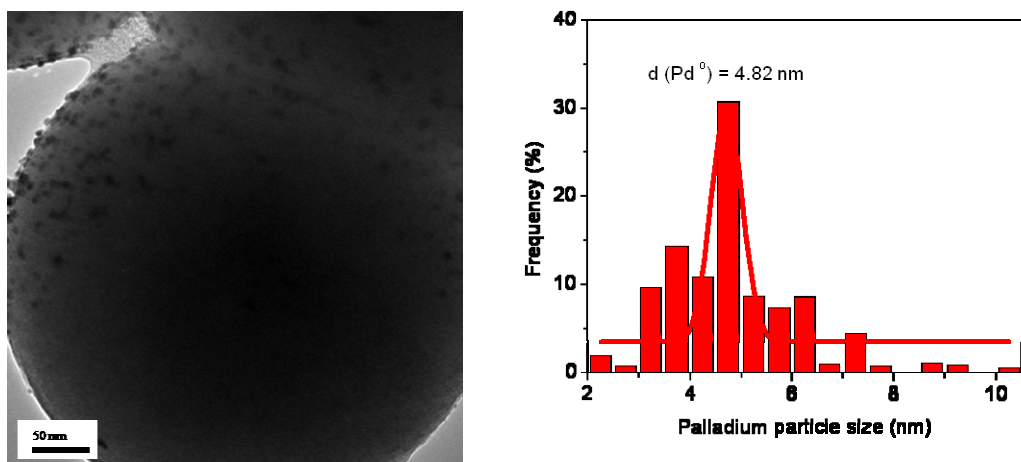


Figure 4.16. TEM image and corresponding particle size distribution graph of 1 % Pd / fCSs 40 catalyst (0.00 % N).

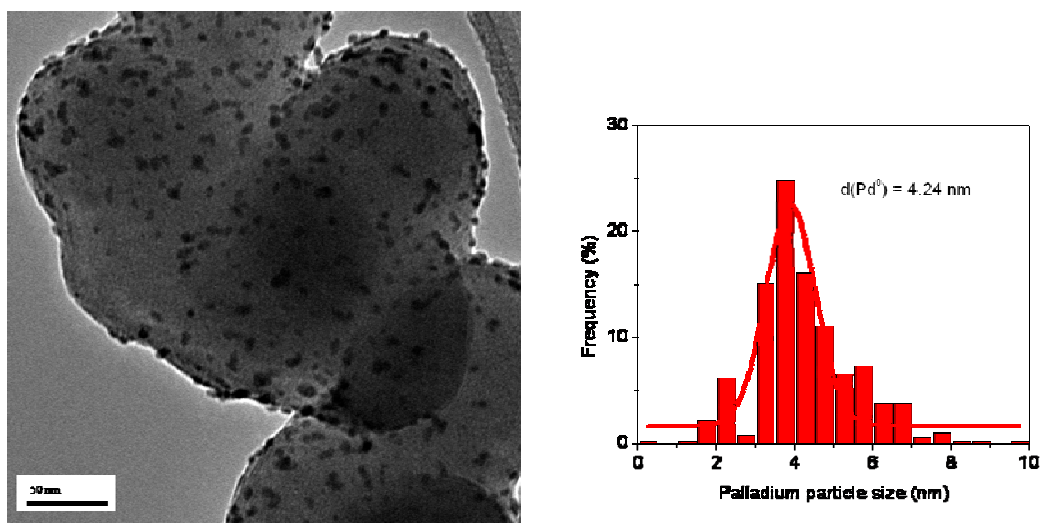


Figure 4.17. TEM image and corresponding particle size distribution graph of 1 % Pd / fNCSs 40 catalyst (0.41 % N).

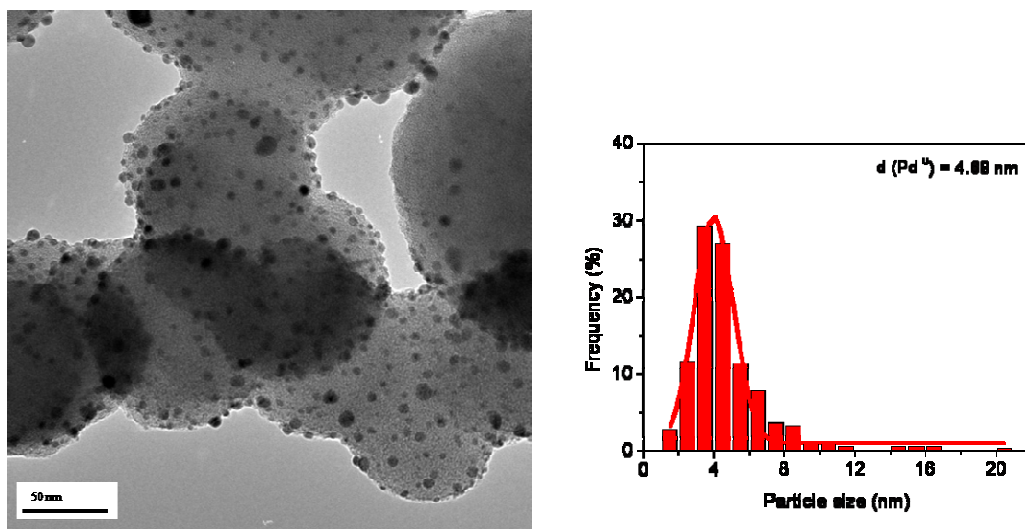


Figure 4.18. TEM image and corresponding particle size distribution graph of 1 % Pd / fNCSs 40 catalyst (2.39 % N).

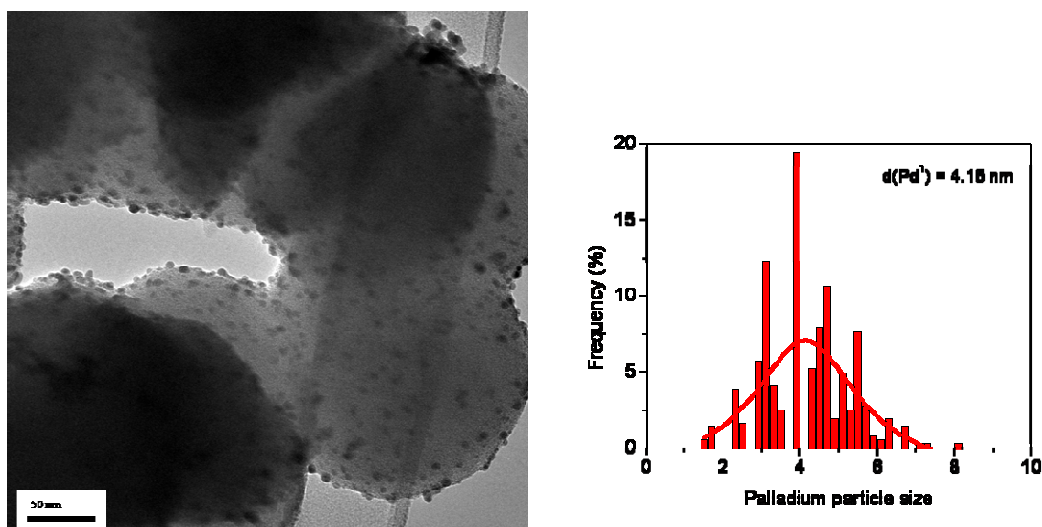


Figure 4.19. TEM image and corresponding particle size distribution graph of 1 % Pd / fNCSs 40 catalyst (3.84 % N).

The presence of Pd in the catalysts was confirmed by the representative TEM - EDX analysis of 1 % Pd / fNCSs 40 catalyst (3.84 % N) (Figure 4.20). The EDX spectrum showed that C, O and Pd elements were present in the catalyst. The Cu detected was due to the use of Cu grids during the analysis.

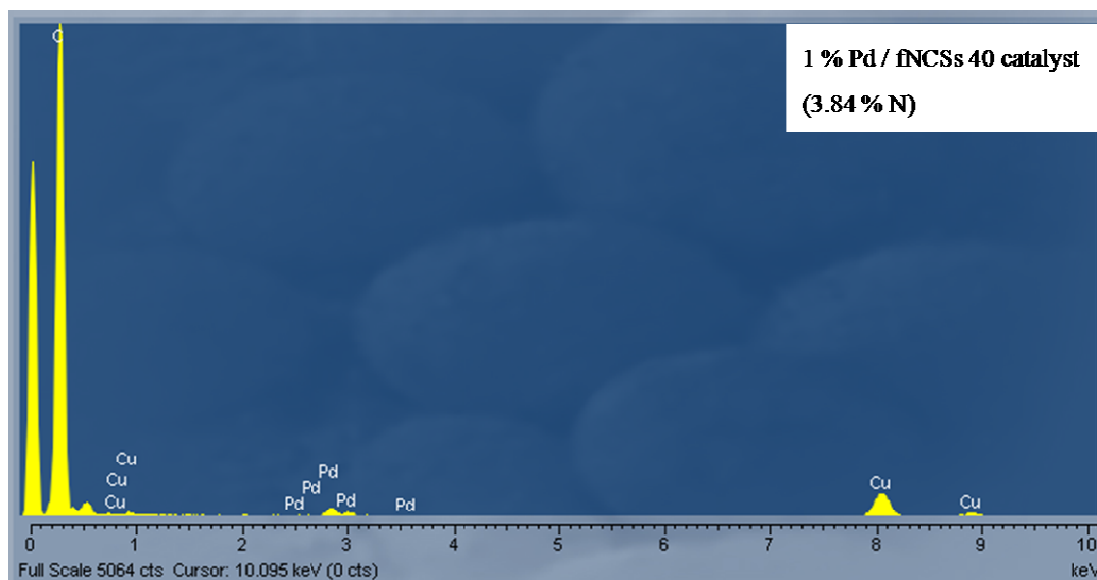


Figure 4.20. EDX spectrum of 1 % Pd / fNCSs 40 catalyst (3.84 % N).

ICP - OES analysis was used to further confirm the presence of Pd in the catalysts. Table 4.9 shows the ICP - OES results of the 4 catalysts. The 1 % Pd / fCSs 40 catalyst (0.00 % N), 1 % Pd / fNCSs 40 catalyst (0.41 % N), 1 % Pd / fNCSs 40 catalyst (2.39 % N) and 1 % Pd / fNCSs 40 catalyst (3.84 % N) had Pd contents of 0.99, 0.99, 1.03 and 0.90 wt. % respectively. The Pd content of all 4 catalysts were close to the targeted 1 wt. % loading of Pd predicted from catalyst preparation.

Table 4.9. Physical properties of the catalysts.

Catalyst	BET surface area (m² / g)	Pore volume (m³ / g)	Pd content (%)^a	Average particle size (nm)^b
1 % Pd / fCSs 40 (0.00 % N)	3.5	0.011	0.99	4.82
1 % Pd / fNCSs 40 (0.41 % N)	3.7	0.014	0.99	4.24
1 % Pd / fNCSs 40 (2.39 % N)	3.8	0.016	1.03	4.68
1 % Pd / fNCSs 40 (3.84 % N)	4.0	0.035	0.90	4.15

^a Determined by ICP-OES analysis, ^b Based on TEM measurements

The BET surface areas and pore volumes of the 4 catalysts are shown in Table 4.9. The BET surface areas for 1 % Pd / fCSs 40 catalyst (0.00 % N), 1 % Pd / fNCSs 40 catalyst (0.41 % N), 1 % Pd / fNCSs 40 catalyst (2.39 % N) and 1 % Pd / fNCSs 40 catalyst (3.84 % N) were 3.5, 3.7, 3.8 and 4.0 m² / g respectively. The pore volumes for all catalysts were in the range of 0.011 - 0.035 m³ / g. The low BET surface areas and pore volumes were due to the absence of porosity within the carbon sphere structures [53, 55, 70].

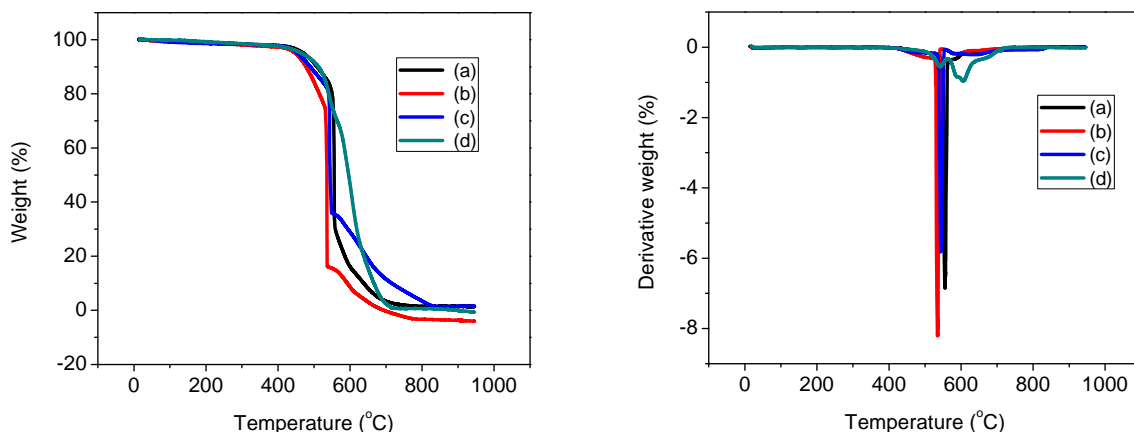


Figure 4.21. TGA and corresponding derivative weight loss graphs of a) 1 % Pd / fCSs 40 catalyst (0.00 % N), b) 1 % Pd / fNCSs 40 catalyst (0.41 % N), c) 1 % Pd / fNCSs 40 catalyst (2.39 % N) and d) 1 % Pd / fNCSs 40 catalyst (3.84 % N).

The TGA and corresponding derivative weight loss graphs of 1 % Pd / fCSs 40 catalyst (0.00 % N), 1 % Pd / fNCSs 40 catalyst (0.41 % N), 1 % Pd / fNCSs 40 catalyst (2.39 % N) and 1 % Pd / fNCSs 40 catalyst (3.84 % N) are shown in Figure 4.21. The peak positions of weight loss of the catalysts are shown in Table 4.10. Two distinct regions of the oxidation of the 4 catalysts were observed. The relative DTG curves of the 4 catalysts were in the regions 533 - 557 °C and 605 - 692 °C. The first region was due to the oxidation of doped or undoped carbon spheres functional groups in contact with Pd metal. The second region was due to the oxidation of carbon with no functional groups that are in contact with Pd nanoparticles. The presence of N in the carbon spheres made the catalysts less thermally stable because of the introduction of defects in the carbon framework.

Table 4.10. Decomposition temperatures of 1 % Pd catalysts containing different N contents of the support.

Sample name	Temperature range (°C)	
	Region I	Region II
1 % Pd / fCSs 40 catalyst (0.00 % N)	557	692
1 % Pd / fNCSs 40 catalyst (0.41 % N)	535	685
1 % Pd / fNCSs 40 catalyst (2.39 % N)	544	671
1 % Pd / fNCSs 40 catalyst (3.84 % N)	540	605

The XRD patterns of 1 % Pd / fCSs 40 catalyst (0.00 % N), 1 % Pd / fNCSs 40 catalyst (0.41 % N), 1 % Pd / fNCSs 40 catalyst (2.39 % N) and 1 % Pd / fNCSs 40 catalyst (3.84 % N) are shown in Figure 4.22. Each profile exhibited 3 peaks at reflections of approximately 28.4°, 45.7° and 51.2°, which corresponded to the (002), (100) and (004) graphite planes respectively. No diffraction peaks corresponding to Pd were observed in all the catalysts. This showed that there was a high dispersion of the Pd nanoparticles on the carbon spheres supports and also that a very low loading of Pd was used.

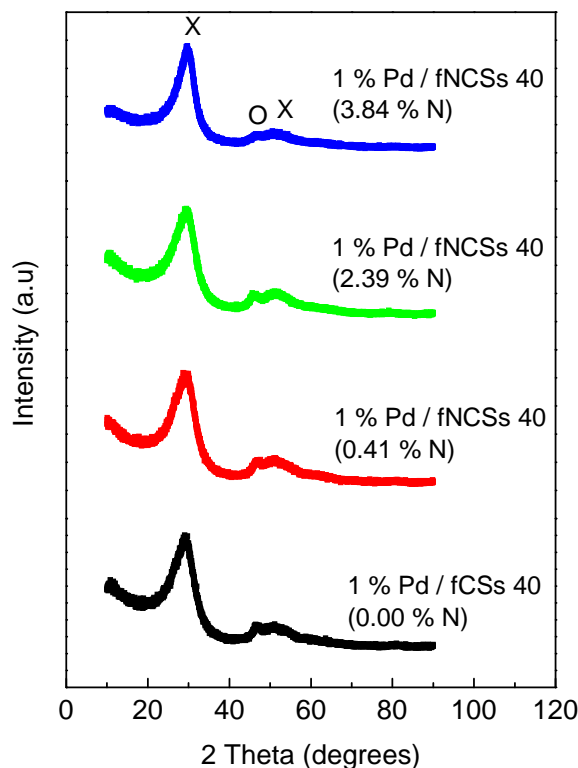


Figure 4.22. Powder XRD patterns of 1 % Pd fNCSs 40 catalysts containing different N contents of support. (X = C).

4.3.2.3 Catalytic test reactions

A study was performed to evaluate the catalytic performances of Pd nanoparticles supported on four different types of carbon sphere catalyst supports for the liquid phase hydrogenation of CALD. The influence of the support was evaluated on the catalytic activity. The hydrogenation results are shown in Figure 4.23 and Table 4.11. According to the results obtained, the most effective catalyst in terms of activity (expressed as conversion) is 1 % Pd / fNCSs 40 (2.39 % N) catalyst, the conversion of CALD was 91 % at reaction time 3 hours. This was then followed by 1 % Pd /

fNCSs 40 (3.84 % N), 1 % Pd / fNCSs 40 (0.41 % N) and lastly 1 % Pd / fCSs 40 (0.00 % N) catalyst with conversions to CALD of 59, 54 and 48 % respectively at reaction time of 3 hours. The catalytic results show that the Pd supported on N free carbon spheres (1 % Pd / fCSs 40 (0.00 % N)) exhibited the lowest CALD conversion when compared to the Pd supported on N doped carbon sphere catalysts. As the particle sizes of the catalysts were all nearly the same, the effect is due to the presence of N. Chizari *et al* reported that an improved catalytic activity on N doped supports was due to an electronic alteration of metal particles due to the electronic modification of support by the insertion of N atoms in the carbon structure [41]. Although the 1 % Pd / fNCSs 40 catalyst (3.84 % N) contained a higher percentage of nitrogen, it had a lower conversion to CALD of 59 % when compared to the 1 % Pd / fNCSs 40 catalyst (2.39 % N) which had a conversion of CALD of 91 % at reaction time 3 hours. Increasing the amount of N in the support up to a certain N level has a negative effect on the hydrogenation of CALD as evidenced by the above results. The catalytic activity of 1 % Pd / fNCSs 40 catalysts increased as the N content was increased from 0.00 % to 2.39 % N and decreased as the N content was further increased to 3.84 % N. The increase in catalytic activity of the 1 % Pd / fNCSs 40 catalysts as the N content was increased from 0.00 % to 2.39 % N was attributed to the increased number of N anchorage sites for the Pd nanoparticles as the N doping on carbon supports increased. The nitrogenated sites provide a strong metal - support interaction which efficiently anchors the metal precursor on the carbon sphere supports and stabilizes the final metal nanoclusters [36, 65, 67]. This in turn has an effect of increasing the dispersion of Pd nanoparticles on support which in turn increased catalytic activity. It has been reported that N doped carbon nanostructures containing pyridinic type N and or pyrrolic type N species exhibited high catalytic activity in oxygen reduction reactions (ORR) and Fischer - Tropsch (FT) synthesis [38, 71, 72]. The pyridinic N and pyrrolic N sites bind to Pd atoms on the NCS surfaces. The 1 % Pd / fNCSs 40 (2.39 % N) catalyst contained 27.79 % of pyridinic N and 56.97 % pyrrolic N + quaternary N species whereas the 1 % Pd / fNCSs 40 (3.84 % N) contained 29.38 % pyridinic N, 45.06 % quaternary N and 25.56 %

molecular N and nitrogen oxide species and finally the 1 % Pd / fNCSs 40 (0.41 % N) contained 79.50 % pyrrolic N and 20.50 % molecular N and nitrogen oxide species. This shows that there appears to be a direct correlation between the % N content of pyridinic and pyrrolic N species and the catalytic activity of CALD.

The fully hydrogenated product 3-phenyl-1-propanol contributed to less than 10 % selectivity in both cases for the 1 % Pd / fNCSs 40 catalyst (0.41 % N) and 1 % Pd / fNCSs 40 catalyst (3.84 % N). The selectivities to HCALD at reaction times of 4 hours for the 1 % Pd / fCSs 40 catalyst (0.00 % N), 1 % Pd / fNCSs 40 catalyst (0.41 % N), 1 % Pd / fNCSs 40 catalyst (2.39 % N) and 1 % Pd / fNCSs 40 catalyst (3.84 % N) were 100.0, 98.4, 100.0 and 93.4 % respectively. The selectivities to HCALD were all above 90.0 % in all catalysts. According to the results obtained, the hydrogenation activity was not affected by the particle sizes of the catalysts but by the type of N species in the catalyst. These results were similar to those obtained in literature by Amadou et al. [40]. They found that the hydrogenation activity was not a structure sensitive reaction i.e. it was not dependant on the particle size.

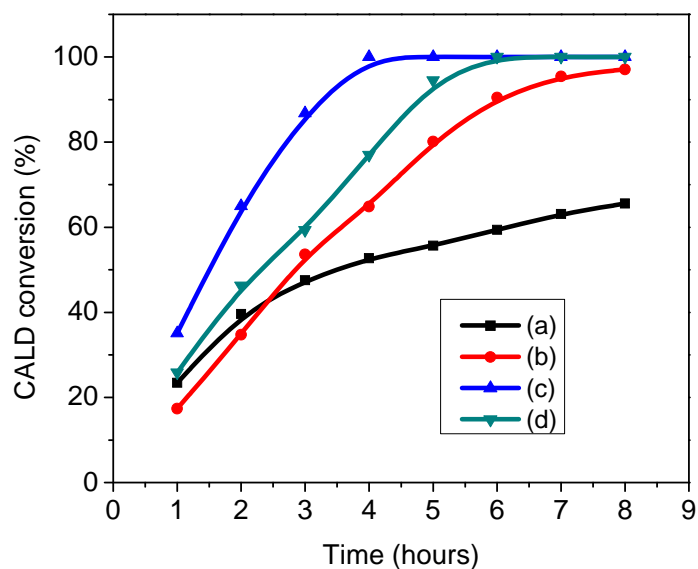


Figure 4.23. Catalytic activity, expressed in terms of conversion as a function of time for the CALD hydrogenation of a) 1 % Pd / fCSs 40 catalyst (0.00 % N), b) 1 % Pd / fNCSs 40 catalyst (0.41 % N), c) 1 % Pd / fNCSs 40 catalyst (2.39 % N) and d) 1 % Pd / fNCSs 40 catalyst (3.84 %N).

Table 4.11. The effect of different N contents in support on the hydrogenation of CALD.

Catalyst name	Activity (%)	Reaction time (hours)							
		1	2	3	4	5	6	7	8
1 % Pd / fCSs 40 (0.00 % N)	Conversion	24	40	48	53	56	59	63	66
	HCALD selectivity	100.0	100.0	100.0	100.0	100.0	100.0	100.0	100.0
1 % Pd / fNCSs 40 (0.41 % N)	Conversion	17	35	54	65	80	91	95	97
	HCALD selectivity	100.0	100.0	100.0	98.4	96.0	95.6	94.5	94.6
	3P1P selectivity	0.00	0.00	0.00	1.60	4.0	4.4	5.3	5.4
1 % Pd / fNCSs 40 (2.39 % N)	Conversion	37	66	91	100	100	100	100	100
	HCALD selectivity	100.0	100.0	100.0	100.0	100.0	100.0	100.0	100.0
1 % Pd / fNCSs 40 (3.84 % N)	Conversion	26	46	59	77	95	100	100	100
	HCALD selectivity	100.0	100.0	96.8	93.4	91.7	92.4	93.2	93.3
	3P1P selectivity	0.00	0.00	3.19	6.58	8.26	7.57	6.77	6.67

No cinnamyl alcohol was observed. Reaction conditions: CALD = 1.26 ml, hexan-1-ol = 100 ml, 1 % Pd / fNCSs 40 catalyst weight = 100 mg, T = 60 °C and H₂ (g) = 50 ml / min. N content was determined by CN elemental analysis.

4.4 Conclusion

We have demonstrated the use of NCSs as a catalyst support. Well dispersed palladium nanoparticles with a reasonably narrow size distribution could be deposited on the NCSs by a simple liquid phase reduction method. The 1 % Pd / fNCSs displayed high catalytic activities for the hydrogenation of CALD reaction. The palladium particles supported on CSs and NCSs functionalized at different temperatures of 55 % HNO₃ for 24 hours had mean particle sizes ranging between 4.68 and 7.51 nm. The palladium nanoparticles supported on CSs with different nitrogen contents were well dispersed with mean particle sizes centred between 4.15 and 4.82 nm.

The liquid phase hydrogenation of CALD was significantly influenced by

- The amount of oxygen surface groups on the support. Low concentration of oxygen surface groups on the catalysts resulted in high catalytic activity (expressed as conversion) of 87 and 91 % for 1 % Pd / fNCSs 40 and 1 % Pd / fNCSs 60 catalysts respectively at reaction time 3 hours. However with 1 % Pd / fNCSs 80 catalyst, the conversion to CALD at reaction time 3 hours was 10 %. Functionalization at 80 °C for the NCSs support increased the number of oxygen groups.
- The presence or absence of N in the carbon sphere support. N incorporation led to a significant improvement of catalytic activity compared to the N free catalysts. The activity improvement was attributed to the electronic modification of the active phase
- The amount of N and the N type in the catalyst also had an effect on the activity and selectivity of the catalyst.

- The total absence of microporosity in the catalysts. The high selectivities to HCALD for all the catalysts was attributed to the absence of microporosity in the catalysts which increases the accessibility of the reactants to the palladium sites
- The strong metal - support interaction between the palladium metal nanoparticles and the support has an effect of increasing catalyst activity and selectivity.

4.5 References

1. Astruc, D., F. Lu, and J.R. Aranzaes, *Nanoparticles as Recyclable Catalysts: The Frontier between Homogeneous and Heterogeneous Catalysis*. Angewandte Chemie International Edition, 2005. **44**(48): p. 7852-7872.
2. Gilhespy, M., M. Lok, and X. Baucherel, *Polymer-supported nitroxyl radical catalyst for selective aerobic oxidation of primary alcohols to aldehydes*. Chemical Communications, 2005(8): p. 1085-1086.
3. Yeung, C.M.Y., K.M.K. Yu, Q.J. Fu, D. Thompsett, M.I. Petch, and S.C. Tsang, *Engineering Pt in Ceria for a Maximum Metal–Support Interaction in Catalysis*. Journal of the American Chemical Society, 2005. **127**(51): p. 18010-18011.
4. Rodríguez-reinoso, F., *The role of carbon materials in heterogeneous catalysis*. Carbon, 1998. **36**(3): p. 159-175.
5. Moreno-Castilla, C. and F.J. Maldonado-Hódar, *Carbon aerogels for catalysis applications: An overview*. Carbon, 2005. **43**(3): p. 455-465.
6. Auer, E., A. Freund, J. Pietsch, and T. Tacke, *Carbons as supports for industrial precious metal catalysts*. Applied Catalysis A: General, 1998. **173**(2): p. 259-271.
7. Serp, P. and J.L. Figueiredo, *Carbon materials for catalysis*. 2009: John Wiley & Sons.

8. Wang, Z.L. and Z.C. Kang, *Graphitic structure and surface chemical activity of nanosize carbon spheres*. Carbon, 1997. **35**(3): p. 419-426.
9. Serp, P., R. Feurer, Y. Kihn, P. Kalck, J.L. Faria, and J.L. Figueiredo, *Novel carbon supported material: highly dispersed platinum particles on carbon nanospheres*. Journal of Materials Chemistry, 2001. **11**(8): p. 1980-1981.
10. Kang, Z.C. and Z.L. Wang, *Chemical activities of graphitic carbon spheres*. Journal of Molecular Catalysis A: Chemical, 1997. **118**(2): p. 215-222.
11. Moyo, M., M.A.M. Motchelaho, H. Xiong, L.L. Jewell, and N.J. Coville, *Promotion of Co/carbon sphere Fischer–Tropsch catalysts by residual K and Mn from carbon oxidation by KMnO₄*. Applied Catalysis A: General, 2012. **413–414**(0): p. 223-229.
12. Xiong, H., M. Moyo, M.A.M. Motchelaho, L.L. Jewell, and N.J. Coville, *Fischer–Tropsch synthesis over model iron catalysts supported on carbon spheres: The effect of iron precursor, support pretreatment, catalyst preparation method and promoters*. Applied Catalysis A: General, 2010. **388**(1–2): p. 168-178.
13. Deshmukh, A.A., R. UlIslam, M.J. Witcomb, W.A.L. vanOtterlo, and N.J. Coville, *Catalytic Activity of Metal Nanoparticles Supported on Nitrogen-Doped Carbon Spheres*. ChemCatChem, 2010. **2**(1): p. 51-54.
14. Shao, Y., J. Sui, G. Yin, and Y. Gao, *Nitrogen-doped carbon nanostructures and their composites as catalytic materials for proton exchange membrane fuel cell*. Applied Catalysis B: Environmental, 2008. **79**(1): p. 89-99.
15. Ewels, C.P. and M. Glerup, *Nitrogen Doping in Carbon Nanotubes*. Journal of Nanoscience and Nanotechnology, 2005. **5**(9): p. 1345-1363.
16. Gallezot, P. and D. Richard, *Selective hydrogenation of α , β -unsaturated aldehydes*. Catalysis Reviews, 1998. **40**(1-2): p. 81-126.
17. Kluson, P. and L. Cervený, *Selective hydrogenation over ruthenium catalysts*. Applied Catalysis A: General, 1995. **128**(1): p. 13-31.

18. Ponec, V., *On the role of promoters in hydrogenations on metals; α,β -unsaturated aldehydes and ketones*. Applied Catalysis A: General, 1997. **149**(1): p. 27-48.
19. Coq, B. and F. Figueras, *Structure–activity relationships in catalysis by metals: some aspects of particle size, bimetallic and supports effects*. Coordination Chemistry Reviews, 1998. **178–180**, Part 2(0): p. 1753-1783.
20. Mills, P.L. and R.V. Chaudhari, *Multiphase catalytic reactor engineering and design for pharmaceuticals and fine chemicals*. Catalysis Today, 1997. **37**(4): p. 367-404.
21. Mohr, C. and P. Claus, *Hydrogenation properties of supported nanosized gold particles*. Science Progress, 2001. **84**: p. 311-334.
22. Muller, A. and J. Bowers, *WO Patent Application WO 99/08989*. First Chemical Corporation, 1999.
23. Zhang, Y., S. Liao, Y. Xu, and D. Yu, *Catalytic selective hydrogenation of cinnamaldehyde to hydrocinnamaldehyde*. Applied Catalysis A: General, 2000. **192**(2): p. 247-251.
24. Toebes, M.L., F.F. Prinsloo, J.H. Bitter, A.J. van Dillen, and K.P. de Jong, *Influence of oxygen-containing surface groups on the activity and selectivity of carbon nanofiber-supported ruthenium catalysts in the hydrogenation of cinnamaldehyde*. Journal of Catalysis, 2003. **214**(1): p. 78-87.
25. Toebes, M.L., Y. Zhang, J. Hájek, T. Alexander Nijhuis, J.H. Bitter, A. Jos van Dillen, D.Y. Murzin, D.C. Koningsberger, and K.P. de Jong, *Support effects in the hydrogenation of cinnamaldehyde over carbon nanofiber-supported platinum catalysts: characterization and catalysis*. Journal of Catalysis, 2004. **226**(1): p. 215-225.
26. Vu, H., F. Gonçalves, R. Philippe, E. Lamouroux, M. Corrias, Y. Kihn, D. Plee, P. Kalck, and P. Serp, *Bimetallic catalysis on carbon nanotubes for the selective hydrogenation of cinnamaldehyde*. Journal of Catalysis, 2006. **240**(1): p. 18-22.

27. Solhy, A., B.F. Machado, J. Beausoleil, Y. Kihn, F. Gonçalves, M.F.R. Pereira, J.J.M. Órfão, J.L. Figueiredo, J.L. Faria, and P. Serp, *MWCNT activation and its influence on the catalytic performance of Pt/MWCNT catalysts for selective hydrogenation*. Carbon, 2008. **46**(9): p. 1194-1207.
28. Machado, B.F., H.T. Gomes, P. Serp, P. Kalck, and J.L. Faria, *Liquid-Phase Hydrogenation of Unsaturated Aldehydes: Enhancing Selectivity of Multiwalled Carbon Nanotube-Supported Catalysts by Thermal Activation*. ChemCatChem, 2010. **2**(2): p. 190-197.
29. Coloma, F., A. Sepúlveda-Escribano, J.L.G. Fierro, and F. Rodríguez-Reinoso, *Gas phase hydrogenation of crotonaldehyde over Pt/Activated carbon catalysts. Influence of the oxygen surface groups on the support*. Applied Catalysis A: General, 1997. **150**(1): p. 165-183.
30. Toebe, M.L., T. Alexander Nijhuis, J. Hájek, J.H. Bitter, A. Jos van Dillen, D.Y. Murzin, and K.P. de Jong, *Support effects in hydrogenation of cinnamaldehyde over carbon nanofiber-supported platinum catalysts: Kinetic modeling*. Chemical Engineering Science, 2005. **60**(21): p. 5682-5695.
31. Plomp, A.J., H. Vuori, A.O.I. Krause, K.P. de Jong, and J.H. Bitter, *Particle size effects for carbon nanofiber supported platinum and ruthenium catalysts for the selective hydrogenation of cinnamaldehyde*. Applied Catalysis A: General, 2008. **351**(1): p. 9-15.
32. Guo, Z., Y. Chen, L. Li, X. Wang, G.L. Haller, and Y. Yang, *Carbon nanotube-supported Pt-based bimetallic catalysts prepared by a microwave-assisted polyol reduction method and their catalytic applications in the selective hydrogenation*. Journal of Catalysis, 2010. **276**(2): p. 314-326.
33. Kente, T., S. Dube, N.J. Coville, and S.D. Mhlanga, *Application of Gallium Nitride Nanostructures and Nitrogen Doped Carbon Spheres as Supports for the Hydrogenation of Cinnamaldehyde*. Journal of Nanoscience and Nanotechnology, 2013. **13**(7): p. 4990-4995.

34. Nieto-Márquez, A., D. Toledano, P. Sánchez, A. Romero, and J.L. Valverde, *Impact of nitrogen doping of carbon nanospheres on the nickel-catalyzed hydrogenation of butyronitrile*. Journal of Catalysis, 2010. **269**(1): p. 242-251.
35. Xiong, H., M. Moyo, M.K. Rayner, L.L. Jewell, D.G. Billing, and N.J. Coville, *Autoreduction and Catalytic Performance of a Cobalt Fischer–Tropsch Synthesis Catalyst Supported on Nitrogen-Doped Carbon Spheres*. ChemCatChem, 2010. **2**(5): p. 514-518.
36. Yoon, H., S. Ko, and J. Jang, *Nitrogen-doped magnetic carbon nanoparticles as catalyst supports for efficient recovery and recycling*. Chemical Communications, 2007(14): p. 1468-1470.
37. Nongwe, I., V. Ravat, R. Meijboom, and N.J. Coville, *Efficient and reusable Co/nitrogen doped hollow carbon sphere catalysts for the aerobic oxidation of styrene*. Applied Catalysis A: General, 2013. **466**(0): p. 1-8.
38. Xiong, H., M. Moyo, M.A. Motchelaho, Z.N. Tetana, S.M.A. Dube, L.L. Jewell, and N.J. Coville, *Fischer–Tropsch synthesis: Iron catalysts supported on N-doped carbon spheres prepared by chemical vapor deposition and hydrothermal approaches*. Journal of Catalysis, 2014. **311**(0): p. 80-87.
39. Lepró, X., E. Terrés, Y. Vega-Cantú, F.J. Rodríguez-Macías, H. Muramatsu, Y.A. Kim, T. Hayahsi, M. Endo, M. Torres R, and M. Terrones, *Efficient anchorage of Pt clusters on N-doped carbon nanotubes and their catalytic activity*. Chemical Physics Letters, 2008. **463**(1–3): p. 124-129.
40. Amadou, J., K. Chizari, M. Houllé, I. Janowska, O. Ersen, D. Bégin, and C. Pham-Huu, *N-doped carbon nanotubes for liquid-phase CC bond hydrogenation*. Catalysis Today, 2008. **138**(1–2): p. 62-68.
41. Chizari, K., I. Janowska, M. Houllé, I. Florea, O. Ersen, T. Romero, P. Bernhardt, M.J. Ledoux, and C. Pham-Huu, *Tuning of nitrogen-doped carbon nanotubes as catalyst support for liquid-phase reaction*. Applied Catalysis A: General, 2010. **380**(1–2): p. 72-80.
42. Chen, Y., J. Wang, H. Liu, M.N. Banis, R. Li, X. Sun, T.-K. Sham, S. Ye, and S. Knights, *Nitrogen Doping Effects on Carbon Nanotubes and the Origin of*

- the Enhanced Electrocatalytic Activity of Supported Pt for Proton-Exchange Membrane Fuel Cells*. The Journal of Physical Chemistry C, 2011. **115**(9): p. 3769-3776.
43. Cabiac, A., T. Cacciaguerra, P. Trens, R. Durand, G. Delahay, A. Medevielle, D. Plée, and B. Coq, *Influence of textural properties of activated carbons on Pd/carbon catalysts synthesis for cinnamaldehyde hydrogenation*. Applied Catalysis A: General, 2008. **340**(2): p. 229-235.
 44. Motchelaho, M.A.M., H. Xiong, M. Moyo, L.L. Jewell, and N.J. Coville, *Effect of acid treatment on the surface of multiwalled carbon nanotubes prepared from Fe–Co supported on CaCO₃: Correlation with Fischer–Tropsch catalyst activity*. Journal of Molecular Catalysis A: Chemical, 2011. **335**(1–2): p. 189-198.
 45. Boehm, H.P., *Some aspects of the surface chemistry of carbon blacks and other carbons*. Carbon, 1994. **32**(5): p. 759-769.
 46. Moreno-Castilla, C., M.A. Ferro-Garcia, J.P. Joly, I. Bautista-Toledo, F. Carrasco-Marin, and J. Rivera-Utrilla, *Activated Carbon Surface Modifications by Nitric Acid, Hydrogen Peroxide, and Ammonium Peroxydisulfate Treatments*. Langmuir, 1995. **11**(11): p. 4386-4392.
 47. McKee, G.S.B. and K.S. Vecchio, *Thermogravimetric Analysis of Synthesis Variation Effects on CVD Generated Multiwalled Carbon Nanotubes*. The Journal of Physical Chemistry B, 2005. **110**(3): p. 1179-1186.
 48. Jones, J.M. and K. Mark Thomas, *Carbon-13 materials as models for NO_x and N₂O release during coal char combustion*. Carbon, 1995. **33**(8): p. 1129-1139.
 49. Zhu, Q., K. Grant, and K.M. Thomas, *The incorporation of nitrogen into isotropic carbons and its release during temperature-programmed combustion*. Carbon, 1995. **33**(1): p. 35-46.
 50. Brown, S.D. and K.M. Thomas, *A comparison of NO release from coals and entrained-flow reactor chars during temperature-programmed combustion*. Fuel, 1993. **72**(3): p. 359-365.

51. Ferrari, A.C. and J. Robertson, *Interpretation of Raman spectra of disordered and amorphous carbon*. Physical Review B, 2000. **61**(20): p. 14095-14107.
52. Chuang, C.C., J.H. Huang, W.J. Chen, C.C. Lee, and Y.Y. Chang, *Role of amorphous carbon nanowires in reducing the turn-on field of carbon films prepared by microwave-heated CVD*. Diamond and Related Materials, 2004. **13**(4–8): p. 1012-1016.
53. Nieto-Márquez, A., I. Espartero, J.C. Lazo, A. Romero, and J.L. Valverde, *Direct synthesis of carbon and nitrogen–carbon nanospheres from aromatic hydrocarbons*. Chemical Engineering Journal, 2009. **153**(1–3): p. 211-216.
54. Xiong, H., M.A.M. Motchelaho, M. Moyo, L.L. Jewell, and N.J. Coville, *Correlating the preparation and performance of cobalt catalysts supported on carbon nanotubes and carbon spheres in the Fischer–Tropsch synthesis*. Journal of Catalysis, 2011. **278**(1): p. 26-40.
55. Nieto-Márquez, A., J.L. Valverde, and M.A. Keane, *Selective low temperature synthesis of carbon nanospheres via the catalytic decomposition of trichloroethylene*. Applied Catalysis A: General, 2009. **352**(1–2): p. 159-170.
56. Sun, S., G. Zhang, Y. Zhong, H. Liu, R. Li, X. Zhou, and X. Sun, *Ultrathin single crystal Pt nanowires grown on N-doped carbon nanotubes*. Chemical Communications, 2009(45): p. 7048-7050.
57. Li, W., C. Liang, W. Zhou, J. Qiu, Zhou, G. Sun, and Q. Xin, *Preparation and Characterization of Multiwalled Carbon Nanotube-Supported Platinum for Cathode Catalysts of Direct Methanol Fuel Cells*. The Journal of Physical Chemistry B, 2003. **107**(26): p. 6292-6299.
58. Belin, T. and F. Epron, *Characterization methods of carbon nanotubes: a review*. Materials Science and Engineering: B, 2005. **119**(2): p. 105-118.
59. Qin, Y.-H., J. Yue, H.-H. Yang, X.-S. Zhang, X.-G. Zhou, L. Niu, and W.-K. Yuan, *Synthesis of highly dispersed and active palladium/carbon nanofiber catalyst for formic acid electrooxidation*. Journal of Power Sources, 2011. **196**(10): p. 4609-4612.

60. Chen, L., G. Hu, G. Zou, S. Shao, and X. Wang, *Efficient anchorage of Pd nanoparticles on carbon nanotubes as a catalyst for hydrazine oxidation*. *Electrochemistry Communications*, 2009. **11**(2): p. 504-507.
61. Louis, B., D. Bégin, M.-J. Ledoux, and C. Pham-Huu, *Chapter 23 - Advances in the Use of Carbon Nanomaterials in Catalysis*, in *Ordered Porous Solids*, V. Valtchev, S. Mintova, and M. Tsapatsis, Editors. 2009, Elsevier: Amsterdam. p. 621-649.
62. Guerrero-Ruiz, A., P. Badenes, and I. Rodríguez-Ramos, *Study of some factors affecting the Ru and Pt dispersions over high surface area graphite-supported catalysts*. *Applied Catalysis A: General*, 1998. **173**(2): p. 313-321.
63. van Dommele, S., A. Romero-Izquierdo, R. Brydson, K.P. de Jong, and J.H. Bitter, *Tuning nitrogen functionalities in catalytically grown nitrogen-containing carbon nanotubes*. *Carbon*, 2008. **46**(1): p. 138-148.
64. Pels, J.R., F. Kapteijn, J.A. Moulijn, Q. Zhu, and K.M. Thomas, *Evolution of nitrogen functionalities in carbonaceous materials during pyrolysis*. *Carbon*, 1995. **33**(11): p. 1641-1653.
65. Zamudio, A., A.L. Elías, J.A. Rodríguez-Manzo, F. López-Urias, G. Rodríguez-Gattorno, F. Lupo, M. Rühle, D.J. Smith, H. Terrones, D. Díaz, and M. Terrones, *Efficient Anchoring of Silver Nanoparticles on N-Doped Carbon Nanotubes*. *Small*, 2006. **2**(3): p. 346-350.
66. Higgins, D.C., D. Meza, and Z. Chen, *Nitrogen-Doped Carbon Nanotubes as Platinum Catalyst Supports for Oxygen Reduction Reaction in Proton Exchange Membrane Fuel Cells*. *Journal of Physical Chemistry C*, 2010. **114**(50): p. 21982-21988.
67. Jiang, K., A. Eitan, L.S. Schadler, P.M. Ajayan, R.W. Siegel, N. Grobert, M. Mayne, M. Reyes-Reyes, H. Terrones, and M. Terrones, *Selective Attachment of Gold Nanoparticles to Nitrogen-Doped Carbon Nanotubes*. *Nano Letters*, 2003. **3**(3): p. 275-277.

- 68. Villa, A., D. Wang, P. Spontoni, R. Arrigo, D. Su, and L. Prati, *Nitrogen functionalized carbon nanostructures supported Pd and Au-Pd NPs as catalyst for alcohols oxidation*. Catalysis Today, 2010. **157**(1-4): p. 89-93.
- 69. Chen, G.-X., J.-M. Zhang, D.-D. Wang, and K.-W. Xu, *First-principles study of palladium atom adsorption on the boron- or nitrogen-doped carbon nanotubes*. Physica B: Condensed Matter, 2009. **404**(21): p. 4173-4177.
- 70. Serp, P., R. Feurer, P. Kalck, Y. Kihn, J.L. Faria, and J.L. Figueiredo, *A chemical vapour deposition process for the production of carbon nanospheres*. Carbon, 2001. **39**(4): p. 621-626.
- 71. Rao, C.V., C.R. Cabrera, and Y. Ishikawa, *In search of the Active Site in Nitrogen - Doped Carbon Nanotube Electrodes for the Oxygen Reduction Reaction*. The Journal of Physical Chemistry Letters, 2010. **1**(18): p. 2622-2627.
- 72. Chen, Z., D. Higgins, and Z. Chen, *Electrocatalytic activity of nitrogen doped carbon nanotubes with different morphologies for oxygen reduction reaction*. Electrochimica Acta, 2010. **55**(16): p. 4799-4804.

CHAPTER 5

The effect of variation of reaction conditions on the hydrogenation of cinnamaldehyde over palladium supported nitrogen doped catalysts.

5.1 Introduction

Selective hydrogenation of organic compounds is a crucial process in the manufacture of petrochemicals and fine chemicals. The metals often employed in such reactions are palladium and platinum. The main reaction scheme for the selective hydrogenation of cinnamaldehyde (CALD) was shown in Figure 4.1.

The hydrogenation of cinnamaldehyde (CALD) may proceed via different reaction pathways (Figure 4.1). The hydrogenation of the C=C bond gives the saturated aldehyde, hydrocinnamaldehyde (HCALD). The hydrogenation of the C=O bond gives the saturated alcohol, cinnamyl alcohol (CA). The hydrogenation of the C=C and C=O bonds gives the unsaturated alcohol, 3-phenyl-1-propanol (3P1P). The challenge in catalysis is to selectively hydrogenate either the C=C or C=O bond, leaving the other one not affected. In this work, we selected the hydrogenation of CALD to HCALD to estimate the performances of our catalyst.

Reaction conditions for the selective hydrogenation of CALD are known to significantly affect the activity and selectivity results of a catalytic process [1]. Higher temperatures in general result in higher hydrogenation activities. The effects

of temperature on selectivity is complicated, as the selectivities can increase, decrease or remain constant with increasing temperature as reported in literature [2-5]. It has also been described that increasing hydrogen pressures increases the conversion of CALD and decreases the selectivities to HCALD and CA while increasing the selectivity to 3P1P [6]. In one study it was observed that increasing hydrogen pressure also increased the conversion of CALD [2]. The selectivities to cinnamyl alcohol were seen to decrease and the conversion of CALD were seen to increase as the hydrogen pressure increased [7]. In another report, the catalyst used had the effect of producing a constant selectivity to cinnamyl alcohol with increasing pressure [8]. Another reaction parameter which was seen to affect the selectivity and activity in the hydrogenation of CALD was the reaction solvents. Depending on the use of polar or non-polar solvents, the hydrogenation activities were different [5-8].

The effect of reaction parameters such as solvents, temperature, flow rates of hydrogen and catalyst mass on the hydrogenation of cinnamaldehyde using Pd / fNCSs catalysts was studied. The catalyst stability was also tested since the use of NCSs as supports in the hydrogenation of CALD has not been studied at great length. Leaching tests were thus conducted.

5.2 Experimental

5.2.1 Synthesis of NCSs

NCSs were synthesized using a non-catalytic chemical vapor deposition (CVD) method where acetylene (C_2H_2) was used as a carbon source and acetonitrile (CH_3CN) was the N source as described in detail in section 4.2.1. Functionalization of the NCSs was carried out by treatment with 55 % nitric acid (HNO_3) for 24 hours

at 40 °C. The functionalized NCSs (fNCSs) were washed using deionized water until the pH of the filtrate was 7. The fNCSs were then dried in an oven for 12 hours at 80 °C. The sample obtained was denoted as fNCSs 40 (functionalized NCSs at 40 °C).

5.2.2 Synthesis of catalysts using liquid phase reduction method

The catalysts were prepared by the liquid phase reduction method of metal in ethylene glycol solution as described in detail in section 4.2.2.

5.2.3 Characterization

Characterization of the as-synthesized NCSs, fNCSs 40 and 1 % Pd / fNCSs 40 catalyst was performed using the same techniques used in section 4.2.3.

5.2.4 Catalyst testing

The hydrogenation of cinnamaldehyde was carried out as described in section 4.2.4 with reaction variables explained in detail in Table 5.1.

Table 5.1. Variation of conditions for the hydrogenation of cinnamaldehyde.

Reaction variables	CALD concentration (M)	Solvent	Temperature (°C)	Hydrogen flow rate (ml / min)	Catalyst mass (mg)
Reaction 1	0.01 M	Ethanol	40	50	100
		Propan-2-ol	40	50	100
		Butan-2-ol	40	50	100
		Hexan-1-ol	40	50	100
		1-heptanol	40	50	100
		Octan-2-ol	40	50	100
Reaction 2	0.01 M	Hexan-1-ol	40	50	100
		Hexan-1-ol	50	50	100
		Hexan-1-ol	60	50	100
		Hexan-1-ol	70	50	100
Reaction 3	0.01 M	Hexan-1-ol	60	25	100
		Hexan-1-ol	60	50	100
		Hexan-1-ol	60	75	100
		Hexan-1-ol	60	100	100
Reaction 4	0.01 M	Hexan-1-ol	60	50	50
		Hexan-1-ol	60	50	100
		Hexan-1-ol	60	50	150
		Hexan-1-ol	60	50	200

5.3 Results and Discussion

5.3.1 Support and Catalyst Characterization

The characterization results for the as-synthesized NCSs, fNCSs 40 and 1 % Pd / fNCSs 40 have been described fully in Chapters 3 and 4. Tables 5.2 and 5.3 gives a summary of the characterization results of the supports and catalysts for ease of reference.

Table 5.2. Physical and chemical properties of supports and catalysts.

Sample name	Average diameter (nm)	D-band (cm ⁻¹)	G-band (cm ⁻¹)	I _D /I _G	Decomposition temperature (°C)	BET surface area (m ² / g)	Pore volume (cm ³ / g)	Average Pd particle size (nm) ^a	Pd content (wt. %) ^b
As-synthesized NCSs	669	1357	1590	1.38	607, 802	1.51	0.0030	-	-
fNCSs 40	-	1373	1598	1.40	610, 760	1.67	0.0028	-	-
1 % Pd / fNCSs 40	-	-	-	-	544, 671	3.80	0.016	4.68	1.03

^a Determined from TEM analysis, ^b Determined by ICP - OES analysis

Table 5.3. CN elemental and XPS analysis results.

Sample name	CN elemental analysis (%)		XPS analysis (at. %)					
			Nitrogen species (%)					
	C	N	C	N	O	Pyridinic N	Pyrrolic + Quaternary N	Molecular N
As-synthesized NCSs	93.90	2.50	93.00	3.00	4.00	27.79 (398.6 eV)	56.97 (401.0 eV)	15.24 (404.5 eV)
fNCSs 40	94.88	2.48	NA	NA	NA	NA	NA	NA

NA = Not analyzed for XPS

5.3.2 Hydrogenation of CALD

5.3.2.1 Effect of solvents

The nature of the solvent plays a very important role in catalytic reactions conducted in the liquid phase. The choice of the solvent is dependent on factors which include solvent polarity, hydrogen solubility, the interaction between the solvent and the catalyst as well as reactant and product solubility [9]. Variation of different solvents was carried out to see the effects on the hydrogenation of CALD and the results are shown in Figure 5.1 and Table 5.5. The solvents studied were ethanol, propan-2-ol, butan-2-ol, hexan-1-ol, 1-heptanol, octan-2-ol and ethyl acetate. All other reaction parameters were kept constant as shown in Table 5.5. Table 5.4 shows the physical properties of the alcohols used in this study. The results obtained showed that the catalytic performance was strongly affected by the type of solvent, but a direct correlation between the solvents properties and their efficiencies could not be established.

Ethanol, as solvent, gave the highest conversion to cinnamaldehyde (90.4 %) at a reaction time of 8 hours. This was followed by butan-2-ol, hexan-1-ol, octan-2-ol, 1-heptanol, propan-2-ol and lastly ethyl acetate with CALD conversions of 64, 63, 60, 53, 46 and 41 % respectively. Ethanol produced many side reaction products (selectivity of 66.8 %). It has been cited in the literature that the use of alcohols during the hydrogenation of CALD results in acetal formation as a by-product and this often resulted in a decreasing catalytic activity and or selectivity [1, 10]. The conversion to CALD increased with increase in reaction time. The selectivities to HCALD and 3P1P increased from 15.2 - 23.2 % and 2.9 - 10.1 % respectively for reaction times ranging from 1 to 8 hours. The selectivity to the by-products was the only one which decreased as the reaction time increased from 1 to 8 hours from 81.9 -

66.8 %. However in this study, by-product formation was only observed when ethanol was used as a reaction solvent. All the other alcohols did not produce any by-products in the hydrogenation of CALD.

The solubility of hydrogen in the solvent may play a significant role in the hydrogenation of cinnamaldehyde. The selectivities to HCALD in this study gave the following sequence: octan-2-ol \leq 1-heptanol \leq hexan-1-ol < ethyl acetate < propan-2-ol < butan-2-ol < ethanol. From these HCALD selectivity results, it was seen that hydrogen solubility is directly proportional to the molecular weight of the alcohols used [11]. The selectivity to HCALD in ethyl acetate was higher than in propan-2-ol, butan-2-ol and ethanol. These results were in good agreement with those obtained by Guo et al [6]. Hexan-1-ol, 1-heptanol and octan-2-ol gave 100 % selectivity to HCALD at a reaction time of 8 hours. This was then followed by ethyl acetate, propan-2-ol, butan-2-ol and lastly ethanol with selectivities to HCALD of 97.0, 93.3, 67.7 and 23.2 % respectively at reaction time of 8 hours. Butan-2-ol, ethanol, propan-2-ol and ethyl acetate produced 3-phenyl-1-propanol (3P1P) by further hydrogenation of HCALD (32.3, 10.1, 7.6 and 3.1 % respectively). In all the hydrogenation reactions no cinnamyl alcohol (CA) was produced. HCALD was the predominant product at all reactions studied using the different solvents showing that the hydrogenation of the C=C bond was favoured under these conditions.

Table 5.4. Properties of alcohols used in the study.

Solvents	Boiling point (°C)	Molecular weight (mol / g)	*E_T (30) Kcal / mol
Ethanol	78	46.1	51.9
Propan-2-ol	82	60.1	48.7
Butan-2-ol	98	74.1	47.1
Hexan-1-ol	156	102.2	48.8
1-Heptanol	176	116.2	48.5
Octan-2-ol	174-181	130.2	-
Ethyl acetate	76.5-77.5	88.1	38.1

*E_T: Empirical parameter of solvent polarity from spectroscopic measurements [12].

Table 5.5. Hydrogenation results of CALD over 1 % Pd / fNCSs 40 catalyst in different solvents.

Solvents	Conversion (%)	Selectivity (%)			
		HCALD	3P1P	CA	Others
Ethanol	90	23.2	10.1	0	66.8
Propan-2-ol	46	93.3	7.6	0	0
Butan-2-ol	64	67.7	32.3	0	0
Hexan-1-ol	63	100.0	0	0	0
1-Heptanol	53	100.0	0	0	0
Octan-2-ol	60	100.0	0	0	0
Ethyl acetate	41	97.0	3.1	0	0

Reaction conditions: CALD = 1.26 ml, catalyst weight = 100 mg, 100 ml solvent, T = 40 °C, time = 8 hours and reductant = H₂, 50 ml / min.

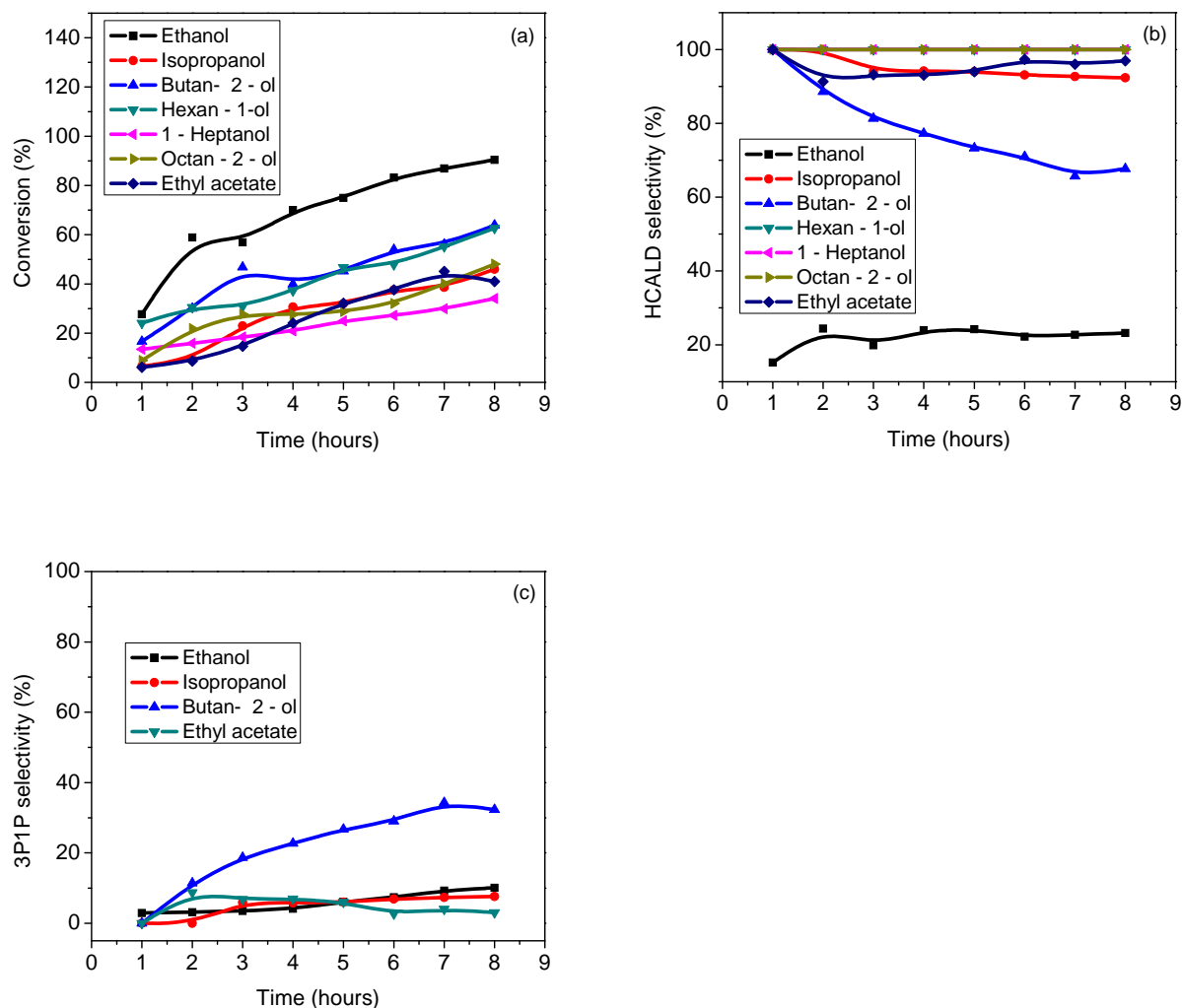


Figure 5.1. Hydrogenation of CALD over 1 % Pd / fNCSs 40 catalyst performed using different solvents. (a) Conversion of CALD as a function of time, (b) HCALD selectivity as a function of time and (c) 3P1P selectivity as a function of time.

From the solvent effect results hexan-1-ol was chosen as the best solvent to use for further studies due to the high activity and selectivity observed and the absence of side reaction products. It is also an easy solvent to handle, it is readily available and reasonably inexpensive. Its boiling point (156 - 157 °C) allows it to be used over a wide range of temperatures.

5.3.2.2 Effect of temperature

The effect of the reaction temperature on the hydrogenation of CALD over 1 % Pd / fNCSs 40 catalysts is shown in Figure 5.2 and Table 5.6, where the conversion of CALD and the selectivity towards HCALD and 3P1P are plotted and tabulated. All other reaction parameters were kept constant except the variation of reaction temperature. The reaction temperatures which were under investigation were 40, 50, 60 and 70 °C. The conversion of CALD increased with time of reaction for each temperature. However there was no clear trend in the selectivity to HCALD as the reaction temperature was increased. The selectivity to HCALD was > 90 % throughout all reaction temperatures investigated and approached 100 % in some cases. By-product formation was absent at all reaction temperatures investigated. 3P1P was produced at reaction temperatures of 50 and 70 °C from the further hydrogenation of HCALD and its presence was below 5 % in both cases.

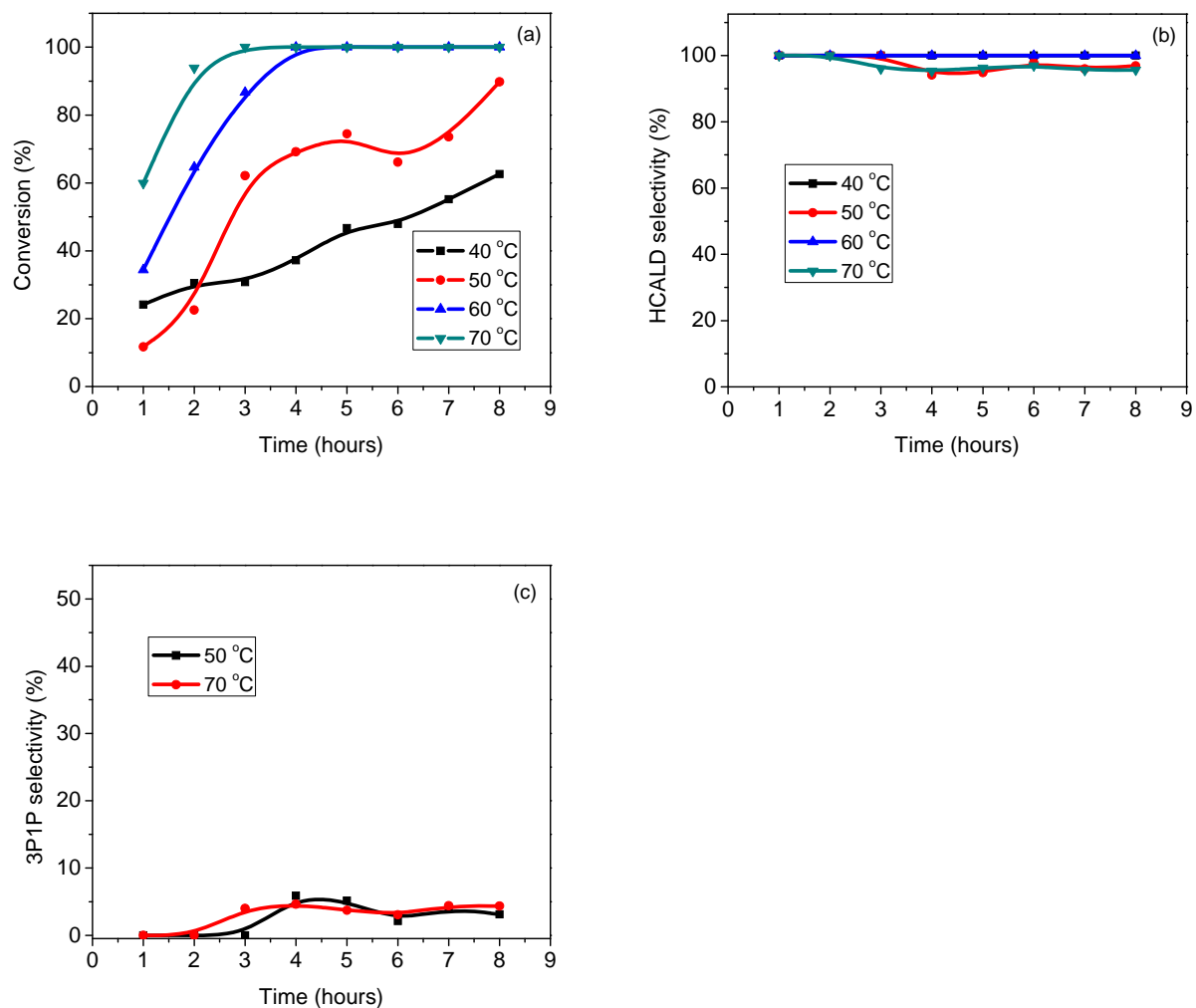


Figure 5.2. Hydrogenation of CALD over 1 % Pd / fNCSs 40 catalyst performed at different temperatures. (a) Conversion of CALD as a function of time, (b) HCALD selectivity as a function of time and (c) 3P1P selectivity as a function of time.

Table 5.6. Hydrogenation results of CALD over 1 % Pd / fNCSs 40 catalyst under different reaction temperatures of hexan-1-ol.

Temperature (°C)	Conversion (%)	Selectivity (%)		
		HCALD	3PIP	CA
40	63	100.0	0	0
50	90	96.9	3.1	0
60	100	100.0	0	0
70	100	95.6	4.4	0

Reaction conditions: CALD = 1.26 ml, solvent = hexan-1-ol (100 ml), catalyst weight = 100 mg, time = 8 hours and reductant = H₂, 50 ml / min.

The optimum temperature for the hydrogenation of CALD was chosen as 60 °C because it gave the best results in terms of both conversion of CALD and selectivity to HCALD.

5.3.2.3 Effect of hydrogen flow rates

The hydrogenation of CALD was carried out at different flow rates of hydrogen (25, 50, 75 and 100 ml / min) while maintaining other reaction conditions constant as shown in Table 5.7. The results of the hydrogenation reactions are shown in Figure 5.3 and Table 5.7. The results showed that increasing the hydrogen flow rates resulted in an increase in the conversion of CALD. The catalytic activity (expressed as conversion of CALD) increased with an increase in hydrogen flow rate. This was explained by the adsorption of H₂ on the catalyst surface in the form of active H-ad-species creating a micro-environment with a higher concentration, thus increasing the rate of surface hydrogenation reactions. Indeed, dissociative adsorbed hydrogen is frequently invoked for modeling hydrogenation reactions over Pt catalysts [9]. The

selectivity of HCALD increased from 87.8 % to 100.0 % by increasing the flow rate of hydrogen from 25 to 50 ml / min at a reaction time of 8 hours. The selectivity of HCALD then decreased as the flow rate of hydrogen was increased from 75 to 100 ml / min. the selectivity to HCALD decreased as the flow rate was increased from 75 to 100 ml / min because the HCALD was being further hydrogenated to 3P1P but the selectivity to 3P1P were less than 7 %.

Table 5.7. Hydrogenation results of CALD over 1 % Pd / fNCSs 40 catalyst under different hydrogen flow rates.

Flow rate of H ₂ (ml / min)	Conversion (%)	Selectivity (%)		
		HCALD	3P1P	CA
25	46.0	87.8	12.2	0
50	62.6	100.0	0	0
75	68.3	95.3	4.7	0
100	71.8	93.1	6.9	0

Reaction conditions: CALD = 1.26 ml, solvent = hexan-1-ol (100 ml), T = 60 °C, catalyst weight = 100 mg and time = 8 hours.

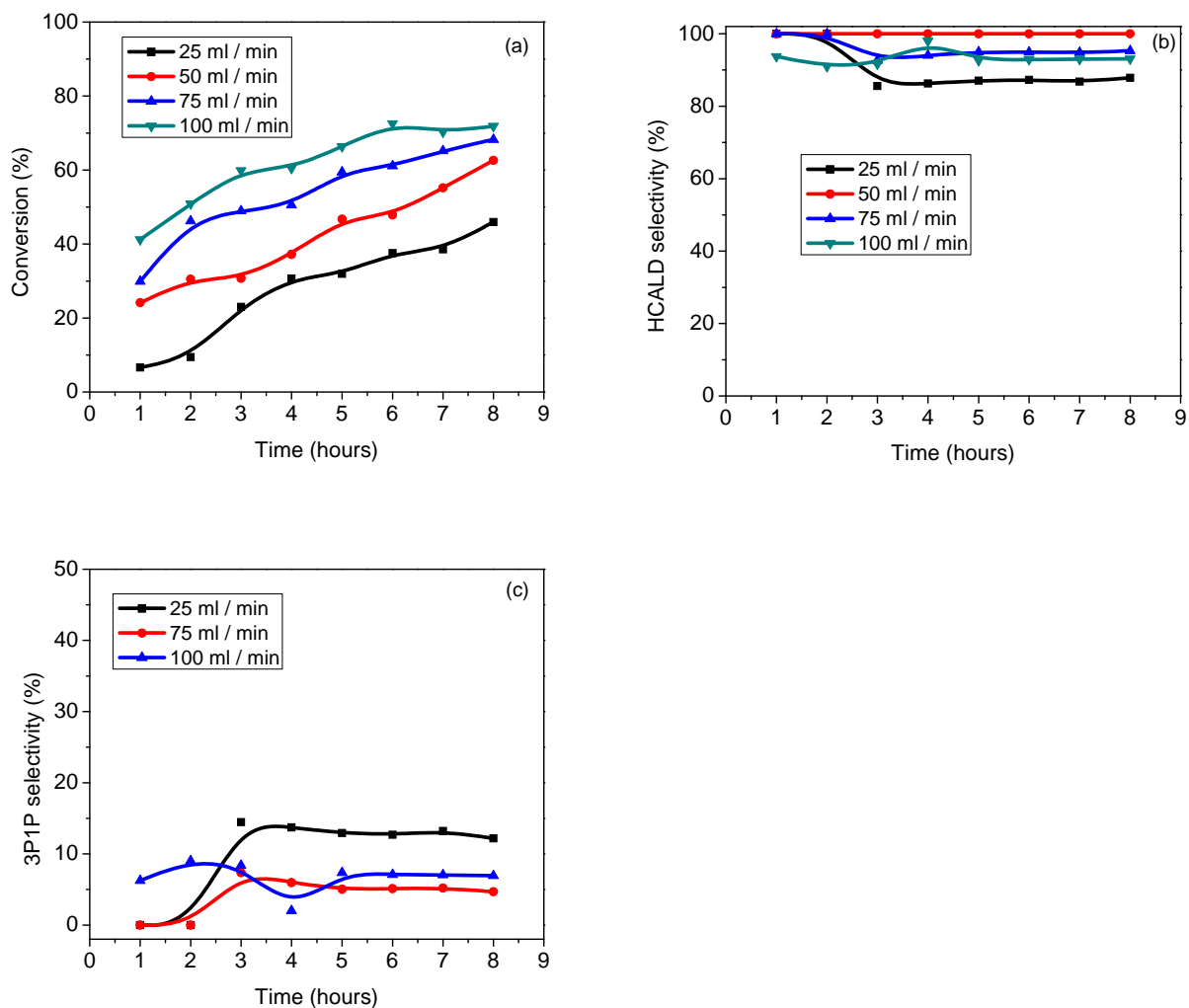


Figure 5.3. Hydrogenation results of CALD over 1 % Pd / fNCSs 40 catalyst under different hydrogen flow rates. (a) Conversion of CALD as a function of time, (b) HCALD selectivity as a function of time and (c) 3P1P selectivity as a function of time.

The flow rate of hydrogen of 50 ml / min was chosen although it had a lower conversion of CALD than flow rates of 75 and 100 ml / min because it produced 100 % selectivity to HCALD.

5.3.2.4 Mass transfer effects

Mass transfer can play an important role in liquid phase hydrogenation reactions using porous catalysts. In order to check that mass transfer was not controlling the rate of the reaction, the conversion of cinnamaldehyde was measured over a range of different catalyst masses. The conversion of CALD increased as the amount of catalyst was increased from 0.05 g to 0.200 g (Figure 5.4). The absence of mass transfer limitations was confirmed by a near straight line plot of conversion of CALD against catalyst mass [2].

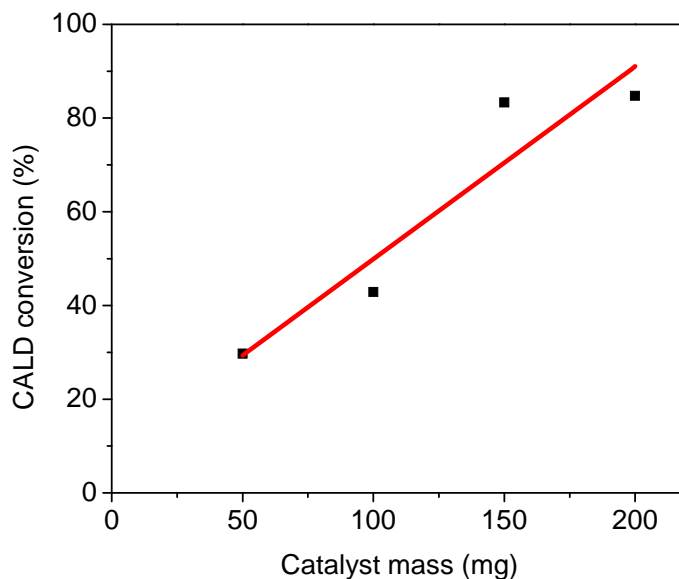


Figure 5.4. CALD conversion as a function of catalyst mass. (Conditions: CALD = 1.26 ml, solvent = hexan-1-ol (100 ml), catalyst weight = 50, 100, 150 and 200 mg, T = 60 °C, reductant = H₂, 50 ml / min).

5.3.2.5 Catalyst leaching and recyclability

To test for Pd leaching, the 1 % Pd / fNCSs 40 catalyst was filtered off from the reaction mixture. CALD (1.26 ml) was added to the filtrate solution and the hydrogenation reaction was carried out with no catalyst present. The reaction conditions used were 1.26 ml of CALD, 100 ml of hexanol, 50 ml / min H₂ (g), 60 °C and 8 hours. The results of the leaching test are shown in Figure 5.5. The conversion of CALD was 0 % from 1 hour to 8 hours showing the absence of Pd leaching during the hydrogenation of CALD. This suggests a strong metal - support interaction between the Pd and the NCSs [13].

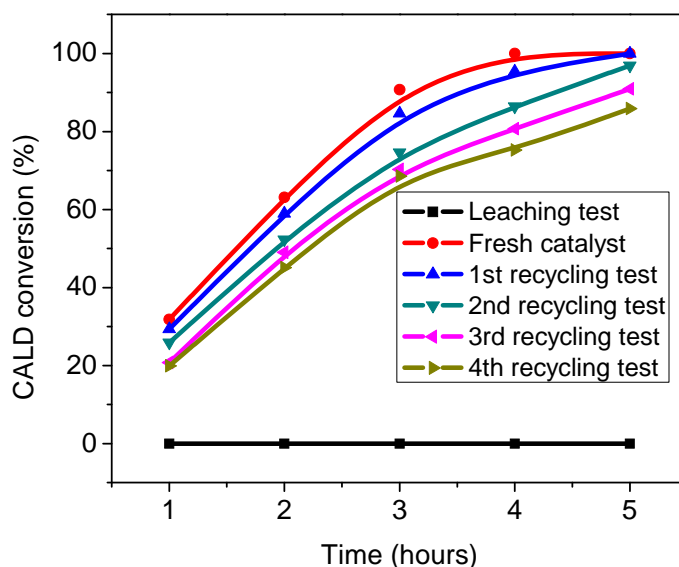


Figure 5.5. Influence of catalyst leaching and stability on the hydrogenation of CALD. (Conditions: CALD = 1.26 ml, solvent = hexan-1-ol (100 ml), catalyst weight = 100 mg, $T = 60\text{ }^{\circ}\text{C}$, reductant = H_2 , 50 ml / min).

Recycling of catalysts in heterogeneous catalysis is important from a viewpoint of an industrial application. The stability of the 1 % Pd / fNCSs 40 catalyst was tested to see if there was any deactivation that occurred during the catalytic runs. Catalyst recycling experiments were carried out using the experimental conditions given in Figure 5.5. The catalyst was tested and after the reaction; it was filtered off from the reaction solvent and washed with hexan-1-ol to remove the hydrogenation products. It was then used again to retest the same reaction under the same conditions. The recycling tests were done 4 times. Figure 5.5 shows the recycling test results which were expressed as CALD conversion as a function of time. After the catalyst had undergone 4 recycling tests, the conversion of CALD decreased from 100 to 83 % at reaction time 5 hours. From these results there appears to be a small deactivation of the 1 % Pd / fNCSs 40 catalyst during the recycling experiments. This loss is due to

catalyst loss during the filtration and recovery process. This was confirmed by carrying out a reaction on the filtered solvent (Figure 5.5). No reaction was detected. These results showed that the 1 % Pd / fNCSs 40 catalysts were very stable when used for the hydrogenation of CALD. The stability of the catalyst is due to nitrogen doping which not only facilitates the high dispersion of Pd nanoparticles on the carbon sphere surfaces but also results in a stronger interaction between Pd and the supports. This strong metal support interaction prevents Pd loss during the course of the reaction. Amadou et al. [14] also observed similar results where a Pd / N-CNT catalyst was more stable after re-use for the hydrogenation of CALD compared to Pd / CNT and Pd / activated carbon catalysts.

5.4 Conclusions

The selective hydrogenation of CALD was carried out over a 1 % Pd / fNCSs 40 catalyst. The effects of reaction solvents, temperature and flow rates of hydrogen were studied. Based on this exploratory study, the optimum conditions to be used for the hydrogenation reactions were: CALD = 1.26 ml, solvent = hexan-1-ol (100 ml), catalyst weight = 100 mg, T = 60 °C, reductant = H₂, 50 ml / min. These conditions were seen as the optimum conditions for the hydrogenation of CALD when using 1 % Pd / fNCSs 40 catalyst because of the following reasons:

- High activity (expressed in terms of conversion) and selectivity to HCALD observed.
- Absence of side reaction products.
- No catalyst leaching and the catalyst was very stable after 4 recycling tests.

5.5 References

1. Gallezot, P. and D. Richard, *Selective hydrogenation of α , β -unsaturated aldehydes*. Catalysis Reviews, 1998. **40**(1-2): p. 81-126.
2. Breen, J.P., R. Burch, J. Gomez-Lopez, K. Griffin, and M. Hayes, *Steric effects in the selective hydrogenation of cinnamaldehyde to cinnamyl alcohol using an Ir/C catalyst*. Applied Catalysis A: General, 2004. **268**(1-2): p. 267-274.
3. Neri, G., L. Bonaccorsi, and S. Galvagno, *Kinetic Analysis of Cinnamaldehyde Hydrogenation over Alumina-Supported Ruthenium Catalysts*. Industrial & Engineering Chemistry Research, 1997. **36**(9): p. 3554-3562.
4. Tronconi, E., C. Crisafulli, S. Galvagno, A. Donato, G. Neri, and R. Pietropaolo, *Kinetics of liquid-phase hydrogenation of cinnamaldehyde over a platinum-tin/nylon catalyst*. Industrial & Engineering Chemistry Research, 1990. **29**(9): p. 1766-1770.
5. Hájek, J., N. Kumar, P. Mäki-Arvela, T. Salmi, D.Y. Murzin, I. Paseka, T. Heikkilä, E. Laine, P. Laukkanen, and J. Väyrynen, *Ruthenium-modified MCM-41 mesoporous molecular sieve and Y zeolite catalysts for selective hydrogenation of cinnamaldehyde*. Applied Catalysis A: General, 2003. **251**(2): p. 385-396.
6. Guo, Z., Y. Chen, L. Li, X. Wang, G.L. Haller, and Y. Yang, *Carbon nanotube-supported Pt-based bimetallic catalysts prepared by a microwave-assisted polyol reduction method and their catalytic applications in the selective hydrogenation*. Journal of Catalysis, 2010. **276**(2): p. 314-326.
7. Shirai, M., T. Tanaka, and M. Arai, *Selective hydrogenation of α -, β -unsaturated aldehyde to unsaturated alcohol with supported platinum catalysts at high pressures of hydrogen*. Journal of Molecular Catalysis A: Chemical, 2001. **168**(1-2): p. 99-103.

8. Koo-amornpattana, W. and J.M. Winterbottom, *Pt and Pt-alloy catalysts and their properties for the liquid-phase hydrogenation of cinnamaldehyde*. Catalysis Today, 2001. **66**(2–4): p. 277-287.
9. Singh, U.K. and M.A. Vannice, *Kinetics of liquid-phase hydrogenation reactions over supported metal catalysts — a review*. Applied Catalysis A: General, 2001. **213**(1): p. 1-24.
10. Maki-Arvela, P., J. Hajek, T. Salmi, D. Y. Murzin, *Chemoselective hydrogenation of carbonyl compounds over heterogeneous catalysts*. Applied Catalysis A: General, 2005. **292**: p. 1-49.
11. Wainwright, M.S., T. Ahn, D.L. Trimm, and N.W. Cant, *Solubility of hydrogen in alcohols and esters*. Journal of Chemical & Engineering Data, 1987. **32**(1): p. 22-24.
12. Reichardt, C. and T. Welton, *Empirical Parameters of Solvent Polarity*, in *Solvents and Solvent Effects in Organic Chemistry*. 2010, Wiley-VCH Verlag GmbH & Co. KGaA. p. 425-508.
13. Chizari, K., I. Janowska, M. Houllé, I. Florea, O. Ersen, T. Romero, P. Bernhardt, M.J. Ledoux, and C. Pham-Huu, *Tuning of nitrogen-doped carbon nanotubes as catalyst support for liquid-phase reaction*. Applied Catalysis A: General, 2010. **380**(1–2): p. 72-80.
14. Amadou, J., K. Chizari, M. Houllé, I. Janowska, O. Ersen, D. Bégin, and C. Pham-Huu, *N-doped carbon nanotubes for liquid-phase CC bond hydrogenation*. Catalysis Today, 2008. **138**(1–2): p. 62-68.

CHAPTER 6

The effect of different methods of catalyst preparation on the hydrogenation of cinnamaldehyde using nitrogen doped carbon spheres as supports and palladium as metal.

6.1 Introduction

The catalyst preparation method has been known to affect the outcome of the selective hydrogenation of CALD [1]. Catalyst preparation methods affect mainly the metal dispersion, which is very important in order to obtain high activity and selectivity in catalytic reactions. In this paper, two main methods for the introduction of metal precursors onto the carbon surface were used, the liquid phase reduction method and the incipient wetness impregnation methods.

The most widely used technique to achieve the deposition of metals on carbon material supports is the incipient wetness impregnation (IWI) method in which the purified carrier material is impregnated with a solution of metal precursor, then dried, calcined and or reduced so as to obtain metal particles dispersed on the support [2, 3]. The other method, the liquid phase reduction method uses ethylene glycol (EG) as a solvent and reducing agent. The main advantage of using this method is that it is short, it does not have a lot of steps like ageing, drying, calcination and or reduction. It is a simple method. A metal precursor salt is suspended in a polyol (EG) and heated to a specific temperature, which allows the salt to completely dissolve and react as necessary before the desired nanoparticles precipitate on the substrate.

In this paper, 1 % Pd / fNCSs 40 catalysts were prepared by different Pd deposition methods. The physicochemical characterizations of the NCSs supports and the corresponding Pd/fNCSs 40 catalysts were evaluated. The influence of the Pd deposition method and the NCSs properties on the dispersion and size distribution of Pd nanoparticles were discussed. The catalysts were tested for the hydrogenation of cinnamaldehyde.

6.2 Experimental

6.2.1 Synthesis of NCSs

The NCSs were synthesized according to the procedure in section 4.2.1 where acetylene was used a carbon source, acetonitrile heated to 80 °C as the N source and a carbonization temperature and time of 950 °C and 90 minutes respectively. Nitrogen gas was used when the temperature was heating to 950 °C and cooling from 950 °C to room temperature after the reaction. The flow rate of the gases was 100 ml / min. Functionalization of the NCSs was done according to procedure in section 5.2.1.

6.2.2 Catalyst preparation

The polyol and incipient wetness impregnation methods were employed to prepare palladium catalysts (1 wt. % Pd) supported on acid functionalized nitrogen doped carbon spheres. The metal precursor solution of 0.05 M Pd (acetate) was prepared by dissolving 0.5625 g of Pd (acetate) salt in 50 ml of acetone.

6.2.2.1 Liquid phase reduction method

The detailed procedure for the preparation of the catalysts using the liquid phase reduction method is described in section 4.2.2. The catalyst produced using the liquid phase reduction method was named Polyol 1 % Pd / fNCSs 40 catalyst.

6.2.2.2 Incipient wetness impregnation method

1 wt % Pd catalysts were also prepared using the incipient wetness impregnation method. The 0.05 M metal precursor solution (0.95 ml) was added drop wise to fNCSs 40 support (0.5 g) under vigorous stirring until a paste like solid was obtained. The wet like solid was dried overnight at room temperature. The air dried solid was named as - synthesized 1 % Pd / fNCSs 40 catalyst. Parts of the air dried solids underwent thermal treatments. The 1st thermal treatment was calcination which decomposes the Pd salt into its corresponding oxide. The as - synthesized 1 % Pd / fNCSs 40 catalyst was calcinated in air at 250 °C for 2 hours at a heating rate of 10 °C / min. The resulting catalyst was named Impregnation 1 % Pd / fNCSs 40 calcined. The Impregnation 1 % Pd / fNCSs 40 calcined catalyst was further reduced in hydrogen gas (20 ml / min) at 400 °C for 2 hours at a heating rate of 10 °C / min. The sample was cooled down under nitrogen flow (50 ml / min). The resultant catalyst was named Impregnation 1 % Pd / fNCSs 40 reduced.

6.2.3 Characterization

The characterization of the catalysts was done using TEM equipped with an EDX, nitrogen adsorption / desorption analysis, ICP-OES analysis, TPR and powder X-ray

diffraction techniques. The detailed characterization techniques are described in the Appendix section.

6.2.4 Hydrogenation of CALD

The catalysts prepared using different methods were tested for the selective hydrogenation of cinnamaldehyde according to the procedure described in section 4.2.2.

6.3 Results and Discussion

6.3.1 Catalyst characterization results

The TEM images of Pd catalysts synthesized using different catalyst preparation methods and their corresponding particle size distribution graphs are shown in Figure 6.1. The histograms of Pd particle size distribution are obtained from measurements of over 200 particles. The Polyol 1 % Pd / fNCSs 40 catalyst, Impregnation 1 % Pd / fNCSs 40 calcined and Impregnation 1 % Pd / fNCSs 40 reduced catalysts had average Pd particle sizes of 4.68, 6.68 and 7.18 nm respectively. The Polyol 1 % Pd / fNCSs 40 catalyst had the smallest Pd particle sizes because of its easy preparation method. The highest temperature the catalyst is subjected to is 195 °C whereas for the catalysts prepared using the incipient wetness impregnation method the catalysts are subjected to calcination temperatures of 250 °C and reduction temperatures of 400 °C which caused the average Pd particles to increase because of the formation of the PdO and Pd respectively. However using the polyol and impregnation methods as catalyst preparation methods produced Pd nanoparticles which were well dispersed on the fNCSs supports. This was attributed to the preparation methods and the presence of

nitrogen atoms which increase the number of anchorage sites for the adsorption of the palladium precursor salt [4-6].

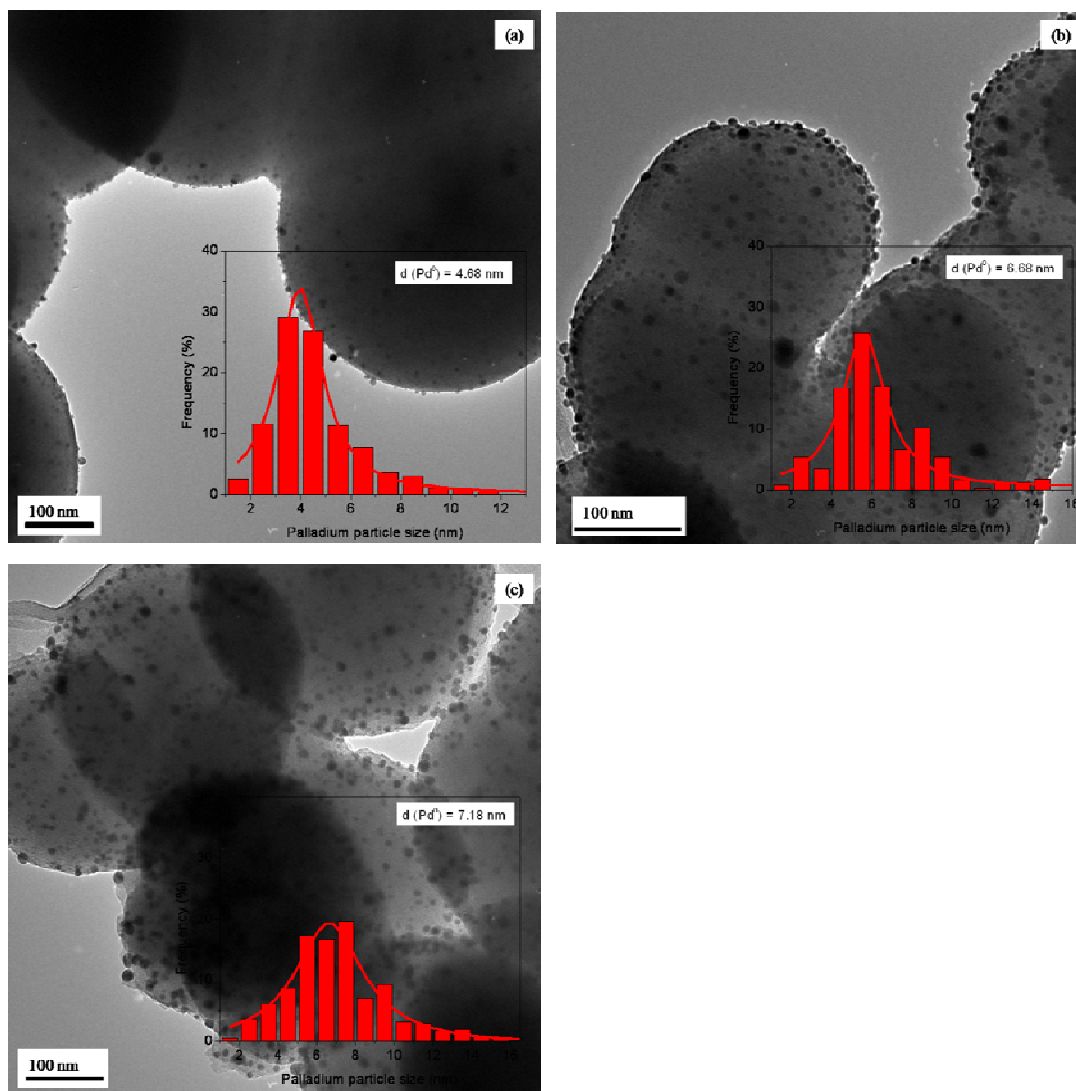


Figure 6.1. TEM images and corresponding particle size distribution graphs of a) Polyol 1 % Pd / fNCSs 40 catalyst, b) Impregnation 1 % Pd / fNCSs 40 calcined catalyst and c) Impregnation 1 % Pd / fNCSs 40 reduced catalyst

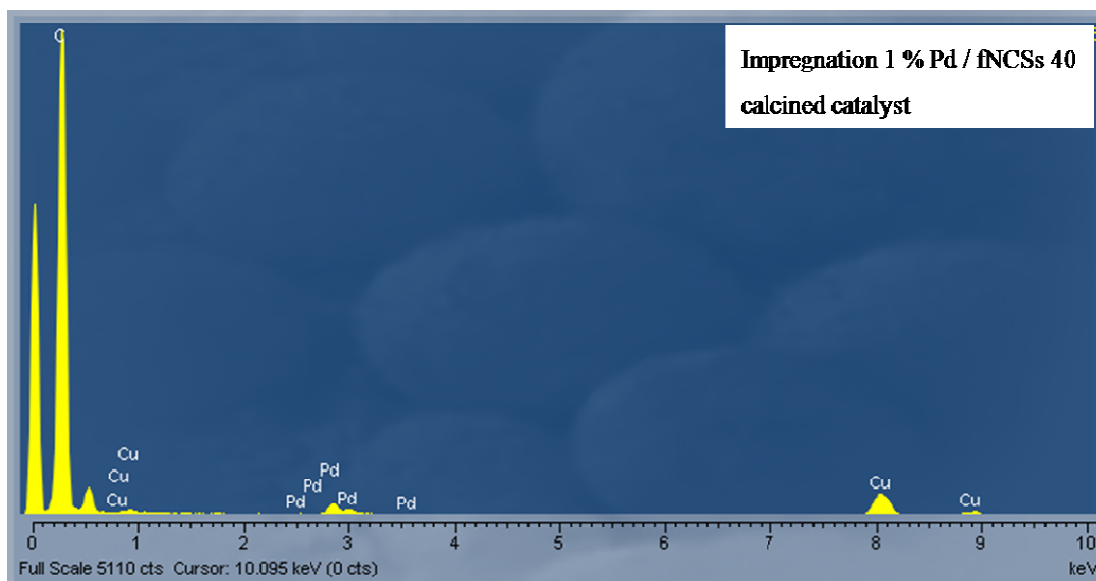


Figure 6.2. EDX spectrum of Impregnation 1 % Pd / fNCSs 40 calcined catalyst

A representative EDX spectrum of Impregnation 1 % Pd / fNCSs 40 calcined catalyst is shown in Figure 6.2. The EDX spectrum shows that Pd was successfully deposited on the fNCSs support.

The BET surface areas and pore volumes of the catalysts synthesized using different preparation methods are presented in Table 6.1. The BET surface areas and pore volumes of the catalysts were low.

Table 6.1. Physical properties of the catalysts.

Catalyst	BET surface area (m² / g)	Pore volume (cm³ / g)	*Pd content (%)
Polyol 1 % Pd / fNCSs 40	3.8	0.016	1.03
Impregnation 1 % Pd / fNCSs 40 calcined	3.6	0.015	0.99
Impregnation 1 % Pd / fNCSs 40 reduced	3.4	0.012	1.01

*Determined by ICP - OES analysis.

The ICP - OES analysis results showed that the Pd loading was 1.03, 0.99 and 1.01 % for the Polyol 1 % Pd / fNCSs 40 catalyst, Impregnation 1 % Pd / fNCSs 40 calcined and Impregnation 1 % Pd / fNCSs 40 reduced catalysts respectively (Table 6.1). The targeted loading of 1 wt. % Pd was successfully achieved in the 3 catalysts.

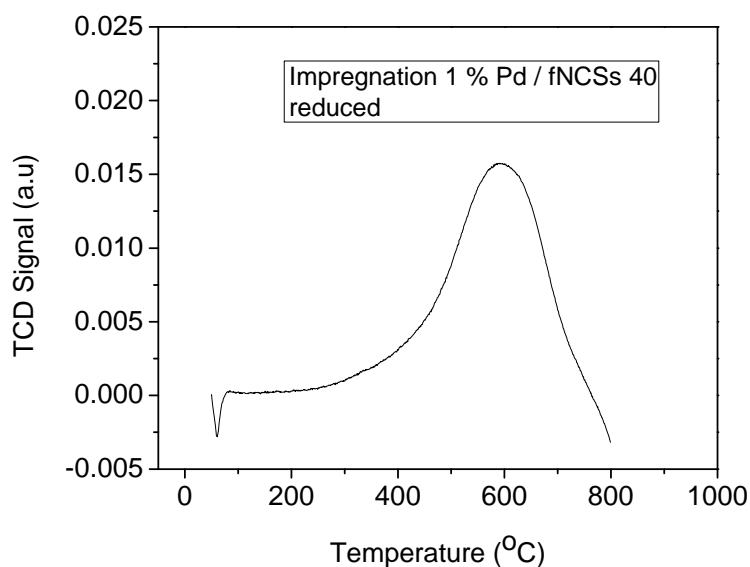


Figure 6.3. TPR profile of Impregnation 1 % Pd / fNCSs 40 reduced catalyst.

From the TPR graph (Figure 6.3) of the Impregnation 1% Pd / fNCSs40 reduced catalyst which was prepared using the incipient wetness impregnation method, it can be seen that there is a negative peak at a temperature of approximately 62 °C which is due to the desorption of physically adsorbed H₂ by the nitrogen doped carbon sphere support during the pretreatment process in a 5 volume % H₂ in Ar flow [7]. The peak at approximately 596 °C is assigned to the gasification of the carbon support. It shows that the Pd is completely reduced by the NCSs support [8].

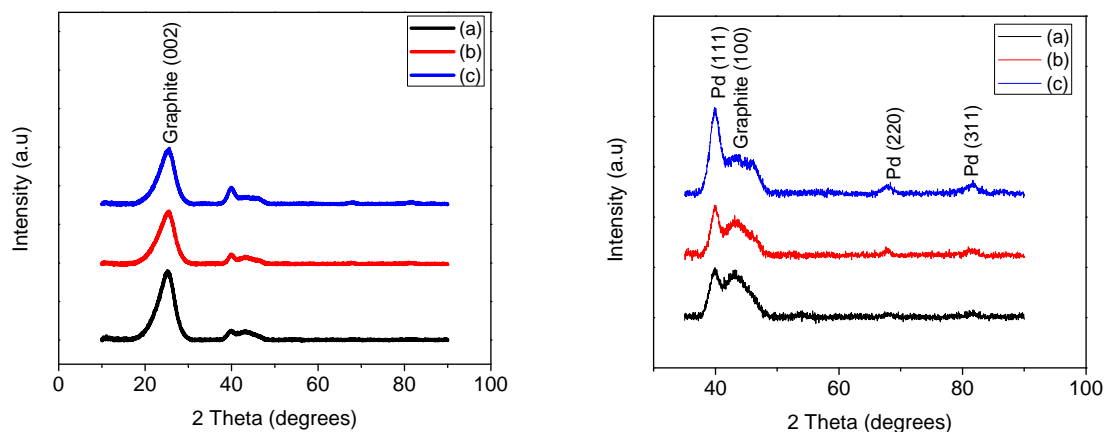


Figure 6.4. XRD patterns of a) Polyol 1 % Pd / fNCSs 40 catalyst, b) Impregnation 1 % Pd / fNCSs 40 calcined catalyst and c) Impregnation 1 % Pd / fNCSs 40 reduced catalyst.

The XRD patterns of the 3 catalysts: Polyol 1 % Pd / fNCSs 40, Impregnation 1 % Pd / fNCSs 40 calcined and Impregnation 1 % Pd / fNCSs 40 reduced catalysts are shown in Figure 6.4. The diffraction peaks at approximately 25.6° and 43.5° observed in the XRD patterns of the 3 catalysts are attributed to the hexagonal graphite structure of (002) and (100) [9, 10]. Besides these peaks of graphite, diffraction peaks at approximately 40.0°, 68.2° and 81.7° were also observed corresponding to the 2θ values of Pd (111), (220) and (311) crystal faces of face centered cubic (fcc) crystalline of the Pd particles in the Pd/fNCSs 40 catalysts [11].

6.3.2 Hydrogenation of CALD

The performance of the 3 catalysts prepared using the incipient wetness impregnation method and the liquid phase reduction method were tested in the hydrogenation of cinnamaldehyde is shown in Figure 6.5 and Table 6.2. As shown in Figure 6.5 and

Table 6.2, the catalyst prepared using the liquid phase reduction method exhibited better results compared with the catalysts prepared using the incipient wetness impregnation method. Blank tests carried out over the fNCSs 40 support alone showed no catalytic activity. The conversion of CALD at reaction time 4 hours for the following catalysts, Polyol 1 % Pd / fNCSs 40, Impregnation 1 % Pd / fNCSs 40 calcined and Impregnation 1 % Pd / fNCSs 40 reduced is 100, 57 and 43 % respectively. Okhlopko et al. and Gurrath et al. have reported that the performances of platinum group metals (PGMs) supported on carbon catalysts prepared by the reduction with hydrogen depends on the reduction temperature and the residual moisture in the hydrogenation reaction [12, 13]. Similar results were catalysts prepared using liquid phase reduction method showed better catalytic performance than those prepared using hydrogen as reductant were obtained by Jhung et al. [14]. The Pd particle sizes of Polyol 1 % Pd / fNCSs 40, Impregnation 1 % Pd / fNCSs 40 calcined and Impregnation 1 % Pd / fNCSs 40 reduced catalysts are 4.68, 6.68 and 7.18 nm respectively (Figure 6.1). The hydrogenation activity decreases with increasing Pd particle size. The catalysts which were reduced using either liquid phase or hydrogen gas were 100 % selective towards HCALD from reaction time 1 hour to 8 hours. These results showed that the reduction of catalysts in the hydrogenation of CALD using Pd nanoparticles deposited on functionalized NCSs is a necessary step to improve the catalytic performance of the catalyst. The Impregnation 1 % Pd / fNCSs 40 calcined catalyst was 100 % selective towards HCALD for the 1st 2 hours of the reaction. However as the reaction time increased from 3 to 8 hours, the catalyst was selective towards HCALD and 3P1P. Calcination of the Pd catalysts during the impregnation method is not sufficient enough to reduce Pd although the Pd is completely reduced as shown using TPR (Figure 6.3).

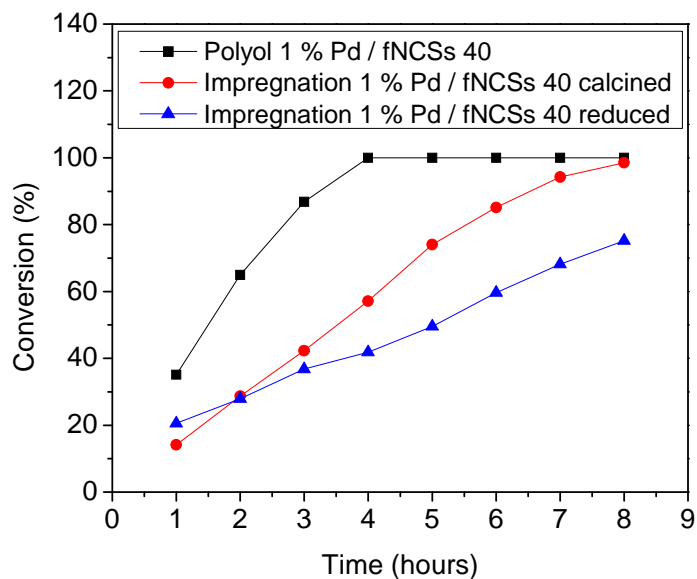


Figure 6.5. Catalytic activity, expressed in terms of conversion as a function of time for the CALD hydrogenation of the 1 % Pd / fNCSs 40 catalysts prepared by different methods.

Reaction conditions: CALD = 1.26 ml, hexan-1-ol = 100 ml, 1 % Pd / fNCSs 40 catalyst weight = 100 mg, T = 60 °C and H₂ (g) = 50 ml / min.

Table 6.2. Catalytic activity of 1 % Pd / fNCSs 40 catalysts prepared by different methods for cinnamaldehyde hydrogenation.

Catalyst	Activity (%)	Reaction time (hours)							
		1	2	3	4	5	6	7	8
Polyol 1 % Pd / fNCSs 40	Conversion	36	67	92	100	100	100	100	100
	HCALD ^a	100.0	100.0	100.0	100.0	100.0	100.0	100.0	100.0
	3P1P ^b	0.00	0.00	0.00	0.00	0.00	0.00	0.00	0.00
Impregnation 1 % Pd / fNCSs 40 calcined	Conversion	14	29	42	57	74	85	94	100
	HCALD ^a	100.0	100.0	94.9	94.0	93.7	93.6	92.0	90.1
	3P1P ^b	0.00	0.00	5.15	6.00	6.34	6.41	7.98	9.86
Impregnation 1 % Pd / fNCSs 40 reduced	Conversion	21	28	37	42	50	60	68	75
	HCALD ^a	100.0	100.0	100.0	100.0	100.0	100.0	100.0	100.0
	3P1P ^b	0.00	0.00	0.00	0.00	0.00	0.00	0.00	0.00

No cinnamyl alcohol was observed. ^aHCALD selectivity, ^b3P1P selectivity. Reaction conditions in Figure 6.2.

6.4 Conclusion

The incipient wetness impregnation method and the liquid phase reduction method were successfully used for the deposition of Pd nanoparticles on functionalized nitrogen doped carbon sphere supports. The catalysts prepared from the two methods were tested for the hydrogenation of cinnamaldehyde. The catalyst prepared from the liquid phase reduction method had the best catalytic performance in terms of both CALD conversion and selectivity to HCALD. The conversion to CALD was 100 % at reaction time 4 hours and the selectivity to HCALD was 100 % from reaction time 1 hour to 8 hours for the Polyol 1 % Pd / fNCSs 40 catalyst. However the catalyst activities (expressed in terms of conversion) for the catalysts prepared using the IWI method were 57 % and 42 % for the Impregnation 1% Pd / fNCSs 40 calcined and Impregnation 1 % Pd / fNCSs 40 reduced catalysts respectively. The Impregnation 1 % Pd / fNCSs 40 reduced catalyst was 100 % selective to HCALD throughout the reaction whereas the Impregnation 1% Pd / fNCSs 40 calcined catalysts was selective to both HCALD and 3P1P from reaction time 3 hours. The catalysts all had the same number of oxygen surface groups and contained the same N content so the differences in the catalyst performances could have been due to the method of preparation of the catalysts and also the Pd particle sizes.

6.5 References

1. Guo, Z., Y. Chen, L. Li, X. Wang, G.L. Haller, and Y. Yang, *Carbon nanotube-supported Pt-based bimetallic catalysts prepared by a microwave-assisted polyol reduction method and their catalytic applications in the selective hydrogenation*. Journal of Catalysis, 2010. **276**(2): p. 314-326.

2. Coq, B., J. Marc Planeix, and V. Brotons, *Fullerene-based materials as new support media in heterogeneous catalysis by metals*. Applied Catalysis A: General, 1998. **173**(2): p. 175-183.
3. de Jong, K.P., *Synthesis of supported catalysts*. Current Opinion in Solid State and Materials Science, 1999. **4**(1): p. 55-62.
4. Chen., Y., J. Wang, H. Liu, R. Li, X. Sun, S. Ye, and S. Knights, *Enhanced stability of Pt electrocatalysts by nitrogen doping in CNTs for PEM*. Electrochemistry Communications, 2009. **11**(10): p. 2071-2076.
5. Chizari, K., I. Janowska, M. Houll , I. Florea, O. Ersen, T. Romero, P. Bernhardt, M.J. Ledoux, and C. Pham-Huu, *Tuning of nitrogen-doped carbon nanotubes as catalyst support for liquid-phase reaction*. Applied Catalysis A: General, 2010. **380**(1-2): p. 72-80.
6. Ayala, P., M. Arenal, M. Rummeli, A. Rubio, and T. Pichler, *The doping of carbon nanotubes with nitrogen and their potential applications*. Carbon, 2010. **48**(3): p. 575-586.
7. Li, Y., G.-H. Lai, and R.-X. Zhou, *Carbon nanotubes supported Pt-Ni catalysts and their properties for the liquid phase hydrogenation of cinnamaldehyde to hydrocinnamaldehyde*. Applied Surface Science, 2007. **253**(11): p. 4978-4984.
8. Xiong, H., M. Moyo, M.K. Rayner, L.L. Jewell, D.G. Billing, and N.J. Coville, *Autoreduction and Catalytic Performance of a Cobalt Fischer-Tropsch Synthesis Catalyst Supported on Nitrogen-Doped Carbon Spheres*. ChemCatChem, 2010. **2**(5): p. 514-518.
9. Belin, T., and F. Epron, *Characterization methods of carbon nanotubes: a review*. Materials Science and Engineering: B, 2005. **119**(2): p. 105-118.
10. Li, W., C. Liang, W. Zhou, J. Qiu, Z. Zhou, G. Sun, and Q. Xin, *Preparation and Characterization of Multiwalled Carbon Nanotube-Supported Platinum for Cathode Catalysts of Direct Methanol Fuel Cells*. The Journal of Physical Chemistry B, 2003. **107**(26): p. 6292-6299.

11. Cheng, N., H. Lv, W. Wang, S. Mu, M. Pan, and F. Marken, *An ambient aqueous synthesis for highly dispersed and active Pd/C catalyst for formic acid electro-oxidation* Journal of Power Sources, 2010. **195**(21): p. 7246-7249.
12. Okhlopkova, L.B., V.A. Likholobov, M. Gurrath, and H.P. Boehm, *Properties of Pt/C and Pd/C catalysts prepared by reduction with hydrogen of adsorbed metal chlorides: Influence of pore structure of the support*. Applied Catalysis A: General, 2000. **204**(2): p. 229-240.
13. Gurrath, M., T. Kuretzky, H.P. Boehm, L.B. Okhlopkova, A.S. Lisitsyn, and V.A. Likholobov, *Palladium catalysts on activated carbon supports: Influence of reduction temperature, origin of the support and pretreatments of the carbon surface*. Carbon, 2000. **38**(8): p. 1241-1255.
14. Jhung, S.H., J.H. Lee, J.M. Lee, J.H. Lee, D.Y. Hong, M.W. Kim, and J.S. Chang, *Effect of Preparation Conditions on the Hydrogenation Activity and Metal Dispersion of Pt/C and Pd/C Catalysts*. Bulletin of the Korean Chemical Society, 2005. **26**(4): p. 563-568.

CHAPTER 7

Summary and Concluding Remarks

The main aim of the work described in this thesis was to study the effect of chemically modifying the surfaces of carbon spheres with non - carbon groups (nitrogen) on the carbon - catalyst (Pd) interaction. The effect of functionalizing the carbon sphere surface using different functionalizing procedures was also investigated. These effects were expected to have an impact between the metal particles and the carbon surface and consequently on the catalytic activity of the metals. In this thesis carbon spheres were functionalized and doped with nitrogen and their catalytic activity in the hydrogenation of cinnamaldehyde was tested. The selective hydrogenation of cinnamaldehyde to hydrocinnamaldehyde was chosen as a showcase to fully explore the different support effects for this reaction in detail.

Nitrogen doped carbon spheres were successfully synthesized by a non - catalytic chemical vapour deposition method using acetylene as the carbon source and acetonitrile as the nitrogen source. The influence of variation of synthesis parameters: temperature, time and flow rates of gases during the pyrolysis stage were investigated and found to have an effect on the physical and chemical properties of the resultant nitrogen doped carbon spheres produced. Increasing the time and temperature and the variation of flow rate of gases during the pyrolysis stage was found to affect the average diameter, degree of disorder and thermal stability of the NCSs.

The liquid phase reduction method was used to prepare catalysts with well dispersed Pd nanoparticles supported on NCSs. The 1 % Pd / fNCSs catalysts displayed high catalytic activities for the hydrogenation of CALD. The palladium particles supported on CSs and NCSs functionalized at different temperatures of 55 % HNO₃ for 24 hours had mean particle sizes ranging between 4.68 and 7.51 nm. The palladium nanoparticles supported on CSs with different nitrogen contents were well dispersed with mean particle sizes centred between 4.15 and 4.82 nm. The liquid phase hydrogenation of CALD was significantly influenced by the amount of oxygen surface groups on the support, the presence or absence of N in the carbon sphere support, the amount of N and the N type in the catalysts and the total absence of microporosity in the catalysts.

An exploratory study on the selective hydrogenation of cinnamaldehyde was investigated. The influence of reaction solvents, temperature and flow rates of hydrogen were evaluated. Based on the results obtained, the optimum conditions which were used for the hydrogenation reactions in this thesis were: cinnamaldehyde concentration of 0.01 M, hexanol solvent (100 ml), 1 % Pd / fNCSs 40 catalyst (100 mg), temperature of 60 °C and reductant H₂ (50 ml / min). These conditions were chosen as the optimum conditions for the hydrogenation of cinnamaldehyde when using 1 % Pd / fNCSs 40 catalyst because i) high activities and selectivities to hydrocinnamaldehyde were observed, ii) there was absence of side reaction products, iii) no catalyst leaching and iv) the catalyst was stable after 4 recycling tests.

The incipient wetness impregnation method and the liquid phase reduction method were successfully used for the deposition of Pd nanoparticles on functionalized nitrogen doped carbon sphere supports. The catalysts prepared from the two methods were tested for the hydrogenation of cinnamaldehyde. The catalyst prepared from the liquid phase reduction method had the best catalytic performance in terms of both

CALD conversion and selectivity to HCALD. The conversion to CALD was 100 % at reaction time 4 hours and the selectivity to HCALD was 100 % from reaction time 1 hour to 8 hours for the Polyol 1 % Pd / fNCSs 40 catalyst. However the catalyst activities (expressed in terms of conversion) for the catalysts prepared using the IWI method were 57 % and 42 % for the Impregnation 1% Pd / fNCSs 40 calcined and Impregnation 1 % Pd / fNCSs 40 reduced catalysts respectively. The catalysts all had the same number of oxygen surface groups and contained the same N content so the differences in the catalyst performances could have been due to the method of preparation of the catalysts and also the Pd particle sizes.

The results described in this thesis showed that NCSs were successfully synthesized using a non-catalytic CVD method. NCSs were used as supports for palladium catalysts in the hydrogenation of CALD. The role of oxygen surface groups as well as the influence of N content and N type was investigated for the hydrogenation of CALD. Different catalysts preparation methods were employed and the catalysts tested for the catalysis reaction. Future research can be devoted to reveal the mechanism of reactant adsorption on NCSs and reactant adsorption via promoters towards palladium. Other metals such Pt, Ru, Os can be deposited on the NCSs supports and the resultant catalysts tested for the hydrogenation of CALD.

APPENDIX

EXPERIMENTAL

Materials and chemicals

Reagents and Chemicals

Palladium acetate ($\text{Pd}(\text{C}_2\text{H}_3\text{O}_2)_2$), acetonitrile (CH_3CN), triethylamine, nitric acid, toluene, ethylene glycol, acetone, cinnamaldehyde, hydrocinnamaldehyde, 3-phenyl-1-propanol, cinnamyl alcohol, ethanol, propan-2-ol, butan-2-ol, 1-hexanol, 1-heptanol, octan-2-ol, ethyl acetate, 1,4-dioxane, hydrochloric acid (HCl) and sodium hydroxide solution (NaOH). All chemicals were obtained from Sigma - Aldrich and were used as received without any further purification procedures. Deionized water was obtained from the School of Chemistry laboratories where it was produced.

Gases

All gases used in this work were supplied by African Oxygen (AFROX). All gas cylinders supplied by AFROX were accompanied by a certificate of analysis which provided purity of gas mixtures, composition of gases and expiry dates of gas cylinders. The gases used were acetylene (C_2H_2), nitrogen (N_2) and hydrogen (H_2).

Synthesis of NCSs

The synthesis of NCSs was performed according to the procedure reported by Deshmukh *et al* [1] with a few modifications. NCSs were synthesized using a non-catalytic chemical vapor deposition (CVD) method where acetylene (C_2H_2) was used as a carbon source and acetonitrile (CH_3CN) was the N source. N_2 was first flowed through a quartz tube (150 cm) at 100 ml / min while the furnace was heated from room temperature to the desired temperature at a heating rate of 10 $^{\circ}C$ / min to create an inert atmosphere. Once the desired temperature was reached the N_2 flow was switched off and C_2H_2 was bubbled through CH_3CN (80 $^{\circ}C$) at a flow rate of 100 ml / min for the required carbonization time. After the required carbonization time, the C_2H_2 flow was switched off and N_2 was flowed through the system at 100 ml / min until the furnace had cooled down to room temperature. NCSs were then collected from the walls of the quartz tube and weighed. The volume of CH_3CN used in the reaction was also recorded. Summary of experimental conditions used in the CVD process are shown in Table 3.1. Figure A1 shows the schematic diagram of the CVD setup.

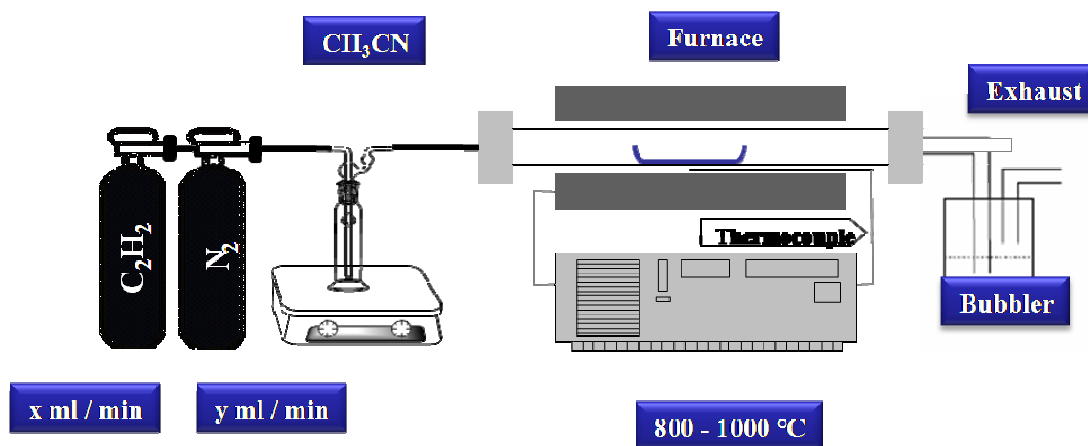


Figure A1. The horizontal CVD setup for the synthesis of nitrogen doped carbon spheres.

Removal of polyaromatic hydrocarbons (PAHs)

NCSs (1.0 g) were placed in a thimble and toluene (150 ml) was added into a round bottomed flask (250 ml). Soxhlet extraction was carried out at reflux for 3 hours. The extracted carbon material was dried in an oven overnight at 80 °C.

Functionalization of NCSs

Functionalization of the NCSs was carried out by treatment with 55 % nitric acid (HNO_3) for 24 hours while varying the temperatures (40, 60 and 80 °C). The functionalized NCSs (fNCSs) were then filtered using deionized water until the pH of the filtrate was 7. The fNCSs were then dried in an oven for 12 hours at 80 °C.

Catalyst synthesis

The polyol and incipient wetness impregnation methods were employed to prepare palladium catalysts (1 wt. % Pd) supported on acid functionalized undoped and doped carbon spheres. The metal precursor solution of 0.05 M Pd (acetate) was prepared by dissolving 0.5625 g of Pd (acetate) salt in 50 ml of acetone.

Liquid phase reduction method

One of the methods for the deposition of Pd nanoparticles on carbon sphere supports was done according to the procedure reported by Chen et al. [2] with a few modifications. For the catalysts prepared using the liquid phase reduction method of metal in ethylene glycol solution, carbon supports (400 mg) were placed into a 500

ml round bottomed flask and ethylene glycol solution (150 ml) was added. The contents of the beaker were sonicated for 15 minutes followed by magnetically stirring for 30 minutes. The metal precursor solution 0.05 M was then added drop wise to the mixture of carbon support and ethylene glycol solution. The concentrations of the precursor solutions in the ethylene glycol solutions were calculated in order to prepare catalysts with metal loadings with a fixed 1 wt %. The resultant solution was magnetically stirred vigorously for a further 3 hours at room temperature followed by refluxing at 195 °C in an oil bath for 3 hours. The solution was then cooled down to room temperature. The metal/carbon sphere powder in the solution was filtered and thoroughly washed 1st with 20 ml of acetone followed by excess distiller water. The resulting carbon supported metal catalyst was dried in air for 8 hours at 80 °C and a mortar was used to homogeneously grind the material to form a powder.

Incipient wetness impregnation method

1 wt % Pd catalysts were also prepared using the incipient wetness impregnation method. The 0.05 M metal precursor solution (0.95 ml) was added drop wise to fNCSs 40 support (0.5 g) under vigorous stirring until a paste like solid was obtained. The wet like solid was dried overnight at room temperature. The air dried solid was named As - synthesized 1 % Pd / fNCSs 40 catalyst. Parts of the air dried solids underwent thermal treatments. The 1st thermal treatment was calcination which decomposes the Pd salt into its corresponding oxide. The as - synthesized 1 % Pd / fNCSs 40 catalyst was calcinated in air at 250 °C for 2 hours at a heating rate of 10 °C / min. The resulting sample was named Calcined 1 % Pd / fNCSs 40 catalyst. The calcined 1 % Pd / fNCSs 40 catalyst was further reduced in hydrogen gas (20 ml / min) at 400 °C for 2 hours at a heating rate of 10 °C / min. the sample was cooled down under nitrogen flow (50 ml / min). The resultant sample was named Reduced 1 % Pd / fNCSs 40 catalyst.

Characterization techniques

Transmission Electron Microscopy (TEM)

TEM was used to study the morphology of the materials and to gain information about the particle size distribution of catalysts on carbon sphere supports. TEM investigations were performed using a FEI Technai G² Spirit electron microscope operating at an accelerating voltage of 120 kV. A small amount of sample was suspended in methanol solution by ultra sonication for 3 minutes. A drop of the suspension was then placed onto a copper grid and dried at room temperature. Energy dispersive X-ray (EDX) spectroscopy coupled with TEM was used for confirmation of elemental composition of catalysts.

Fourier transform infrared (FTIR) spectroscopy

FTIR was used to confirm the introduction of functional groups on the carbon spheres after acid functionalization. FTIR measurements were performed on a Bruker Vector FTIR spectrometer in the range 4000 - 400 cm⁻¹.

Zeta potential measurements

The degree of functionalization of the carbon supports was studied using zeta potential measurements. Zeta potentials of as-synthesized and acid functionalized undoped and doped carbon spheres were measured using a Malvern Zetasizer nano-series instrument. The as-synthesized and acid functionalized undoped and doped carbon spheres (0.5 g) were dispersed in deionized water (100 ml) at room

temperature and the pH of the suspension was adjusted from 2.0 to 12.0 by adding either 0.1 M HCl or 0.1 M NaOH. By measuring the zeta potential as a function of pH the point of zero charge was determined.

Raman spectroscopy

Raman spectroscopy was used to determine the graphitic nature of the carbon nanomaterials. It was performed using a micro - Raman attachment of a Jobin - Yvon T64000 Raman spectrometer equipped with a charge couple device (CCD) detector. The laser spot size on the sample was approximately 1.5 microns in diameter, and the excitation wavelength was 514.5 nm from a green line of an argon ion laser.

Thermogravimetric analysis (TGA)

The thermal stability of the carbon supports and catalysts was determined by thermogravimetric analysis (TGA) using a Perkin Elmer TGA 4000 analyzer. Approximately 10 mg of sample was used for the analysis and the samples were heated from room temperature up to 950 °C at a heating rate of 5 °C / min in air atmosphere (20 ml / min).

Nitrogen adsorption / desorption analysis

A Micrometrics Tristar 3000 Surface Area and Porosity Analyzer was used to measure the N₂ adsorption / desorption isotherms according to the Brunauer, Emmett and Teller (BET) method at - 196 °C. This technique was used to determine the BET surface area and pore volumes of carbon supports and catalysts. The samples (~ 0.2 g)

were degassed using a Micrometrics Flow Prep 060 Sample Degas System at 120 °C for 5 hours prior to nitrogen adsorption.

CN elemental analysis

The composition of carbon and nitrogen in the NCSs was determined by CN elemental analysis using a Carlo Erba NA1500 Nitrogen Carbon Sulphur analyzer. Approximately 1.0 - 1.5 mg of sample was used for the analysis, a GC equipped with a thermal conductivity detector (TCD) was used to separate the gases produced.

X-ray photoelectron spectroscopy (XPS)

X-ray photoelectron spectroscopy (XPS) was used to determine the elemental composition in the doped carbon spheres. The binding energy was recorded on a PHI5600 spectrometer equipped with a monochromatic Al K α source (1486.6 eV).

Powder X-ray diffraction (XRD)

Information on the crystallographic structure of carbon supports and catalysts was obtained using a Bruker D2 phaser equipped with a Lynxeye detector. A Co K α radiation at 30 kV was used. The scan ranged from $10^\circ < 2\theta < 90^\circ$ in 0.026° steps. Samples were ground to fine powders and packed flatly in sample holders before analysis.

Inductively Coupled Plasma - Optical Emission Spectroscopy (ICP - OES)

The metal weight-loading of the samples was determined using ICP-OES. The measurements were performed using a SPECTRO CIROSCCD ICP-Spectrometer. Each sample was destructed by heating in aqua regia (1:3 mixture of HNO₃: HCl) before analysis.

Temperature programmed reduction (TPR)

A Micrometrics AutoChem 2910 instrument was used for the determination of the degree of reduction and reducibility of the catalysts. The sample (~ 100 mg) was 1st pretreated by heating it from room temperature to 500 °C at a heating rate of 10 °C / min for 30 minutes then cooled to 50 °C under Ar. After pretreatment, reduction of the sample followed where the following conditions were used: 5 % H₂ + 95 % Ar gas mixture at a flow rate of 50 ml / min at 1 bar pressure was heated to 900 °C at 10 °C / min heating rate. Change in the amount of hydrogen flowing in both the reference and reactor was monitored by TCD.

Catalytic reaction

The equipment setup for the hydrogenation of cinnamaldehyde is shown in Figure A2.

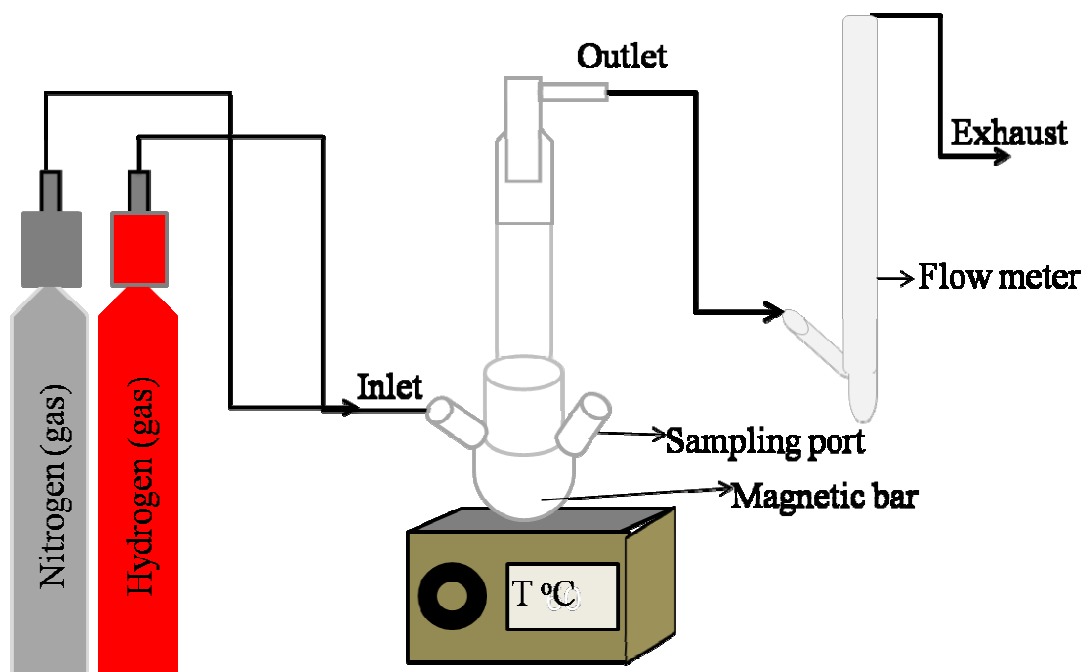


Figure A2. Experimental setup used for the hydrogenation of cinnamaldehyde reaction.

The selective hydrogenation of cinnamaldehyde was carried out at atmospheric pressure in a 250 ml three necked round bottomed flask equipped with a magnetic stirrer, reflux condenser, gas inlet and sampling port. The three necked round bottomed flask was maintained in an oil bath at specific temperatures. In a typical catalytic run, the reaction mixture contains 1.26 ml of cinnamaldehyde; 100 ml of solvent and 0.1 g of catalyst were added to the flask. Nitrogen gas was bubbled through the solution for 30 minutes, while the oil bath was heating from room

temperature to the desired reaction temperature to remove traces of dissolved oxygen in the system. After this hydrogen gas (H_2) at desired flow rate was continuously fed into the system while the contents were stirred. The duration of each reaction was 8 hours. Chemical analysis of the reaction products was performed by taking samples of the reaction solution periodically and analyzing by gas chromatography (GC) equipped with a flame ionization detector (FID) and a ZB-1 capillary column ($30\text{ m} \times 0.32 \times 0.53\text{ }\mu\text{m}$). Blank experiments using raw carbon spheres, functionalized carbon spheres and as-synthesized and functionalized nitrogen doped carbon spheres was carried out to reveal that the CALD conversion is zero, and any product is not detected by GC. Reagent and products will be identified by comparison with authentic standards (GC grade). Qualitative analysis was carried out by calculating the area of the chromatographic peaks from the computer. Table 3.2 shows the catalytic reaction variables used in this study.

Gas chromatographic analysis

The Gas chromatographic conditions were as follows:

GC model:	Varian 3700
Detector:	Flame ionization detector (FID)
Detector temperature:	350 °C
Column type:	ZB-1 Capillary column 30 m × 0.32 × 0.53 μm
Injector temperature:	250 °C
Carrier gas:	Argon
Flow rate:	30 ml / min
Oven temperature:	130 °C

Data analysis and calculations

The results of the catalytic reaction runs were analyzed in terms of reactant conversion and product selectivity [3]:

$$\text{Conversion (\%)} = 100 \times [CALD]_0 - [CALD]_t \div [CALD]_0 \quad (1)$$

$$\text{Selectivity (\%)} = 100 \times [X]_t \div \sum [X]_t \quad (2)$$

where $[\text{CALD}]_0$ represents the initial concentration of CALD at time 0, $[\text{CALD}]$ represents the concentration of CALD at a given time t and $[\text{X}]_t$ represents the concentration of the main identifiable hydrogenation products of CALD, namely cinnamyl alcohol, hydrocinnamaldehyde, 3 - phenyl - 1 - propanol and others at a given time t .

References

1. Deshmukh, A.A., R. Ul Islam, M.J. Witcomb, W.A.L. van Otterlo, and N.J. Coville, *Catalytic Activity of Metal Nanoparticles Supported on Nitrogen-Doped Carbon Spheres*. ChemCatChem, 2010. **2**(1): p. 51-54.
2. Chen, Y., J. Wang, H. Liu, M.N. Banis, R. Li, X. Sun, T.-K. Sham, S. Ye, and S. Knights, *Nitrogen Doping Effects on Carbon Nanotubes and the Origin of the Enhanced Electrocatalytic Activity of Supported Pt for Proton-Exchange Membrane Fuel Cells*. The Journal of Physical Chemistry C, 2011. **115**(9): p. 3769-3776.
3. Cabiac, A., T. Cacciaguerra, P. Trens, R. Durand, G. Delahay, A. Medevielle, D. Plée, and B. Coq, *Influence of textural properties of activated carbons on Pd/carbon catalysts synthesis for cinnamaldehyde hydrogenation*. Applied Catalysis A: General, 2008. **340**(2): p. 229-235.